PETROLEUM RESEARCH JOURNAL

Velocity Investigation and Depth Conversion Using Calibrated Seismic Velocity in Soluq Depression Area, NE-Libya .....
Saad M. El-Shari 1

An Evaluation of the Waha Limestone South Al Jabal Field, Sirt Basin .....
Ali M. Massoud Elmesmari 21

Anisotropic Prestack Depth Migration In C97 And NC98,Libya .....
C. Hanitzsch and A.S. Ben Abdulla 35

Integration of Remote Sensing and Geophysical Data: A Case Study of Structural Development and Petroleum Prospectivety of Western Sirt Basin, Libya .....
Khalifa M. Abdunaser and Giuma Reeh 45

Late Tertiary Subsidence and Tilting in the Sirt Basin and their Seismic Signatures ....
M. S. Zanati and M. Roohi 59

Seismic Reprocessing: Case Study Barrut Arch, Concession 72, Sirt Basin, Libya .....
Ali Abuagela, and Naji Miladi 77

Improved Static Corrections over Sand Dunes for Seismic Line NC151-V532, Western Libya .....
Abdurrazag M.A. Ushah and N.R. Goulty 95

Reservoir Characterization in Concession C97-I, Eastern Sirt Basin, Libya .....
Luca de Vincenzi and Ziad Ayub 103

A Unique High Resolution Imaging Process - a Key to the Understanding of the Reservoir .....
Stuart Hirsch, Gary Perry, and Michael Fleming 107

Pitfalls in 3D preSDM Imaging .....
Ian F. Jones 113

VOLUME 20 - (2007)

Libyan Petroleum Institute
P.O. Box 6431, Tripoli
Great Socialist People's Libyan Arab Jamahiriya

Petroleum Res. J. Vol. 20 (2007); P. 1–20, 11 Figs.

Velocity Investigation and Depth Conversion Using Calibrated Seismic Velocity in Soluq Depression Area, NE-Libya

Saad M. El-Shari*

تحقيق السرعة وتحويل العمق باستخدام معايرة السرعة الزلزالية في منطقة منخفض سلوق شمال شرق ليبيا

سعد م. الشاري

يهدف هذا التحليل إلى تحديد الفرق بين السرعات ذات الاشتقاق السيزمي والسرعات المستمدة من المسوحات المبدئية والسرود الصوتية وإلى اختبار التأثير المحتمل لهذا الفرق على تحديد توزيع السرعة الحقيقية. وحيث من المفترض أن المنطقة تحت الدراسة تقع على خط التماس بين بيئتين فإن الرسوبيات قد تجمعت في بيئات مختلفة وبذلك فإنه من المتوقع وجود تغيير في المحتوى الصخري في كلا الاتجاهين الرأسي والأفقي. وفي هذه الحالة، فإن افتراض سرعة واحدة لن يكون صحيحا، حيث أن تغيرات سريعة قد تحدث في السرعة بين نقطة وأخرى ولذلك فإن تحديد دوال السرعة الحقيقية في المنطقة يعد عملا مهما ويتطلب أكبر قدر من الدقة.

تتألف بيانات السرعة المتوفرة لهذا التحليل من مسوحات السرعة في الآبار وقياسات السرود الصوتية في تسعة آبار. وتشتمل مجموعة البيانات قياسات السرعة الانعكاسية في 54 مقطعا سيزميا. ويحدد الجزء الأول من تحليل المقطع ومتوسط السرعات من مصادر هذه البيانات. وقد تم إنجاز مقارنة دقيقة لهذه السرعات المختلفة التي تم تحديدها مسبقا. وأخيرا تم تصحيح السرعات المقطعية لكي يتم التعويض على التأثير المفتعل تلقائيا الملاحظ خلال ربط الآبار. وتوضح رسومات مستويات السرعات السيزمية زيادة في السرعة مع العمق كما هو متوقع من عمليات التراص الطبيعية.

وعموما فإن رسومات السرعة تمثل مضاهاة مقبولة مع المتوقع جيولوجيا للتركيبات تحت السطحية وسوف تقود تفسيرات خرائط العمق والسرعة لكل تتابع سيزمي على حده مع ما يتوفر من بيانات جيولوجية وجيوفيزيائية، إلى تفسيرات نهائية أكثر دقة لمنطقة الدراسة.

Abstract: *Investigation of the difference between the seismic derived velocities and the check-shot and sonic log velocities, to examine what effect the difference might have on the determination of the true velocity distribution was conducted. Since the investigated area is assumed to be located on a hinge-line, sediments have been deposited in different environments and thus a change in lithology in both vertical and horizontal directions is expected. In such a situation, an assumption of constant velocity would not be valid, since rapid changes in velocity from one point to another may occur. Therefore, determination of the true velocity functions in the area is an important task, requiring as much accuracy as possible.*

The velocity data available for this analysis consists of borehole velocity survey and sonic log measurements from nine boreholes. The data set also includes seismic reflection velocity

* Exploration Dept. AGOCO, P.O. Box 263 Binghazi-Libya.
E-mail: smbelshari@yahoo.com

measurements from 54 seismic profiles. The first part of the analysis determines interval and average velocities from these data sources. A critical comparison of these different determined velocities has been done. The derived average and interval velocities are finally corrected using the mean average and interval velocity error, in order to compensate for a systematic biasing influence observed from the well ties. Contour plotting of the seismic velocities shows a general increasing velocity with depth, as expected with normal compaction. Generally, the velocity plots represent a reasonable correlation with the geological expectation of the subsurface structure. The interpretation of the depth and velocities maps for individual seismic sequences, together with all available geological and geophysical data, will lead to a more complete final interpretation in the study area.

INTRODUCTION

The area of the present study is located on concession NC129 of AGOCO (Fig. 1). Geologically, the area approximately lies on a hinge-line between the Mesozoic-Tertiary Sirt Basin to the west and the stable Cyrenaica Platform to the east. The Ajdabiya Trough forms the most eastern part of the Sirt Basin, while the Soluq Depression is the western part of the Cyrenaica Platform (Fig. 1).

Analyses of true velocity variation are very useful for local stratigraphic interpretation and lithologic evaluation, and for conversion of two way time to depth. Many technical papers have been published on the subject of velocity analysis. Among them are the following which focus on the concept of velocity and its application to structural-stratigraphic interpretation: Al-Chalabi (1974 and 1979), Lindseth (1982), Banik (1984), Peikert (1985), Dobrin and Savit (1988) and Sheriff and Geldart (1995).

The overall aim of this research is to compute and interpret the velocity distribution across the hinge-line between the Sirt Basin and Cyrenaica Platform. The velocity distribution fields for each depositional sequence in the area are calculated, and used to indicate lithologic and stratigraphic changes to help evaluate the geological and tectonic history of the area. Reliable depths to the top of each sequence, by converting travel times using calibrated average velocity information, is also produced.

During the last four decades, a number of regional

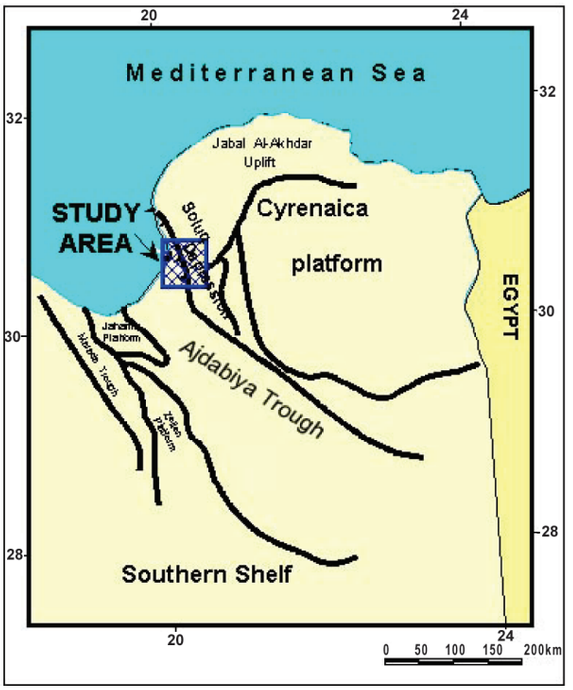


Fig. 1. Location map of the study area, and the major tectonic elements in NE- Libya.

and local geological studies, in the Sirt Basin and Cyrenaica Platform have been published (Barr (1972), Burke and Dewey (1974), Berggren (1969, 1974), Van Houten (1983) and Anketell and Ghellali (1991). Most of the geological studies done on NE Libya have concentrated on the surface outcrops in the Al Jabal al Akhdar region. Rohlich (1974) described the principle stratal features and evaluated the tectonic development of Al Jabal Al Akhdar exposures. El-Arnauti and Shelmani (1985) studied the stratigraphy and structural development of the Palaeozoic and Mesozoic in the subsurface of the Cyrenaica Platform. El-Shari (2004) studied the stratigraphic sequences and analysed the subsidence and sedimentation rates across the hinge-zone between Sirt Basin and Cyrenaica Platform.

GEOLOGICAL SETTING OF SOLUQ DEPRESSION

The most prominent surface morphologies in the Cyrenaica region are Al Jabal al Akhdar uplift in the north, the Soluq Depression in the southwest and the Cyrenaica Platform in the east and southeast (Fig. 1). In the southern part of the area, a partially marine Palaeozoic sequence has unconformably overlain the basement, while in the east and northeast, the

basement is overlain by a wedge of marine Palaeozoic rocks which thickens towards the east (El-Arnauti and Shelmani, 1985). The Palaeozoic rocks are widespread in the Cyrenaica region and show variation of thickness, which can be attributed to the post-early Palaeozoic tectonic activity and subsequent erosion (Sola and Ozcick, 1990).

The Soluq Depression, which lies mainly on the Cyrenaica Platform, is connected with the Ajdabiya Trough of the Sirt Basin. Within this depression, the main structural trend is northwest-southeast. During Triassic, Jurassic and Early Cretaceous times, the Soluq Depression was high with NE dipping Palaeozoic strata, which was subjected to erosion (Yanilmaz *et al.*, 1989). The Lower Cretaceous is absent in this region, where the basin is probably underlain by Lower Palaeozoic age rocks.

During Late Cretaceous, the fluctuation in sea level resulted in the deposition of limestone interbedded with shale. At this time, a local depocentre developed, and over 2500m of Upper Cretaceous sediments were deposited. The axis of the basin, and its depocentre, shifted towards the east during Palaeocene and Eocene times. During the Oligocene and Miocene, periodic fluctuations in sea level resulted in cyclic shoaling-upward carbonate cycles. Figure 2 shows that the sedimentary succession is dominated by marine carbonates, but significant amounts of shale were also deposited in the area. During low stands of sea level, evaporites were deposited upon shallow parts of the platform.

DATA BASE AND METHODOLGY

The database for this analysis is comprised of 507 velocity analysis tabulations from 54 seismic reflection profiles, continuous velocity logs, and well velocity surveys from nine wells. The seismic lines form an approximate 2 km square grid over a rectangular area of around 60 x 60 km. The locations of the wells and the seismic lines used in this project are shown in Figure 3.

The seismic data quality over the studied area is generally good. The seismic data pointed to a basin-to-shelf depositional setting (Fig. 4). In such an area, lateral and vertical changes in geology are expected to reflect different depositional environments. In order to evaluate the lateral facies changes, and to control the distance between the expected major features of the area, a close seismic line spacing was chosen.

The analysis begins by determining the velocity from these three different sources of data. Then, results of the velocities derived from the seismic reflection data and those derived from the sonic logging and well velocity surveys in the boreholes are compared. The derived average and interval

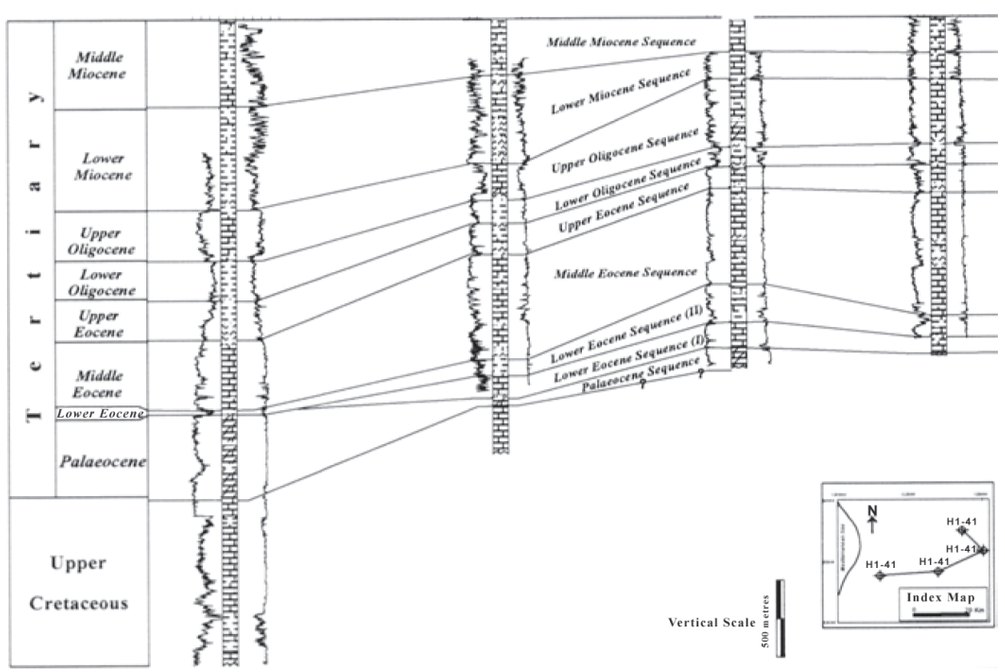


Fig. 2. Chronostratigraphic correlation with lithostratigraphy of the penetrated sedimentary sequences of four wells located on the hinge-zone of the Cyrenaica Platform with Sirt Basin, the correlation of the wells is based on the final lithological composite log and on the interpretation of gamma-ray and sonic logs. Log curves have been plotted with a sampling interval of 3 meters, and the datum is mean sea level.

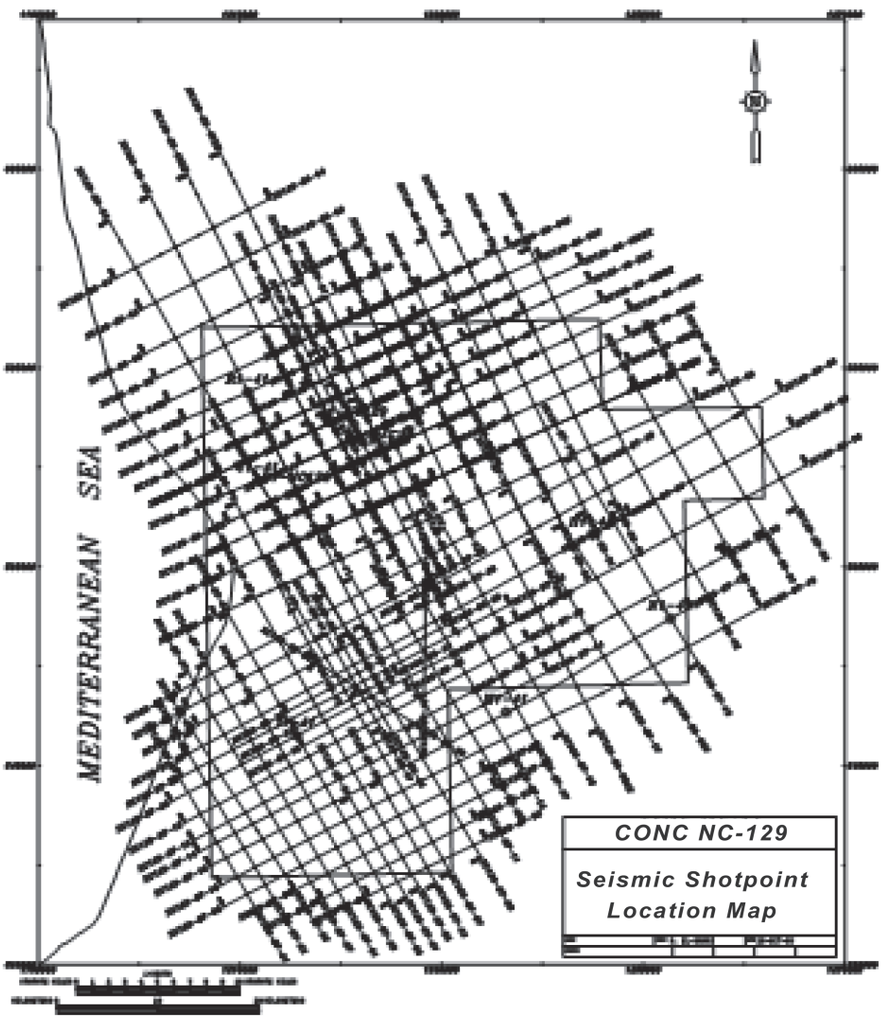


Fig. 3. Seismic reflection profiles and wells location in Concession NC-129.

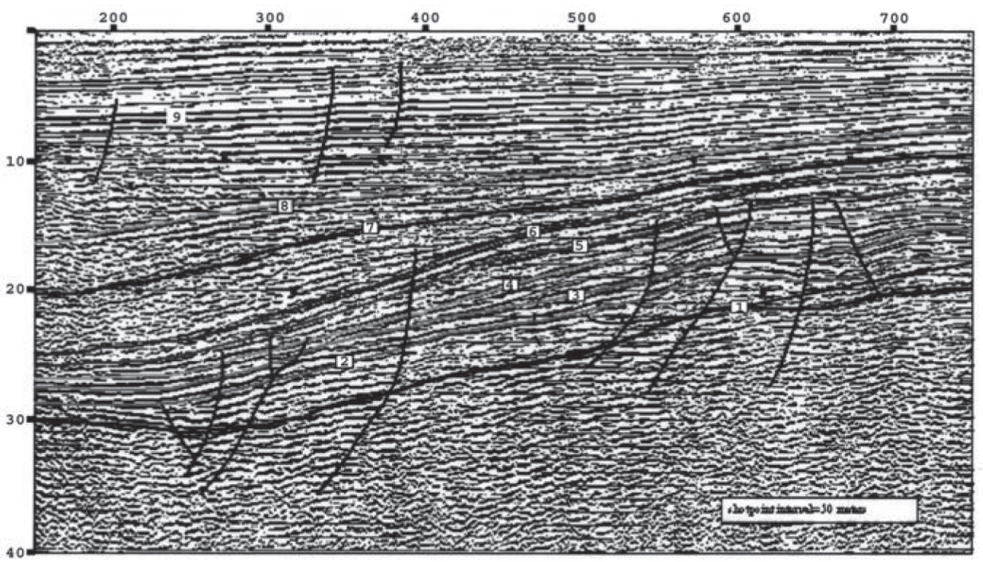


Fig. 4. Seismic interpretation along line NC129-87-08. The boundaries between the sequences shown as following; (1) base Palaeocene sequence, (2) top Palaeocene sequence, (3) top Lower Eocene sequence I, (4) top Lower Eocene sequence II, (5) top Middle Eocene sequence, (6) top Upper Eocene sequence, (7) top Lower Oligocene sequence, (8) top Upper Oligocene sequence, (9) top Lower Miocene sequence. Note that all faults are of extensional type and mostly downthrown in the direction of the basin (after El-Shari, 2004).

seismic velocities have been edited to exclude unrealistic values, and adjusted to tie with well information.

After the final calibration of both average and interval seismic reflection velocities, velocity maps have been constructed. The interval velocity and its changes, related to stratigraphy and lithology of the particular section, are of great value in the geological interpretation. Using the calibrated average velocity, a depth map for each depositional sequence has been constructed for the area of study.

VELOCITY DETERMINATION

Observation of lithologic well logs in the study area indicates that the subsurface geology, and hence, velocity distribution, of most sedimentary sections, is likely to be complex. Rapid variations of physical properties with depth characterise the sedimentary succession. In addition to heterogeneity within layers of similar material, the interfaces separating the layers are frequently discontinuous, due to faulting and unconformity.

Generally, there are only two sources of subsurface velocity information: wells and seismic data. Borehole check shots and sonic log provide reliable measurements of the vertical velocity-depth function local to the well bore, and also precise details of the velocity variation within any chosen interval. However, the spatial distribution of wells is usually insufficient to constrain the lateral variations of velocity that must be defined over a prospect. In contrast, the seismic reflection data generally provide coverage across both high and low areas. The seismic reflection data give reliable estimates of subsurface velocities if the velocity layering, and hence the geological structure, is exactly horizontal.

However, for this research, an accurate method of velocity-determination that will improve the interpretation of the seismic reflection data is desired. The velocity is also used for the conversion of seismic travel times to depths and for computation and mapping of interval velocities, which are important indicators of subsurface lithology. Since the investigated area is assumed to be located on a hinge-line, sediments have been deposited in different environments and thus a change in lithology in both vertical and horizontal directions is expected. In such a situation, an assumption of constant velocity would not be valid, since rapid changes in velocity from one point to another may occur. Therefore, determination of the true velocity functions in the area is an important task.

COMPARISON OF VELOCITIES FROM THREE DATA SOURCES

The comparison of the velocities derived from the seismic reflection data and those derived from sonic logging and well velocity surveys in the boreholes is carried out in this section. Many authors have noted the differences between travel times (and associated velocities) derived from the sonic log and well velocity surveys, either using the check-shot technique or the vertical seismic profile (VSP) (*e.g.* O'Brien and Lucas, 1971; Stewart *et al.,* 1984; De *et al*., 1994).

The sonic logs provide comprehensive velocity information of the subsurface, measuring the transit time over very small intervals of the geological column. It is common, however, to have errors in travel times (and thus errors in the derived velocities) because of the instrument problems, borehole conditions and. In addition, the determination of sonic velocity in carbonates commonly shows less accuracy due to the development of vuggy porosity, caused by irregular dissolution of grains and rocks in limestones and dolomites.

However, the well velocity survey is characterised by the measurement of the direct travel time of seismic signal from source to receiver through the ground, which enables the tool to measure travel time accurately. The well velocity survey, therefore, is considered the most reliable source of vertical velocities measured within the borehole. In this study, the well velocity survey was used to improve the accuracy of the initial velocity functions.

Every tool has some degree of reliability for travel time measurements and, of course, their associated derived velocities. The main reason for the observed differences between the sonic log and the well velocity survey, is that the sonic logging tool uses an ultra-sonic source of high frequency of 15-20 khz, propagating very short distances (several feet) along a path adjacent to the borehole. In contrast, the well velocity survey uses a seismic source of low frequency of 50-100 hz, which may be offset several hundred feet from the wellhead. O'Brien and Lucas (1971), Stewart *et al*. (1984) and De *et al*. (1994), conclude that frequency dependent dispersion is the main contributing factor to observed discrepancies between the sonic logs and well velocity surveys. In addition, the propagation path of the well velocity survey samples the ground many tens of feet from

the borehole, whereas, the sonic log samples the material close to the borehole wall only. However, the amount of the velocity data obtained from the surface seismic survey is relatively large compared with other *in situ* velocity measurements. It has a lower cost than well velocity surveys and sonic logging, and provides data coverage over large areas, but it has been shown that the seismic velocities derived by normal move out velocity methods do not always measure the same physical parameters as well as survey velocities (*e.g.* Al-Chalabi, 1979; Levin, 1978; Lindseth, 1982).

The comparison curves of the two-way times, calculated from each source versus depth, are displayed in Figure 5. The depth values in the seismic reflection data are estimated using average velocity, which is calculated from the stacking velocity at each well. Constant stacking velocity was assumed in the

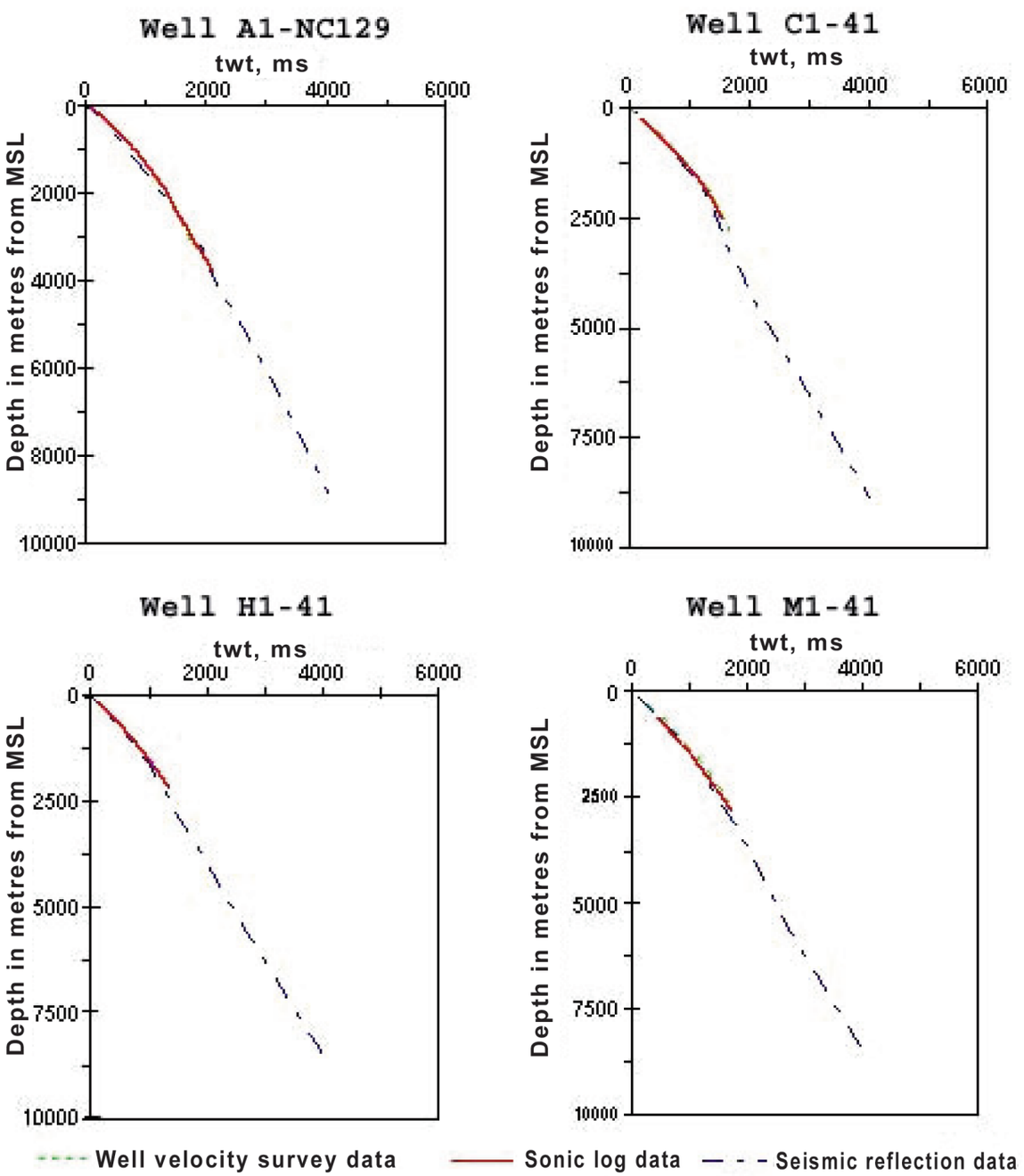


Fig. 5. Comparison of two-way travel times derived from three sources data; seismic reflection profiles, sonic logs and well velocity surveys.

deeper parts of all seismic profiles. The plots show a systematic difference between the two-way travel times obtained from seismic reflection data and those obtained from the sonic logs and well velocity surveys. In all wells, the two-way travel times measured from the seismic reflected data are slightly but systematically shorter than those measured from the other two sources. Most wells display good agreement of the measured two-way travel times from the well velocity surveys and sonic logs. A diversion between the three curves is noticed at depths of about 2000 meters, and clearly increases with depth. However, the resolution of the seismic reflection data decreases as depth increases, making the seismic reflection data less reliable.

Figure 6 shows comparison plots between velocity data derived from the three data sets. The resulting comparison indicates the well survey velocities are systematically lower than the sonic log velocities at most depths. The difference between the sonic log average velocities and well survey velocities range between +16 and -7 percent, with an average of +2.3

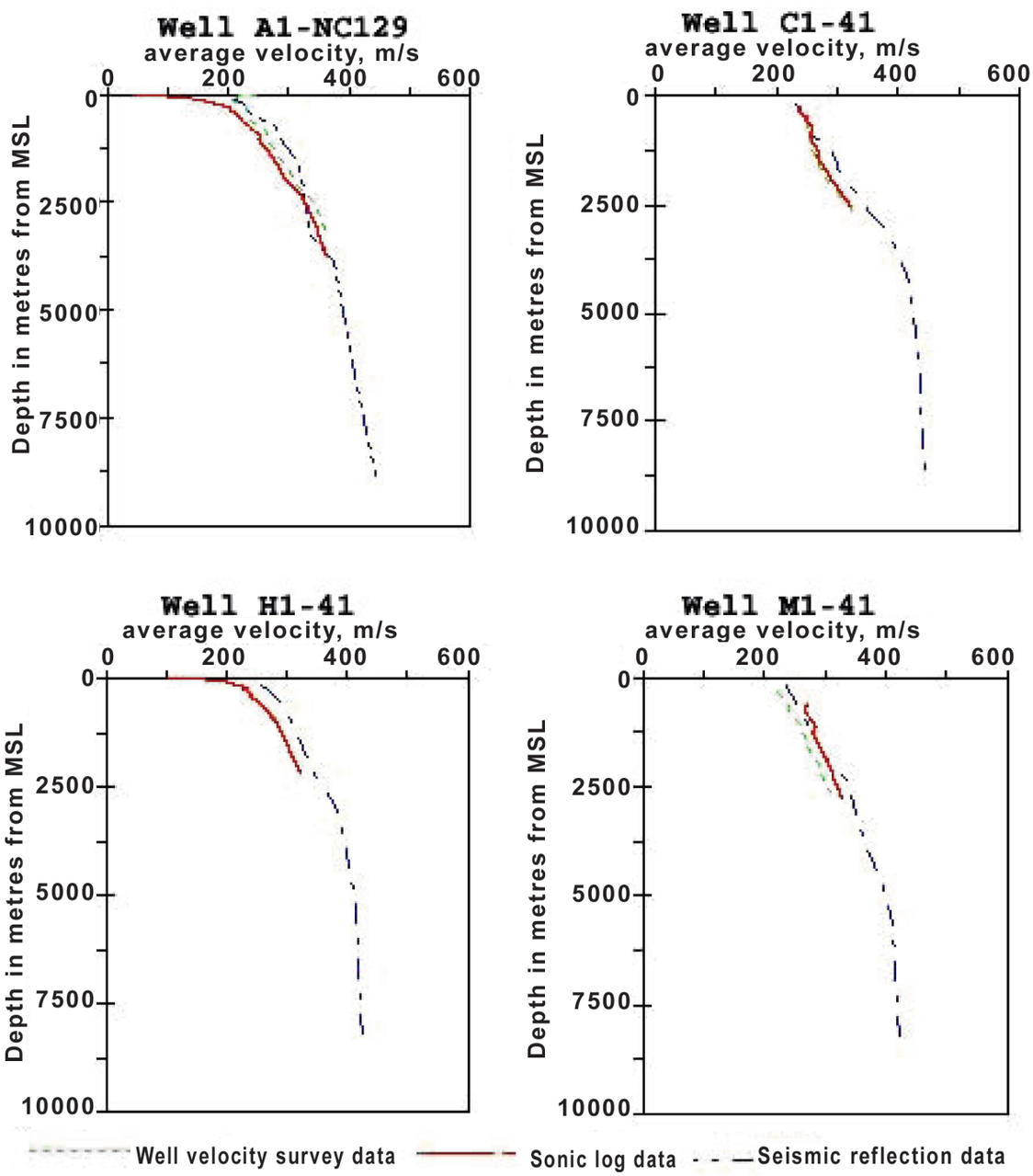


Fig. 6. Comparison of average velocity derived from three sources data; seismic reflection profiles, sonic logging, and well velocity surveys.

percent. This positive drift is consistent with normal dispersion in which the higher frequency waves travel at higher velocities. On the contrary, De *et al*. (1994) concluded that the velocity differences between well velocity surveys and sonic surveys range from +16 to -5 percent, with an average of +6.9 percent. The seismic reflection velocity in this analysis is found higher than the velocity derived from the well velocity surveys and sonic logging in most of the wells. In fact, the true velocity distribution can never be fully recovered by the surface seismic reflection method, due to practical limitations on the resolution of velocity information.

SEISMIC VELOCITY

Interpretation

The average and interval seismic reflection velocities versus two-way time, in the form of seismic section display, have been plotted for preliminary interpretation of the velocity distribution in the study area. The average velocities and the interval velocities were calculated using Dix's equation and are represented in a series of iso-velocity plots.

Figure 7 shows plots of iso-(average seismic reflection velocity) as a function of two-way travel time for selected dip seismic profiles located in the southern part of the area. In these plots, increasing average velocity with depth has been observed. Generally, the average velocity plots are smooth and represent a reasonable correlation with a geological expectation of the subsurface structure. The shallow depths show uniform average velocity distribution. At greater depths, the plots show denser contour lines indicating abrupt changes in velocity. Velocity variation between the platform and the basin is interpreted as arising from changes in lithology between the two areas. The low average velocity at the basinward end of the dip profiles may be correlated with increasing shale percentage towards the deep basin.

Figure 8 shows iso-interval velocity plots of selected dip and strike profiles and their corresponding reflection time. Generally, these

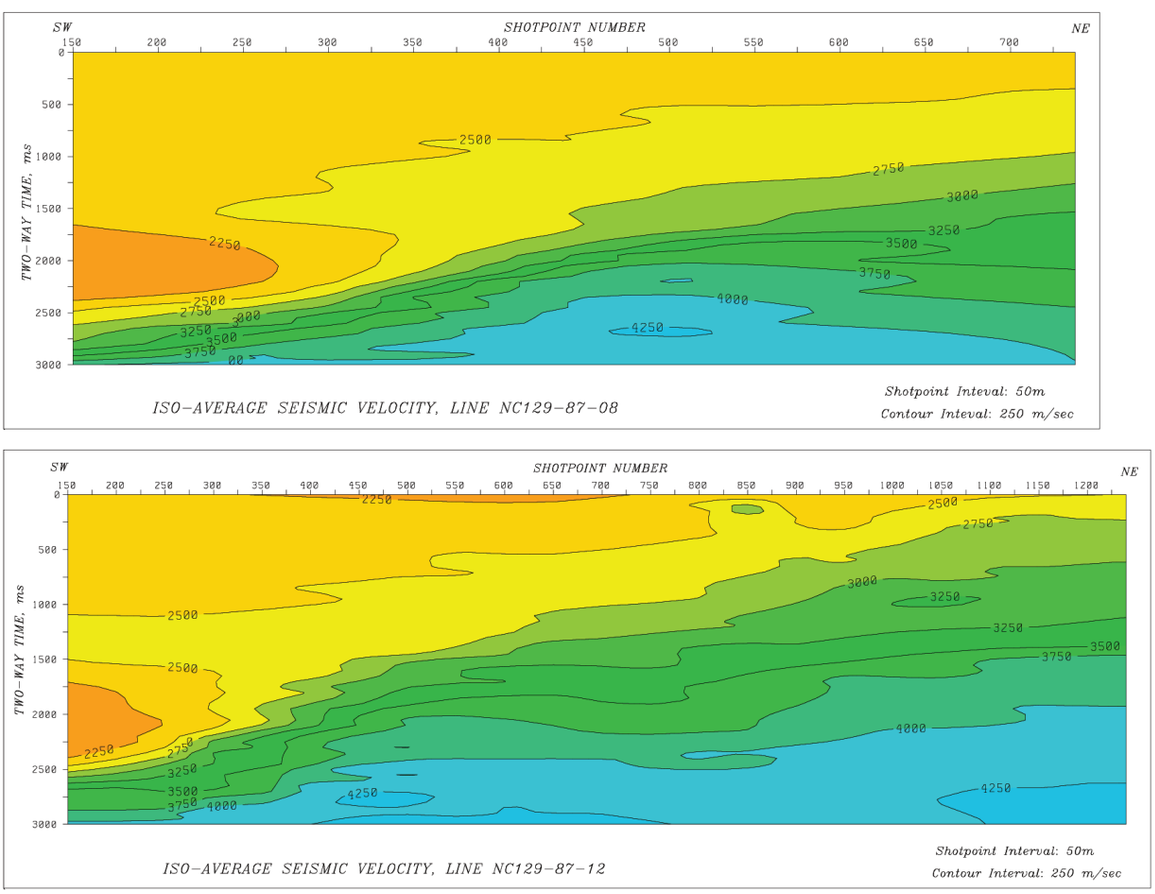


Fig. 7. The iso-average seismic reflection velocity for lines NC129-87-8 and NC129-87-12 (dip lines in the southern part of the area). For lines location see Figure 3.

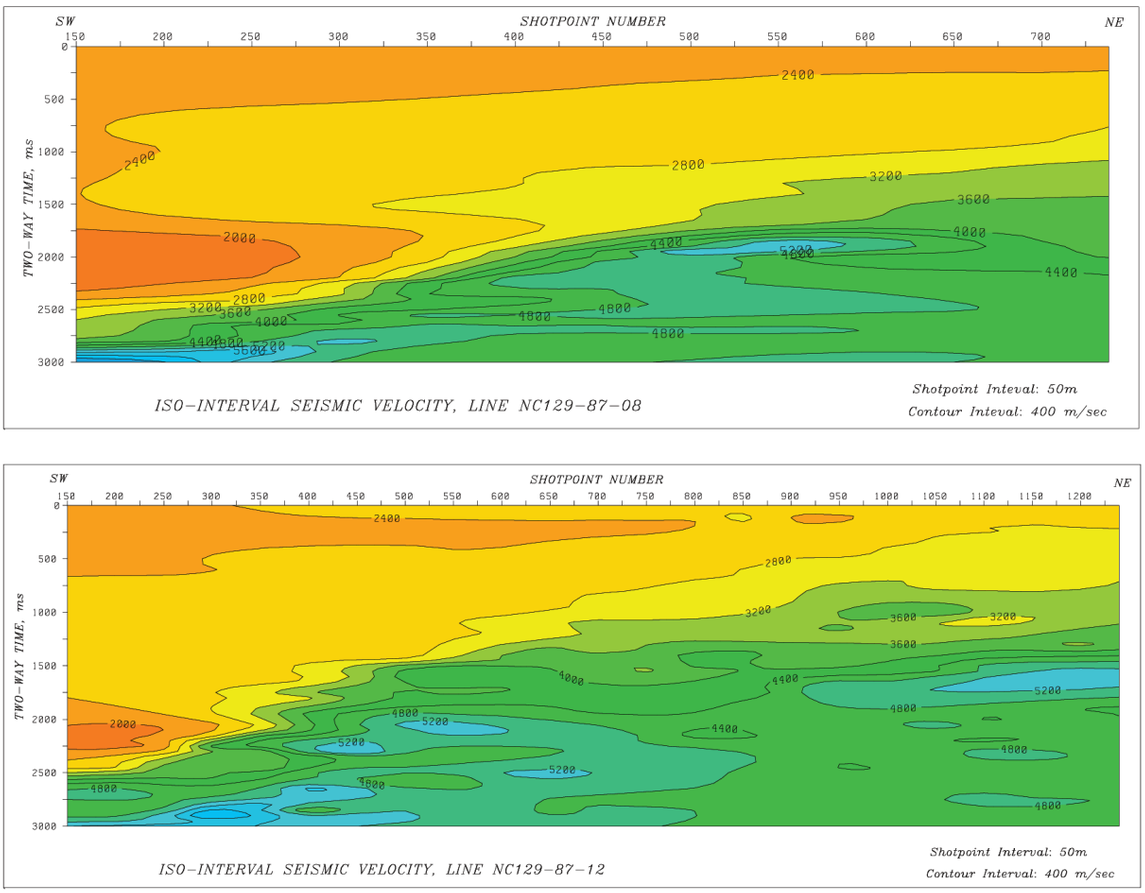


Fig. 8. The iso-interval seismic reflection velocity for lines NC129-87-8 and NC129-87-12 (dip lines in the southern part of the area). For lines location see Figure 3.

contour plots capture the important large-scale velocity behaviour. Lateral variation in the velocity distribution has been observed along these profiles. These velocity anomalies reflect geological conditions related to structural elements and sediment distribution during the Late Cretaceous and Tertiary.

The upper parts of the sections show a uniform increase of interval velocity, consistent with the dip of the section, to a depth of approximately 1.5 sec TWT. Deeper, the interval velocity represents high lateral variations, especially towards the southwest direction. The velocity variation is seen if we compare the right hand side (NE directions) of the dip profiles, NC129-87-8 and NC129-87-12, with the left hand side (SW directions) of the same profiles (Fig. 8). Increasing lithology variation toward the area of a hinge-line is a possible explanation for this lateral interval velocity variation. The relatively highly faulted area may also contribute to these velocity differences. In addition, the development of these faults may affect the depositional environment, which in turn affects the lithology variations of the sediments in those areas. These faults alone, may have an affect on the seismic velocity in those areas.

Velocity Calibration

Determination of velocities from well survey methods is important, since they give the only true check on the precision of the same velocities derived from other sources. Any mature exploration area shows that wells tend to be concentrated in clusters around hydrocarbon discoveries. Also, because hydrocarbons migrate updip, and accumulate towards the climax of the prospect, the locations of the wells tend to be concentrated towards the structural highs. Since few wells have been drilled in structural lows, this drilling represents a significant influence in the sampling of seismic velocities. Also, the structural highs are commonly characterised by apparent thin or missing geological sections. This, commonly combined with large lithological variation from structural highs to lows, contributes to make the

estimation of velocities away from well control a slightly uncertain operation.

The final step in this velocity analysis is to compute an accurate velocity function for the entire study area. The well velocity survey is used to calibrate the initial seismic reflection velocity. It is often very useful to calibrate the velocity field, estimated from exploration seismic data, with the other well velocity sources. However, this method depends on the degree of velocity variation, the amount of well control, and the quality and density of velocity information from seismic data. The seismic reflection velocities have been calibrated using velocities derived from the well data to remove unrealistic variations. The idea of calibration is based on calculated velocity values from a number of widely separated wells, which are averaged and then used to correct the seismic reflection velocities.

VELOCITY MAPPING

In sedimentary rocks, the *P*-wave velocity is dependent upon the wave velocity in the rock matrix, the porosity and the velocity in the fluid filling the pore spaces. Also, the velocity depends on the strength of rock, which reflects the consolidation and sedimentation, both of which tend to increase with age and depth of burial. The rock density generally increases while porosity decreases with burial. In general, the lithology, porosity and depth of burial are considered the most prominent factors affecting the velocity of sediments.

In the Soluq Depression, an interpretation of the seismic information has been made, and well information has been used to correlate seismic reflection horizons with stratigraphy and to estimate the gross interval velocities between horizons. Information from lithologic well logs indicate that the subsurface geology, and hence velocity distribution, of most sedimentary sections is likely to be complex. From the well information, it is recognised that the sedimentary column of the area is composed mostly of an alternation of limestone, shale, and dolomites (Fig. 2).

Average Velocity Maps

The average velocity is usually given as a function of depth and can be considered as a vertical variation in velocity. The average velocity maps have been constructed for the sequences from the top of the Upper Cretaceous sequence to the top of the Lower Miocene sequence which is the shallowest horizon boundary identified in this study. In the average velocity maps, increasing velocity with depth has been observed. The compaction process, and consequent loss of porosity, is the primary cause for the increase of velocity with depth. The significant difference in the average velocity of individual sequences mostly occurs between the area toward the deep basin and the platform.

Figure 9a displays the average velocity above the top of Upper Cretaceous sequence. In general, the contour pattern in this map shows some irregularity in the velocity distribution. The complexity of the velocity at this level may be attributed to the decrease in quality of velocity data. In the lower depositional sequences (the Palaeocene sequence and the Lower Eocene sequence), the average velocity distribution is generally unsystematic (Figs. 9b and 9c). However, a general increase of velocity has been observed towards the southwest, consistent with an increasing depth of burial towards the basin. The Middle Eocene sequence and all overlying sequences are characterised by increased velocity towards the east and southeast (Fig. 9d). Limestones and shales are the predominant lithologies in these sequences, with a considerable increase in shale percentage, towards the deep basin. The increased shale percentage towards west and southwest is the most reasonable explanation of decreasing velocity towards that direction.

Interval Velocity Maps

The interval velocity maps represent the pattern of velocity variation within the sequences and reflect the controlling variables of lithological variation and depth of burial. Particular details of velocity structure and an investigation of the lateral velocity variation provide parameters such as depositional environment, source area location, burial history, structural style and structural position. In general faults cause discontinuities in the interval velocity data. The interval velocity maps are constructed for the entire Tertiary sedimentary succession in the Soluq Depression.

The Palaeocene Sequence

Figure 10a shows contour plotting of the interval velocity within the Palaeocene sequence. The contour patterns generally have an irregularity in their

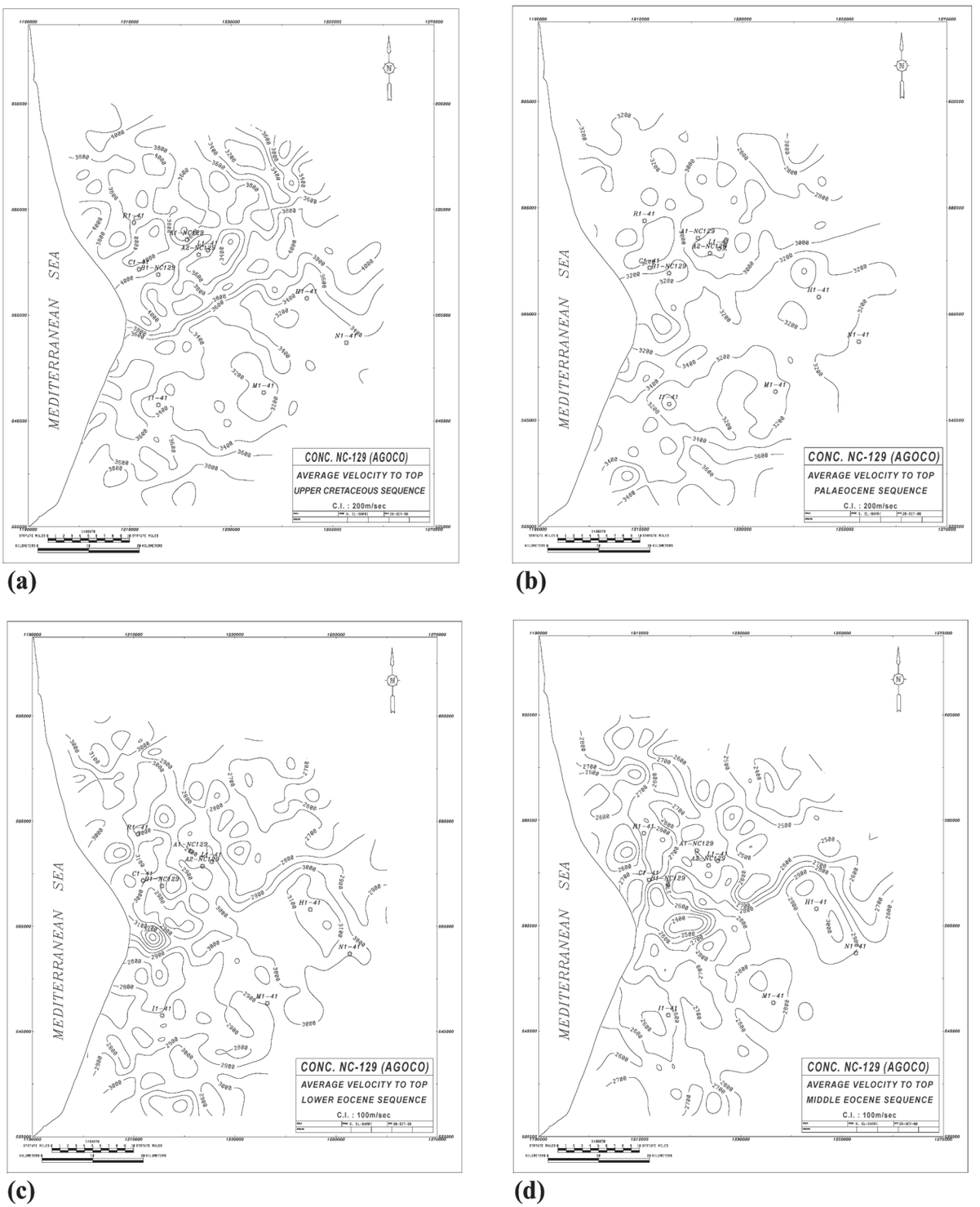


Fig. 9. Average velocity contour map to top of; a) Upper Cretaceous (b) Palaeocene, (c) Lower Eocene, and (d) Middle Eocene sequences.

measurement in that area. However, the lateral velocity variation in the Lower Eocene sequence is interpreted as controlled by sedimentary facies variation, and the effect of the fault structures. The variation of depth of burial throughout the sequence may also effect the interval velocity distribution.

The Middle Eocene Sequence

The interval velocity distribution within the Middle Eocene sequence (Fig.10c) shows a different appearance from that of the previous sequences (The Palaeocene sequence and the

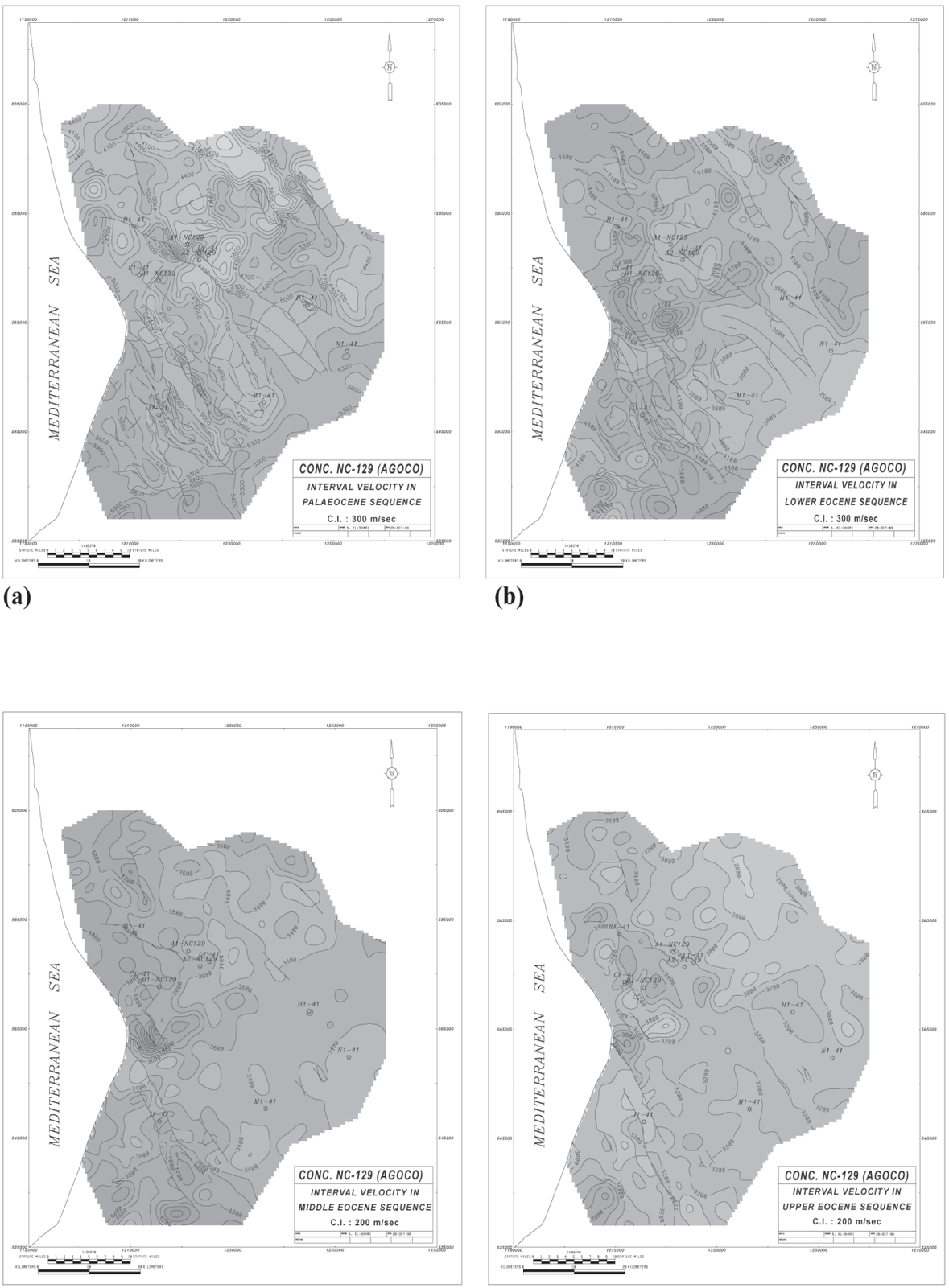
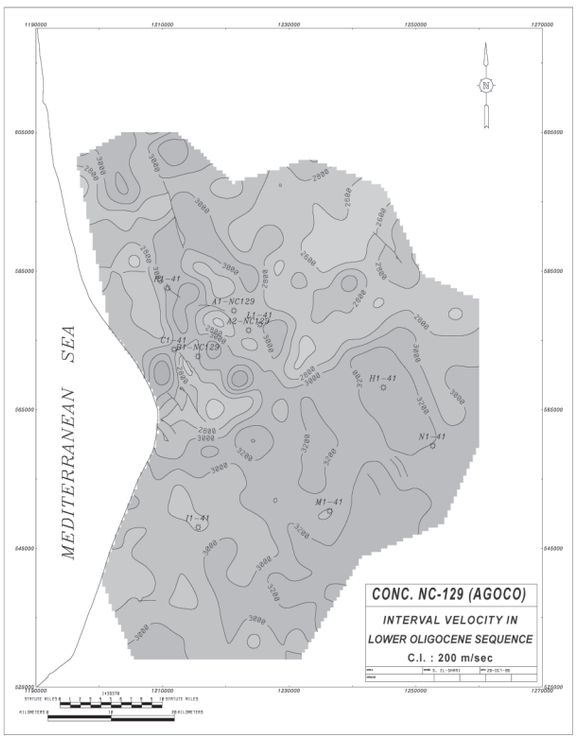
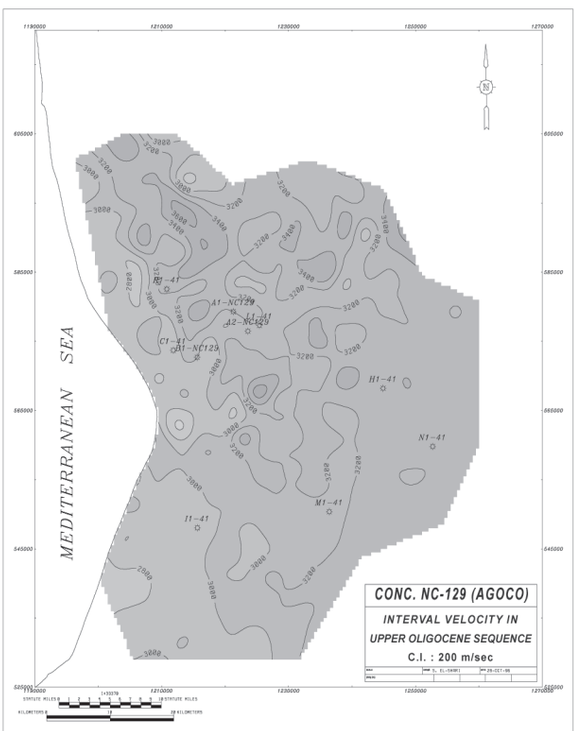


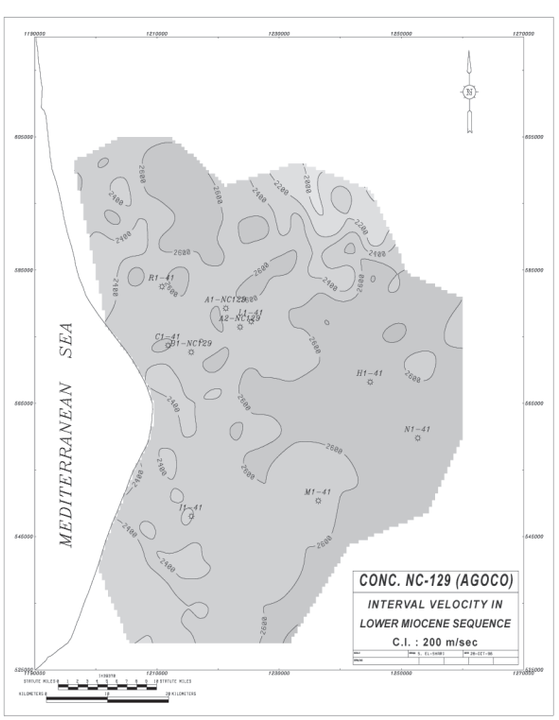
Fig. 10. Interval velocity contour map within the depositional sequences in the Soluq Depression; (a) the Palaeocene, (b) the Lower Eocene, (c) the Middle Eocene, (d) the Upper Eocene.



(e)



(f)



(g)

Fig. 10. Interval velocity contour map within the depositional sequences in the Soluq Depression; (e) the Lower Oligocene, (f) the Upper Oligocene, and (g) the Lower Miocene.

Lower Eocene sequence). The contour pattern in this map shows wider contour line spacing over most of the area, which indicates some uniformity in velocity distribution. The interval velocity in the northern and eastern areas only ranges between 3400 and 3600 m/sec. However, the faulted areas around and northwest of well I1-4 show relatively dense contours, which suggest a sudden change in interval velocity within the sequence occurring in these areas. The maximum interval velocity in the faulted areas reaches a value of about 4200 m/sec.

The Middle Eocene sequence is composed of relatively uniform lithology throughout the area (Fig. 2). The well information of M1-41, N1-41, H1-41 and C1-41 shows that argillaceous limestone, interbedded occasionally with shale beds, is the dominant lithology. The map shows increasing velocity towards the west and southwest. Generally, the velocity increase gradually, but have relatively steep gradients where the shelf margin is present at the area of well I1-41. Based on well data, the increasing velocity trend may be consistent with an increase of relatively dense carbonates towards the basin. The sequence depth of burial increases toward the southwest and is more significant beyond the shelf margin area, which accounts for increasing interval

velocity toward the southwest where porosity reduction and compaction might be expected with increasing depth.

The Upper Eocene Sequence

Figure 10d is a contour plot of the interval velocity within the Upper Eocene sequence. The velocity in this map is in the ranges from 3000 to 3400 m/sec. Well data in the Soluq Depression shows lateral lithofacies changes in the sequence. It mainly consists of argillaceous limestones interbedded with shales. Lithological logs from wells located in the northwestern (A1-NC129, B1-NC129 and C1-41) show that chalky and argillaceous limestones are the common rock types. The limestone interbeds with shale in the western and southern wells (N1-41 and H1-41). In general, the velocity gradually increases towards the west. The areas towards the basin show relatively close contour patterns, indicating sudden changes in the distribution of the interval velocity within the sequence.

The Lower Oligocene Sequence

The interval velocity distribution in the Lower Oligocene sequence is shown in Figure 10e. The velocity contours in this map show some irregularity, especially in the northwestern area, which reflects some lateral interval velocity variation. Velocity in the range is 3000 - 3200 m/sec is the most dominant. Lower velocity values are encountered in the western and northeastern parts of the area, where slightly increasing velocity generally marks the sequence southeastwards. The well information shows that the Lower Oligocene sequence represents lateral changes in lithofacies throughout the Soluq Depression. Limestone and shale interbedded with some marl beds are the predominant lithologies in the sequence. A thick shale sequence was deposited in the west and southwest, while interbedded shales and carbonates were deposited in the east. There are only a few normal faults of NW-SE orientation marked on the map. However, these faults appear to be without any significant affect on the interval velocity distribution. Therefore velocity distribution within the sequence may be controlled by the lateral lithological variation.

The Upper Oligocene Sequence

Figure 10f shows the interval velocity map of the Upper Oligocene sequence. The map of this sequence shows a different appearance from that of the previous sequences. The contour patterns in this map generally display a uniform velocity distribution within the sequence. The dominant interval velocity range is 3000- 3200 m/sec. The general increasing velocity trend is toward the east. The well data shows limestone interbedded with some beds of shale and marl as the predominant lithology in the sequence (Fig. 2). Dolomitic limestone and anhydrite beds occasionally occur within the sequence. In southern areas, the lithology of the sequence is mainly fossiliferous limestone interbedded with shale (wells; I1-41, M1-41, N1-41 and H1-41). The dolomitic limestone and anhydrite percentage increases in the eastern wells. In the northern areas, fossiliferous limestone interbedded with marls is the predominant rock type. This lithology variation may be correlated with the interval velocity distribution in the sequence. No fault structures appear in this level, and the lithology may be the main cause of velocity variation.

The Lower Miocene Sequence

The interval velocity within the Lower Miocene sequence is displayed in the contour map of Figure 10g. On this map, no significant sudden change in interval velocity marked the horizon, and consistent lateral variation in velocity distribution can be seen. The well data shows the Lower Miocene sequence is mainly composed of shale and argillaceous limestone throughout the basin**.** The shale is the predominant lithology in the lower part of the sequence and fossiliferous limestone interbedded with some intervals of shales appears in the middle part. In the upper part, the lithology of this unit is primarily shale with some argillaceous limestone. The shale percentage increases towards the west and southwest. The interval velocity distribution largely reflects the gradual lithological variation within the sequence. The velocity in the sequence is generally consistent with the shale-increasing trend.

Time to Depth Conversion

One of the significant results in this project is to determine reliable depths to the top of each depositional sequence in the Soluq Depression. The time to depth conversion in this research was carried out using velocities derived from surface seismic data calibrated by well velocity data. Time to depth conversion for complicated geological models

including laterally variable velocities and reflector structure strictly requires more accurate velocity consideration. The calibrated average velocities together with the two-way travel times, to the top of each depositional sequence, have been used to calculate the depths of these sequences.

Depth Map of Upper Cretaceous Sequence

Figure 11a shows the depth contour map of the Upper Cretaceous depositional sequence. In general, the depth gradually increases towards the southwest. Close contour spacing in the map, which is concentrated west of well I1-41, indicates a sudden increase in sequence depth at the shelf margin. The general trend of normal faults dissecting the Upper Cretaceous sequence is NW-SE. Differential subsidence across the hinge-line between the Sirt Basin and Cyrenaica Platform, together with the effect of the fault displacement, are the main reasons for the sudden increase in depth towards the deep basin. The Upper Cretaceous sequence in the Soluq Depression is only penetrated in wells A1-NC129, I1-41 and M1-41. The comparison of the sequence depths in these wells with the constructed depth map shows misties especially in well I1-41. However, this disagreement is expected at this level due to the following reasons:

(a) The Upper Cretaceous Sequence is the most intensively faulted horizon. These faults have a detrimental effect on the accuracy of both picking horizon times and velocity measurements.

(b) The decreasing seismic resolution with depth affects the precise picking of the horizon time on the seismic profile.

(c) Lower accuracy of seismic reflection velocity estimation with increasing travel time.

(d) Less control points for seismic velocity calibration as the horizon is only penetrated in a few wells.

Depth Maps of Palaeocene, Lower Eocene and Middle Eocene Sequences

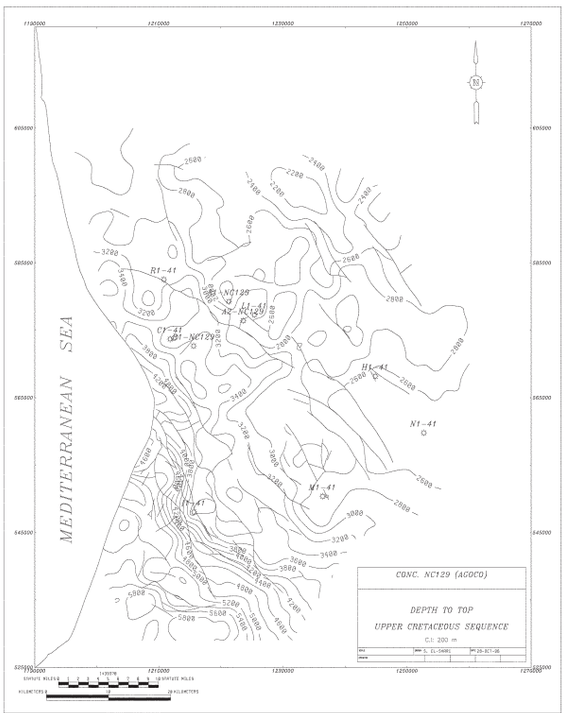
The depth maps of these sequences are shown in Figures 11b, 11c and 11d respectively. In general these maps show slightly increasing depth generally marks the sequences southwestwards. An exception is the shelf margin at well I1-41, where sudden increases in depth are observed. The sequences are intensively dissected by many normal faults dipping mainly southwards. The main faults in the sequences appear to be concentrated in a belt roughly tending NW-SE, where some of them have a WNW-ESE trend. These faults may have an influence in the irregularity of the depth contours. Close contours on these maps are seen to the west of well I1-41, indicating a sudden increase of depth to the southwest. The location of the area on a hinge-line may be the main reason for the abrupt increase in depth towards the deep basin. Subsidence, which is expected to increase towards the deep basin, as well as the displacement of normal faults, may be the most plausible reasons for this change in the depth gradient towards the southwest. However, the shape of the contour pattern in the Middle Eocene sequence is more regular. This may be attributed to decreasing of the fault structures in this horizon compared with the underlying horizons.

Depth Maps of Upper Eocene, Lower Oligocene, Upper Oligocene and Lower Miocene Sequences

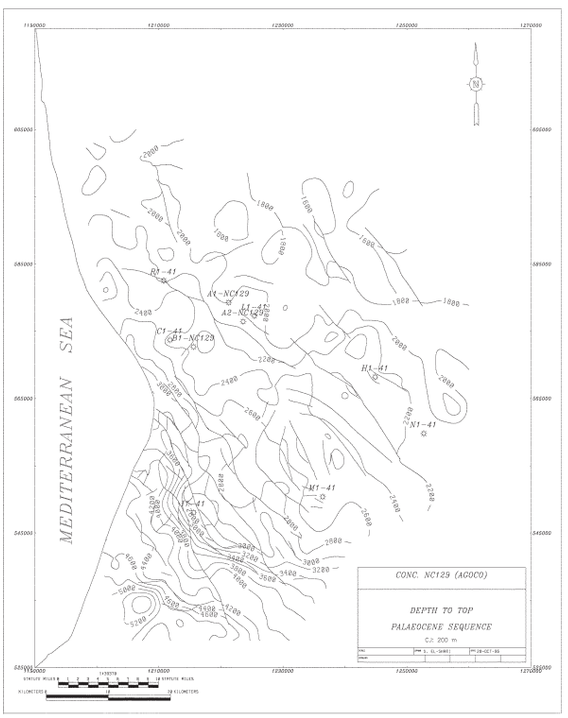
The depth structure maps of these depositional sequences are shown in Figures 11e, 11f, 11g and 11h respectively. In general, the contour pattern in these maps represent gradual and uniform increasing in depth of the sequences towards the southwest. A very gentle increase in depth has been observed up to the area of well I1-41. To the west of this well the contour line spacing indicates an abrupt increase in depth towards the deep basin. Here again the increasing depth gradient toward the southwest indicates increasing basin subsidence as we move southwestwards. Thermal subsidence of post-rift sequences in the basin is expected to be the main reason for the increasing depth gradient in this direction because there are no major effects of fault displacement in these sequences. However, the gradient of increasing depth southwestward in the Upper Oligocene and Lower Miocene sequences is obviously lower than the increasing depth gradient in the underlying sequences in the same trend. This may be interpreted as a decrease of the effect of the basin thermal subsidence with time.

CONCLUSIONS

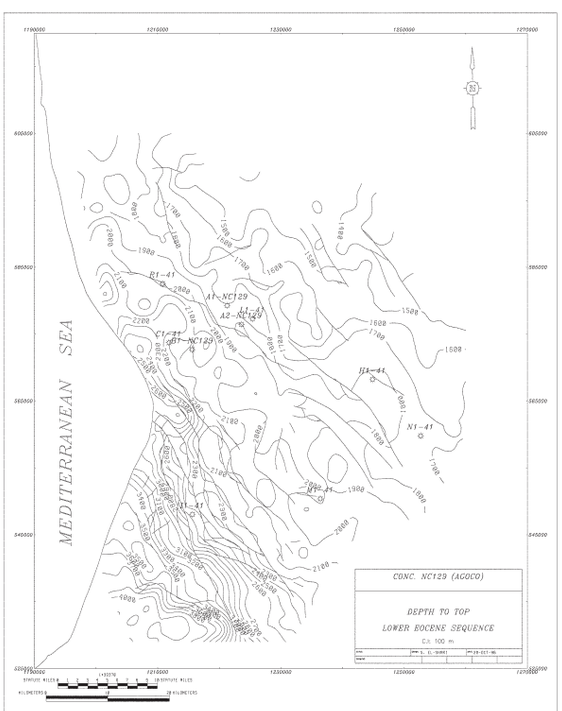
Analyses of true velocity variation are very useful for local stratigraphic interpretation and lithologic evaluation, and for conversion of time to depth for each sequence in the subsurface of the Soluq Depression. In order to satisfy these objectives, the velocity analysis done in this research was based on



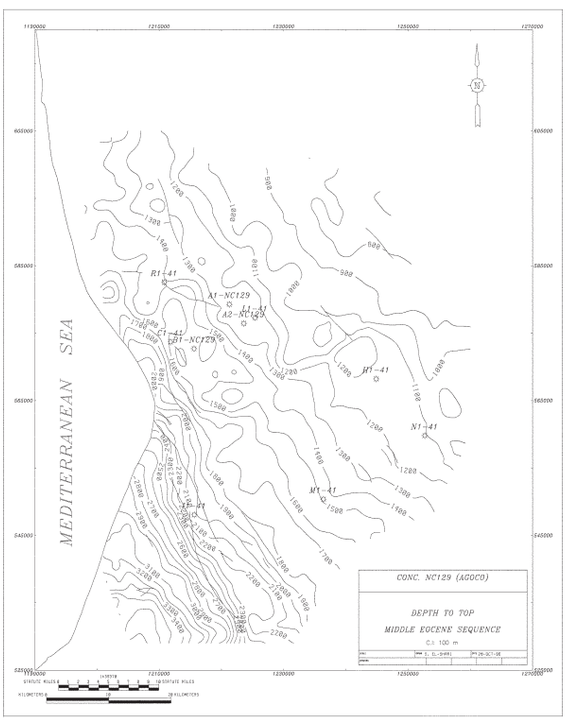
(a)



(b)

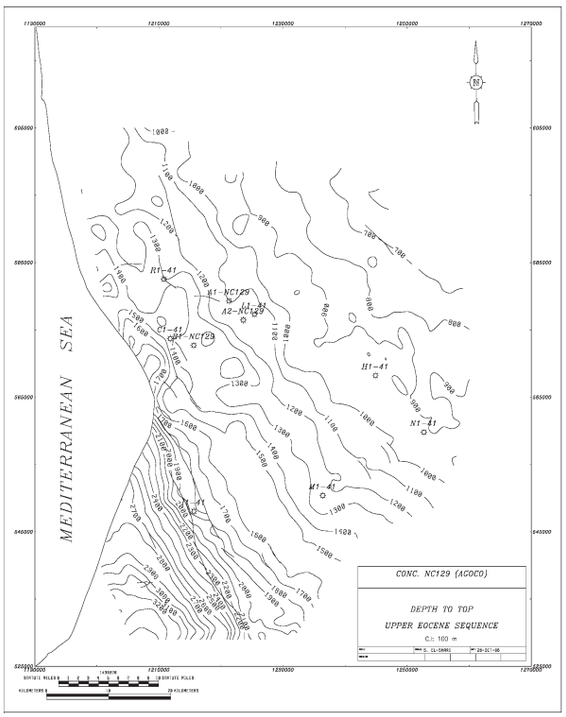


(c)

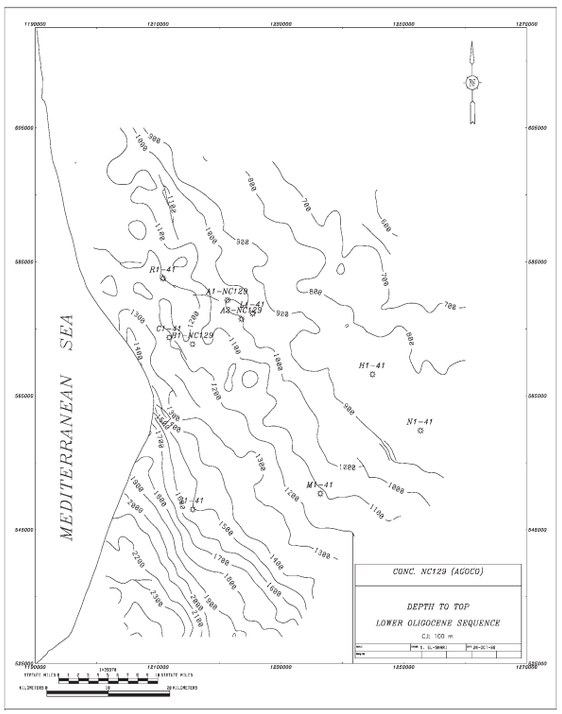


(d)

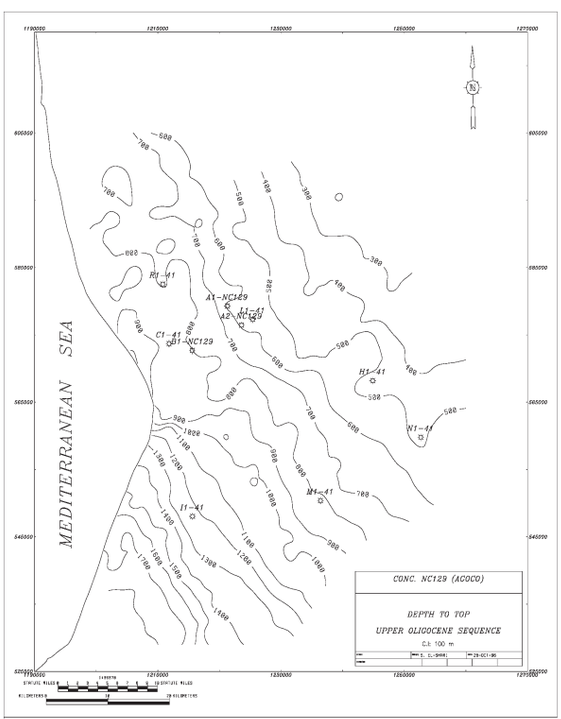
Fig. 11. Depth structural contour map of the depositional sequences in Soluq Depression; (a) top Upper Cretaceous (b) top Palaeocene, (c) top Lower Eocene, (d) top Middle Eocene.



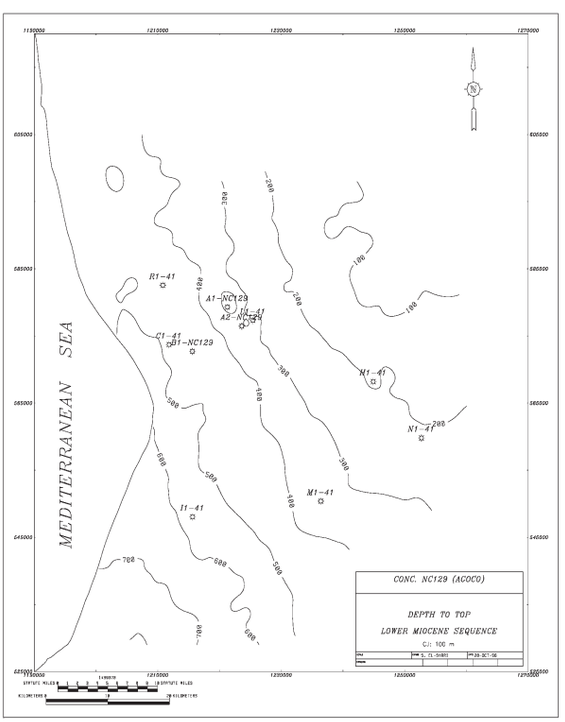
(e)



(f)



(g)



(h)

Fig. 11. Depth structural contour map of the depositional sequences in Soluq Depression; (e) top Upper Eocene, (f) top Lower Oligocene, (g) Upper Oligocene, and (h) top Lower Miocene.

velocities extracted from three data sources: well velocity surveys, sonic logs, and seismic reflection measurements. Contour plotting of the seismic reflection average velocities shows a general increasing velocity with depth, as expected with normal compaction.

The velocity comparison indicates that the seismic reflection data consistently shows a higher velocity than that measured from well data. The comparison also shows that the velocities derived from sonic logs were consistently higher than those from well surveys. To obtain a realistic velocity value, well data were used as a reference in a calibration operation to smooth the seismic reflection velocities. Seismic reflection velocity should not be used directly to infer true subsurface velocities for time to depth conversion if accuracy is important.

Between the deep basin and the platform areas, there are significant differences in the average velocity to the tops of most sequences. In general, increases of average velocity have been observed towards the southwest for the Palaeocene and Lower Eocene sequences. This is consistent with increasing depth of burial basinward. A decrease in velocity towards the west and southwest direction is characteristic of the Middle Eocene sequence, and all the overlying sequences. The most reasonable explanation of this trend is the increasing shale percentage in the same direction.

The patterns of velocity variation within the sequences are represented on the interval velocity maps, and reflect the controlling variables of lithological variation and depth of burial. Lateral changes in velocity have been observed in the Palaeocene and the Lower Eocene sequences. Determination of interval velocity is made more complicated here by the effect of faults on the accuracy of seismic velocity estimation and also, in some instances, the control of those faults on the lateral facies distribution. Transfer zones between these faults may act as conduits for local sediment transport in basin stratigraphy.

The interval velocity maps generally display relatively less irregularity in velocity distribution in the Middle Eocene and Upper Eocene sequences. The main factors affecting velocity distribution are variations of both lithology and depth of burial. For the Lower Oligocene sequence and above, the interval velocity maps generally display uniform velocity distribution, decreasing towards the southwest. The lateral lithofacies variation largely controls the velocity distributions in these sequences. The main reason for velocity decreasing towards the southwest direction is the deposition of thick sequences of shale in the same direction.

The final results of the depth conversion are depth maps with perfect well ties, and with reasonable depth estimates away from wells. All of the depositional sequences display surfaces dipping towards the southwest (basin direction). In the southwest, the dip gradient is much steeper. Fault displacement and thermal relaxation in the post-rift period are two main reasons for gradients towards the centre of the basin. The development of a hinge-line between the Cyrenaica Platform and the Sirt Basin may explain why the increase in dip is more significant beyond the area of the shelf-slope break. The increasing gradient toward the southwest may be due to increasing thermal subsidence in the post-rift period towards the deep basin, compared with the platform.

ACKNOWLEDGEMENTS

First, I must express my great thanks to Allah, who enabled me to complete this work and my countless thanks to him will never be sufficient. I would like to express my gratitude to Dr Roger Scrutton of Edinburgh University, for his help and suggestions during all stages of this research. Special thanks are due to Mr. Abdu-Elhamed Shahlol of AGOCO, for his encouragement and enormous helping during the early stages of this research. Thanks are also expressed to AGOCO, for kindly releasing confidential data, on which the work has been based.

REFERENCES

Al-Chalabi, M., 1974. An analysis of stacking, rms, average, and interval velocities of horizontally layered ground. *Geophysics. Prosp.,* **22**, 458-475.

Al-Chalabi, M., 1979. Velocity determination from seismic reflection data. *In:* A. A. Fitch (*ed*.), *Developments in Geophysical Exploration Method*, **1**, 1-68.

Anketell, J. M. and Ghellali, S. M., 1991. A palaeogeographic map of the Pre-Tertiary surface in the region of the Jifarah plain and its implication to the structural history of northern Libya. *In:* M. J. Salem, A. M. Sbeta, and M. R. Bakbak, (*eds.*). *The Geology of Libya,* Elsevier, **6**. 2407-2416.

Banik, N. C., 1984. Velocity anisotropy of shales and depth estimation in the North Sea basin. *Geophysics*, **49**.1411-1419.

Barr, F. T., 1972. Cretaceous stratigraphy and planktonic foraminifera of Libya. *Palaeont*., **18**.1-46.

Berggren, W. A., 1969. Biostratigraphy and planktonic foraminifera zonation of the Tertiary system of the Sirte Basin of Libya. North Africa. *In*: P. Bornnimann and H. H. Renzi (*eds.*). *Proc. 1st Int. Conf. Plank. Microfossils*, **1**, 104-120.

Berggren, W. A., 1974. Palaeocene benthonic foraminiferal biostratigraphy, biogeography and palaeoecology of Libya and Mali. *Micropalaeontology.* **20**, 449-465.

Burke, K. and Dewey, J. F., 1974. Two plates in Africa during the Cretaceous?. *Nature*, **249**,313-316.

De, G. S., Winterstein, D F. and Meadows, M. A., 1994. Comparison of P- and S-wave velocities and Q's from VSP and sonic log data. *Geophysics,* **59**, 1512-1529.

Dobrin, M. B. and Savit, C. H., 1988. *Introduction to Geophysical Prospecting* (Forth Edition). McGraw-Hill book company.

El-Arnauti, A. and Shelmani, M., 1985. Stratigraphic and structure setting. *In*: B. Thusu and B. Owens (*eds*.), Palynostratigraphy of Northeast Libya. *J. Micropalaeontology*, **4**, 1-10.

El-Shari, S. M., 2004. Stratigraphic effects and tectonic implications at hinge-zone area between Sirte Basin and Cyrenaica Platform, NE Libya. *G*eology of East Libya, *Sedimentary Basins of Libya,* Third Symposium (abstract).

Levin, F. K., 1978. The reflection, refraction and diffraction of waves in media with an elliptical velocity dependence. *Geophysics*, **46,** 528-537.

Lindseth, R. O., 1982. *Digital Processing of Geophysical Data, a Review,* Continuing Education Program, Society of Exploration Geophysics, Tulsa, 278p.

O'Brien, P. N. S. and Lucas, A. L., 1971. Velocity dispersion of seismic waves. *Geophysical Prospecting*, **19**, 1-26.

Peikert, E. W., 1985. Stratigraphic velocity interpretation; national petroleum reserve-Alaska. *In*: O. R. Berg and D. G. Woolverton (*eds*.), Seismic stratigraphy II: An integrated approach to hydrocarbon exploration. *Am. Assoc. Petrol. Geol. Memoir* **39**, 209-222.

Rohlich, P., 1974. Geological Map of Libya. 1:250000 Sheet NI 34-15, *Al-Bayda Explanatory Booklet*. Ind. Res. Cent. Tripoli, 70p.

Sheriff R. E. and Geldart L. P., 1995. *Exploration Seismology* (Second Edition). Cambridge. 592p.

Sola, M. and Ozcick, B., 1990. On the hydrocarbon prospectivity of the north Cyrenaica region, Libya. *Petrol. Res. J*., **2**, 25-41.

Stewart, R. R., Huddleston P. D. and Kan K. K., 1984. Seismic versus sonic velocities: A vertical seismic profiling study. *Geophysics*, **49**(8), 1153-1168.

Van Houten, F. B., 1983. Sirte Basin, north central Libya; Cretaceous rifting above a fixed mantle hotspot?. *Geology*, **11**, 115-118.

Yanilmaz, E.; Ahmed S. and Amsaad, I., 1989. *Regional Geology of Cyrenaica* (*Northeast Libya*). Internal report, AGOCO, Exploration Department.

Petroleum Res. J. Vol. 20 (2007); P. 21–34, 13 Figs.

An Evaluation of the Waha Limestone South Al Jabal Field, Sirt Basin

Ali M. Massoud Elmesmari*

تقييم الحجر الجيري (الواحة) جنوب حقل الجبل

علي م. مسعود المسماري

تأخذ بنية حقل الجبل الحالية تركيبة محدبة في اتجاه الشمال الشرقي-الجنوب الغربي، وهي بارزة المظهر نتيجة حدوث ارتفاع طبوغرافي في عصر ما قبل الكريتاسي الذي تم تحويره لاحقا بواسطة التصدع والتعرية والترسيب المتقدم إبان عصر الكريتاسي وبواسطة التصدع أثناء عصريْ الباليوسين والأيوسين، وهناك صدع كبير يحاذي هذا التركيب من جهة الغرب ويفصل بين غور الحفة ومرتفع زلطن، كما يوجد صدعان آخران صغيران يميلان بعيدا عن الصدع الرئيسي ويقطعان التركيب البنيوي ومن المحتمل أن يغلقا التركيبة المحدبة للحقل من الغرب إلى الشمال الغربي.

يعتبر حجر الواحة الجيري التابع للكريتاسي العلوي الهدف الأول لصخور المكمن في منطقة رصيف زلتن، ويتراوح سمك صخور المكمن من الصفر عند ذروة التركيبة المحدبة إلى أكثر من 350 قدم عند الحواف، ويمكن ملاحظة بعض خواص المقاطع الزلزالية المنعكسة من خلال التنبؤ وموقع مكمن الواحة عند تواجد مقطع سميك منه، يولد تباين قوة مقاومة الصوت عند قمة الكلاش (فوق الواحة) والباهي/القرقاف (مباشرة تحت الواحة) انعكاسات تحدد معالم الغلاف الذي يوجد بداخله تكوين الواحة.

تم اكتشاف معظم المصايد النفطية بحقل الجبل اعتمادا على الدراسة الحقلية والمسح الزلزالي، ومنذ تأسيس الحقل فقد وصل الإنتاج حاليا مرحلة الاسترداد الثانية. قادت هذه الدراسة إلى البحث عن مصايد بنيوية صغيرة متواجدة مع هذا الحقل العملاق وخاصة في الجزء الجنوبي منه. وبالرغم من اعتبار أن هذه الظواهر الصغيرة قليلة المخاطر نسبيا، خاصة عند استعمال التقنية السيزمية، فإن موقع شاذات التركيبة المأمول قد تم التعرف عليها، ومن المحتمل أن تكون هدفا للحفر وهو ما يسمح للشركة من تحديد موضع قدم للنفط وتطوير الإنتاج في هذا الحقل.

Abstract: *The present day structure of Al Jabal Field is a NE-SW trending anticline structure. The prominent shape of this structure is the product of a Pre-Cretaceous topographic high, which was modified by faulting, erosion and transgressive sedimentation during the Cretaceous and by faulting during the Palaeocene and Eocene. A major fault, bounding this structure on the west, defines Al Hagfah Trough/Zaltan Platform. Two other minor faults splay off from this major fault, cut the main structure and probably seal Al Jabal structural anticline from the west to the northwest.*

The Upper Cretaceous Waha Limestone is a primary reservoir target on the Zaltan Platform. The reservoir ranges from zero thickness on the crests of topographic highs to over 350 feet on their flanks. Certain seismic reflection characteristics are noted in relation to the prediction and location of the Waha reservoir where a thick Waha section is usually present. Strong acoustic impedance contrasts at the top of the Kalash (above the Waha) and the Bahi/ Gargaf (immediately below the Waha) generate

* Sirte Oil Company.

reflections that define the envelope in which the Waha exists.

Most of the traps were discovered in Al Jabal Field on the basis of geological fieldwork and seismic surveys since the field was established have now reached their secondary recovery stage. This study led the search for smaller satellite structures to be associated with this giant field, particularly in its southern part of the field. Although these small features are considered to be of relatively low risk, especially with using the seismic techniques, the locality of new prospective structure anomalies has been defined, and could be a drilling target, which would enable the company to spot the oil leg target and develop production in this field.

INTRODUCTION

Waha Formation in Al Jabal Field is the principle Upper Cretaceous producing formation, a saturated light oil reservoir with a gas cap and aquifer. The Waha Limestone varies in lithologic composition from sandstone to limestone and ranges in thickness from its depositional edge to over 350 feet in the northern part of the field (El Ghoul, 1996). This study focuses on prospective areas in the southern part of this field by looking for satellite structures and by analysing the effect of thickness variation of reservoir rock unit. Although there is minimum well data within studied area, the appearance of Waha Limestone elucidates fair distributed thickness to be a capable reservoir rock unit in this region. The identification of these potential structures could be useful with the prediction of production in Al Jabal Field.

Location of the Study Area

Al Jabal Field is located in South Concession 6 on the updip edge of the Zaltan Platform in onshore Sirt Basin. Esso discovered this field in 1962 and drilled wildcat P1-6. Production of Al Jabal Field started in 1964, and a total of over 60 wells have been drilled to date (Wallace, 1988). The greatest part of the Concession 6 is located on the Zaltan Platform. This platform is bounded on the west by large scale syn-depositional faulting that separated the Zaltan Platform from Al Hagfah Trough to the west.

The area of study is located in the southern portion of Al Jabal Field (Fig. 1) between latitude N 28° 28‘36", N 28°41‘54", and longitude E 19° 49‘14", E 20° 01‘44".

Petroleum System in Studied Area

Source Rock

The Sirte Shale is composed primarily of shale and some limestone. It is believed to be the hydrocarbon source rock that was deposited in Al

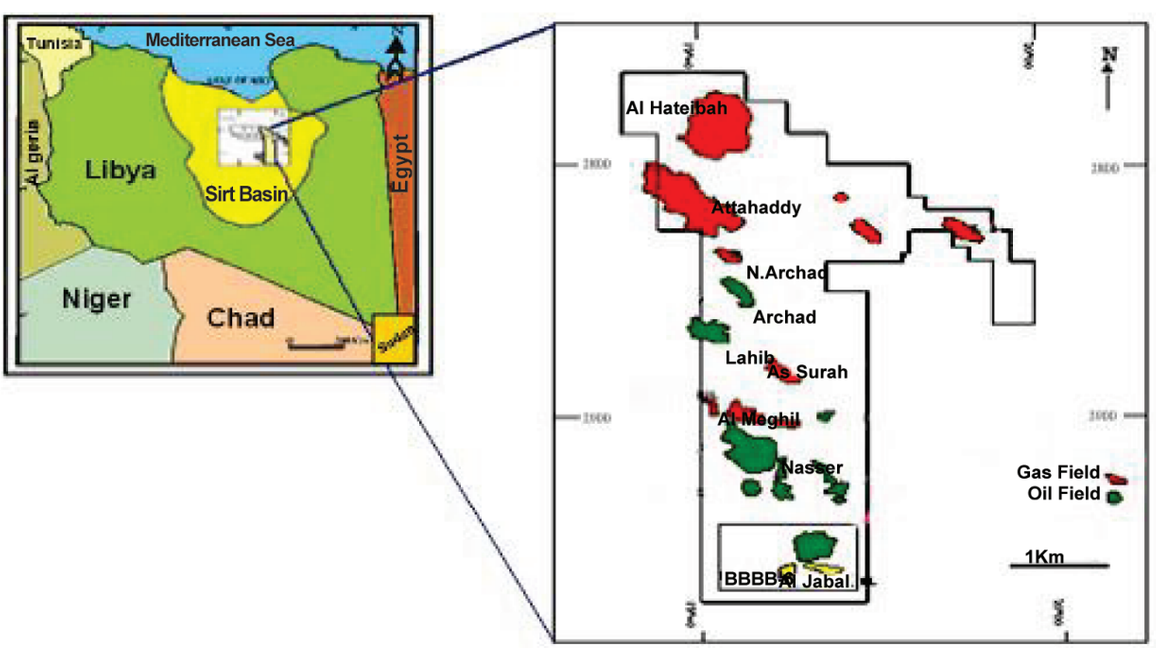


Fig. 1. Study area, locations map.

Hagfah Trough for the Waha, Bahi and Gargaf reservoirs (Fig. 2). This figure shows the total and minimum petroleum system in Concession 6 (El Ghoul, 1996).

Reservoir Rock

The main primary producing reservoir in Al Jabal Field is the Upper Cretaceous Waha Limestone in the southern part of Concession 6 (Fig. 2). The Waha is composed primarily of skeletal limestone and calcarenite sands. It represents deposition in the high-energy zone at or near wave base as the first Cretaceous seas on-lapped the Zaltan Platform (Barr and Weegar, 1972). The best Waha oil reservoirs are usually on the old highs where Sirte Shale was not present. Waha Limestone ranges in thickness from its depositional edge to over 350 feet (Waha Limestone thickness in well 4B2-6 is 11 feet, and 357 feet in well P1-6).

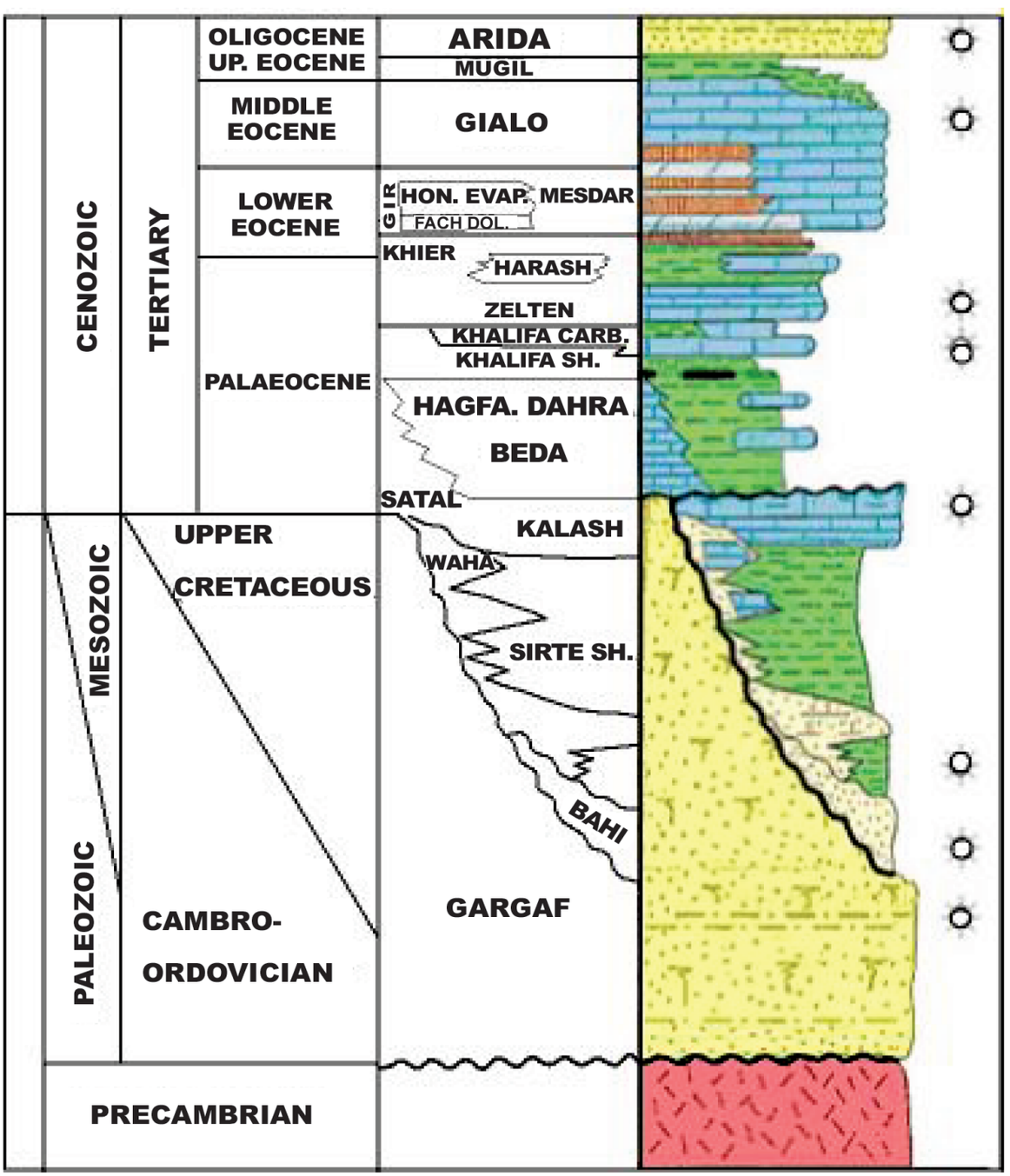


Fig. 2. Generalized columnar stratigraphic section of Concession 6.

Seal Rock

The Kalash Limestone is the most widespread Cretaceous sediments unit and covers all of the Concession 6 (McDowell, 1988), both the Zaltan Platform and the Al Hagfah Trough. It is a tight micritic limestone and represents deep water carbonates deposition (Barr and Weegar, 1972), and it is not normally a reservoir. The Kalash Limestone is supported by massive shale (Hagfa Shale), which acts as a seal for Upper Cretaceous reservoir rock in the Zaltan Platform (Fig. 2). Hagfa Shale is widespread in central and western Sirt Basin. It is Lower Palaeocene (Danian) in age, and consists mainly of a shale sequence with occasional thin limestone interbeds.

Trap Style

The trap style in Al Jabal Field is a combination of stratigraphic and structural traps. The anticline at Al Jabal is a NE-SW trending feature with faults on the western and northwestern flanks of the field. In addition, major unconformities, bounding the Waha reservoir at the top and base contribute to the complexity of the reservoir sequence at Al Jabal (Wallace, 1988). The field illustrates an excellent example of a combination of a stratigraphic-structural trap in many Libyan oil fields.

Oil Migration

The Sirt Basin is an example of a dominant vertical migrated petroleum system, wherein Upper Cretaceous oil charges multiple reservoirs along fault zones adjacent to horsts and grabens (Ahlbrandt, 2001).

OBJECTIVES

Most palaeotopographic giant structural traps were discovered in the early stage of exploration in the Al Jabal Field, with the aim of developing production of this field as its secondary stage of recovery by looking for new localities of potential satellite structures and constructing time and thickness maps for seal and reservoir layers in the South Al Jabal Field.

The purpose of this study involves evaluating the Waha Limestone as a reservoir unit, and Kalash Limestone, which is a widespread Upper Cretaceous sedimentary unit in Concession 6. Additionally as an excellent mappable seismic reflector, and fairly easy to follow as it is overlain by massive shale of Hagfa Shale that on certain seismic reflection shows strong acoustic impedance contrasts at the top of Kalash enabling calculating of the thickness of Waha reservoir and seal rocks. Mapping the shallower formation, which is (the Middle Eocene Gialo) can illustrate the general, and overall structural picture of the studied area.

AVAILABLE DATA

Seismic Database

All seismic data provided is vibroseis and covered the southern part of the Al Jabal Field. These data, the last proposed on this field, were shot in years 2000 and 2001, associated with previous seismic proposed in the recent years, which were shot in years 1998 and 1999. The seismic data used in this study includes 15 lines of migrated 2D and consist of 302 km. Six out of 15 seismic lines are strike lines and 9 of them are dip. The strike lines orientate in NW-SE direction whereas the dip lines in NE-SW (Fig. 3). A seismic base map with a scale of 1:50,000 have been used.

Well Database

The well data used in this study have been collected from 17 wells that were drilled below Kalash level, in Al Jabal Field (Fig. 3). Well data information includes composite logs containing spontaneous potential (SP), gamma ray (GR), resistivity (LLD), and sonic logs.

METHODOLOGY

A seismic programme of 302 km has been selected from the database of Sirte Oil Company (SOC) in Al Jabal Field to determine the main seismic reflectors in the area of study and the presence of potential hydrocarbon traps. Synthetic seismograms were used from 12 wells to tie the well data with seismic profiles. The main seismic marker in the area is the Upper Cretaceous Kalash Limestone, being the strongest and continuous reflector and an excellent mappable seismic marker. The Kalash Limestone is believed to be a good seismic reflector marker for the Waha

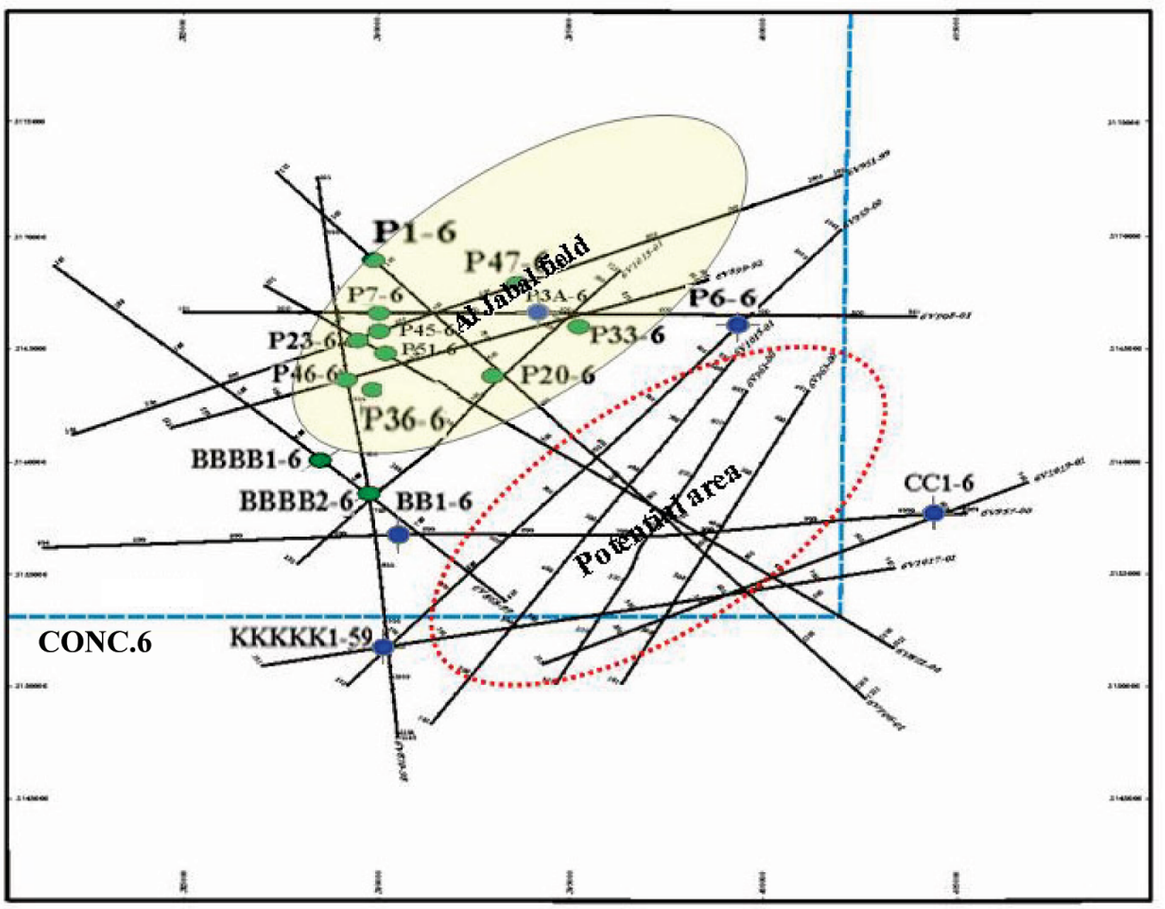


Fig. 3. Base map Al Jabal Field.

Limestone reservoir that contacts the Kalash with the Waha, which has a minor variation in acoustic impedance contrast.

Two-way time structure map was generated for the top of Kalash posted on a base map every 40 shot points by using 20 (ms) as a contour interval, and another two-way time structure map was generated for the top of Gialo Limestone, demonstrating the general structure of the area, and could illustrate new shallower structures.

Two cross-sections were generated across the field in two different directions by using sub sea depth at (-6600 ft) as a datum within Hagfa Shale that overlies the Kalash Limestone.

Well data information was used also to illustrate the distribution of the formations' thicknesses. Two isopach maps in vertical sequence succession were generated for Kalash, and Waha limestones.

SEISMIC INTERPRETATION

The purpose of the seismic interpretation was to define and map the south part of Al Jabal Field and track any possible structure for development, outpost or exploration drilling. Basic procedures for seismic interpretation were followed involving the identification of strong and continuous seismic reflector. This achieved by tying well data to seismic profiles and tracking the marker horizons. Eleven seismic markers have been traced during the course of this work to verify the presence of hydrocarbon traps within the studied area.

Tying Well Data

Interpretation was started by picking horizons that were displayed on the seismograms from twelve wells in this area. The seismograms generated by using sonic logs to determine the formation tops.

Two seismic lines were used as key lines since they intersect with the most lines in this study. Line 6V957-00 shot in year 2000, extends for approximately 24 km in a W-E direction as a strike line and ties two wells, BB1-6 in the west at shot point 475, and CC1-6 in the east at shot point 1035

(Fig. 4). The second line is 6V872-00, which extends for approximately 23 km in a NW-SE direction as a strike line as well and crosses over well P51-6 (Fig. 5).

The second stage involved the interpretation of all seismic lines used to correlate and tie at every intersection between these lines, closing loops of seismic grid by correlating the recognized horizons on the two key lines and follow them on the other seismic profiles.

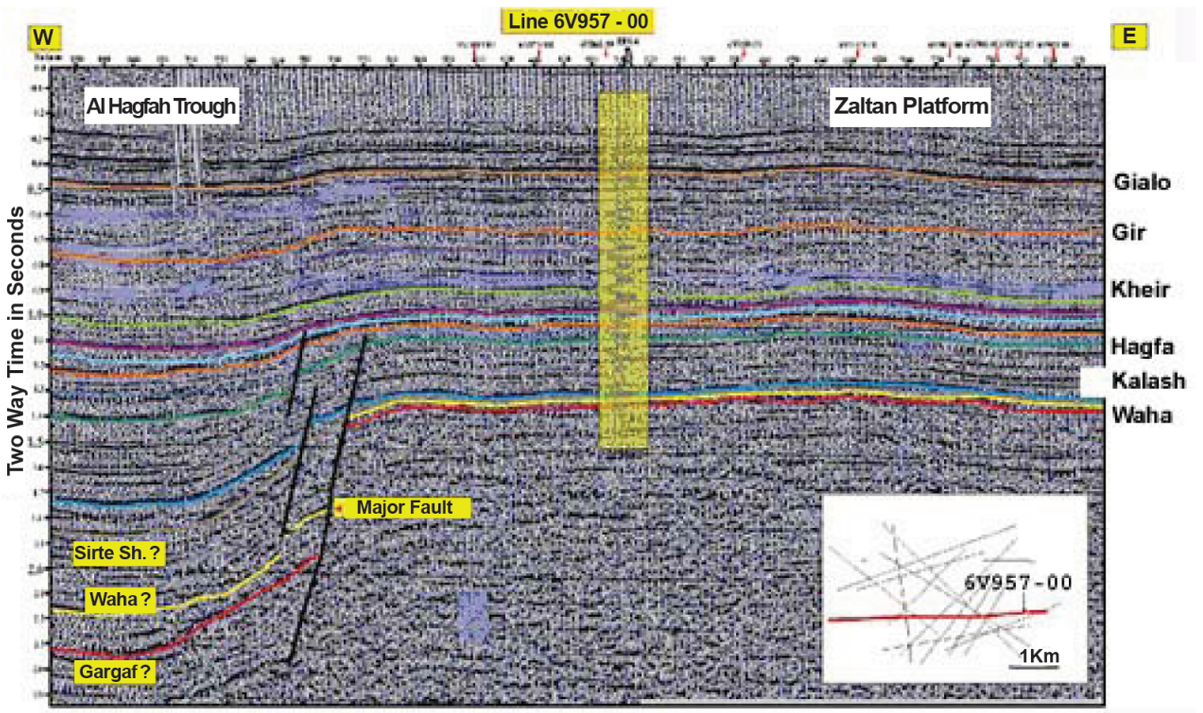


Fig. 4. Seismic profile of line 6V957-00.

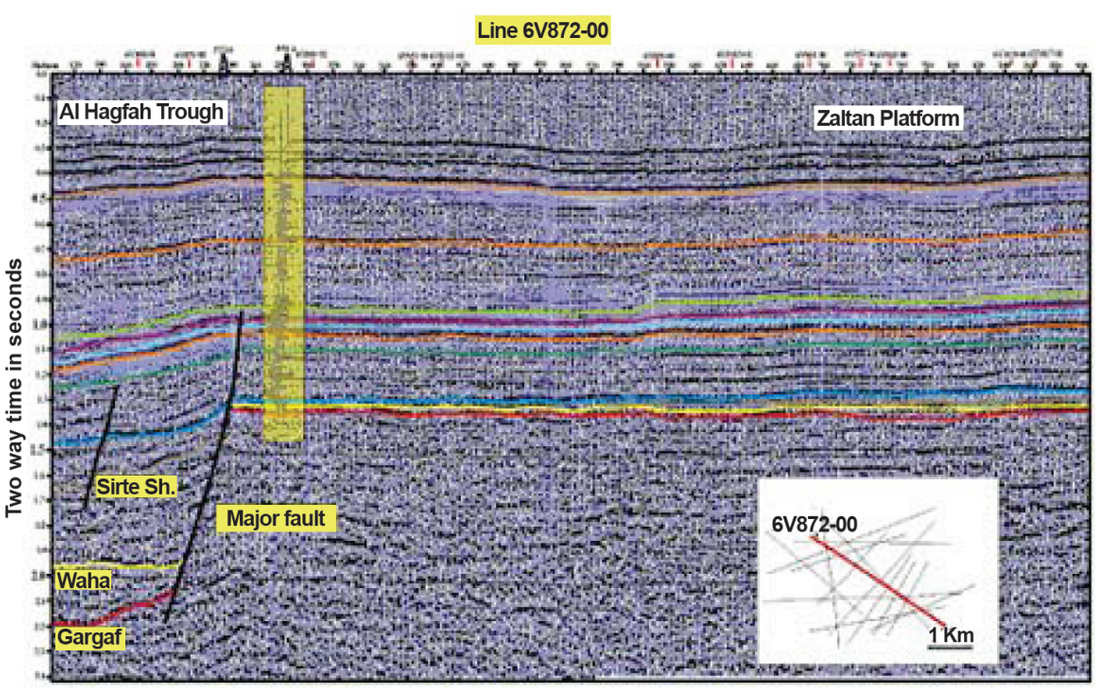


Fig. 5. Seismic profile of line 6V872-00.

Structural Interpretation and Mapping

This phase of interpretation involved the production of satisfactory time structure maps for target horizons to illustrate the general structural picture in the vicinity of Al Jabal Field. Verification of the presence of hydrocarbon traps within the area of study was achieved through the construction of two-way time maps, which may be considered to represent a new mapped structural configuration of the top of the reflector (Kalash). Mapping time values are utilized for the identification of many untested structurally high features that may indicate new Waha sweet spots.

The interpretation enabled the production of time structure maps that were generated on a scale of 1:50,000 for inclusion in this study:

- A time structure map of Top Gialo Middle Eocene (Fig. 6) was generated, because Gialo map illustrates the general and overall picture of the structure of the area. This horizon appears almost flat and it is not disrupted by any tectonic events, which is reasonably undisturbed. A smooth gently dipping Gialo surface was constructed. This surface was then modified as the standard from which all other events were compared.

- A time structure map of Top Kalash Upper Cretaceous (Fig. 7) was generated, since mapping of the Kalash seismic horizon indicates the Waha reservoir. Seismically, top Kalash surface has proved to be an excellent mappable event. This peak is due to the strong acoustic impedance contrasts at the top of Kalash. The Kalash horizon is gentle dipping to the northeast, and in the west most of the Kalash surface has been affected by the major fault and a number of complex normal faults system situated to the west of Al Jabal Field. These faults are trending to the north south towards and downthrown into Al Hagfah Trough. The map can be utilized for identification of many untested structurally high features located in the South Al Jabal Field on the Zaltan Platform.

The Kalash time structure map has clarified some satellite structures; it demonstrates a crest of anticline structure traps. The most interesting structural high anomalies that have been interpreted are on seismic profiles of line 6V957-00, which extends in a W-E direction showing a typical anticline sitting on this line (Fig. 8), and the time computed for this closure is 1.22 sec. Second seismic profile of line 6V1019-01 extends in a SW-NE direction relocates another typical anticline sitting on this line of computed time

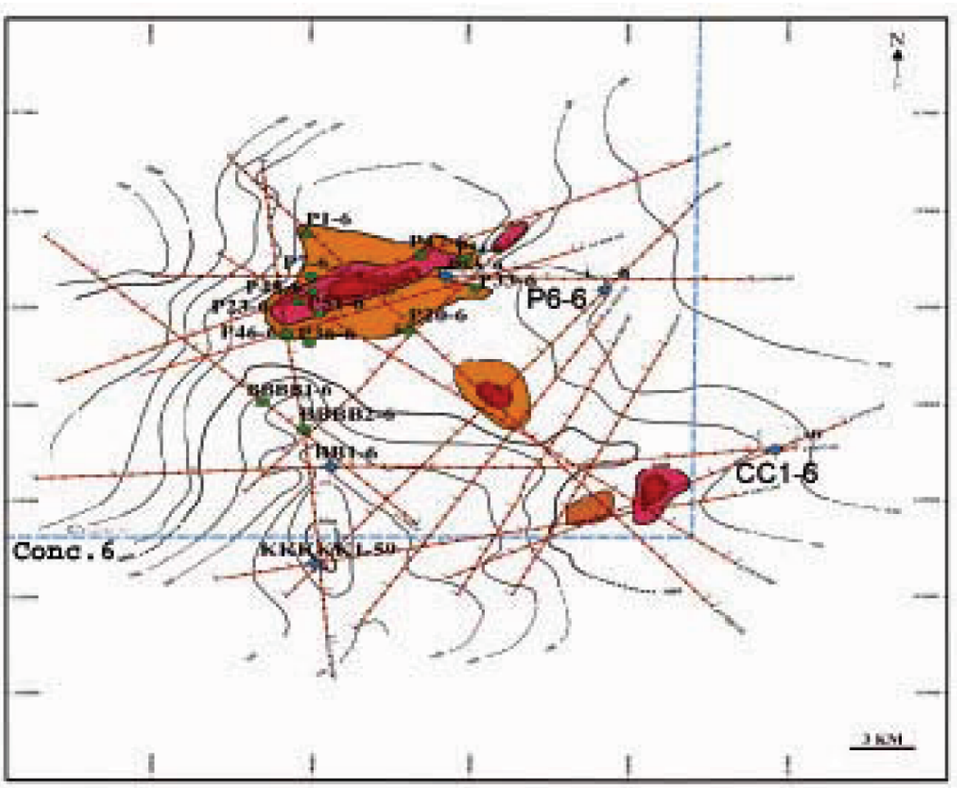


Fig. 6. Time structure map of top Gialo, contour interval (20 ms).

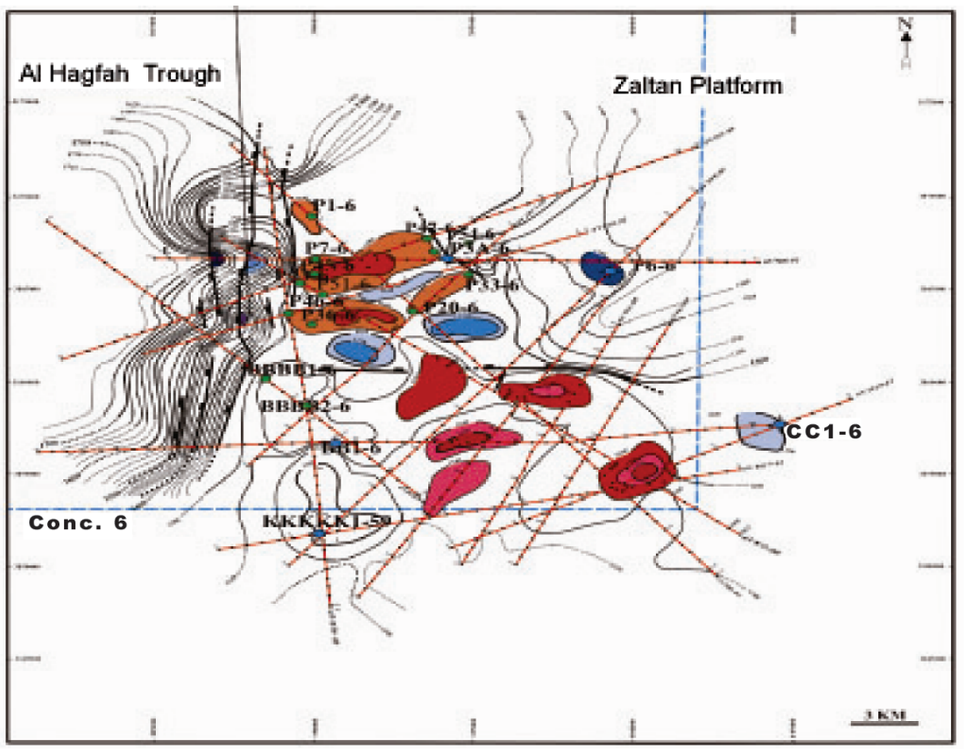


Fig. 7. Time structure map of Kalash, contour interval (20 ms).

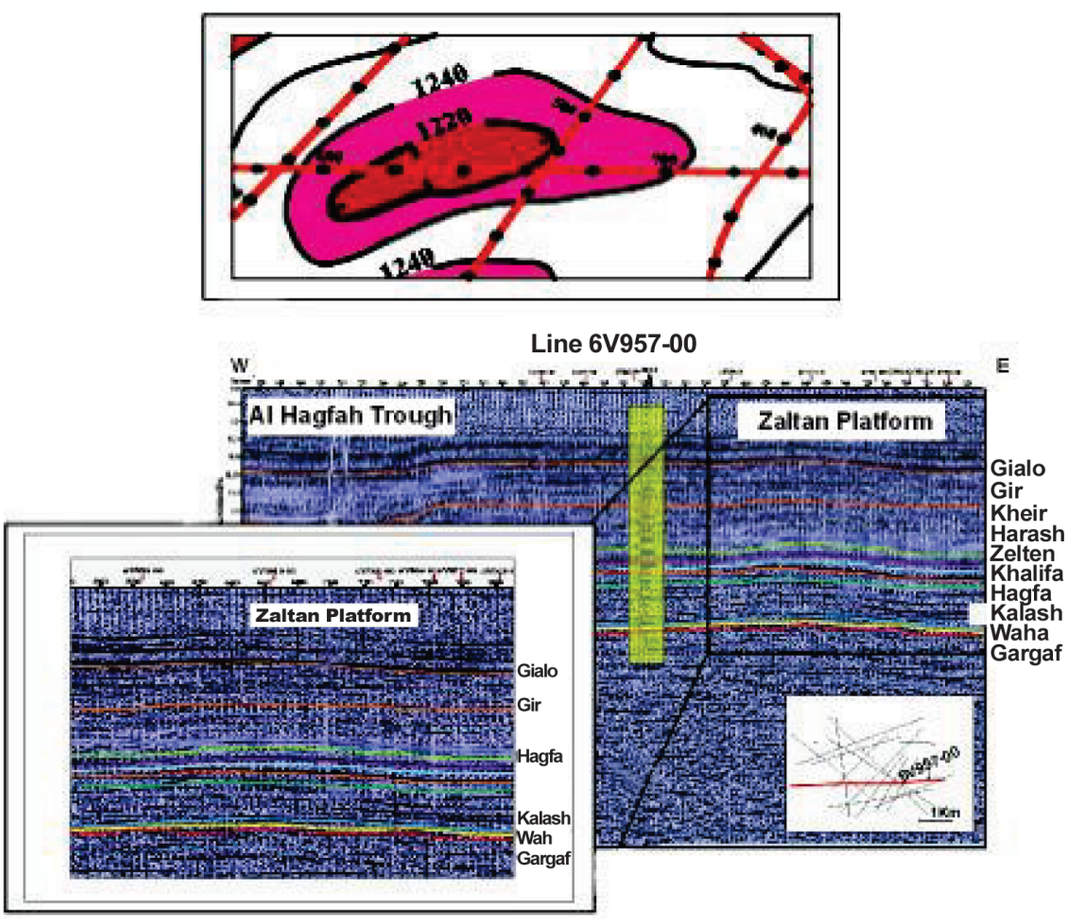


Fig. 8. Enlarged portion along seismic profile of line 6V957-00, showing anticline structure.

1.22 sec as well in the south part of Al Jabal Field in the Zaltan Platform (Fig. 9).

WELL LOGS ANALYSIS

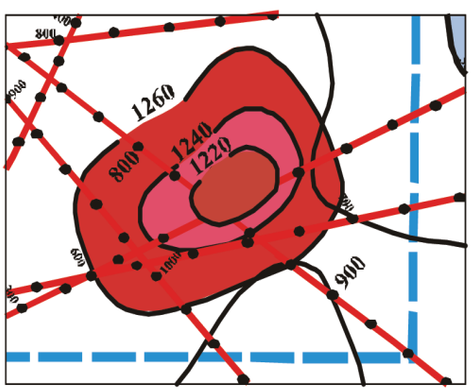
Well Status

The well data information that has been used in this study was collected from 17 wells. Five wells are dry (BB1-6, CC1-6, KKKKK1-95, P3A-6, P6-6) and two are abandoned (BBBB1-6, BBBB2-6). The reasons for dry wells will be discussed later in the text.

Well Correlations

Two geological structural cross-sections were constructed from the well logs for comparison with the interpreted seismic data to achieve the best geological model. These cross-sections were generated using well logs across the studied area in two different directions to elucidate the distribution of thickness and map the tops of the seal and reservoir layers by using sub sea depth measurements at -6600 ft as a datum for both cross-sections within the Hagfa Shale.

The first cross-section A-A‘ was based on seven wells (P1-6 to BB1-6) extending north-



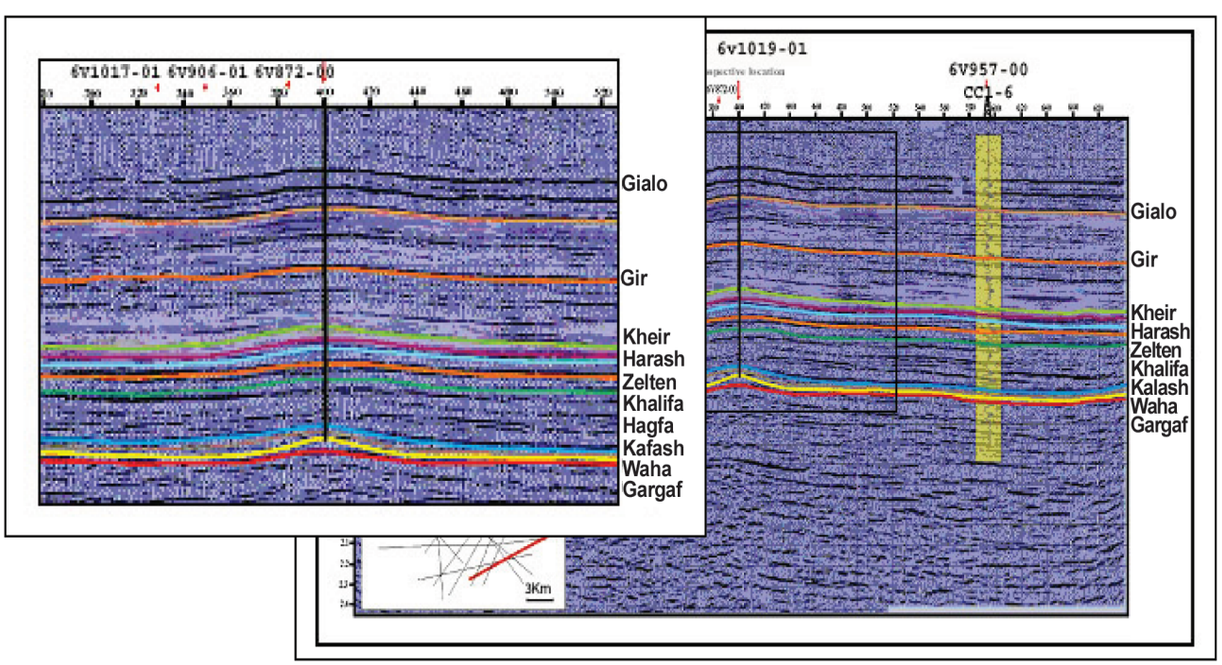


Fig. 9. Enlarged portion along seismic profile of line 6V1019-01, showing anticline structure.

south across the southern area of the field (Fig. 10). In this cross-section well BB1-6 is located at the southern part in the field. This well was drilled in 1964 and it was dry. The results of drilling were three oil shows in the upper section in the Gialo Limestone that tested tight and no significant shows were encountered in the Cretaceous section (Wallace, 1988).

The well BBBB2-6 located about 5 km south of Al Jabal Field was drilled in 1984. This well was abandoned because the results demonstrated tight show in Gialo Limestone and only 11 feet of wet Waha that gave up fresh water (Wallace, 1988).

The second cross-section B-B‘ was based on six wells (P7-6 to CC1-6) extending west- east across three dry wells in the southern part of the field (Fig. 11). Well CC1-6 drilled in 1964, located to the southeast side of the field. No shows in the target section of this well and the test showed salt water.

Well P3A-6, located to the north of the study area, was drilled in 1963, on a high structure, but the reservoir thickness was only 17 feet, and there were no shows in Waha Limestone. The third well in this cross-section is P6-6 located to the south east of well P3A-6. It was drilled in 1963 and it was proposed to drill on a seismic structure of the southeast the field. The well bottomed in metamorphosed igneous basement and no shows were established (Wallace, 1988).

These two cross-sections showed how the thickness of Waha reservoir varies; it attains its maximum thickness up to 357 feet in well P1-6 in the north and reduces to 11 feet in well BBBB2-6 in the southwest.

The Upper Cretaceous Waha Limestone is capped by the chalky Upper Cretaceous Kalash Limestone and generally on-lapped the eroded quartzite highs of the Cambro-Ordovician Gargaf. The thickness variations are discussed below for each formation. Although minimum well data was available for the studied area, these two sections show a fair distributed thickness to be a capable reservoir unit in this region.

Formations’ thickness Distribution

Two isopach maps were generated from well data to calculate the thickness of the lower layers in the

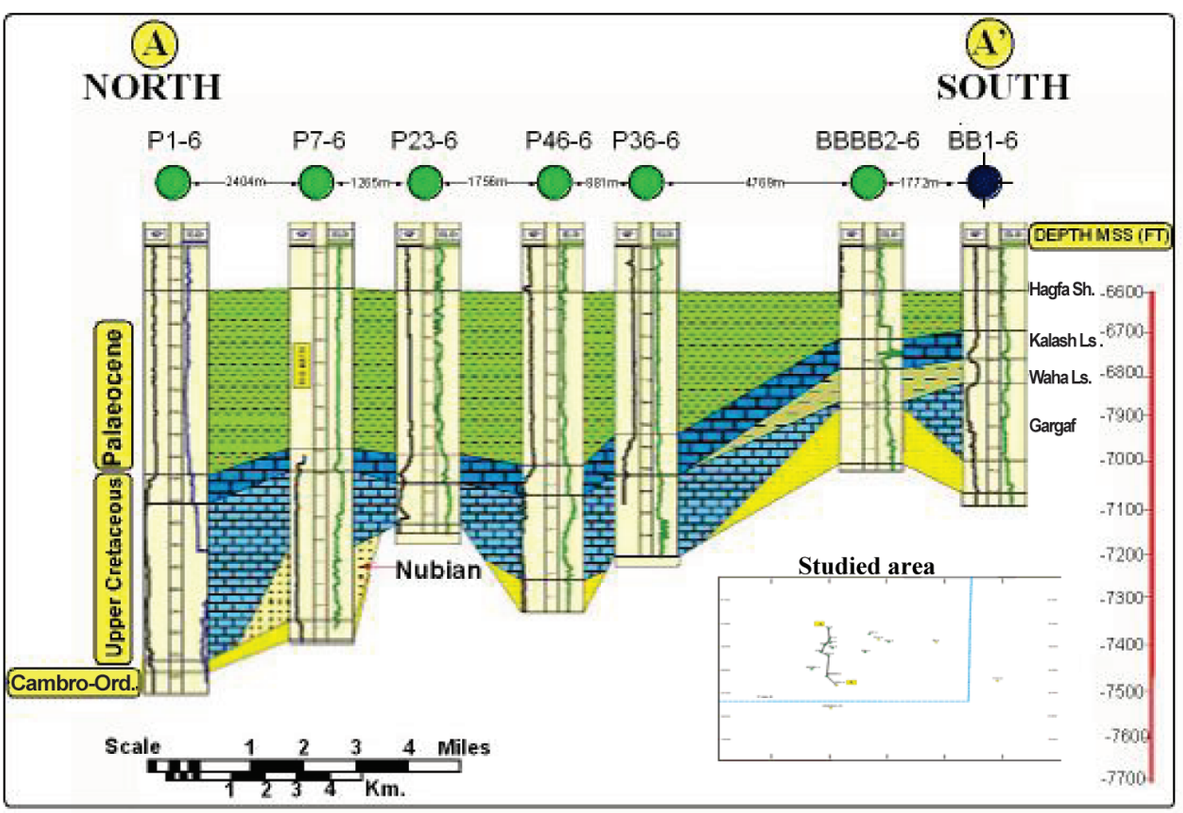


Fig. 10. Geological structural cross-section (A-A‘).

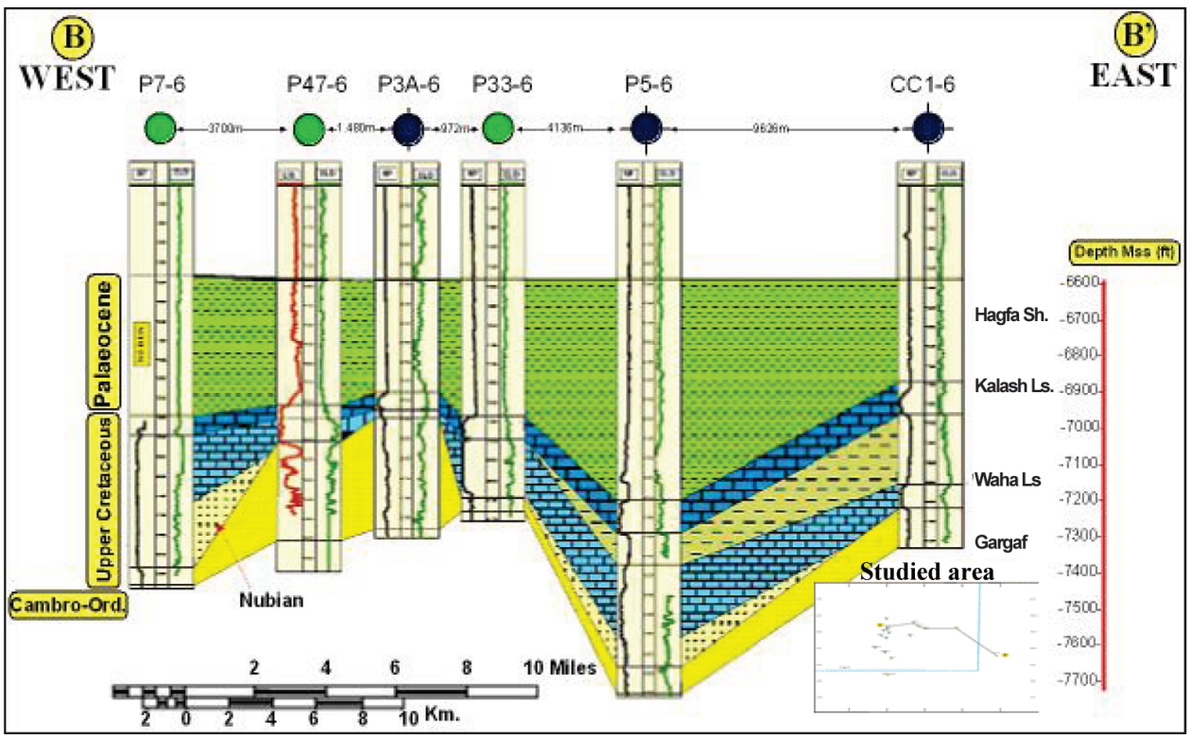


Fig. 11. Geological structural cross-section (B-B').

area of study (Table 1). The following analysis covers the formations' thickness consecutively:

Kalash Limestone

An isopach map of the Kalash was generated, using 10 feet as a contour interval (Fig. 12). This map illustrates the seal rock thickness that is supported by Hagfa Shale in Al Jabal Field. It is evident that Kalash Limestone is widespread in this area, and reasonably sufficient to deduce that the Kalash is an excellent indicator for Waha reservoir in the area of interest. This map shows some reduction in thickness towards the north as it reaches the crest of Al Jabal structure and increases to the south.

The Kalash thickness ranges from 37 feet to the northeast in well P47-6 up to 92 feet in the southwest in well P36-6 (Table 1).

Waha Limestone

An isopach map was produced to estimate the gross thickness using an interval contour of 25 feet for the Waha Limestone in the southern part of the field (Fig. 13). The Waha map clarifies several important trends:

Table 1. Formations' thickness of the lower section in the study area.

Well name	Hagfa Sh (ft)	Kalash (ft)	Waha (ft)
BB1-6	1110	65	170
4B1-6	1106	70	38
4B2-6	1094	72	11
CC1-6	1117	86	64
5K1-59	962	46	184
P1-6	1111	66	357
P3A-6	1034	44	17
P6-6	1107	89	185
P7-6	1113	50	179
P20-6	1078	90	100
P23-6	1005	60	91
P33-6	1056	62	145
P36-6	1033	92	90
P45-6	1049	55	295
P46-6	1051	70	192
P47-6	1022	37	59
P51-6	1063	59	207

First, stratigraphic thinning onto the structure is quite evident. This trend agrees with the regional structural and stratigraphic history of the Sirt Basin during the Upper Cretaceous. Secondly, the western flank of the field illustrates rapid thickening as one moves further away from the structure crest.

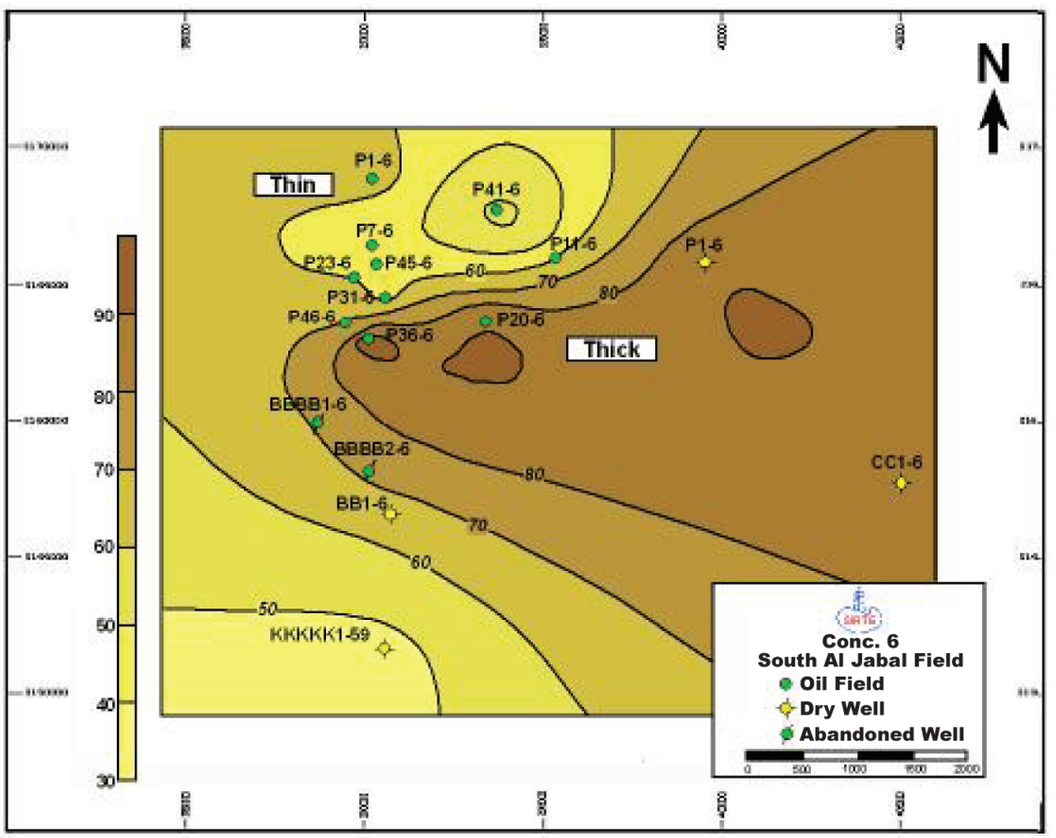


Fig. 12. Isopach map of Kalash, contour interval (10 feet).

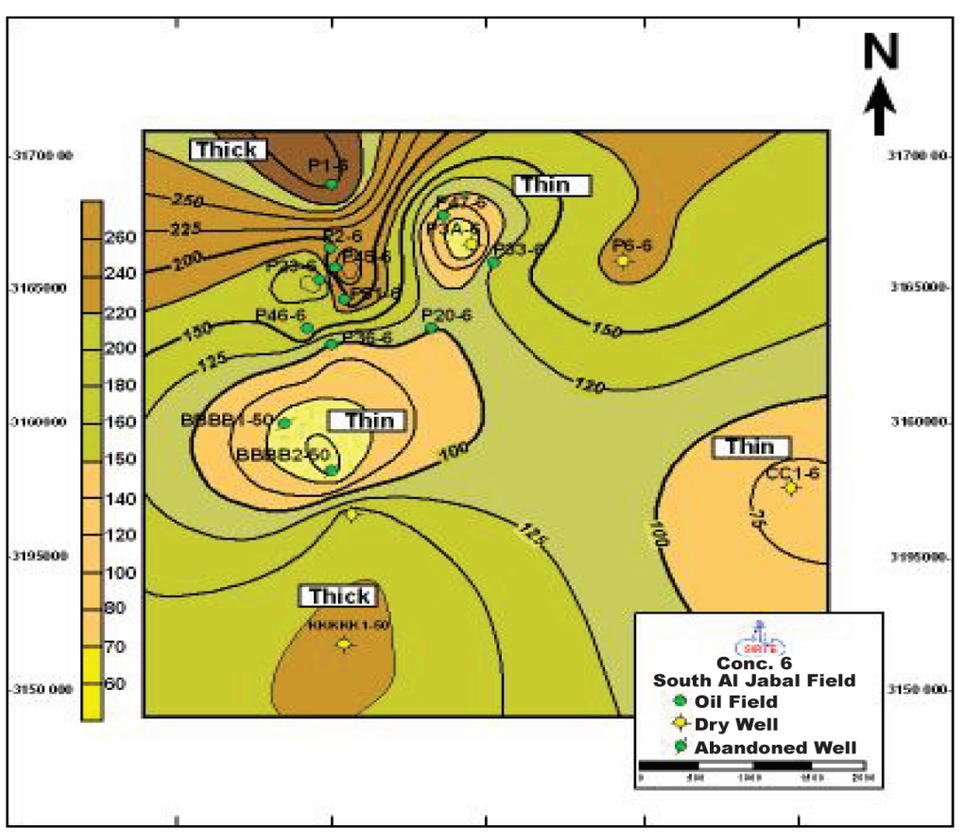


Fig. 13. Isopach map of Waha, contour interval (25 feet).

SUMMARY

Most palaeotopographic structural traps were discovered in Al Jabal Field, so as a secondary recovery stage by focusing on these prospective areas, we can enhance the production in Al Jabal Field.

The results of the Top Kalash two-way time structure illustrated areas of prospectivity, which are in the southern part of the Jabal Field. The time computed for the closure of the crest is 1.22 (sec), and the low contour is 1.26 (sec). These anomalies are considered to be of relatively low risk, especially when using seismic techniques to locate new drilling targets that could develop the production in this field.

The Upper Cretaceous Waha as a reservoir target ranges from 0 on the crest of palaeohighs to over 350 feet on their flanks as it moves away from these palaeohighs, so on these flanks Waha Limestone is almost present.

CONCLUSIONS

1. The anticlinal structure at Al Jabal, Field is in a NE-SW trending feature, with a sealing major fault on the western and northwestern flanks of the field. Two additional faults trend parallel to sub parallel with the major basement faulting at Al Jabal Field.

2. The Upper Cretaceous Waha Limestone in Al Jabal Field is the principal producing formation for Cretaceous sediment units, a saturated light oil reservoir with a gas cap and aquifer. The Waha Limestone varies in lithologic composition from calcarenite to limestone and ranges in thickness from its depositional edge to over 350 feet in the northern part of the field. It is at a depth of 7,000 feet subsea.

3. The Upper Cretaceous Kalash Limestone that is the most widespread Cretaceous sediments unit overlies the Waha Limestone reservoir. It covers all of Concession 6, both the Zaltan Platform and Al Hagfah Trough. It is a tight micritic, and it is believed to be a seal for the Upper Cretaceous reservoir rock supported by massive Hagfa Shale in the Zaltan Platform.

4. The dominant source rock is the Sirte Shale, which is composed primarily of shales and some limestone. These are source rocks for the Waha, Bahi and Gargaf reservoirs and were deposited in Al Hagfah Trough.

5. Several untested significant anomalies, for some satellite structures, have been identified in the southern portion of the field, which could suggest to company to spot the oil leg target and develop the production in this field.

6. Although low control on well data within studied area, the appearance of Waha Limestone shows fair distributed thickness to be a capable reservoir rock unit in this region.

RECOMMENDATION

3D seismic is proposed to re-evaluate discovered leads in the studied area. This new 3D survey would present the opportunity to construct one data set, which will resolve problems related to any seismic mis-tie issues, and make changes for improved stratigraphic resolution in Kalash. This seismic technique should assist in resolving the critical reservoir thickness and build a consistent depth map for reservoir unit.

ACKNOWLEDGEMENT

I would like to express my gratitude to Sirte Oil Company. My special appreciation is expressed to Exploration Management, who offered me the chance, encouragement and permission to use company data for this study.

I further wish to thank my colleagues in Exploration Department, who assisted with the provision of data.

REFERENCES

Ahlbrandt, T. S., 2001. The Sirte Basin Province of Libya—Sirte- Zelten total petroleum system, *U.S. Geological Survey Bulletin* **2202**–F, Department of the Interior.
http://geology.cr.usgs.gov/pub/bulletins/b2202-f/.

Barr, F.T. and Weegar, A. A., 1972. *Stratigraphic Nomenclature of the Sirte Basin,* Libya, Petroleum Exploration Society Libya, Tripoli, 179p.

El Ghoul, A., 1996. An approach to locate subtle Waha structural traps on the Zaltan Platform: geology and geophysics. In: Salem, M.J., Busrewil, M.T., Missaluti, A.A. and Sola, M.A. , (eds), *The Geology of Sirt Basin,**III,*** Elsevier, Amsterdam, 137-154.

McDowell, J. E., 1988. *Concession 6: Cretaceous Study Project*, Sirte Oil Company, Interior Company Report.

Wallace, F.K., 1988. *Jebel Field Geology Study, Concession 6*, Sirte Oil Company, Interior Company Report.

Wennekers, J.H.N., Wallace, F.K. and Abugares, Y.I., 1996, The Geology and Hydrocarbons of The Sirt Basin. A synoposis. In: Salem, M.J., Mouzughi, A.J. and Hammuda, O.S. (eds), *The Geology of Sirt Basin **1***, Elsevier, Amsterdam, 3-56.

Petroleum Res. J. Vol. 20 (2007); P. 35–44, 11 Figs.

Anisotropic Prestack Depth Migration In C97 And NC98,Libya

C. Hanitzsch* and A.S. Ben Abdulla**

هجرة عمق ناجم عن تراص مسبق متباين بعقديْ الامتياز C97 وNC-98، ليبيا

س. هاينتش وعبد الله سالم بن عبد الله

التصوير الزلزالي المحسن تحت نطاقات الصدوع المركبة، حيث تزداد استمرارية الانعكاسات وتتحسن حديّة التركيز على الصدوع وبأقل ضوضاء ممكنة، يمكن الحصول عليه، بهجرة العمق الناجمة عن تراص مسبق متباين الخواص. فهو يحسن نوعية الصور بالتقليل من الضوضاء وباستمرارية أكبر للانعكاسات وتحديد أفضل للصدوع. وللنتائج المتحصل عليها تأثير فعال في حفر آبار جديدة وقد تعمل هذه التقنية على تحسين صور أماكن أخرى مرتقبة في ليبيا تقع تحت نطاقات الصدوع المركبة. ولضمان نجاح هذه التقنية فإن المطلوب من الجيولوجيين والجيوفيزيائيين العاملين في شركات النفط، أن يولوا اهتمامات أكثر وتفاعلات أكبر من تلك التي يمارسونها في تقنيات المعالجة الزلزالية العادية.

Abstract: *Improved seismic imaging below a complex fault zone, more continuity of reflections, better focusing of faults and less noise are achieved by anisotropic Prestack depth migration (PreSDM). It improves the image quality by reducing noise, more continuity of reflections and better fault definition. The obtained results had a major impact on drilling of new wells. The technology of PreSDM may improve imaging of other Libyan prospects that are located below complex fault zones. To achieve success, this technology requires significantly more attention and involvement from oil company's geophysicists and area geologists than standard seismic processing techniques.*

INTRODUCTION

Study Area

An anisotropic Prestack depth migration (PreSDM) project was operated in 2001 – 2004 by Wintershall – Libya with Waha Oil Company being project partner. It covers an area of 1242 Km² mainly in Concessions C97 (Wintershall-Libya operator) and NC-98 (Waha Oil Co. operator) in the eastern Sirt Basin of Libya with small extensions into C100, C102 and NC-59 (Fig.1). In addition to producing oil fields, the area contains several potential exploration prospects. It was one of the first applications of depth imaging in Libya and is one of the largest onshore depth imaging projects world-wide. However, to keep project sizes reasonable the project was split into three phases, assuring consistency between all phases (Fig. 1).

The area of study is generally of low structural relief, but has complex faulting resulting in strong lateral changes in velocity. These lateral changes degraded the seismic image in the original standard time processing.

* (Wintershall-Libya, Corinthia Bab Africa, Commercial Centre, Tripoli, G.S.P.L.A.J.).
** (Waha Oil Co., P.O. Box 395, Tripoli, Libya).

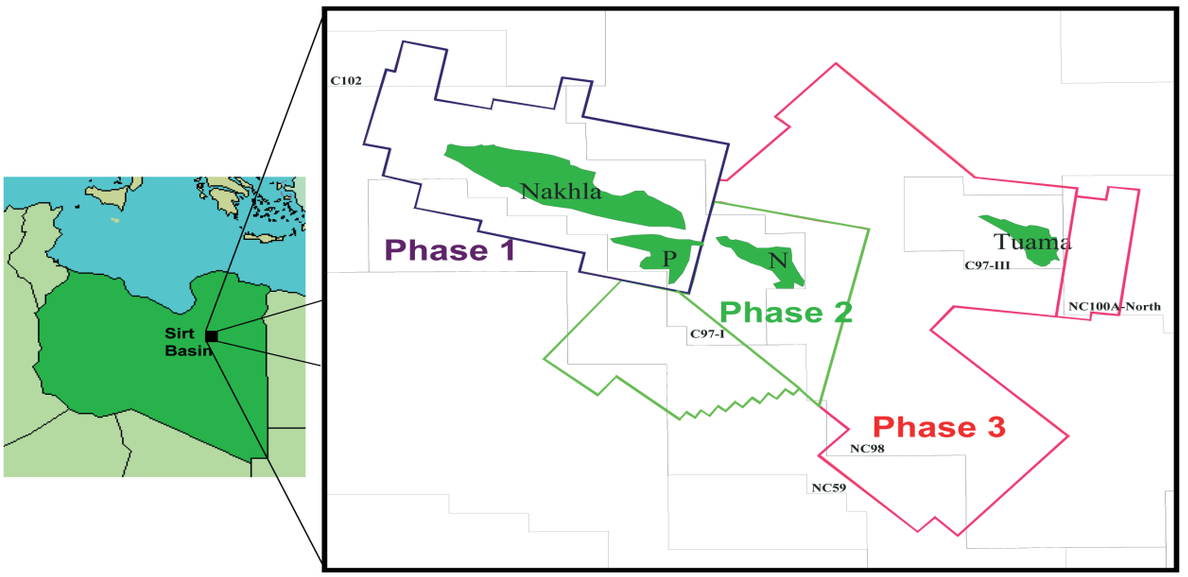


Fig. 1. Project outline. Concessions C97 and NC98 are located in the eastern part of the Sirt Basin.

Objective

The main objective of the project was to improve the image quality below the complex fault zone. Figure 2 shows an overlay of PreSDM seismic and the corresponding section of the obtained velocity / depth model. A system of long and very steep faults cause the large lateral velocity variations. As a consequence, nonhyperbolic moveout is present and therefore standard time processing does not manage to focus the image properly below the fault zone.

Another objective was to obtain a seismic image in "true" depth (*i.e.* that ties existing well marker depths within the seismic bandwidth) therefore vertical transverse isotropy (Thomson's delta and epsilon parameters) was introduced to the velocity model as a first order approximation of anisotropy.

PROJECT STEPS

Data Preparation

When matching seismic with well data as an objective, it is very important to assure the integrity of all data. With about 40 wells located within the project area, a consistent log re-processing including the calculation of time–depth curves based on VSP constrained sonic logs, synthetics in time and depth and consistent picking of well marker depths prior to the project proved extremely valuable. Interpretation of existing time seismic provided the eight horizon maps for the initial model.

Time Pre-processing

Time pre-processing is an important major step prior to depth imaging. In this project, seismic data from eight seismic surveys (acquired between 1991 and 2002 with different parameters) were used which required very careful analysis for matching phase, time and amplitudes. In recent years, techniques for de-noising and demultiple have advanced. The reduction in the noise level of the PreSDM result, compared to the original Poststack time migration result (Fig. 3), is to some degree due to these advancements.

Multiples pose a big problem in many data sets in the region. These are intra-bed multiples that have the same moveout as primaries, and therefore velocity based demultiple techniques failed. Model based techniques were also not successful due to difficulties in defining a proper model. In subsets of the project, Tau-P deconvolution was applied to partly attenuate these intra-bed multiples; In other areas, multiples could not be attenuated without harming the top reservoir primary and therefore remain a challenge for the seismic interpretation.

Velocity Model Building

The geology in the Sirt Basin requires the use of a layered velocity model. Eight layers were parameterized; Each with their own laterally varying V0 and spatially invariant depth gradient and Thomson's anisotropy parameters (delta, epsilon). For the initial model, VSP calibrated sonic logs were

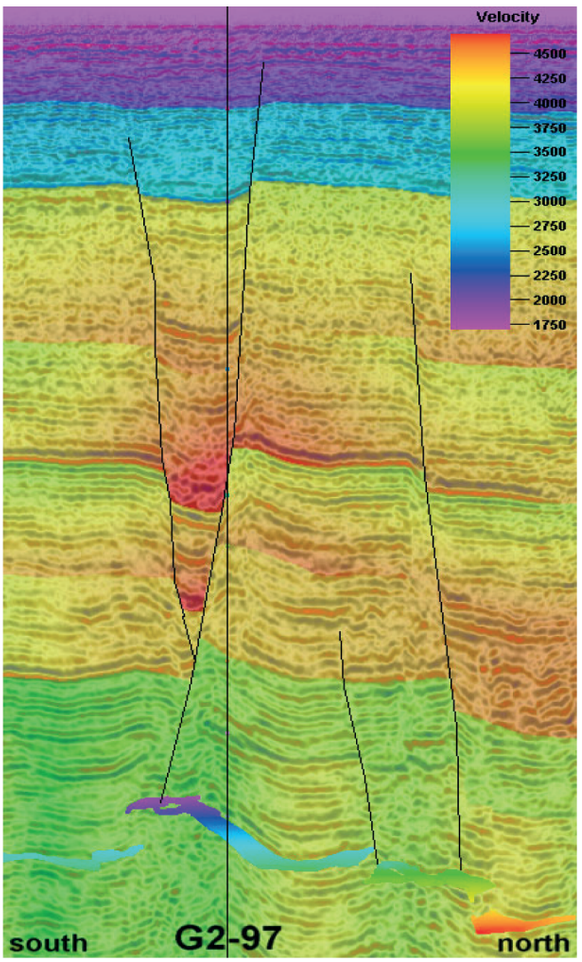


Fig. 2. Overlay of Prestack depth migrated seismic and the corresponding section of the obtained velocity / depth model. A system of long and very steep faults cause the large lateral velocity variations as indicated by the grey background. These lateral velocity changes are the main reason why Prestack depth migration improves the quality of seismic results.

analyzed to determine constant depth gradients for each layer and these were not changed during the model updating. Interpretations of the time seismic and stacking velocities were used in Dix inversion to build the initial model.

In each iteration of velocity model updating, first velocity residuals were picked on the result of a coarse PreSDM (performed with the previous model) then tomographic updates were performed until flatness of image gathers were achieved. When the average well misfit was significant, an anisotropic tomographic update was then performed. Then a structural update migration (usually inlines and crosslines every 500m) was interpreted, and the next iteration could start. Usually four iterations with, two horizons each were performed. Interpretations were performed in the depth domain because vertical depth-time conversions would have introduced significant artifacts around the faults.

Final PreSDM and Post-processing

After completion of the velocity model building process, a full volume PreSDM was applied followed by post migration processing that included residual moveout, stack, and standard Poststack processing steps like deconvolution, filters and scaling.

PROJECT MANAGEMENT

For a successful project, this technology requires significantly more attention and involvement from oil company's geophysicists and area geologists than standard seismic processing techniques. In standard projects, first the seismic processing is performed and only after its completion the result is interpreted. In case of PreSDM, processing and interpretation are coupled. After a first iteration of processing, the interpreter picks the most shallow horizons that are fed back into the next iteration of processing. Only after several iterations of processing and interpretation, a final processing result is obtained that is then subject to final interpretation. Each iteration requires sufficient attention from the oil company's geophysicists and area geologists.

In this project seismic processing was done by WesternGeco in Gatwick and the supervision, coordination and interpretation were performed by Wintershall-Libya in Tripoli and Monarch Technical Services in London, with support from Waha Oil Company. Optimal (fast Internet based) communication and supervision to achieve efficient decision making and team work were key for this successful study.

RESULTS AND DISCUSSION

Figures 3, 4 and 5 compare original Poststack time migration, Prestack time migration and PreSDM (scaled to time for comparison purposes) on a line in the west of the project area. Prestack Kirchhoff time migration (Fig. 4) was tested in an early phase of the project, but although there is some image improvement, compared to the original Poststack time migration (Fig. 3), it is not a convincing improvement. It is the Prestack Kirchhoff depth migration result (Fig. 5) that shows significant improvement in image quality compared to Poststack and Prestack time migration: less noise, more continuous reflections, better focused

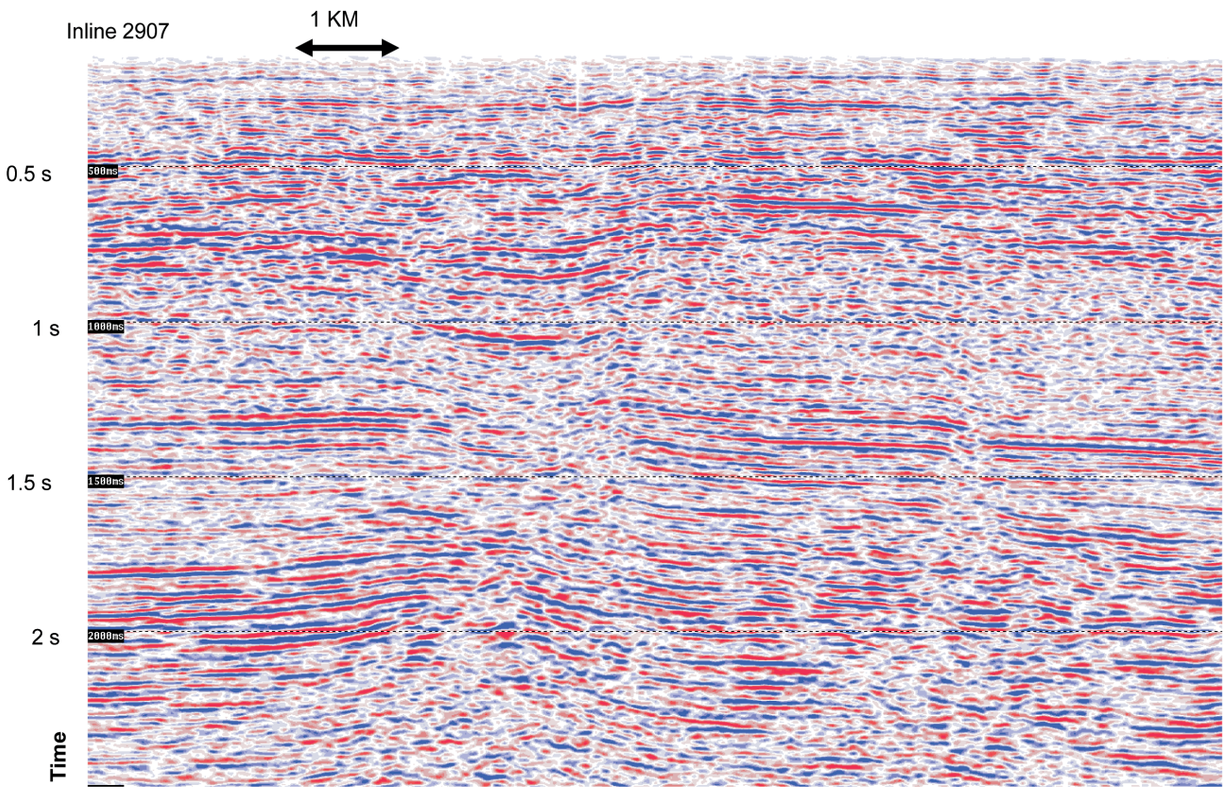


Fig. 3. Standard Poststack time processing result for one inline in the west of the project (for comparison with Figures 4 and 5).

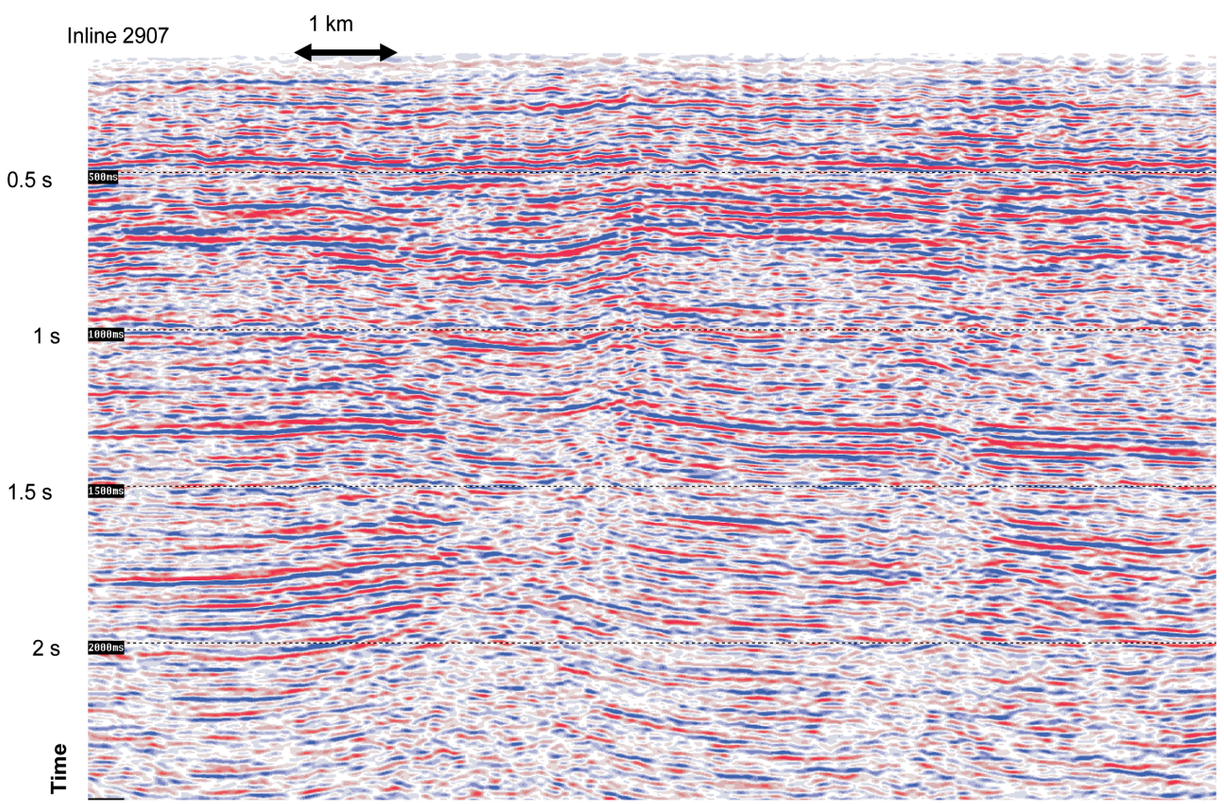


Fig. 4. Prestack Kirchhoff time migration result for the same inline as Figure 3. This test shows some (but not convincing) image improvements compared to Poststack time migration.

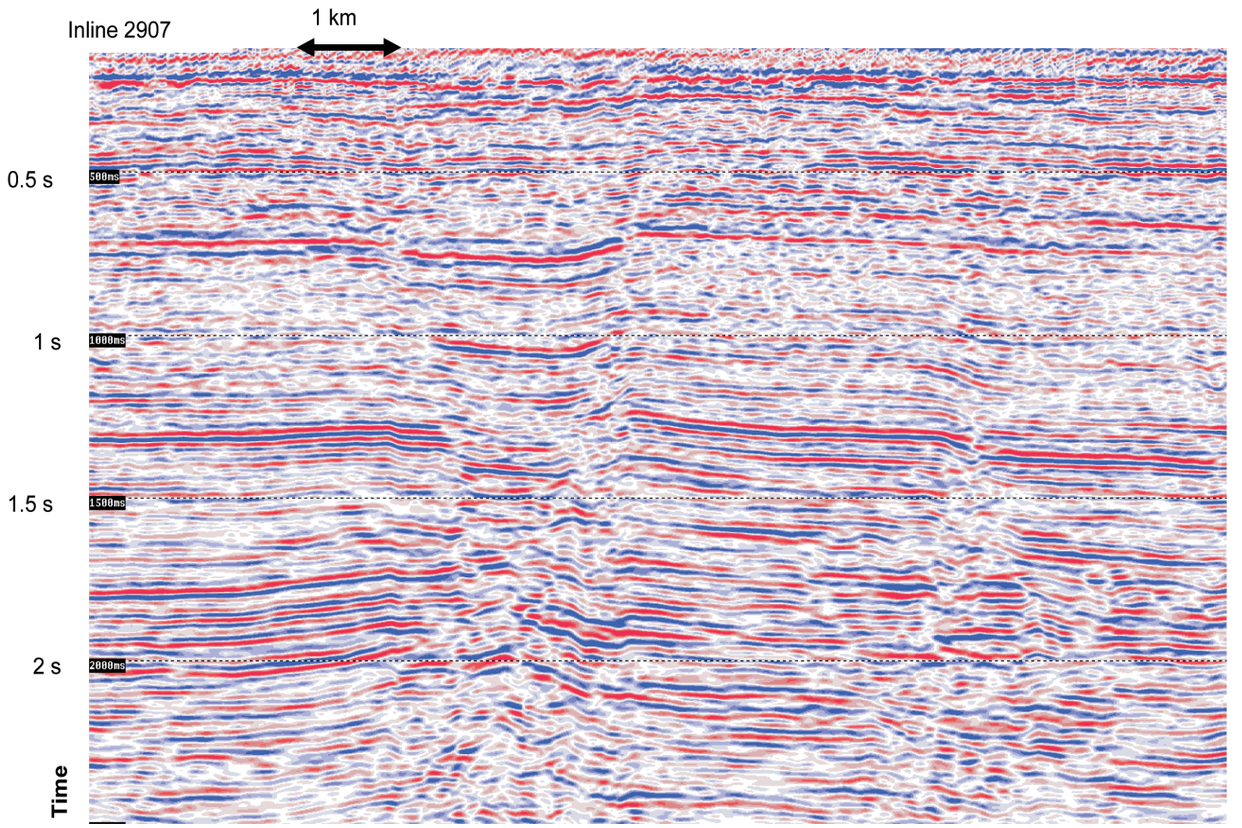


Fig. 5. Prestack Kirchhoff depth migration result (scaled to time for comparison purposes) for the same inline as Figures 3 and 4.

faults and more continuity in the reservoir zone below the faults.

The improved fault definition is even more clear in the comparisons of Figures 6 and 7; the noise reduction and improved reflector continuity is most impressive on Figure 7 where faults that were not visible before on the time migration result become visible. These comparisons are from the centre of the project area.

The Poststack time migration result on the left of Figure 8 shows an apparent time dip that differs significantly from the depth dip (right part of Fig. 8). In Figure 9, the Poststack time migration result shows a false time structure, in depth the reflectors are dipping continuously and don't show a structure. The Prestack depth migration resolves velocity artifacts that are inherent to time seismic as apparent time dip and false structures.

The project had a major impact on one particular well (Fig. 10) originally planned as vertical well to reach a target that appears to be safe on the time seismic, the depth seismic imaged it on the downthrown side of a fault. The well was side tracked by 600m to the up thrown block and hit the target reflector within a few metres of prediction.

The main objective (improved image quality compared to Poststack and Prestack time migration) was achieved and the second objective (to obtain a seismic image in "true" depth that ties *existing* well marker depths within a tolerance of 30 metres) was also achieved. However, one of the wells based on the interpretation of this project came in 112 metres too deep which is far outside the tolerance of the applied technology.

The VSP velocities (left part of Figure 11) showed very high values averaging at 5700m/s within the layer bounded by the horizons Top Megraf and Top Sirte. After further analysis, it was concluded that these anomalous velocities correspond to a steep fault where fluids moved up causing dolomitization of the limestone close to the fault (simplified sketch in the right part of Figure 11). Due to the steepness of the fault, a thick vertical dolomitized section was created. Close to this well, the width of the anomaly (perpendicular to the fault) is in the order of a few hundreds of metres which explains why seismic velocity analysis (every 500 m) was unable to see it. Even high resolution velocity analysis (every 100m) proved unable to see this anomaly due to limited data quality close to the well. The reason why this problem

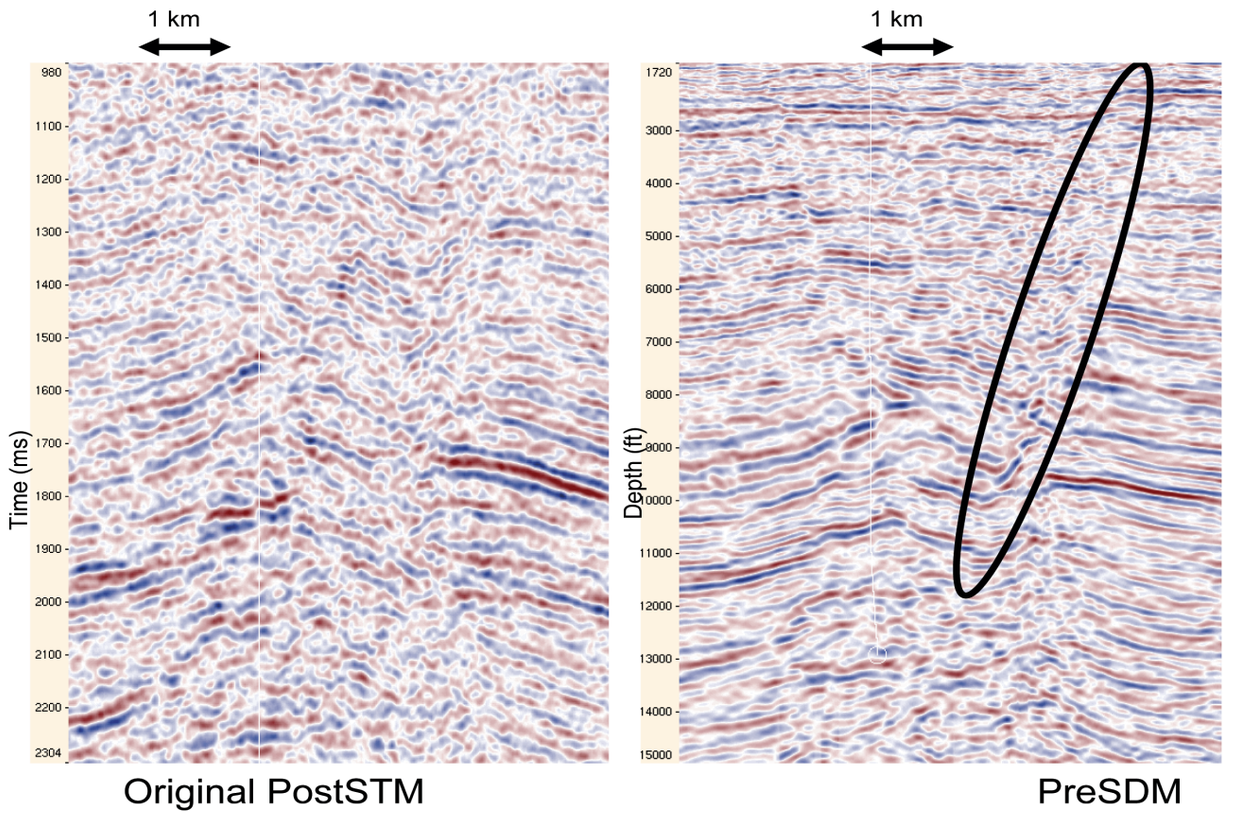


Fig. 6. Prestack Kirchhoff depth migration (right) shows better focussed faults, more continuous reflections, less noise and more continuity in the reservoir zone below the faults compared to original Poststack time migration (left).

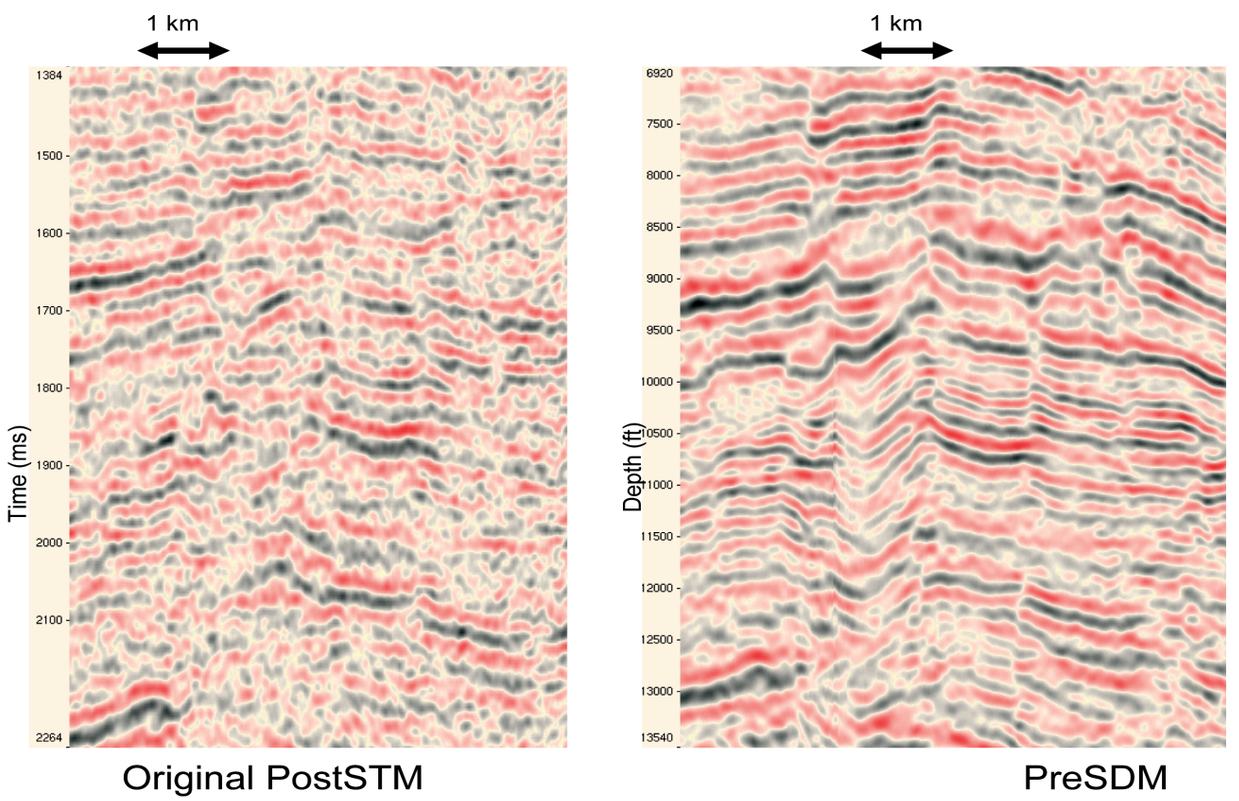


Fig. 7. Prestack Kirchhoff depth migration (right) shows less noise, more continuous reflections and better focussed faults compared to original Poststack time migration (left).

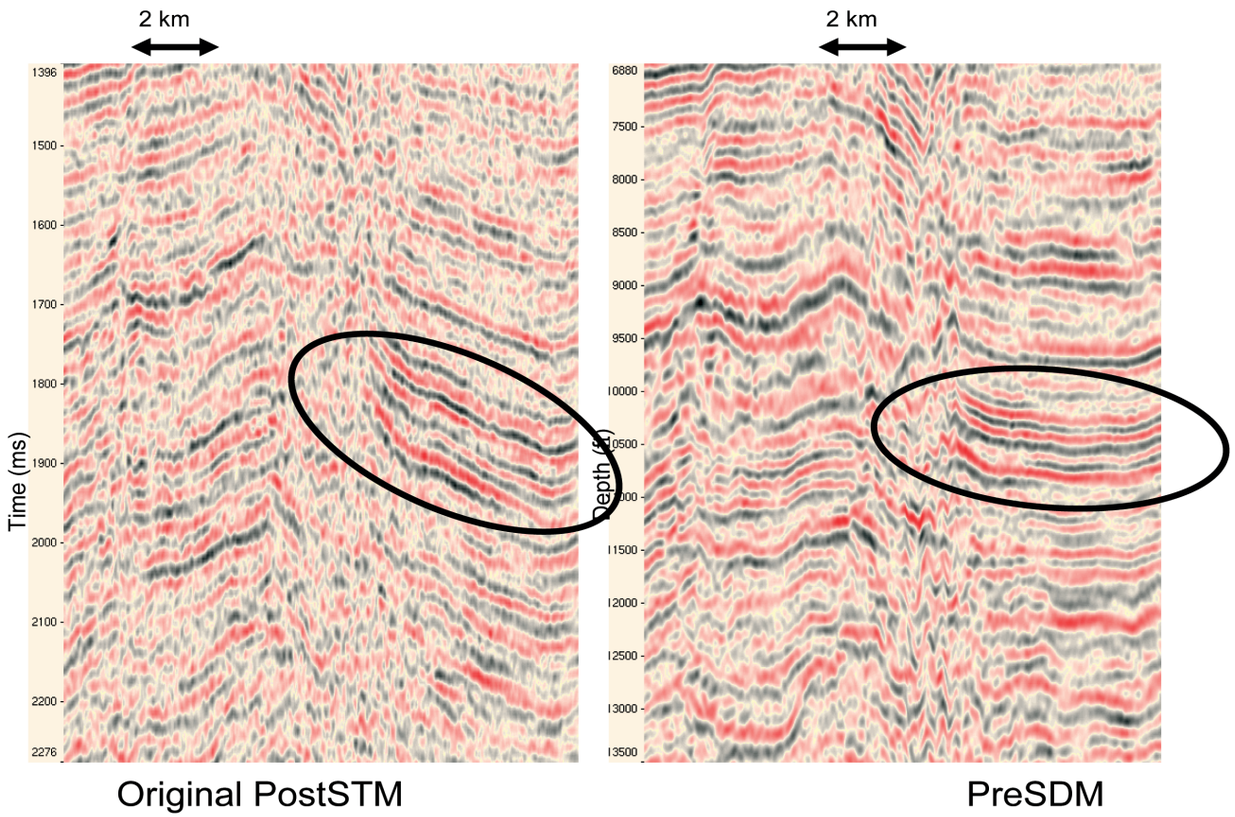


Fig. 8. Prestack Kirchhoff depth migration (right) shows events with a very small dip compared to the apparent time dip visible after Poststack time migration (left).

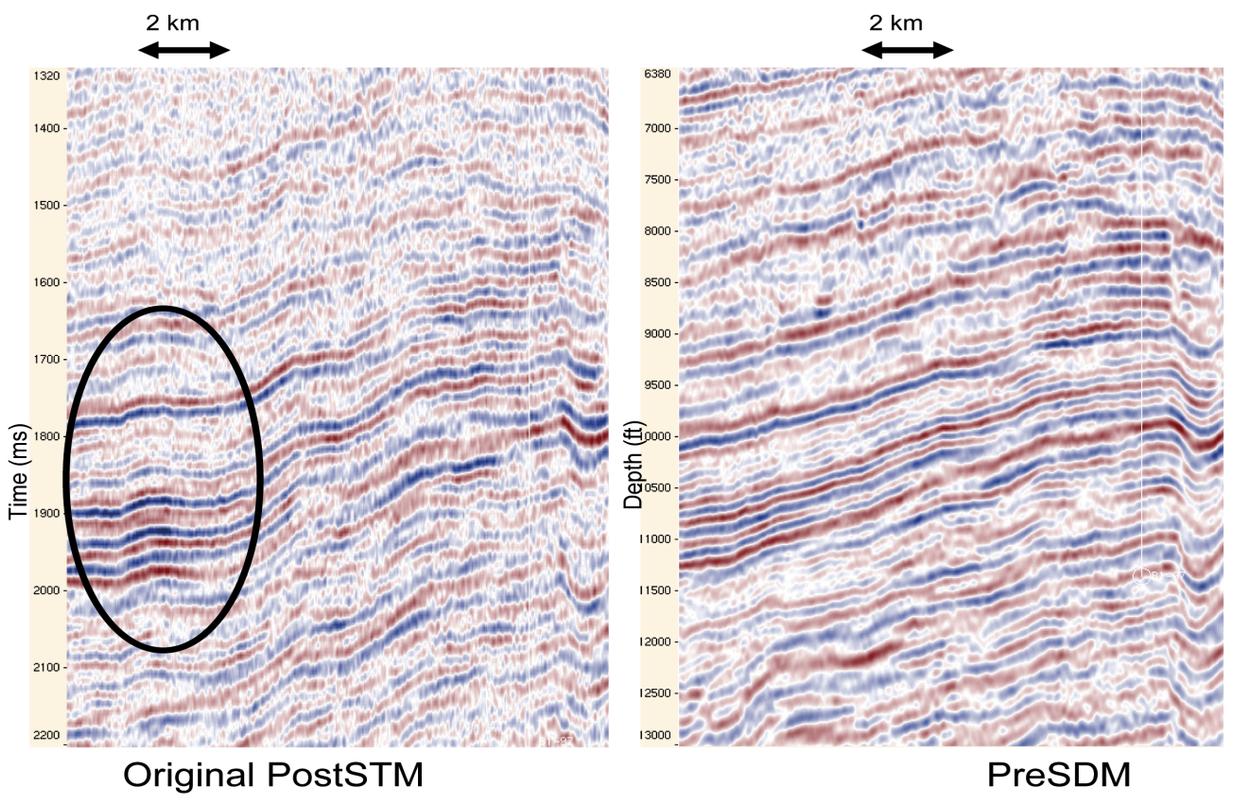


Fig. 9. A false structure visible on the original Poststack time migration (left) disappears after Prestack depth migration (right). This was a velocity artifact.

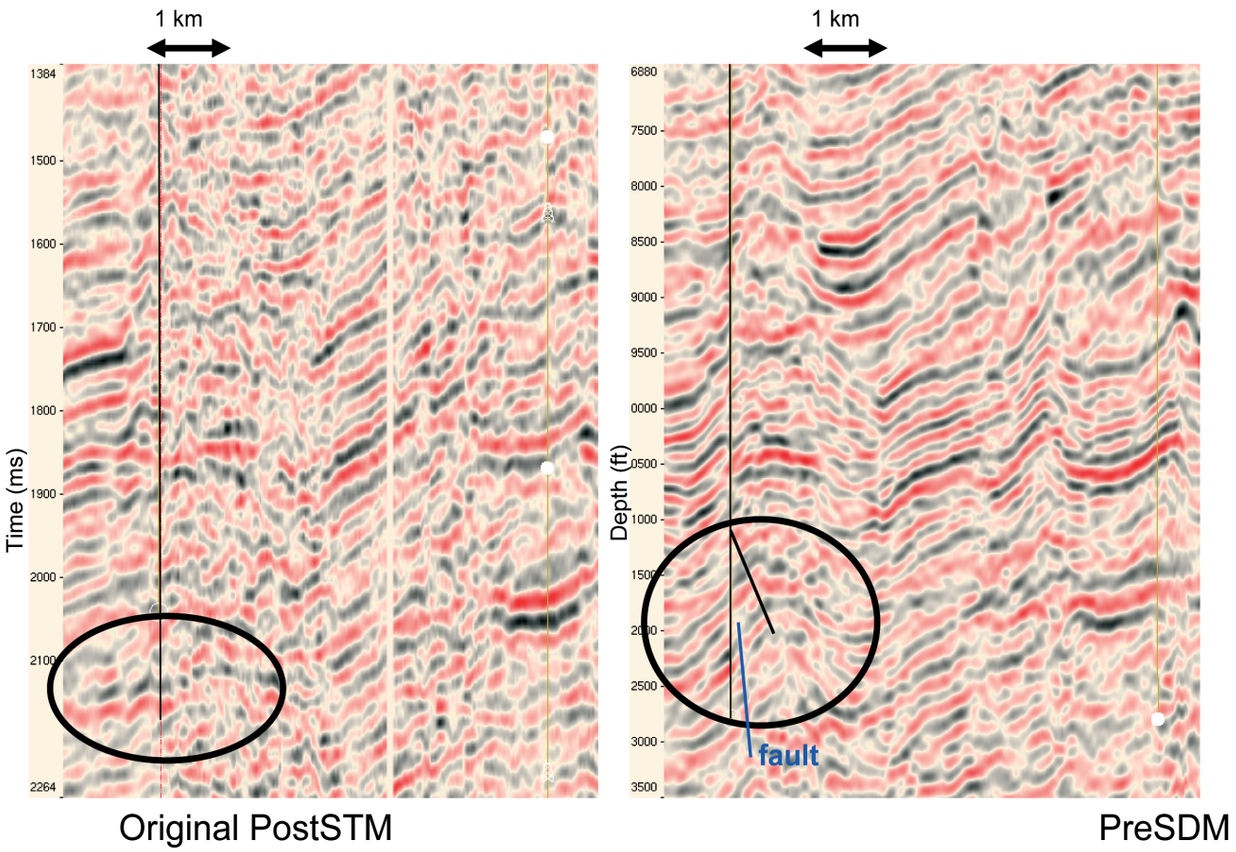


Fig. 10. Major impact on one particular well..

was only encountered after Prestack depth migration is that the Poststack time migrated seismic in the area of this well was so badly distorted that no well had been placed before.

In later phases of the project, special attention was given to identify this anomaly. In the central part of the project, the width has increased to more than five kilometres so that standard velocity analysis was able to see it. In later project phases, much special attention was spent estimating the high resolution character of the velocity model.

Preliminary results from this project have been presented by Hanitzsch *et al*. (2003).

CONCLUSIONS

PreSDM provided a significantly improved image quality compared to Poststack and Prestack time migration: less noise, more continuous reflections, better focused faults and more continuity in the reservoir zone below the faults. Also, artifacts, like apparent dips and false structures on old time seismic data, were removed or corrected after Prestack depth migration.

PreSDM had a major impact on interpretation. In particular, a better integrated fault interpretation was obtained due to the better focus of the overburden. For planning of new wells, it became evident that time seismic images should not be relied on. So far, about a dozen new (exploration and development) wells have been drilled based on the results of this Prestack depth migration project, and in all (but one) cases the target reflector was hit within 60m.

In the study area, dolomitization occurs along steeply dipping faults that can cause very high velocities. If not accounted for in the velocity model, such anomalies can cause depth prediction misfits of more than one hundred metres. Such an anomalous zone can have several hundreds of metres vertical thickness above top Sirte, be very long parallel to faults but only a few hundreds of metres wide perpendicular to fault. Therefore, it is hardly possible to recognize these anomalies with standard velocity analysis and its estimation with high resolution methods can be very challenging depending on data quality. It is sometimes possible to estimate such anomalies from image distortions; they cause deeper down when not taken into account, at least when the background velocities have already been estimated

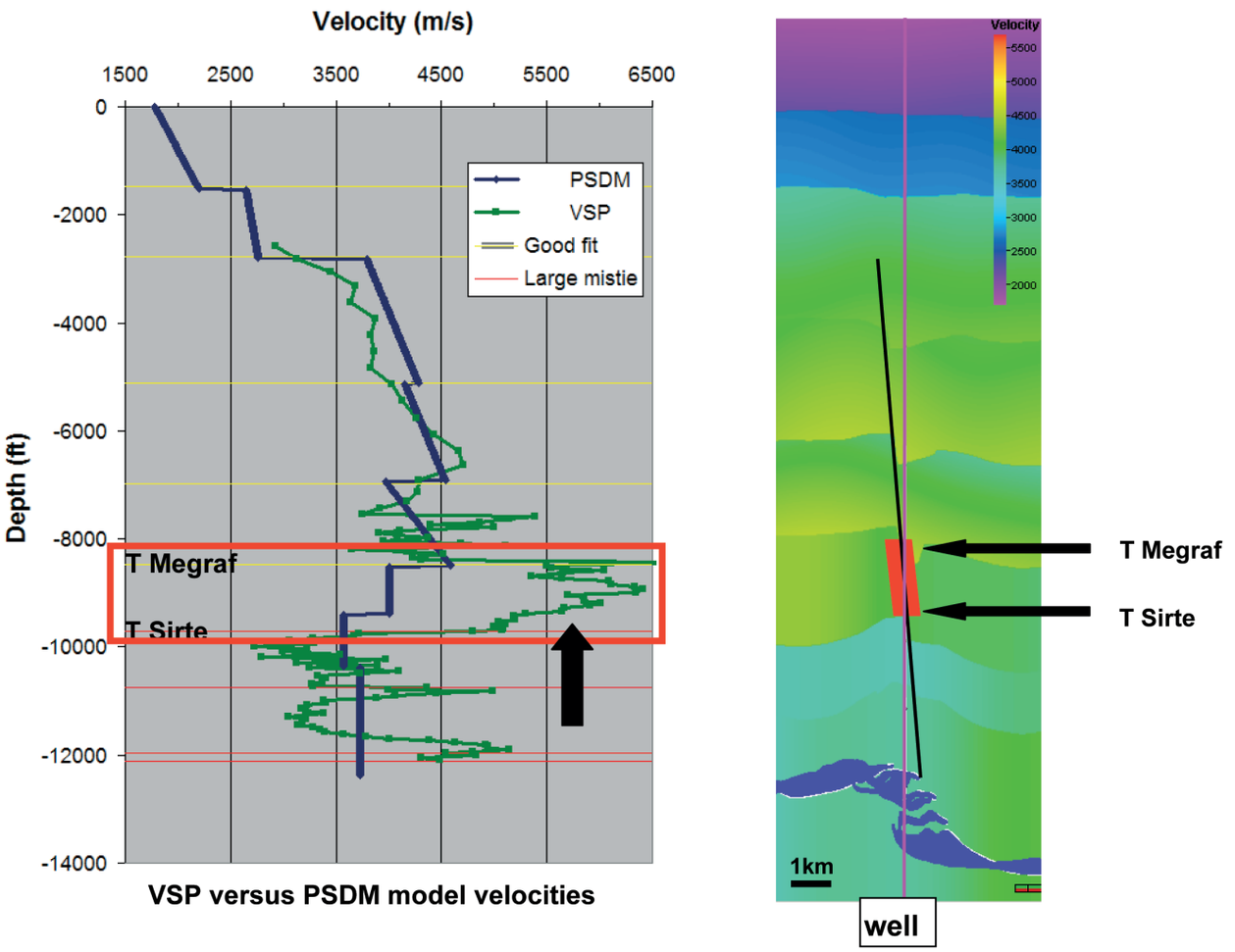


Fig. 11 (left). Measured VSP versus PreSDM model velocities at a particular well location. This well came in 112m deeper than prediction due to the high velocities above Top Sirte. (right). As discussed in the text, these high velocities are due to dolomitization along a major steeply dipping fault.

and data quality is sufficient. This may require several extra iterations during velocity model building. In any case such zones of dolomitization increase the depth prediction uncertainty.

To achieve success, PreSDM requires significantly more attention and involvement from oil company's geophysicists and area geologists than standard seismic processing techniques.

ACKNOWLEDGEMENTS

The authors acknowledge the National Oil Corporation (NOC), Wintershall – Libya, Waha Oil Company and AGIP Oil Company for their important cooperation and contribution to this project. The authors acknowledge B. Braner, B. van der Es, W. Heerde, L. van Veen, L. de Vincenzi (Wintershall – Libya), M. King, N. Sartoretto (Monarch Technical Services), and many colleagues at Waha and at WesternGeco in Gatwick for their technical support. We thank NOC, Wintershall and Waha for permission to publish this work.

REFERENCES

Hanitzsch, C., van der Es, B., King, M., Whitfield, P. and Khlussovich, T., 2003a. Anisotropic prestack depth imaging onshore Libya. 65th Ann. Intern. Mtg., European Association of Geoscientists and Engineers, Expanded Abstracts, **E13**.

Hanitzsch, C., van der Es, B.and Heerde, W., 2003. Prestack depth imaging Onshore Libya. 1st North Africa / Mediterranean Petroleum and Geosciences Conference and Exhibition, European Association of Geoscientists and Engineers, Expanded Abstracts, **S043**.

Petroleum Res. J. Vol. 20 (2007); P. 45–58, 7 Figs.

Integration of Remote Sensing and Geophysical Data: A Case Study of Structural Development and Petroleum Prospectivety of Western Sirt Basin, Libya

Khalifa M. Abdunaser and Giuma Reeh*

دمج معلومات الاستشعار عن بعد والمعلومات الجيوفزيائية: دراسة حالة تطور تكتوني واحتمالات نفطية بمنطقة غرب حوض سرت، ليبيا

خليفة عبد الناصر وجمعة ريح

تم في هذه الدراسة تحليل صور الأقمار الصناعية وتفسير المعلومات الرادارية والجيوفزيائية وبعض سرود الآبار للتعرف على التراكيب الجيولوجية لمنطقة شمال غربي حوض سرت.

إن استعمال التحليل البصري والرقمي لصور الأقمار الصناعية ساعد في تخريط الظواهر والتراكيب التكتونية الإقليمية وعند دمجها مع المعلومات الرادارية تم الحصول على معلومات إضافية أخرى أكثر تفصيلاً. معلومات الجاذبية والمسح المغناطيسي الجوي التي خضعت إلى العديد من التحليل الترددي وتحويل فورير والمصفيات والتحسين الرقمي (المشتقة الرأسية الأولى، الممال الأفقي والكلي) أوضحت أن بعض الشاذات ذات أعماق وأحجام مختلفة.

توجد علاقة قوية بين التكاوين الجيولوجية السطحية والتحت سطحية، وساعدت المعلومات السيزمية في تحديد أعمار وتطور الصدوع. تم توحيد المعلومات السيزمية والجيوفزيائية الأخرى مع تفسير المعلومات الرقمية للأقمار الصناعية باستخدام منظومة المعالجة الرقمية (ER Mapper Software) ووضعها على هيئة طبقات باستخدام منظومة المعلومات الجغرافية (ArcGIS).

تمتاز منطقة الدراسة بتواجد كثيف للتراكيب الجيولوجية ذات الاتجاه شمال شمال غرب إلى جنوب جنوب شرق متعامدة مع تراكيب جيولوجية اقل وضوحاً تأخذ الاتجاه شرق شمال شرق إلى غرب جنوب غرب ويعتقد إنها الأحدث عمراً والتي يحتمل تأثرها باتجاه الحركة الهرسينية التي تتوافق مع التراكيب الجيولوجية الإقليمية لمنطقة غربي حوض سرت.

تم تحديد بعض المجاميع التركيبية والمعالم الاستكشافية المرشدة بناءاً على تواجد التراكيب الجيولوجية السطحية التي تظهر على صور الأقمار الصناعية والتي تتوافق مع التراكيب الجيولوجية التحت سطحية التي تم تحديدها بواسطة المعلومات الجيوفزيائية. ويعتقد إن المعالم التركيبية المرشدة هي مصائد تركيبية كما تظهر على صور الأقمار الصناعية والتي تم تحديدها بناءاً على وجه التشابه مع التراكيب الجيولوجية للحقول النفطية المكتشفة بالمنطقة.

Abstract: *Satellite image analysis, radar data interpretation, gravity, magnetic data available seismic reflection profiles and well logs, have been used to define the geological structure of the northwestern portion of the Sirt Basin, Libya.*

Visual and digital satellite image analysis have enabled, rapid mapping of the regional tectonic structures and features while when merged with radar revealed additional and more detailed information. The gravity and the aeromagnetic data were subjected to several analytical and FFT frequency-based analyses, filtering and image enhancements including first vertical derivative, horizontal gradient and analytic signal have

* Libyan Petroleum Institute, P O Box: 6431, Tripoli-Libya.

showed anomalies from sources of various size and depth.

They established a good relationship between the surface and subsurface structure, such as the identification of basement structure while integration of regional seismic lines helped to establish the structural and timing of fault development. The representative seismic lines and regional Potential Fields data have been co-registered and scaled to fit the digital satellite image interpretation maps using ER MAPPER and ArcGIS software. The study area is characterised by a strong NNW-SSE structural grain with less ENE-WSW trending structures that appear to be superimposed on the NNW-SSE structures. The later trend may be influenced by pre-existing Hercynian structure, which is consistent with the regional structure of the western Sirt Basin.

A number of structural domains and exploration leads were identified based on the surface structures expressed on satellite imagery, and generally, show good correlation with regional subsurface structural features defined by seismic and potential fields data. The leads are primarily structural traps with a related surface expression as interpreted from the data used. The structural setting of existing oil fields in the region were used as analogues for assessing the exploration potential of the surface structures.

INTRODUCTION

The study covers the western Sirt Basin, Libya (Fig. 1). It has been undertaken jointly by the Libyan Petroleum Institute, Infoterra and Teknica and is part of a larger programme to investigate the geology and hydrocarbon evaluation of Tertiary and Mesozoic rocks of the Western Sirt Basin of Libya. The main objective of this study is to delineate the geological structure of northwestern Sirt Basin.

Methodolgy

The study involved the following:

1. Acquisition and processing of 13 scenes of Landsat TM and 31 scenes of ERS SAR
   - The Landsat TM and ERS data were digitally enhanced.
   - Landsat TM Bands 7,4,2 were selected and displayed as red, green, and blue *(RGB);*
2. Generation of a merged Landsat TM/ERS SAR satellite image mosaic;
3. Structural geological interpretation of Landsat TM and ERS SAR satellite imagery;
4. Gravity and Aeromagnetic data were subjected to several analytical and FFT frequency-based analyses, filtering and image enhancements including first vertical derivative, horizontal gradient and analytic signal;
5. Integration of subsurface structure derived

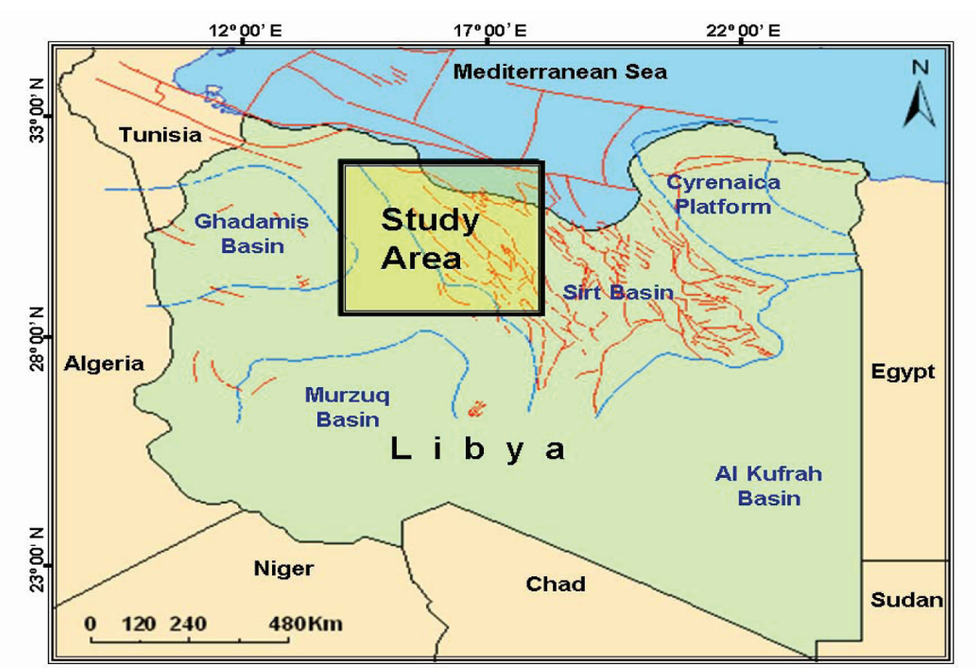


Fig. 1. Location map of western Sirt Basin study area.

from interpreted seismic profile, well correlations, oil fields and potential field data.

Geological interpretation was performed digitally on-screen using ArcGIS software, scales ranging from 1:100,000 – 1:250,000, and hardcopy satellite imagery at a 1:250,000 scale and a 1:500,000 scale was used to provide a 'regional' context during the on-screen geological interpretation.

TECTONICS

The Sirt Basin is the youngest and the greatest petroleum-bearing basin in Libya. The eastern half of the study area has been extensively surveyed for its oil exploration during the past century. The evolutionary history of the Sirt Basin is complex and marked by at least two main tectonic events (Ahlbrandt, 2001; and El-Batroukh and Zentani, 1980); namely the Hercynian Orogeny at the end of Palaeozoic time and the extensional "rifting" event in Pre-Cretaceous to Paleogene time.

The Hercynian Orogeny led to the formation of the entire basin and to the creation of northeast-southwest structural trends. The Pre-Cretacous to Paleogene rifting event led to the generation of a series of northwest-southeast oriented grabens and horsts bounded by deep-seated normal faults that step progressively downward to the east in the basin. Block faulting is the common tectonic style in the Sirt Basin.

The complex tectonic history of the Sirt Basin resulted in the formation of multiple reservoirs and conditions that favored hydrocarbon generation, migration, and accumulation, principally on or adjacent to the horst blocks (Ahlbrandt, 2001). Carbonate reservoirs, mostly of Palaeocene and Eocene age, are also concentrated on the structural highs in the central Sirt Basin (e.g. Az Zahrah Platform). These reservoirs were in turn charged by vertical migration along faults during the peak of petroleum generation period of the early Tertiary.

STRATIGRAPHY

The surface stratigraphy of the western Sirt Basin (Fig. 2) is dominated by sedimentary rocks ranging in age from Late Cretaceous to Tertiary with the exception of scattered Precambrian and Cambro-Ordovician outcrop of the Al Qarqaf Arch in the southwest.

STRUCTURAL GEOLOGICAL INTERPRETATION OF THE SATELLITE IMAGERY

Hun Graben

The Hun Graben is a present-day fault bounded basin 305km long, and 33.5-48km wide (Fig. 3). The graben trends NNW-SSE, although its southern end changes to E-W and links with the Zallah Trough and is infilled mainly by Oligocene Mazul Ninah Formation.

The Hun Graben appears to cross-cut existing northeast draining wadi channels (Fig. 3). Along the western margin of the basin, wadis generally narrow and become incised as they approach the margin of the graben, indicating that they have been rejuvenated by the formation of the graben. The northeast draining channel is deflected as it enters the Hun Graben suggesting that it was possibly modified by development of the Hun Graben in the Oligocene time.

A number of open folds have been interpreted within Mazul Ninah Formation along the margins of the graben. The folds have probably formed in response to drag in the hanging wall to the basin bounding faults or possibly due to roll-over or non-planar fault trajectories in the subsurface. Lava flows of Jabal As Sawda in the SW of the area appear to post-date the N-S trending faults.

Waddan Uplift

This uplift is a gentle NNE tilted block narrowing in the north before it disappears below the coastal plain. It is a convex to the south, bounded by fault with downthrow to the SW, S and SE. The common trend is ENE-WSW, then NNW-SSW to NW-SE. N-S and E-W trending faults are also developed.

The northern half of the uplift is characterised by north and north-northeast dendritic drainage down the sub-horizontal dip slope of the structure. A more organised trellis drainage pattern has developed towards the northern end of the structure parallel to the NNW-SSE and ENE-WSW trending fracture system. Elongated erosional escarpments of more resistant lithologies and/or fault scarps may also control linear NNW-SSE trending wadi channels (Fig. 3). The NNE dip slope is also cross-cut by a N-S trending minor fault system which appears to be the onshore extension of an offshore fault trend. The SE part of the Waddan Uplift appears to be associated

Era	Period		Epoch	Unit Name	Lithology
Cenozoic	Quaternary		Recent	Fluvio-eolian and recent wadi deposits	Fluvio-eolian and recent wadi deposits
			Holocene	Sabkha deposits	Sabkha deposits
			Pleistocene	Ancient wadi terraces	Ancient wadi terraces
	Tertiary	Pliocene	Pleistocene	Al Hishah Fm.	Fine gypsiferous marl, calcarenite, and sandy clay
		Miocene	Langhian	Al Khums Fm.	Limestone, many limestone and calcarenite
		Oligocene	Chattian	Upper Member of Mazul Ninah Fm.	Gypsum manly limestone
			Rupelian	Lower Member of Mazul Ninah Fm.	Gypsum, marl sandy limestone
		Eocene	Lutetian-Priabonian	Wadi Thamat Fm.	Marl, limesone and dolomitic limestone
			Ypresian-Lutetian	Al Jir Fm.	Chalky to manly dolomite and dolomitic limestone
			Thanetian-Ypresian	Bishima Fm.	Gypsiferous marl to manistone, dolomite, chalky dolomite and limestone
		Palaeocene	Thanetian	Shurfah Fm.	Limestone, marl, many limestone, calcarenite and calcilutite
			Danian	Upper Member of Zimam Fm.	Calcenous dolomite to dolomitic limestone
Mesozoic	Cretaceous		Maastrichtian	Lower Member of Zimam Fm.	Marl, marly limestone
			Campanian	Mizdah Fm.	Limestone, marly limestone and gypsiferous
			Turonian-Coniacian	Qasr Tigrinnah Fm.	Limestone, manly limestone, sandstones, and gypsum and clay
Palaeozoic			Cambrian	Al Hassaouna Fm.	Conglomeratic sandstone
Precambrian			Precambrian	Basement	Basement

Fig. 2. Generalized str0atigraphy of the study area (After Mijalkovic, N. 1977, Said, M. 1981, and Zivanovic, M. 1977).

with a downthrown fault block, which is defined by a broad low amplitude anticlinal structure that developed in Wadi Thamat Formation.

Zallah Trough

The limits of Zallah Trough are well defined at the surface and the SW margin is bounded by a north downthrowing, normal fault zone. Large triangular bedding facets or flat-irons indicate E dipping strata into the trough along the eastern end of the Al Qarqaf Arch.

The structure of the Zallah Trough is characterised by an increased intensity of faults and fault related folds (drag-folds which are typically narrow asymmetric monoclinal structures). Larger very low amplitude, periclinal folds with four-way closure and shallow plunge are also present (Figs. 3 and 4).

Elongated asymmetric synclines associated with shallow west limbs and steeper dipping east limbs

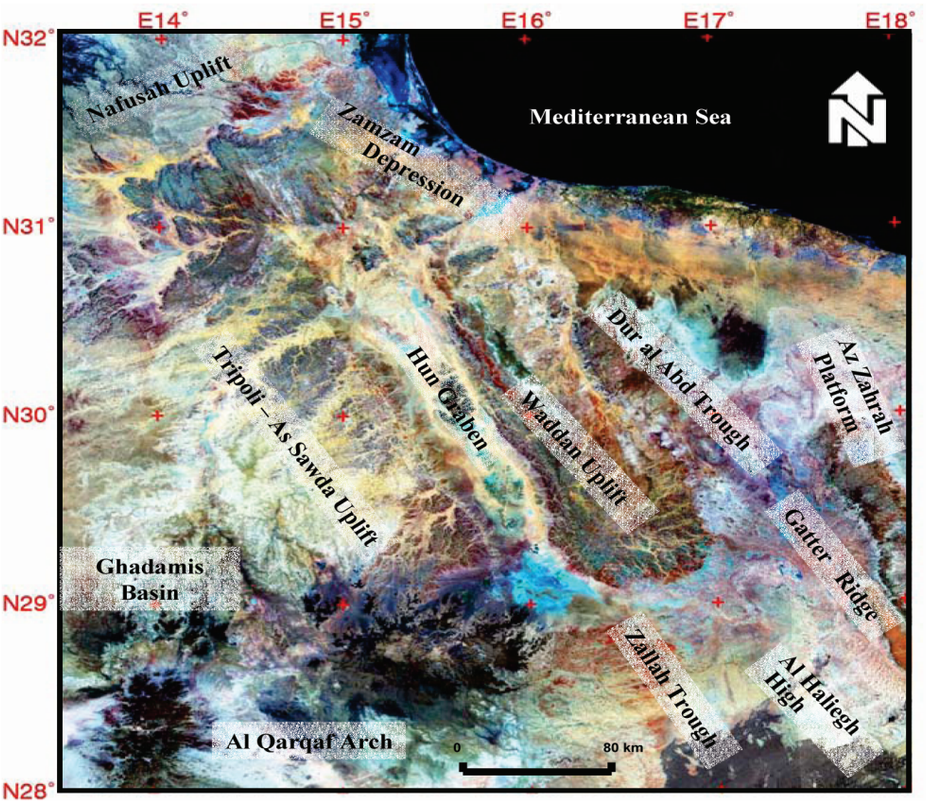


Fig. 3. Landsat 5 TM image bands 7, 4 , 2 displayed as red, green, and blue *(RGB)* shows the main interpreted structural elements of the study area.

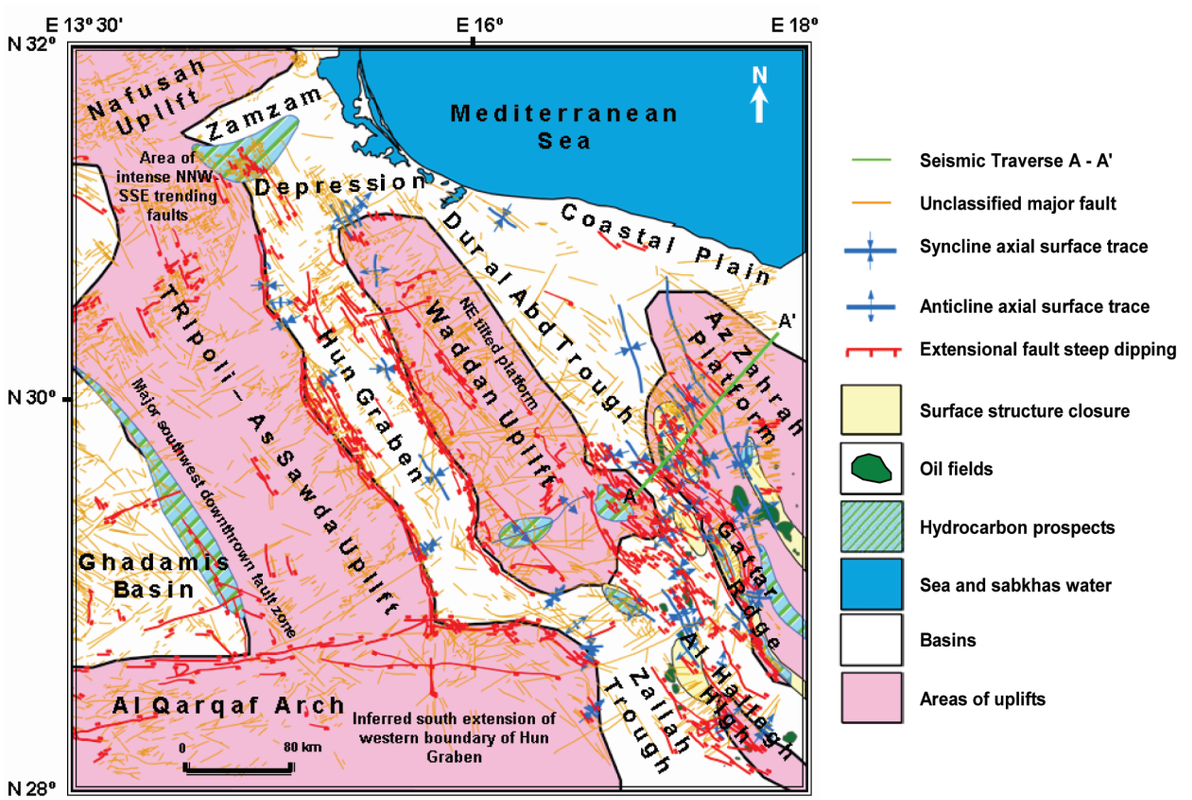


Fig. 4. Structural overview map based on satellite image interpretation.

are developed in the hanging wall and adjacent to west down throwing normal faults. The eastern margin of Zallah Trough is marked by a series of major fault scarps which coincide with a normal fault zone defining the western edge of the Gattar Ridge and Az Zahrah Platform. The preservation of Oligocene sediments is suggestive of subsidence at Late Tertiary-Quaternary times.

The Zallah Trough contains a number of subtle low amplitude periclinal structures which are exposed at surface. Most of these surface structures are associated with the following producing oil fields (Fig. 4).

Karim Oil Field:- It is a NNW-SSE trending periclinal structure expressed at surface in Mazul Ninah and Al Khums formations. It has a gentle plunge to the SSE and may be structurally closed at its northern end by NE-SW trending transverse faults associated with normal displacement. Many NW-SE trending normal faults intersect the structure with a downthrow dominantly to the southwest.

The main axis of the structure is 38km long and its width is 24.5km at surface. It is separated from the Aswad and Zallah oil fields to the north by a narrow NE-SW trending basaltic lava flow that occupies a topographically inverted palaeodrainage system.

Aswad and Zallah Oil Fields:- They are associated with a large subtle domal structure, 27km long by 22.5km wide expressed at surface within Mazul Ninah and Al Khums formations. The Mazul Ninah Formation is exposed in the erosional core of the structure. The fold structure is bounded by a NNW-SSE trending fault on its eastern side with down throw to the west and a similar trending normal faults are occur near the crest of the structure.

Hakim and Fidda Oil Fields:- These oil fields are associated with a narrow NNW-SSE trending surface anticline expressed in Al Khums Formation and Late Tertiary-Quaternary sediments. The anticline is closely associated with faults which are oblique to the main fold structure and are splays to a major fault zone to the east (Fig. 4). The structure is approximately 36.5km long and 4km wide.

Mellugh, Ghani and Zenab Oil Fields:- These fields are located in the vicinity of a NNW-SSE to NW-SE trending arcuate fault zone associated with normal downthrow to the west (Figs. 3 and 4). Localised folds are developed within the fault zone.

Daba, Gsur, Tagrifet and Facha Oil Fields:- They are situated on a NNW-SSE trend north of a synclinal area on the hanging wall side of the boundary fault of the Gattar Ridge. Faults in the vicinity of the fields downthrow to the northeast along strike continuation of the eastern boundary faults of the Waddan Uplift.

Al Haleigh High

The Al Haleigh High is a NNW-SSE trending narrow basement ridge or horst block which protrudes into the southern part of the Zallah Trough (Fig. 4). The surface structure appears to suggest that there is a lateral continuation of this feature northwards to the southern edge of the Waddan Uplift. The Hakim and Fidda oil fields are on strike with the Al Haleigh High, while two broad, low amplitude periclines at surface may be related to the reactivation of faults bounding the Al Haleigh High. The fields are represented at the surface by periclines developed mainly in Wadi Thamat Formation.

Dur al Abd Trough

It forms the northern extension of the Zallah Trough and primarily follows the NNW-SSE trending structural grain of the region. The transition between the Zallah and Dur al Abd Trough coincides with the northern end of the Gattar Ridge, close to the location of the ENE-WSW trending transverse zone. Dur al Abd Trough contains two main fault trends:

- NNW-SSE dominant fault trend of the Sirt Basin, associated with a subsidiary later ENE-WSW transverse fault set;
- N-S trending faults which become evident on the northeastern dipping flank of the Waddan Uplift and extend into the Dur al Abd Trough. These faults represent a new fault trend and may indicate the presence of a different structural regime offshore.

Gattar Ridge

The Gattar Ridge is coincident with a 15km wide, 120km long NNW-SSE trending northeast tilted panel of Al Jir Formation at surface. The western edge of the fault block is bounded by a fault zone up to 1km wide, consisting of overlapping parallel normal faults consistently down throwing to the west.

It is also associated with horsetail splay faults which may indicate a component of sinistral strike-slip. The panel is bounded to the north-northwest by an ENE-WSW trending transverse fault. To the north-northwest, the Gattar Ridge dies out into an area of close spaced faults with NW-SE trend. The faults cross-cut Wadi Thamat Formation, Upper and Lower Members of the Mazul Ninah Formation and Late Tertiary-Quaternary deposits. The dominant fault trend is NNW-SSE (Fig. 4) and subsidiary E-W and NE-SW faults sets are also developed.

Az Zahrah Platform

The northern end of the Az Zahrah Platform (Fig. 4) is expressed at surface in the north by a homoclinal shallow NE dipping and marked by a NNW plunging nose of a large low-amplitude anticline. It is cross-cut by a 15-20km wide NE-SW trending fault zone while the dominant fault trend is NNW-SSE. Many NNW-SSE trending low amplitude gentle flexures are expressed by erosional features and surface geomorphology. An anticlinal monoclinal fold defines the western margin of the platform. The boundaries of the fault zone are defined by:

- NE-SW trending monoclinal flexures in the bedding that provide a relative sense of downthrow across the fault zone; and
- Changes in the amount of plunge of the NNW-SSE trending fold hinges of the Az Zahrah Platform and adjacent Gattar Ridge.

Five major oil fields are located along the western crest of the Az Zahrah Platform:

Bahi Oil Field:- It is situated on the northern end of the Az Zahrah Platform, approximately 14km to the south of the NE-SW trending transverse fault zone in the erosional window developed above the structural crest of the Az Zahrah Platform, 4.5km east of the fault bounded western margin of the platform.

Dahra Oil field: It is situated within a NNW-SSE trending open syncline east of the monoclinal margin. NE-SW trending transverse faults occur in the area.

Jofra Oil Field: The field is situated to the east of the monoclinal margin in a structural position similar to the Dahra field. A significant NE-SW trending, possibly fracture controlled, erosional window is present to the north of the field.

Ali and Almas Oil Fields: The two fields are located on the gentle northeast dipping limb of the Az Zahrah Platform

Eastern Ghadamis Basin

This uplift is characterised by a gentle northeast dipping region of Tertiary strata with a relatively simple structure and well established dendritic drainage pattern. The dominant structural grain is NNW-SSE to NW-SE trending faults associated with down throw to the WSW, opposite to the drainage direction.

Towards the west, a NW-SE to WNW-ESE trending set of faults becomes evident and the fault zone is on-trend with the Pan-African Al Haruj Uplift. This feature forms the divide between the Ghadamis Basin and Zamzam Depression.

Nafusah Uplift

This is a major E-W trending topographic ridge which forms a major drainage divide in the northwestern part of the study area. The uplift is associated with the exposure of Cretaceous lithostratigraphic units in the study area. The structure is considered to be a Late Palaeozoic to Mesozoic Hercynian structure (Klitzsch, 1971; Anketell, 1996). The structure forms the northern boundary of the Ghadamis Basin. The southern margin is fault bounded at least in part in the subsurface, but this is not evident on the satellite imagery. Eocene tectonism is the primary cause for the emplacement of flood basalts. The Nafusah Uplift is associated with N-S and NE-SW trending faults (Fig. 4).

Al Qarqaf Arch

The Al Qarqaf Arch is an E-W trending Hercynian structure located on the southwestern edge of the study area and exposes Neoproterozoic basement rocks and Palaeozoic sedimentary sequences onlapped by Oligocene cover rocks. Regionally the structure forms a WSW-ENE topographic high which separates the Murzuq and Ghadamis basins. The core of the structure is formed by Jabal Hasawnah, which is elevated 800m above mean sea level.

The structural grain of the Al Qarqaf Arch is dominated by ENE-WSW trending faults and resistant ridges (possibly silicified relict fault planes and/or igneous dykes)?. Subsidiary WNW-ESE to NW-SE and N-S trending faults also occur (Fig. 4).

Tripoli-Tibisti and Al Haruj Uplifts

The Tripoli-Tibisti and Al Haruj Uplifts are subsurface Pan-African basement highs which trend NNW-SSE across the western part of the study area to the west of the Hun Graben. The actual position and effect of these structures on the surface geology and geomorphology is unclear. The Tripoli-Tibisti Uplift is coincident with the alignment of volcanic rocks emplaced during the Eocene to Recent. Reactivation of basement faults related to either of these two structures may be responsible for the location of the NNW-SSE trending, west-southwest down throwing normal fault zone (Figs. 3 and 4).

Zamzam Depression

The surface expression of the Zamzam Depression is extremely subtle on the satellite imagery (Fig. 3). The structure represents the eastern extension of the Ghadamis Basin and is overlain by the western margin of the younger Sirt Basin. The Ghadamis Basin and Zamzam Depression are 'separated' by the NNW-SSE trending Tripoli As Sawda Uplift. The Zamzam Depression may be coincident with the northward plunge of the Hun Graben. The region associated with the Zamzam Depression is dominated by NNW-SSE trending faults associated with minor normal displacement (Fig. 3). ENE-WSW trending cross-cutting faults are also developed.

A 10-15km wide ENE-WSW fault zone also transects the northern end of the Hun Graben possible indicating the southern margin of the Zamzam Depression (Fig. 4). The boundaries of the fault zone are indicated by narrow anticline and syncline monoclinal folds

SEISMIC IRETATION

The available seismic data has provided support for the interpretation and understanding of the geological history as a geologic framework that integrates the surface and subsurface geologic data with geophysical data of the western part of the Sirt Basin. The data used was compiled and processed by Teknica Company as part of a larger study on the geology and hydrocarbon evaluation of Tertiary and Mesozoic rocks of the western Sirt Basin of Libya.

This work contains an interpreted seismic traverse profile that has been composed from individual seismic lines of different vintages and different field acquisition and processing parameters. Teknica's procedure for handling line-to-line mis-ties based on different seismic datum has been incorporated into the combined traverse sections. Because there are no long lines that cross the whole study area, several shorter lines (usually of different seismic vintages) had to be combined. This sometimes resulted in data gaps and offsets between the adjoining lines.

The selected section crosses the south-eastern margin of Waddan Uplift to the south-western of the section and extends into the boundary line between Az Zahrah Platform and Maradah Trough to the north-east. It shows the location of, and difference in, structural complexity of the platforms and adjoining troughs and also helps to illustrate the major tectonic elements. The seismic section used in this study is about 225Km in length and shows two gaps, 2.8km and 7km in length (Fig. 5).

The hinge zone between the Waddan Uplift and the Dur al Abd Trough contains many (about 8) large down-to-basin faults, two of which appear to extend to the surface. Many smaller, additional faults with both down-to-basin and down-to-margin throws are believed to be present. The apparent throws of the large eight faults vary between ~ 10 and 350 ms (15 and 525 m). It has been anticipated that all of these hinge zone faults will have some lesser degree of wrench movement.

The dimensions of the Dur al Abd Trough are difficult to determine on this section, but they appear to extend from about point x1 to x2. The sedimentary section extends below the maximum time indicated on plotted seismic section (~ 3000m) and is expected to include rocks of pre-Cretaceous to Oligocene age. Within the trough, the bedding is broken by numerous down-to-basin and antithetic faults; most of which show some growth, indicating either reoccurring normal or wrench faulting in conjunction with slump faulting associated with the rapid compaction of the sedimentary column within the trough as it accumulated basin fill.

In the hinge zone between the Dur al Abd Trough and the Az Zahrah Platform a major anticline broken in places by both down-to-basin and down-to-margin faults exists and its reservoirs have been the target of a large number of Concession 17 wells (Mabruk Field). Some of the large faults of the area extend to, and have been observed cutting through, the Upper Eocene sediments that outcrop at the surface.

Generally on the Az Zahrah Platform, the Cretaceous to Oligocene sedimentary section consists

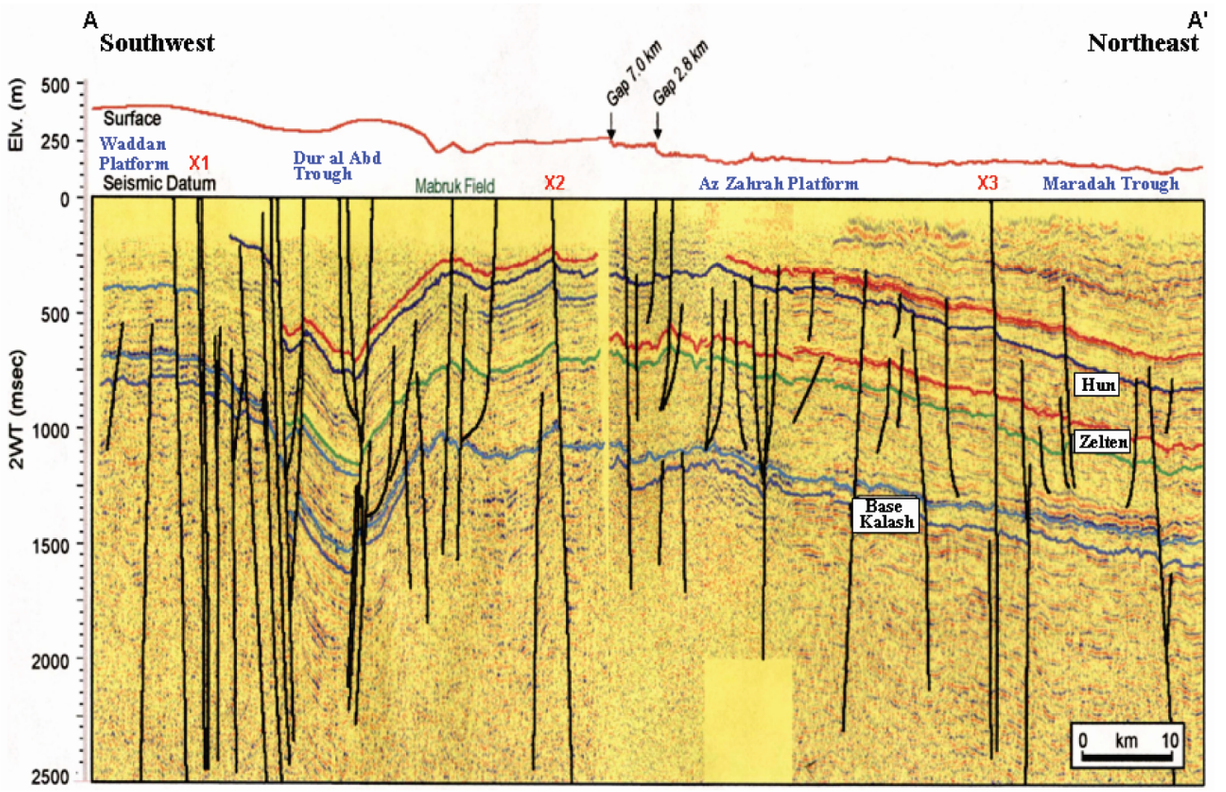


Fig. 5. A selected seismic traverse (A-A') crosses the Waddan Uplift through Dur al Abd Trough and Az Zahrah Platform to the western boundary of Maradah Trough.

of a sequence of almost parallel-bedded strata that dip gently to the northeast (at ~1-5°) and thin by ~5%. The sediments in the Az Zahrah Platform are also fractured by numerous faults, some with pop up compressional features, but the majority have the appearance of being primarily of normal (tensional) origin and may be partially of wrench tectonic origin.

Some normal faults terminate below the near base Kalash seismic time marker. Some faults that are basement rooted extend to the surface. Some faults are antithetic to basement- rooted faults. Basement-rooted faults and those antithetic to them show fault patterns similar to "flower" structures. Several of the larger Az Zahrah Platform faults that are observed on this seismic traverse extend to the surface, where they have been mapped cutting the Upper Eocene and Oligocene formations on the western margin of the platform.

The boundary between the north-eastern edge of the Az Zahrah Platform and the Maradah Trough seems to be present at point x3 close to a large NE dipping, normal fault that extends from the surface to the bottom of the seismic section. This hinge zone is only weakly deformed, being fractured by a small number of faults. The apparent throws of these faults are also small, in the range of 15-30 ms (20-45 m).

In this section, the beds of Maradah Trough dip gently to NE and became flat while the syncline axis of it is probably located to the east of the section.

GRAVITY INTERPRETATION

The gravity data were re-projected to UTM-Zone 33, WGS84 and gridded at a 1 km grid cell size. The observed gravity data were reduced to sea level using the Geodetic Reference System of 1967 (International Union of Geodesy and Geophysics, 1971) and referenced to the International Gravity Standardization Net 1971 gravity datum (Morelli *et al*., 1974).

The observed gravity data were reduced to simple Bouguer gravity with a reduction density of 2.67 g/cm^3.

- Box A. Shows a clear syncline to the north of Az Zahrah Platform.
- Box B. Is confirming the existence of a horst and graben to the southeast of Waddan Uplift.
- Box C. Reveals the clear boundaries between Zallah Trough, Al Haleigh High and Gattar Ridge.

In order to separate the long wavelength regional trend from the short wavelength residual field, a

numerical technique known as trend surface analysis was applied on the Bouguer gravity grid. Removing the regional trend from the data would leave the residual field attributed to the local geological features. The residual Bouguer gravity was calculated up to three polynomial orders. In principal, increasing the order of the polynomial would lead closer approximation of the regional trend to the real data.

There is a pronounced east-west trending high Bouguer anomaly at the northwestern corner of the first order residual of the Bouguer gravity map (Fig. 6). This anomaly crosscuts the major tectonic trends in the area and appears to be due to major basement faults. This trend is probably related to the deepening of the basement towards the Mediterranean Sea to the north. The Al Qarqaf Arch is associated with a broad semi-circular high gravity anomaly. This could be associated with an uplifted basement or igneous intrusions and high topography.

There is a weak correlation between the Bouguer gravity data and the tectonic elements trends and the geological structures at some places on the map. For example, the Waddan Uplift is associated with a low gravity anomaly whereas the north-west part of Hun Graben is associated with a high gravity anomaly. A possible explanation (assuming accurate mapping of the tectonic elements) is that the gravity data is in part controlled by density variation of the sedimentary section (particularly the presence or absence of evaporites) rather than the basement.

Total-horizontal-gravity-gradient Calculation

The aim of total-horizontal-gravity-gradient calculation is to identify faults and define their distribution. A fault is reflected as a gravity gradient belt in Bouguer gravity anomaly. Total-horizontal-gravity-gradient calculation transforms gravity

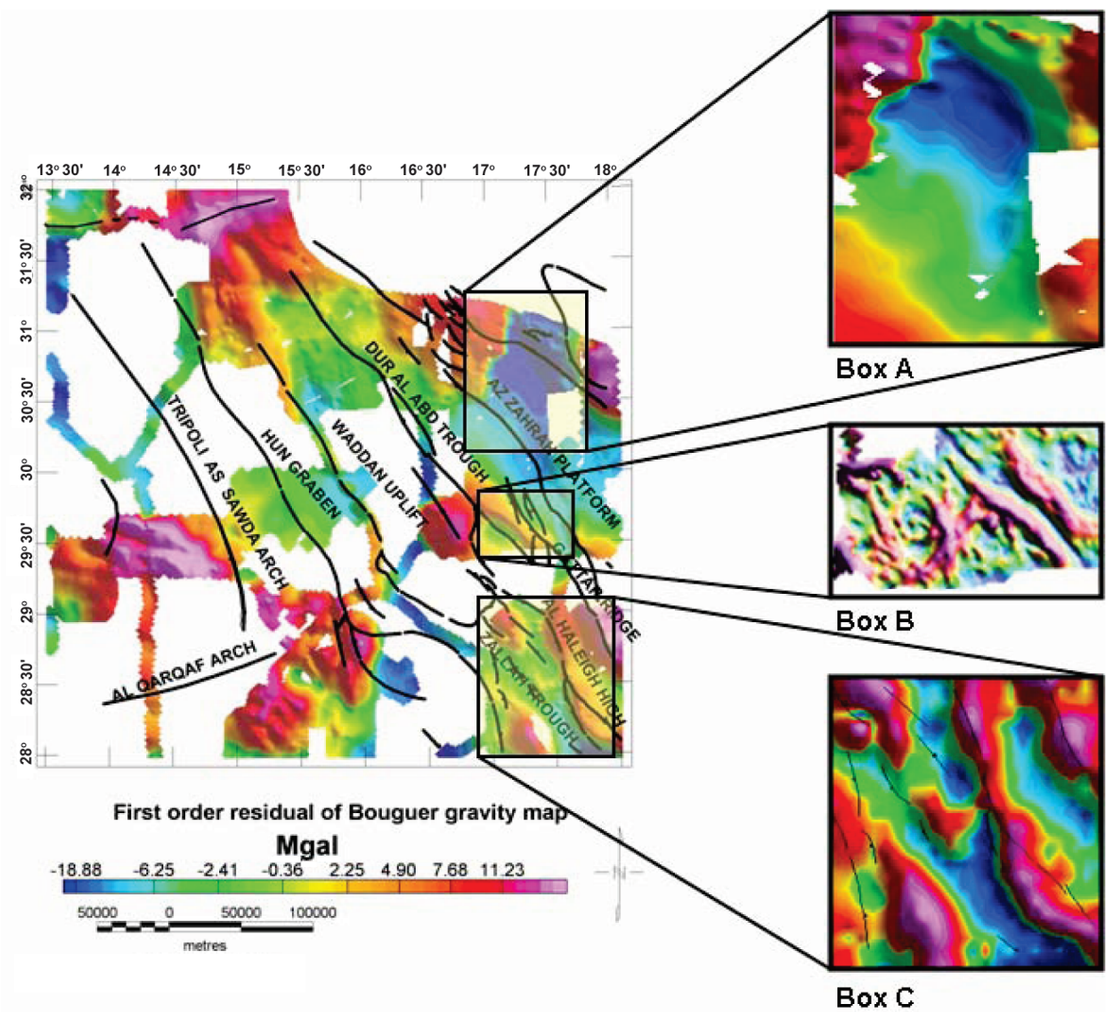


Fig. 6. First order residual Bouguer gravity map Box A shows a clear syncline to the north of Az Zahrah Platform, Box B is confirming the existence of a horst and graben to the southeast of Wadan Uplift and Box C reveals the clear boundries between Zallah rough, El Haleigh High and Gattar Ridge.

gradient belts into gradient maximum belts and further improves the resolution of faults, amplitudes which show the scale of the fault.

The tectonic trends become even more clear on the horizontal gradient map (Fig. 7). The gradient reveals the presence of several northeast-southwest trending anomalies that are not displayed on the tectonic elements maps. Among these anomalies, for example, is one that extends from the Mediterranean Sea and crosses the Az Zahrah Platform toward the southwestward direction of the study area. This anomaly appears to be displaced by the northwesterly trending structures (note the offset of the anomaly within the Az Zahrah Platform) and therefore associated with older geological events in the area.

CORRELATION BETWEEN SURFACE AND SUB-SURFACE STRUCTURES

The study area is characterised by a strong NNW-SSE structural grain which is consistent with the regional structure of the western Sirt Basin. The area has also been divided into a number of structural domains based solely on the surface structures expressed on satellite imagery (Fig. 3). The structural domains generally show good correlation with regional sub-surface structural features defined by seismic and potential field data.

Because of the variable coverage of the gravity data, it is not possible to carry out a complete interpretation of the gravity data. For the same reason, it is difficult to see if there is any correlation

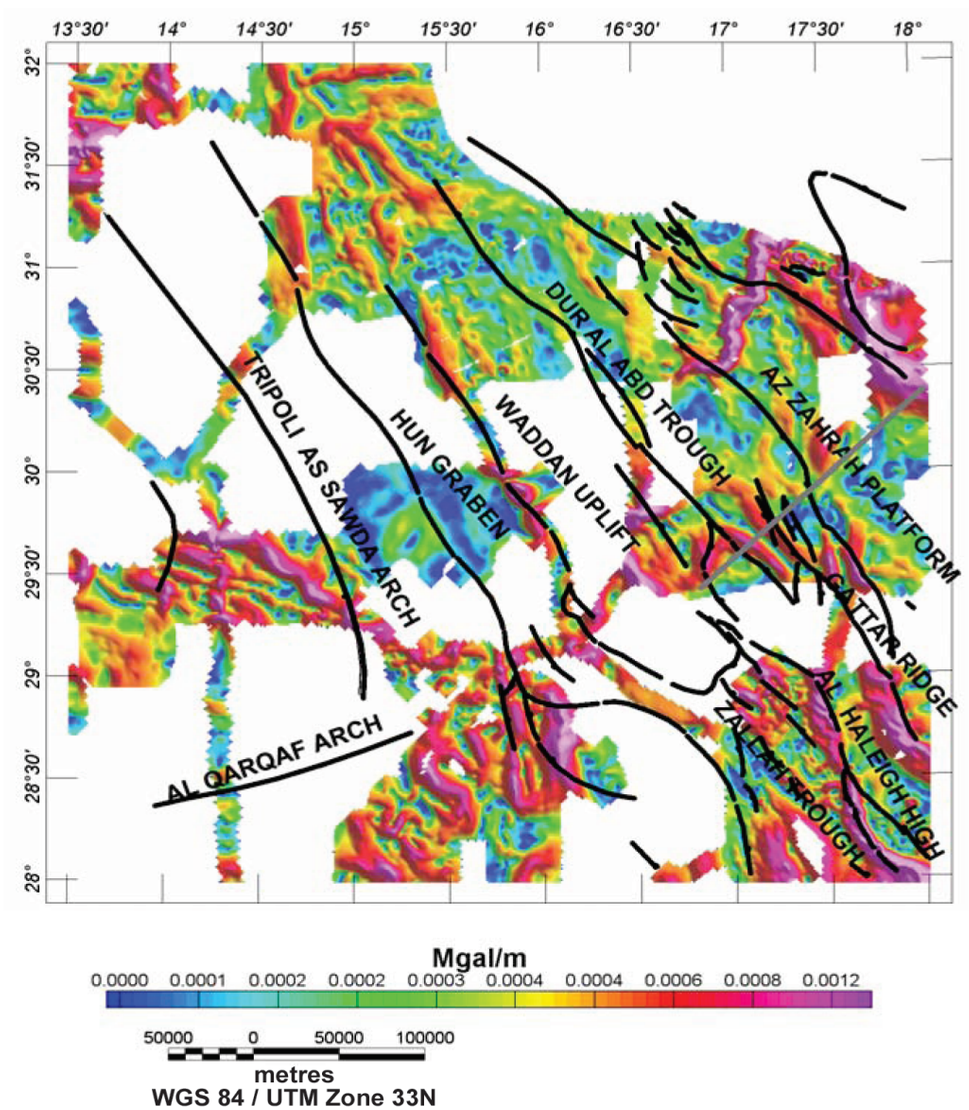


Fig. 7. Total Horizontal gradient of Bouguer gravity map.

between the Bouguer gravity data of the whole area (Fig. 6) and the tectonic elements trends and the geological structures (horsts and grabens). However, there is a good correlation at some places on the map (*e.g.*, Zallah Trough, Al Haleigh High, negative gravity anomaly within Az Zahrah Platform).

Hun Graben

It is a prominent Oligocene age structure bounded by steep cliffs which coincide with fault scarps or at least the eroded scarp slopes. It is not clear from the gravity data whether the graben affects the basement.

Az Zahrah Platform

The northern end of the Az Zahrah Platform (Fig. 4) is expressed at surface in the north by a homoclinal shallow NE dipping and marked by a NNW plunging nose of a large low-amplitude anticline. This anticline seems to be crosscut by a syncline (Fig. 6 Box A) located to the extreme northwest of it; its axis trends NE-SW and probably extending into offshore area. Several of the larger Az Zahrah Platform faults extend to the surface that revealed from satellite images are clearly observed on the seismic traverse as well.

Waddan Uplift

The W, S and SE boundaries are well-defined on the satellite imagery and bounded by normal faults down throwing to the W, S and SE respectively. The hinge zone between the Waddan Uplift and the Dur al Abd Trough contains many (about 8) large down-to-basin faults, two of which appear to extend to the surface. A graben linked to the SE part associated with NNW-SSE trending faults is confirmed by the gravity data (Fig. 6 Box B).

Zallah Trough

This is a well-defined structural domain on the satellite imagery characterised by low-lying relief, structural low region characterised by relatively smaller scale structures and preservation of Oligocene strata. Most of the major faults and broad low amplitude periclinal structures identified from the satellite imagery coincide with similar features obtained from the geophysical data.

The Al Haleigh High

It is defined as a basement high from satellite imagery by the outcrop of older stratigraphic units at the same structural level as younger strata. These areas are bounded on the both sides by faults that coincide with a gravity high (Fig. 6 Box C).

Dur al Abd Trough

Surface bed dips, combined with relatively thinner sedimentary sequence and relatively higher gravity values, indicate that the Dur al Abd Trough is shallower than the Zallah Trough.

EXPLORATION LEADS

A number of exploration leads have been identified in the study area (Fig. 4). They are primarily structural traps with a related surface expression as interpreted from the satellite imagery. The structural setting of existing oil fields in the region were used as analogues for assessing the exploration potential of the surface structures. The following exploration leads have been identified:

- Surface four-way closure (low amplitude periclinal structures) at the southern end of the Waddan Uplif. The structure is along strike from surface closures associated with the Al Haleigh High and the Karim, Aswad and Zallah oil fields.
- Down-faulted trap-door type structure located at the southeastern side of the Waddan Uplift. The structure is dependent on the western bounding fault to be a sealing fault. Migration would be up-dip from the Zallah Trough.
- The western margin or crest of the northeast tilted Gattar Ridge where the Palaeocene carbonates are likely to be highly fractured due to the proximity of the western boundary fault. Due to the amount of downthrow across the Az Zahrah Platform bounding fault to the east, the structure would probably require oil migration from the Zallah Trough.
- Northern end of the Hun Graben. This lead depends on there being a complex structural trap involving the interaction of gentle northeast dipping strata, NNW-SSE boundary faults of the Hun Graben and the ENE-WSW trending fault zone. The prospectivity of this area is dependent on oil generation and migration from the Zamzam Depression, and there being suitable reservoir(s).

• NNW-SSE trending fault zone in the western part of the study area. The fault may provide a structural trap at the eastern margin of the Ghadamis Basin.

CONCLUSIONS

The present study shows a good correlation between surface and subsurface structure defined by seismic and potential fields data. The study area is dominated by a NNW-SSE structural grain related to Cretaceous extensional tectonics and possible influence of pre-existing Pan-African basement structure.

Major ENE-WSW trending structures appear to be superimposed on the NNW-SSE structures. This trend may be influenced by pre-existing Hercynian structure. ENE-WSW structures may have a greater influence of the productivity of the structural traps generally attributed to the NNW-SSE trend.

Preservation of Mazul Ninah and late Tertiary-Quaternary deposits within structural and geomorphological depressions indicates that subsidence is ongoing along the eastern margin of the Zallah Trough and possibly within the Hun Graben.

The study area can be divided into twelve structural domains consisting of the Zallah, Dur al Abd, Hun Graben, Ghadamis and Zamzam Depression; the Waddan uplift, Gattar Ridge, and Az Zahrah Platform; the Nafusah Uplift and Al Qarqaf Arch; the Tripoli-As Sawda Uplift and the intrabasinal Al Haleigh High.

The main structural traps are:

• The crests of major NNW-SSE trending northeast tilted fault blocks developed along the basin margins e.g. Az Zahrah Platform and Gattar Ridge.

• Four-way periclinal fold closures developed as drape structures and/or drape structures related to differential compaction above smaller scale intrabasinal basinal highs such as the northern extension of the Al Haleigh High.

Six exploration leads have been identified, although the main prospective areas are within the Zallah Trough itself and the up-dip crests of adjacent platforms.

The Hun Graben appears to be an Oligocene age structure, which is probably unprospective due to the lack of reservoir and source rocks.

Western Hun Graben structure is generally characterised by a gentle northeast dipping homoclinal panel with no surface expression of any structural trap. Migration would tend to be towards the southwest. Possible seepage may occur along faults associated with the NNW-SSE trending fault zone or further west in the true structural crest of the Tripoli-As Sawda Uplift and adjacent margins of the Ghadamis Basin.

The flank of the western Sirt Basin may be defined by the Hun Graben. However, this structure is only Oligocene and the western limit of the Sirt Basin most likely extends to the west of the Hun Graben, possibly to the eastern edge of the Tripoli-As Sawda Uplift.

ACKNOWLEDGEMENTS

We wish to extend our thanks to Dr Martin Insely of Infoterra, (UK) for his supervision and without him, this paper would not have been possible. We also appreciate the approval and support from the management of the Libyan Petroleum Institute, (Libya) to publish this paper.

REFERENCES

Ahlbrandt, T.S., 2001, The Sirte Basin province of Libya – Sirte-Zelton total petroleum system, *U.S. Geological Survey Bulletin* 2202-F, 29p.

Anketell, J.M. 1996. Structural history of the Sirt Basin and its relationship to Sabratah Basin and Cyrenaican Platform, northern Libya. In: M. J. Salem, M. T. Busrewil, A.A. Misallati, and M.A. Sola (eds). *The Geology of the Sirt Basin*, Elsevier, Amsterdam, **III,** 57-89.

El-Batroukh, S.I., and Zentani, A.S., 1980, Gravity interpretation of Raguba field, Sirte basin, Libya. *Geophysics*, **45**, 1153-1163.

Klitzsch, E. 1971. The structural development of parts of north Africa since Cambrian time. In: C. Gray (ed). *First Symposium on the Geology of Libya* Faculty of Science, University of Libya, Tripoli, 253-262.

Mijalkovic, N. 1977. Geological Map of Libya, Sheet Al Qaddahiyah (NH 33-3), scale 1:250,000, Explanatory Booklet, Industrial Research Centre, Tripoli. 66p.

Morelli, C., Cantar, C., Honkasalo, T., McConnell, R.K., Tanner, J.G., Szabo, B., Uotila, U., and Whalen, C.T., 1974. The international gravity standardization net 1971 (IGSN71). *Int. Assoc. Geod., Spec*. Publ. 4.

Said, M. 1981. Geological Map of Libya, Sheet Bunjim (NH 33-7), scale 1:250,000, Explanatory Booklet, Industrial Research Centre, Tripoli, 92p.

Zivanovic, M. 1977. Geological Map of Libya, Sheet Bani Walid (NH 33-2), scale 1:250,000, Explanatory Booklet, Industrial Research Centre, Tripoli, 71p.

Petroleum Res. J. Vol. 20 (2007); P. 59–76, 23 Figs.

Late Tertiary Subsidence and Tilting in the Sirt Basin and their Seismic Signatures

M. S. Zanati and M. Roohi*

ميل وهبوط حوض سرت خلال الحين الثلاثي المتأخر وبصماته السيزمية

محمد سعد الزناتي ومنصور روحي

يقع حوض سرت في منتصف شمال ليبيا، ويعتبر من أكبر الأحواض إنتاجا للنفط في أفريقيا. وهو غير متماثل الشكل حيث يمتد بعرض 400كم في إتجاه الجنوب الغربي و120كم في اتجاه الشمال الشرقي نتيجة لعملية خفض منفردة تمت على نطاق واسع في فترة ما بعد عصر الأيوسين. ويمثل الموقع المحوري لغور إجدابيا العمق المحوري الحالي لحوض سرت حيث تكون كل الملامح التركيبية في الجزء الغربي للحوض (منخسف هون ومرتفع ودان وغور زلة ورصيف الظهرة – الحفرة وغور مراده ورصيف زلتن) وجزئه الشرقي (رصيف آمال ومنخفض مراغ ومرتفع الرّكب) مائلة وتتحرك تدريجيا إلى الأعمق في اتجاه محور غور إجدابيا.

تعتبر حركة هذا الخفض والميلان التي تمت خلال الحقبة المتأخرة من الحين الثلاثي من أهم الأحداث التكنونية بحوض سرت. بدأت ذروة تولد النفط من الصخور الغضارية الرئيسية المولدة له بالحوض والتي تنتمي للعصر الطباشيري العلوي (الكامبيني-التيروني) إبان الأوليغوسين والمايوسين، عندما كان عمق صخور المصدر مدفونا تحت عمق 4000 متر. لذلك فقد حدث تولد وهجرة وتجمع النفط بعد هبوط كبير في فترة ما بعد عصر الأيوسين وفي وقت تشكلت فيه البنية والملامح الحالية للحوض.

يعتقد أن البصمات السيزمية مثل أنعكاسات حركات الكتل المرتبطة بإزاحة صدعية كبيرة في أفق المناطق المنخفضة (بعض من كتل ما قبل الكريتاسي العلوي تعلوها تكاوين غير سميكة من الكريتاسي العلوي) وحدوث صدوع عادية أو ذات ميل مضربي، نتيجة اختلاف ميل الكتل، ووجود قوة ضغط جانبية محلية على الأفق السطحي في آفاق غور المنطقة الضحلة (مولدة صورة بنيوية معقدة) وسمات خطية بنيوية تنتمي إلى الحين الثلاثي المتآخر، وذات اتجاه شمال غرب-جنوب شرق وشمال شرق-جنوب غرب، حدثت جميعها نتيجة هبوط وميلان رئيسيان أثناء الحين الثلاثي المتأخر.

Abstract: *Sirt Basin, situated in the north-central part of Libya, is the largest oil producer in Africa. Present asymmetrical configuration of the Sirt Basin with southwestern flank being about 400km wide and northeastern flank about 120km wide, is a result of a single, broad, large scale, post Eocene subsidence. The axial position of deep Ajdabiya Trough represents the present axis of the Sirt Basin. All the structural features in the western flank of the basin (Hun Graben, Waddan Uplift, Zallah Trough, Az Zahrah-Al Hufrah Platform, Maradah Trough, Zaltan Platform) and eastern Sirt Basin (Amal Platform, Maragh Low, Ar Rakb High) are tilted and have moved progressively deeper towards the axis of the Ajdabiya Trough.*

These major late Tertiary subsidence and tiltings are considered as one of the most important tectonic events of the Sirt Basin. The peak of the oil generation from the Upper Cretaceous Campanian-Turonian shales as the

* Exploration Department, Waha Oil Company, P.O. Box 395, Tripoli, Libya.

principal petroleum source rocks in the Sirt Basin was mainly during the Oligocene-Miocene time when the burial depth of these source rocks was below a depth of 4000m. Therefore, generation, migration, and accumulations occurred mainly after the huge post Eocene subsidence, at a time when the present structural configuration of the basin had already been established.

Seismic signatures such as reversal block movements associated with larger fault displacements in the shallower horizons (some deeper pre-Upper Cretaceous blocks have thinner overlying Upper Cretaceous formations); scissor faults and/or strike slip faults as a result of differential block tiltings; localized lateral compressional forces in the shallow horizons of the trough areas (generating complicated structural pictures); and NW-SE and NE-SW trending late Tertiary structural lineaments are thought to be mainly due to the late Tertiary major subsidence and tiltings.

INTRODUCTION

Structural evolution of the Sirt Basin shows that the gradual subsidence, associated with syndepositional fault movements, of the NW-SE trending platforms and troughs ended with a major subsidence associated with tiltings in late Tertiary time (Roohi, 1996a).

A very unique combination of thick sediments of up to 10,000 m with rich source rocks in the troughs versus much thinner sediments with prolific reservoir rocks on the platforms accounts for the productivity of the basin.

The main objective of this paper is to analyze the importance of this major late Tertiary tectonic event, and demonstrate that the present structural configuration of the Sirt Basin is the result of this movement. Structural complexities observed in seismic which are related to this subsidence and its associated tiltings are also discussed.

As the result of this post-Eocene tectonic event all the blocks in the western and eastern flanks of the Sirt Basin subsided rather abruptly. They progressively moved deeper and tilted towards the axis of the Ajdabiya Trough to establish the present structural configuration of the basin (Fig. 1).

The most important significance of the late Tertiary major subsidence is the oil generation, migration, and accumulations which occurred after this tectonic event (Roohi, 1996a). Therefore, seismic analyses of the complicated structural

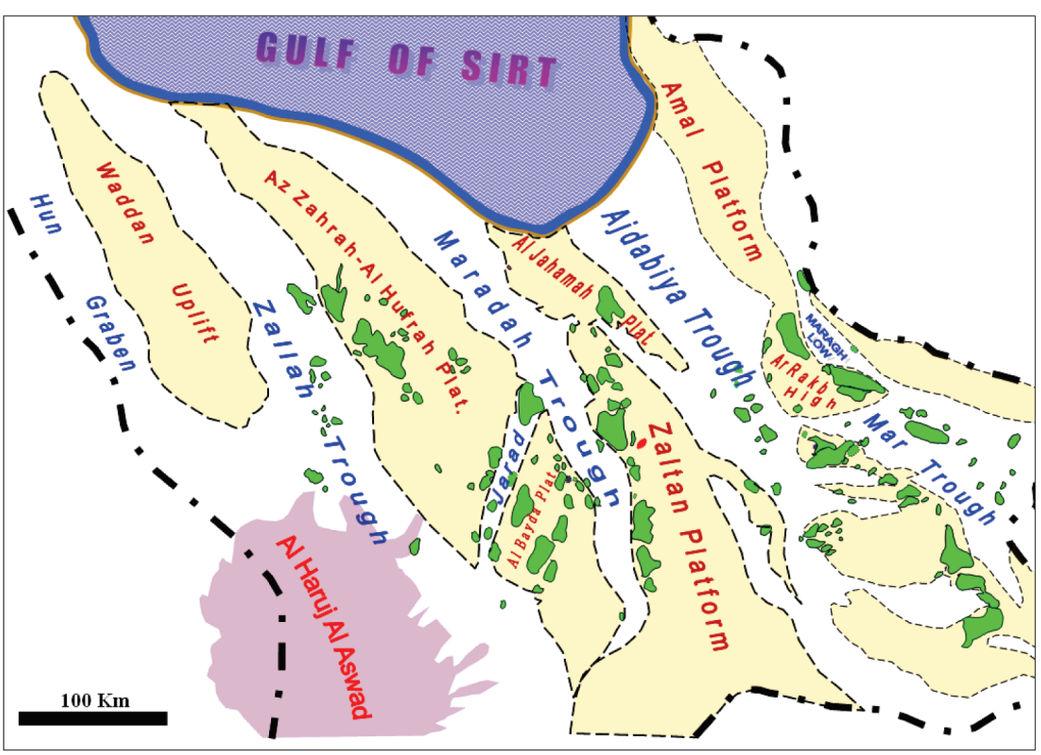


Fig.1. Sirt Basin, structural elements.

relationship of the shallow and deep horizons are challenging work for the geophysicists in prospect evaluations in the deep areas as well as along the edges of platforms.

STRUCTURAL HISTORY AND DEFORMATION OF SIRT BASIN

Figure 2 shows the major tectonic elements in North Libya and their general regional trends. Palaeozoic basins (Ghadamis, Murzuq) and highs (Qarqaf Arch, Tibisti Arch) have NE-SW trends. Subsurface data indicate that Ghadamis and Murzuq basins had plunged northeastward and ended in the western margin of the Sirt Basin; meanwhile, the northeastward continuation of the two uplifts of Qarqaf and Tibisti shows that further to the east they were joined together and had created Sirt Arch.

The Sirt Arch was broken by a series of NW-SE trending faults in Lower Cretaceous time and gradually the area collapsed into a series of alternating northwest-southeast trending horsts (platforms) and grabens (troughs). This drastic change in the structural framework of the area resulted in the initiation of the Sirt Basin superimposed on NE-SW trending Palaeozoic tectonics.

The Cretaceous structural deformation in the Sirt Basin was followed by Cenomanian marine transgression and a thick sequence of Upper Cretaceous-Tertiary shallow marine shales and carbonates associated with evaporites and sands were deposited. Horsts remained relatively stable, while the grabens, accompanied by syndepositional fault movements, subsided to a depth in excess of 6000 metres in the deepest part of the basin, filled with marine sediments.

The major tectonic features in the broad western flank of the Sirt Basin are: (from west to east) Hun Graben, Waddan Uplift, Zallah Trough, Az Zahrah-Al Hufrah Platform, Maradah Trough, and Zaltan Platform. Ajdabiya Trough is in the axial position, and the strongly fault controlled smaller horst and graben blocks, including Amal Platform, Ar Rakb High, Maragh Low, Jalu-As Sarir Structural High, and Mar Trough comprise the narrow eastern flank of the asymmetrical Sirt Basin. These horsts and grabens extend from onshore areas northwestward into a complex offshore terrain (Fig. 1).

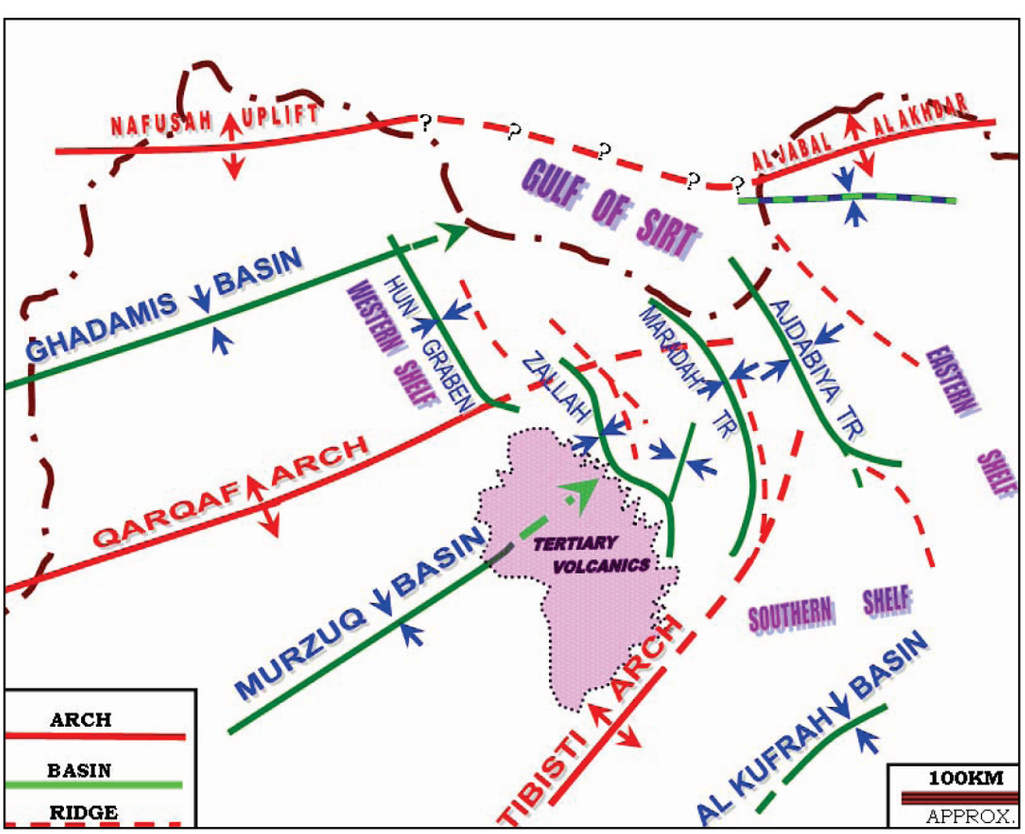


Fig. 2. Major tectonic elements, North Libya (compiled from different sources).

A significant down warping movement took place rather abruptly during the Late-Eocene to Oligocene time and the present-day asymmetrical structural configuration of the Sirt Basin is the result of this major late Tertiary subsidence.

LATE TERTIARY SUBSIDENCE AND TILTING

A regional study was carried out over the Az Zahrah-Al Hufrah Platform in the Western Sirt Basin to evaluate the Waha Oil Company concessions. The conclusion of this study was that the eastern edge of the platform (along the western edge of Maradah Trough) was structurally higher than the western edge during the deposition of Upper Cretaceous-Tertiary formations (Fig. 3). Presently their structural situations are completely reversed and the Az Zahrah-Al Hufrah High has a superior structural position in the region (Fig. 4). Detailed study of tectonic history of the area has shown that this structural deformation happened after Eocene time in which the entire platform was tilted towards east-northeast (Fig. 5), towards the axis of Ajdabiya Trough; and a favorable condition for upward hydrocarbon migration from the Maradah Trough to the present position of giant fields of Az Zahrah-Al Hufrah and Bahi were created (Roohi, 1996b).

The results of the Az Zahrah-Al Hufrah Platform study were applied to the other major tectonic features in the Sirt Basin. All the platforms, as well as all troughs, had a very similar tectonic history, and they all were subsided progressively deeper and tilted towards the axis of the Ajdabiya Trough in post Eocene time (Figs. 6-7). Of course, with the exception

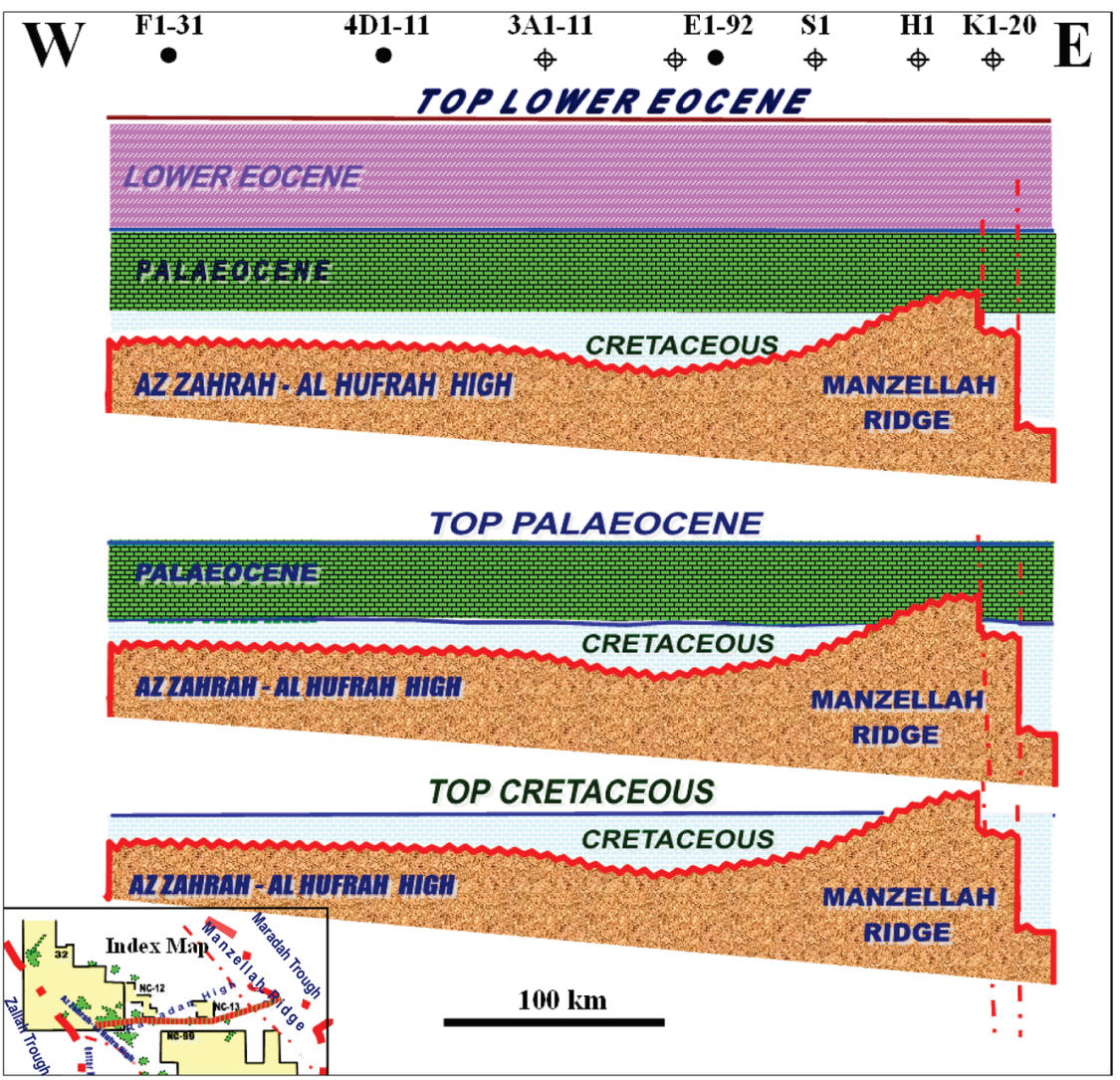


Fig. 3. Az Zahrah-Al Hufrah Platform, historical development.

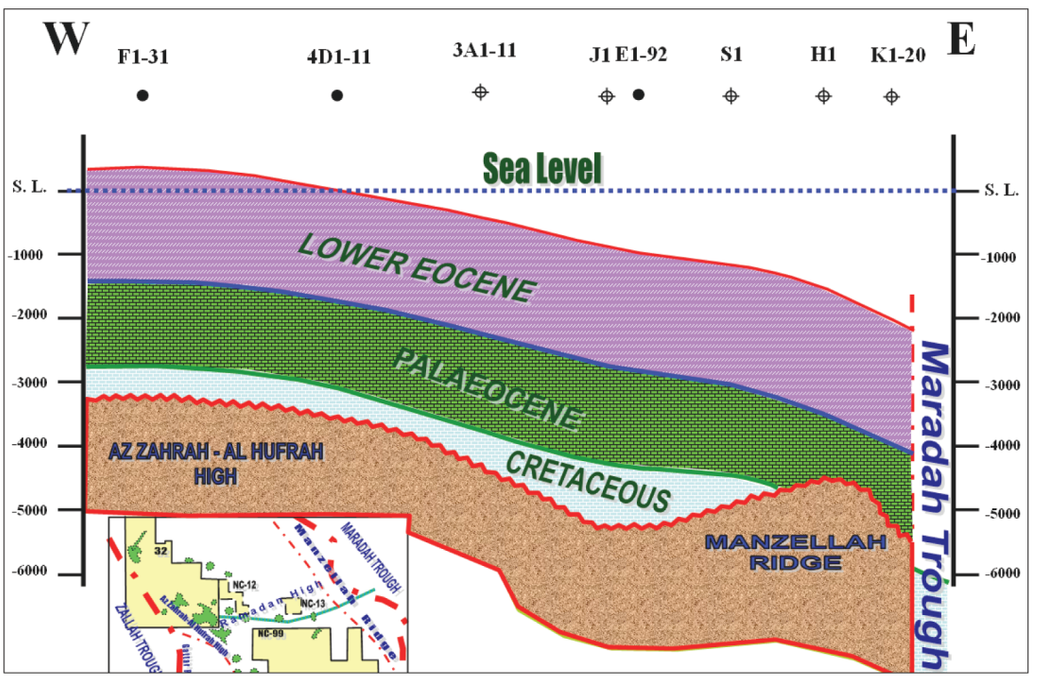


Fig. 4. Az Zahrah-Al Hufrah Platform, present configuration.

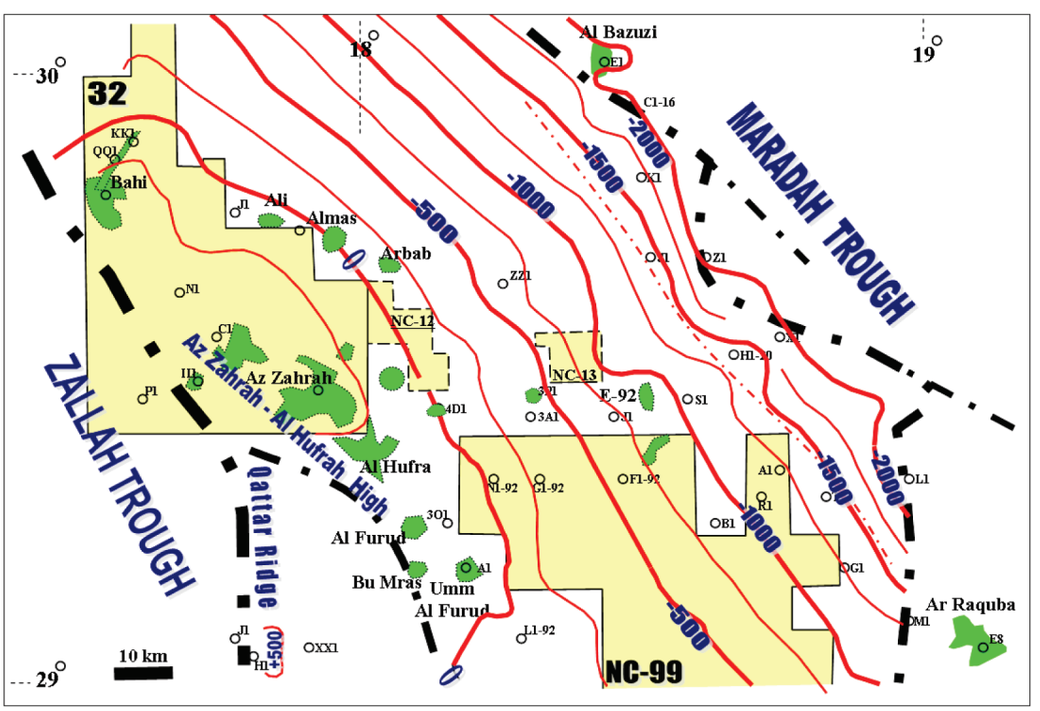


Fig. 5. Az Zahrah-Al Hufrah Platform, structure top Lower Eocene Gir Formation (C.I.=250 ft.).

of Zallah Trough in the western Sirt Basin, the pictures of the troughs are more speculative due to the lack of deep drillings in the trough areas. However, by taking into account the total post Eocene picture of the basin (Fig. 8), it is reasonable to believe that troughs have gone through the same history as the platform areas.

One significance of late Tertiary subsidence and tiltings of the Sirt Basin is that the prolific rich marine shales of Upper Cretacous age, developed

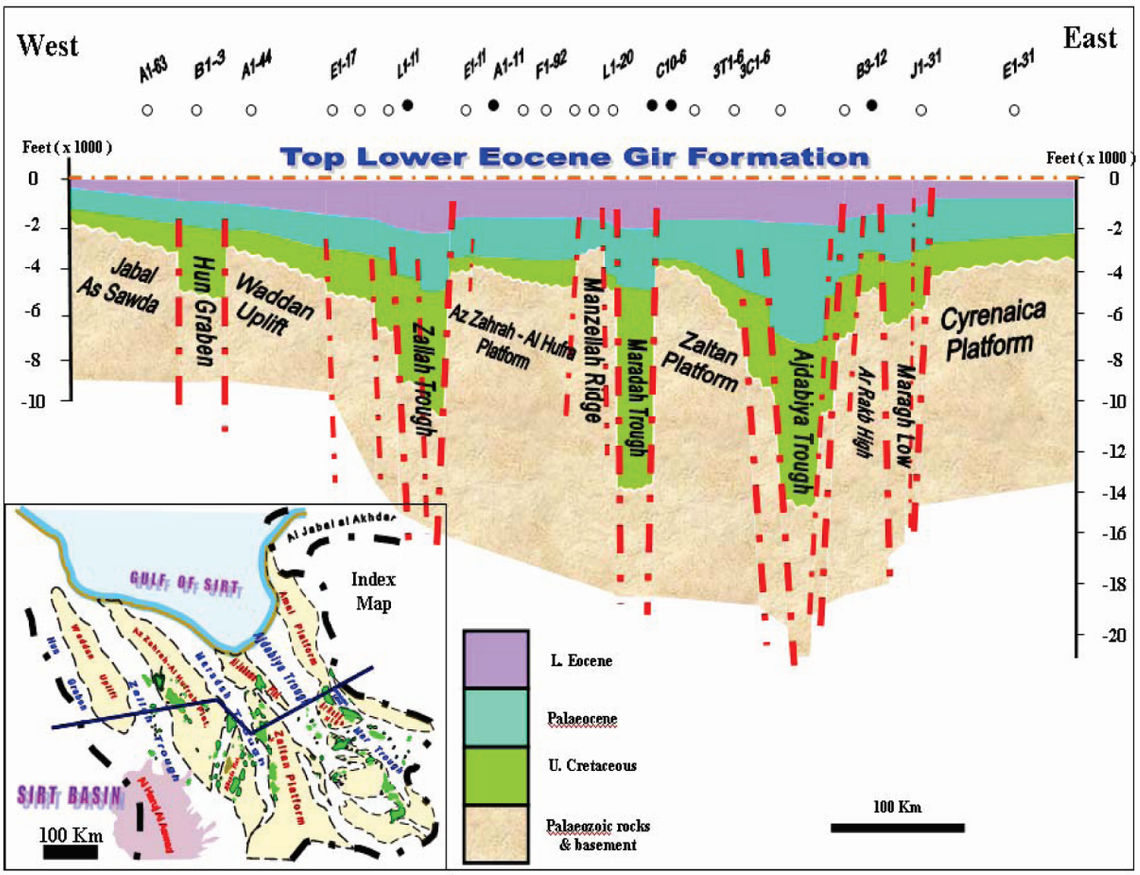


Fig. 6. Reginal cross-section across the Sirt Basin leveled to top Lower Eocene Gir Formation.

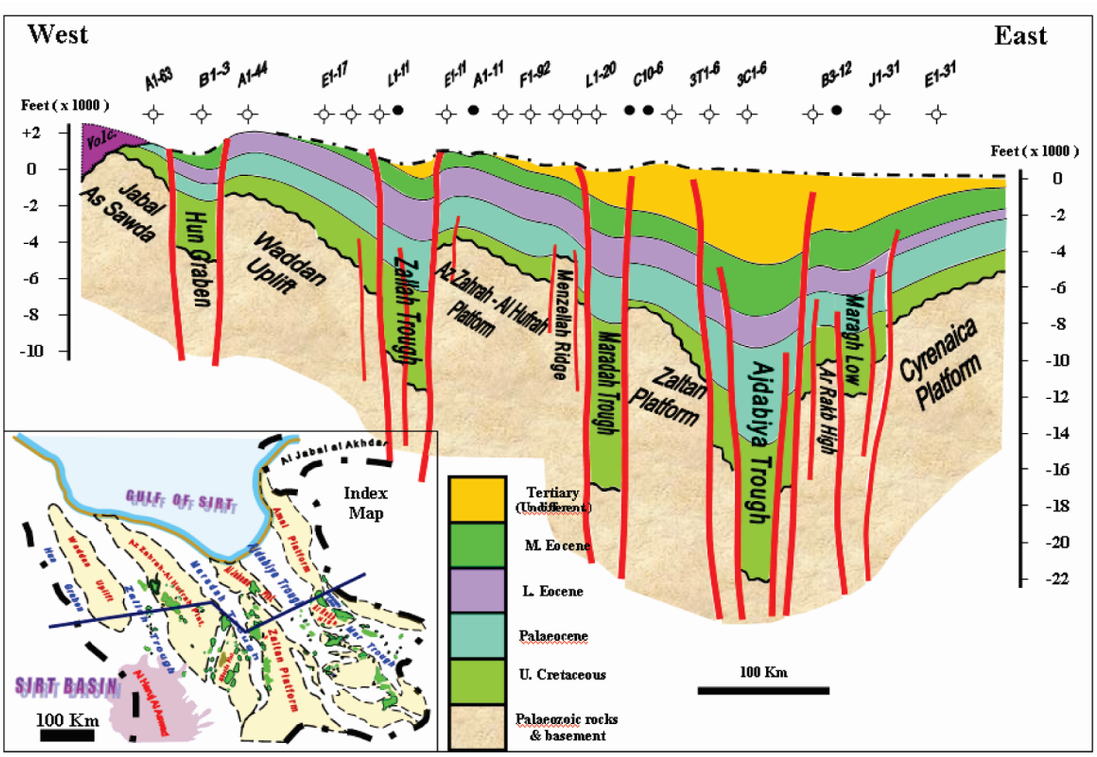


Fig. 7. Regional cross-section across the Sirt Basin, showing present picture.

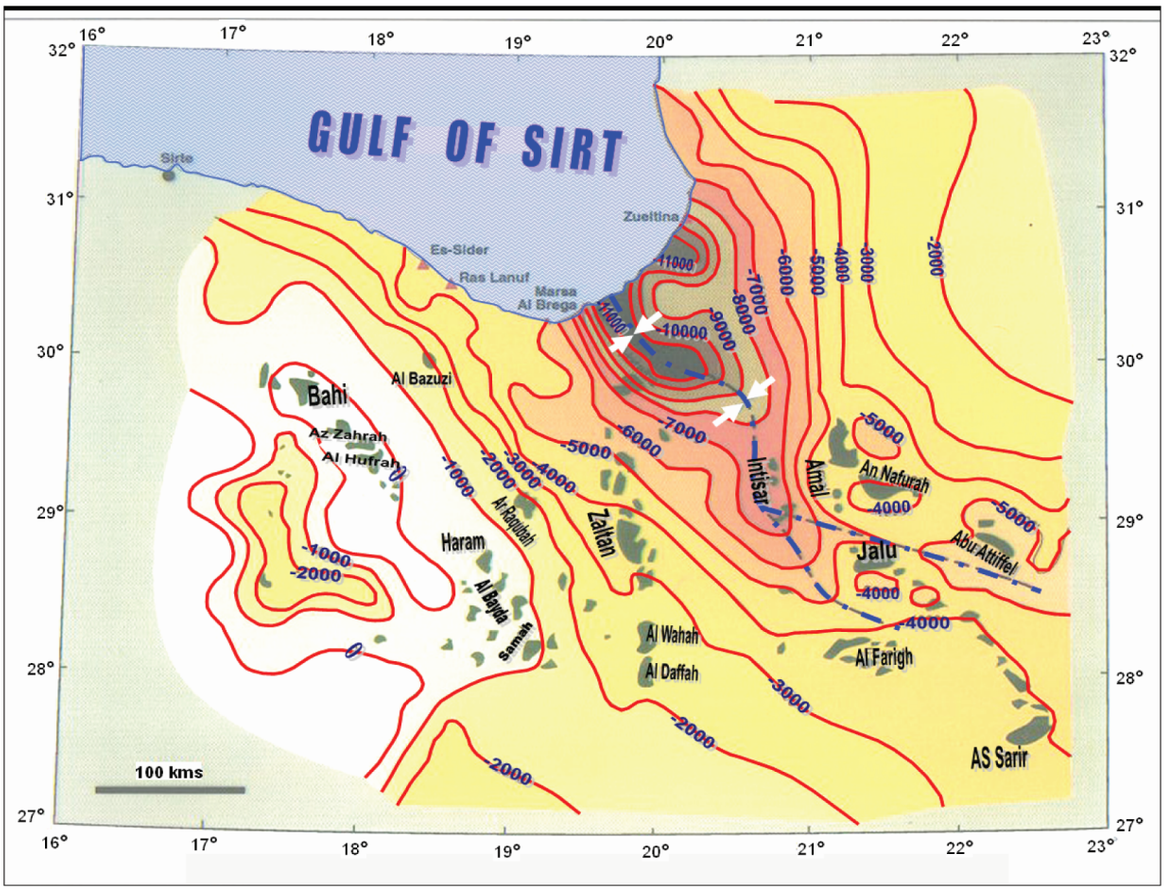


Fig. 8. Sirt Basin, structure top Lower Eocene Gir Formation (C.I. =1000 ft.).

in the troughs as the petroleum source rocks, reached the depth of hydrocarbon generations below 10,000 feet. Geochemical modeling of source rocks in the Sirt Basin shows that the peak of oil generation was during the Oligocene-Miocene (Figs. 9-11), after the major late Tertiary subsidence; and the migration happened later in post Oligocene time. Hydrocarbons generated in the deep trough areas migrated up onto the platforms and into the multiple age reservoirs. Block faultings also resulted in placing the deep clastic reservoirs in juxtaposition with mature source rocks in the deep trough areas. Major faults, with periodic reactivation, were acting as conduits for vertical hydrocarbon migration in the Sirt Basin.

SEISMIC SIGNATURES

Structural deformation of the Sirt Basin from pre-Eocene to post-Eocene picture (see Figs. 6 and 7) requires considerable differential movements between platforms and troughs along the bounding faults; and different magnitudes of subsidence to comply with the present structural configuration of the basin. Figure 7 clearly shows the tilings of all the platforms as well as troughs towards the axis of Ajdabiya Trough due to this major late Tertiary subsidence.

A series of available seismic lines, from only the Waha Oil Company concessions, are provided to see some of the seismic signatures of these late Tertiary tectonic events such as: tiltings; differential block movements; and lateral compressional forces in the shallow horizons of the trough areas.

An E-W trending seismic line covers the Az Zahrah-Al Hufrah Platform and clearly shows the northeastward post-Eocene tilting towards the axis of Ajdabiya Trough (Fig. 12). Unfortunately, the line does not extent into the Maradah Trough to the east, and therefore, the situation of the eastern margin of the platform is not shown. However, structural complications as well as indications of missing formation at depth, along the eastern margin, can be observed.

Figure 13 shows a seismic line of the structural configurations of Az Zahrah-Al Hufrah Platform with the Zallah Trough to the west. Re-activation

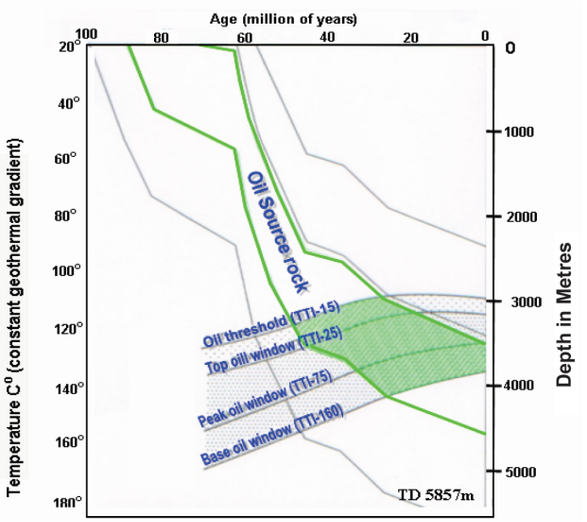


Fig. 9. Time-temperature index of maturity (TTI), well 5P1-59.

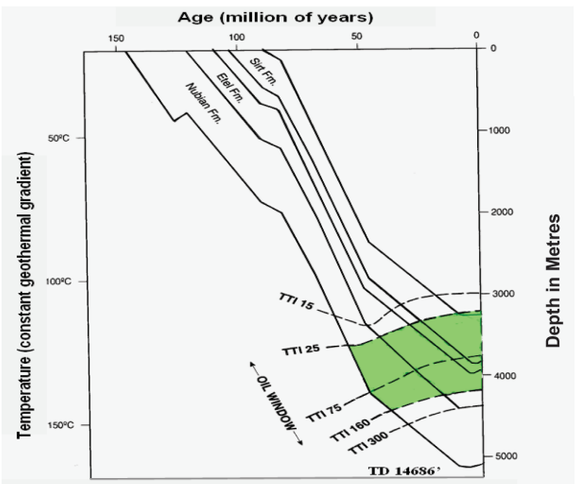


Fig. 10. Burial history (TTI), well DD2a-59.

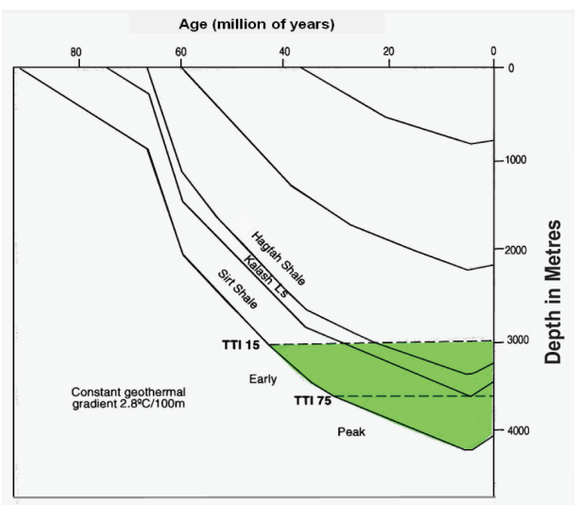


Fig. 11. Burial history (TTI), Maradah Trough, adjacent to Ar Raguba Field.

of the major bounding fault (Az Zahrah Fault) with huge differential movements in Late Tertiary time together with the northeastward tiltings of both Az Zahrah-Al Hufrah Platform and Zallah Trough, exerted a lateral compression over the shallow horizons in the trough area.

Shale, anhydrite, and salt in the Eocene formation; have created,under the localized lateral compression, different structures in comparison with the deep formations.

A northeast-southwest trending seismic line from Concession 31 in the western margin of the Amal Platform in the eastern flank of the Sirt Basin is presented in Figure 14. It clearly shows the post Eocene westward tilting of the platform towards the Ajdabiya Trough.

To comply with the present picture of the Sirt Basin; late Tertiary tilting in the eastern flank of the Sirt Basin is in the opposite direction of western flank (Fig. 15).

Jarad is a narrow trough, along the NE-SW trending palaeo-tectonic feature, separating the Az Zahrah-Al Hufrah Platform from its southeastern extension called Al Bayda Platform (Fig. 1). An E-W trending seismic line across this narrow trough is shown in Figure 16. During the late Tertiary tilting, the two platforms of Az Zahrah-Al Hufrah and Al Bayda did not tilt exactly at the same direction and/or same magnitude. Compared to the Al Bayda Platform, Az Zahrah-Al Hufrah underwent a higher angle of tilting. It seems that the magnitude of tilting and subsidence of different platforms and troughs are related to the depth variation of the Ajdabiya Trough. Ajdabiya Trough becomes gradually shallower towards the southeast and tectonic blocks in the Sirt Basin follow the same picture.

Considering the differential movements between the Az Zahrah-Al Hufrah and Al Bayda platforms, the tilting of the Az Zahrah-Al Hufrah towards the northeast and Al Bayda Platform with different angle and less magnitude of subsidence towards east-northeast a localized lateral compressional force was created in the Jarad Trough area and different structural pictures between the shallow and deep horizons were developed.

There are several potential oil fields on the Al Bayda Platform, all of which are controlled by faults of different magnitudes. Major faults trend NE-SW, more or less parallel to the Jarad Trough, and were possibly created by the reactivation of pre-Upper Cretaceous faults in late Tertiary time. These major

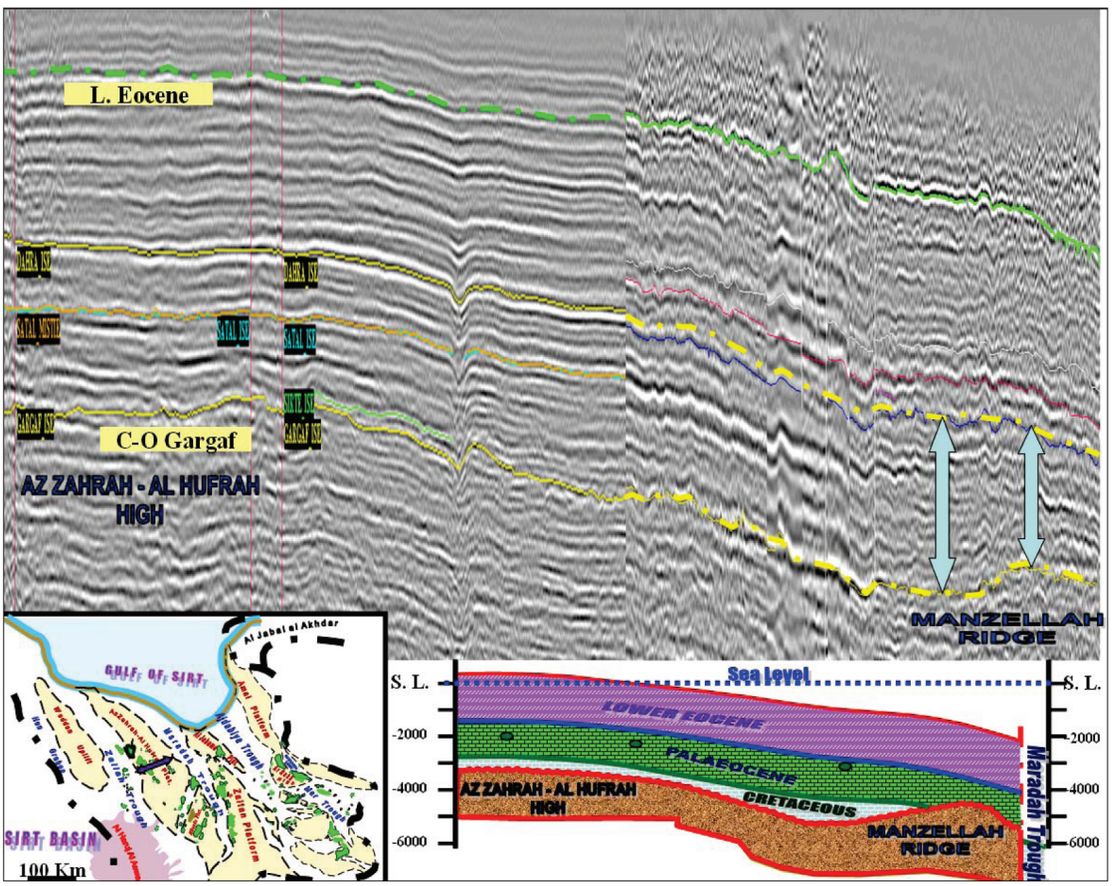


Fig. 12. E-W trending line across the Az Zahrah-Al Hufrah Platform.

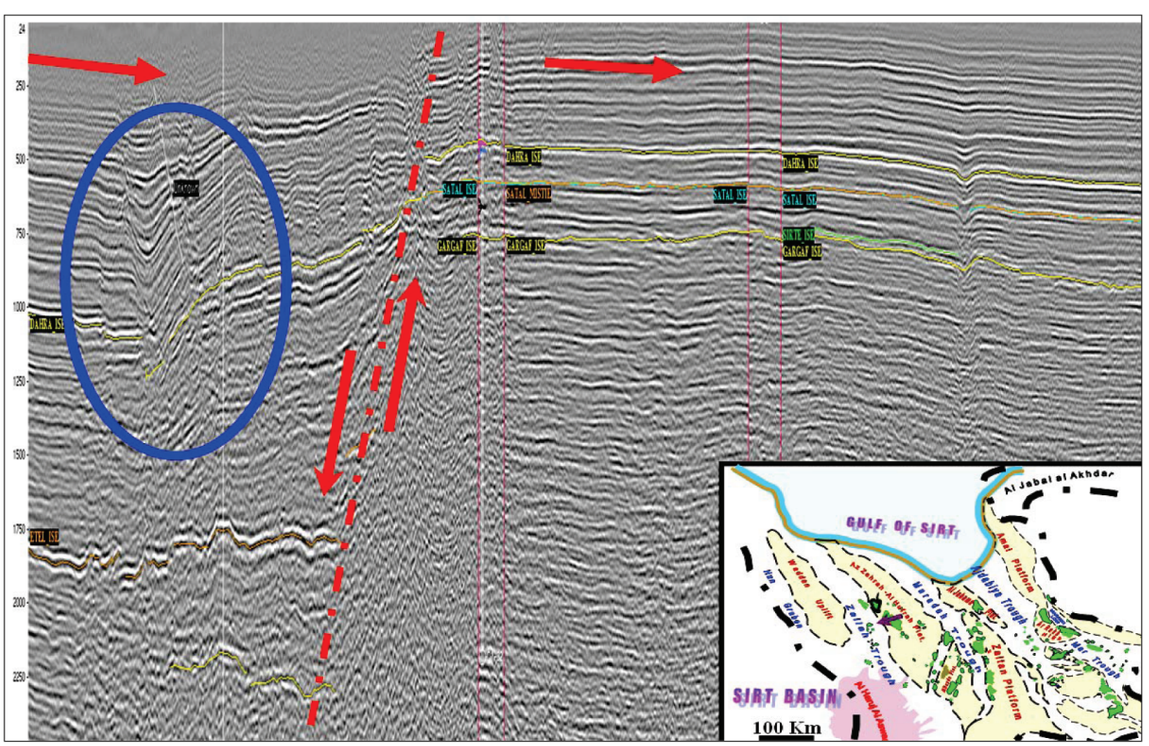


Fig. 13. E-W trending line, western edge the Az Zahrah-Al Hufrah Platform.

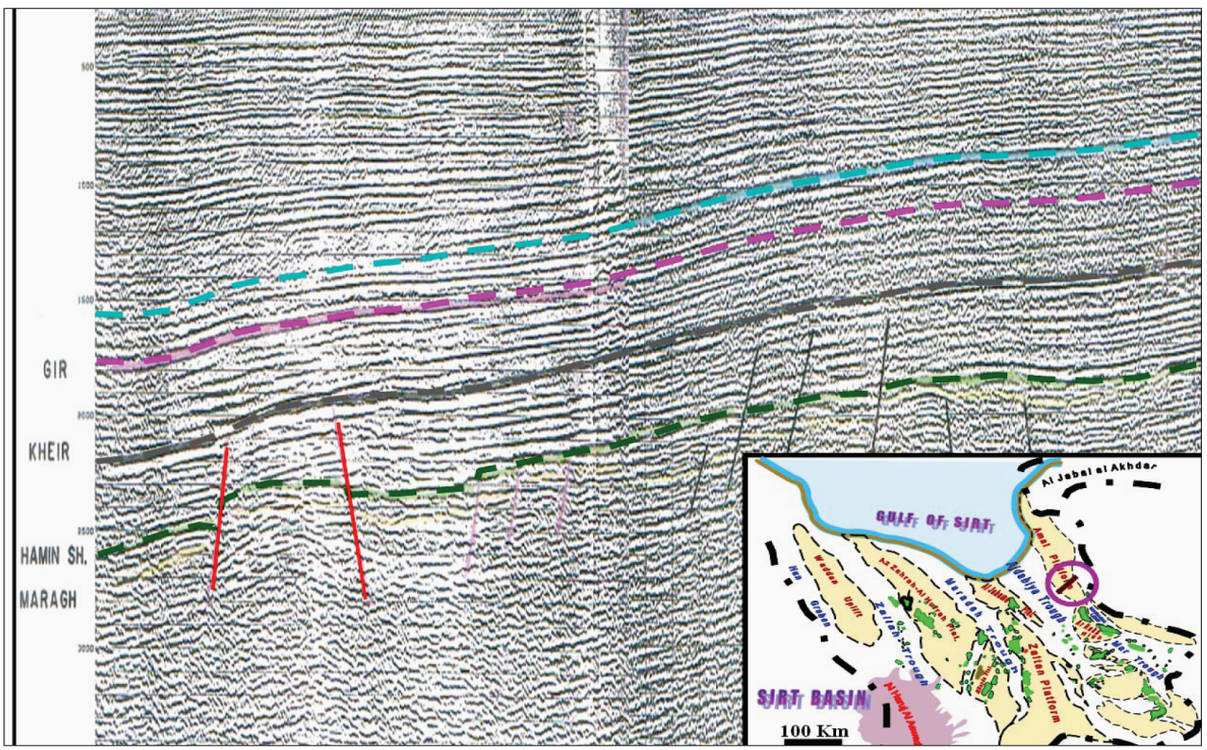


Fig. 14. NE-SW trending line, Concession 31, Amal Platform.

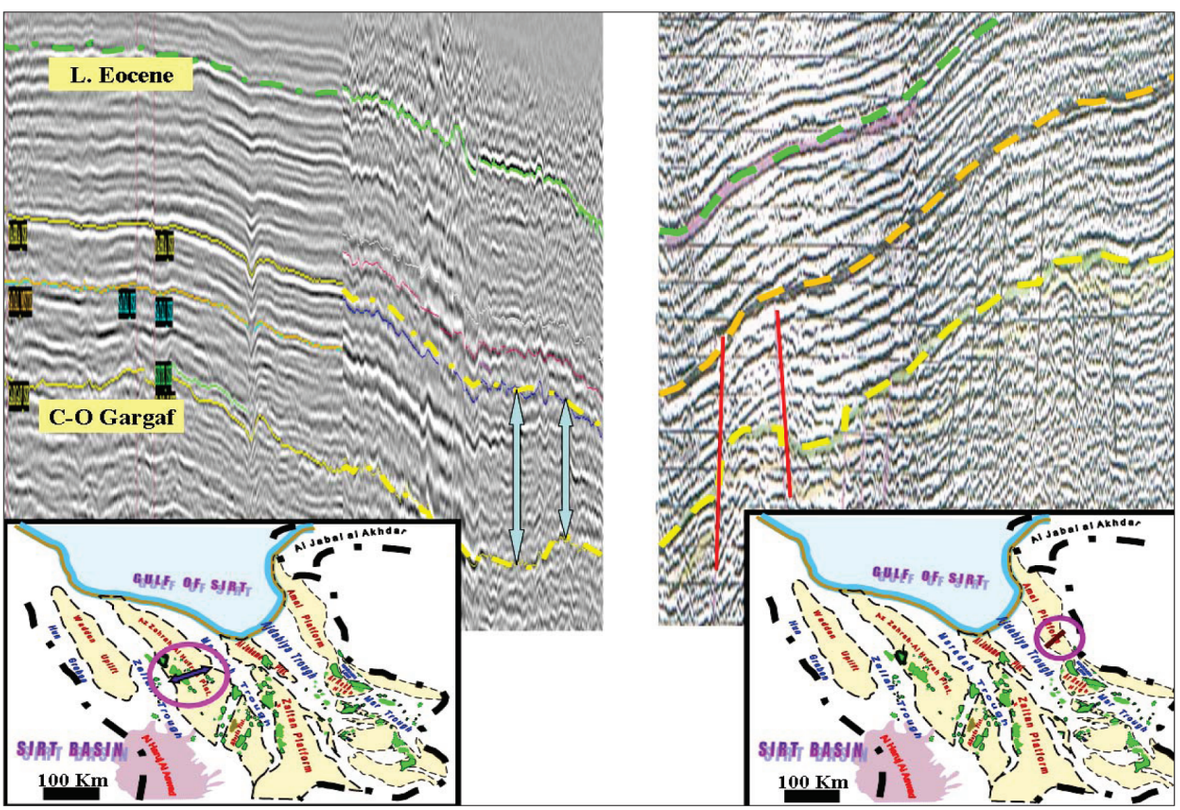


Fig. 15. Direction of tilting of Az Zahrah-Al Hufrah and Amal Platform, towards the axis of the Ajdabiya Trough.

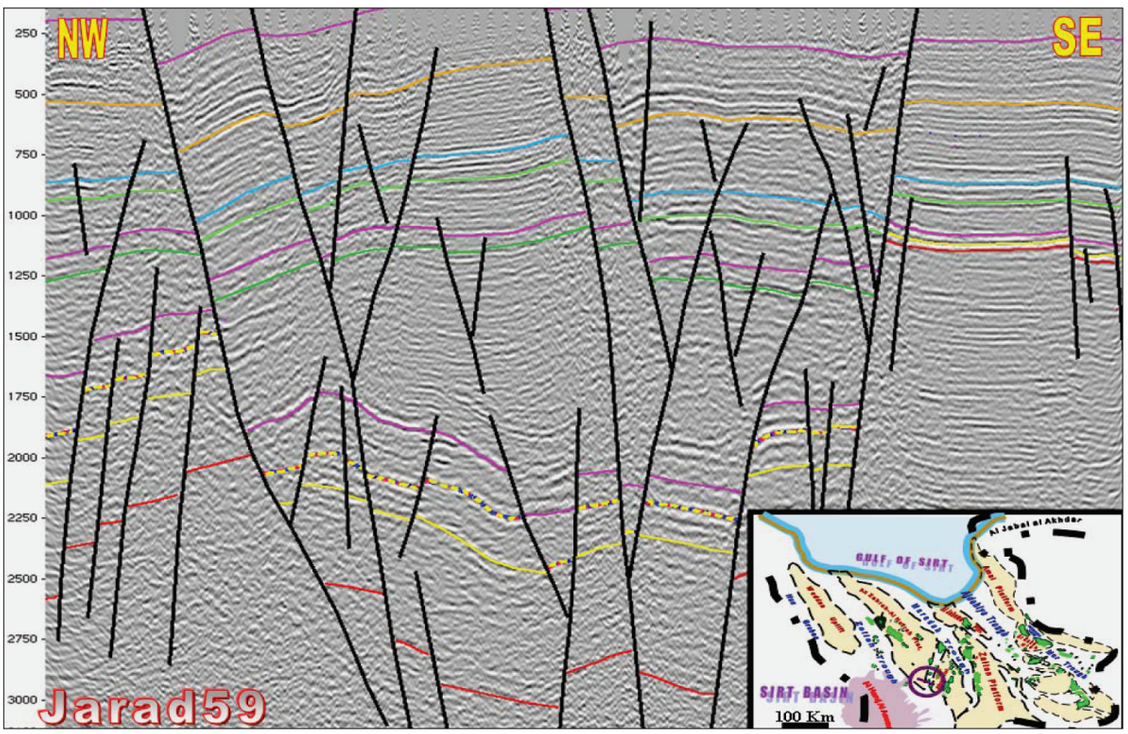


Fig. 16. NW-SE trending line across the Jarad Trough.

faults are mostly right lateral and associated with echelon faults.

The following maps (Fig.17a) are from the area, just to the northeast of Balat field on the Al Bayda Platform (AA structure). The coherency display map at the level of Lower Eocene Gir Formation shows the same fault pattern of Lower Palaeocene Beda producing pay. This indicates that during the east-northeastward late Tertiary tilting, Al Bayda Platform was broken into several blocks along the NE-SW trending pre-Upper Cretaceous faults.

To comply with present structural picture of the Sirt Basin, northwest blocks of the Al Bayda Platform moved farther and tilted more towards the Ajdabiya Trough compared to southeastern blocks. These right lateral faults systems (strike slip faults) seems to be the result of differential block movements.

This NE-SW trending seismic line (Fig.17b) covers the eastern block of the above map and clearly shows the late Tertiary northeastward tilting.

Although Figure 18 covers a very small portion of the eastern edge of the Al Bayda Platform (Zaggut Field), it clearly shows the northeastward late Tertiary tilting as well as the complications along the eastern platform bounding fault with the Maradah Trough.

Figure 19 is a NE-SW trending seismic line across the giant field of Al Wahah, along the western edge of the Zaltan Platform. The late Tertiary northeastward tilting of the platform is apparent. The western platform bounding fault with the Maradah Trough to the west is indicated in this seismic line as well.

This line is in a similar structural position as the western edge of the Az Zahrah-Al Hufrah Platform with the Zallah Trough (Fig. 13). However we do not see the crumbling picture of the shallow horizon in the trough. The reason is that here we do not see a huge late Tertiary reactivation of the bounding fault; and also because of the narrowness of the Maradah Trough, formations did not have room to subside in relation to the Zaltan Platform. Therefore, the compressional force created in the Zallah Trough due to the differential movements between the platform and trough does not exist in this area.

Both Zaltan Platform and Maradah Trough are tilted almost uniformly together towards the axis of the Ajdabiya Trough. The structural map of the Gir Formation covering the Sirt Basin (Fig. 8) shows only a small indication of the Maradah Trough.

The seismic line across the giant field of Al Daffah, along the western edge of the Zaltan Platform (Fig. 20) exhibits a similar tilting as Figure 19. It is tilted towards northeast and complicated along the edge of the platform. There are some indication of late Tertiary structural lineaments (slump feature); perhaps created by the

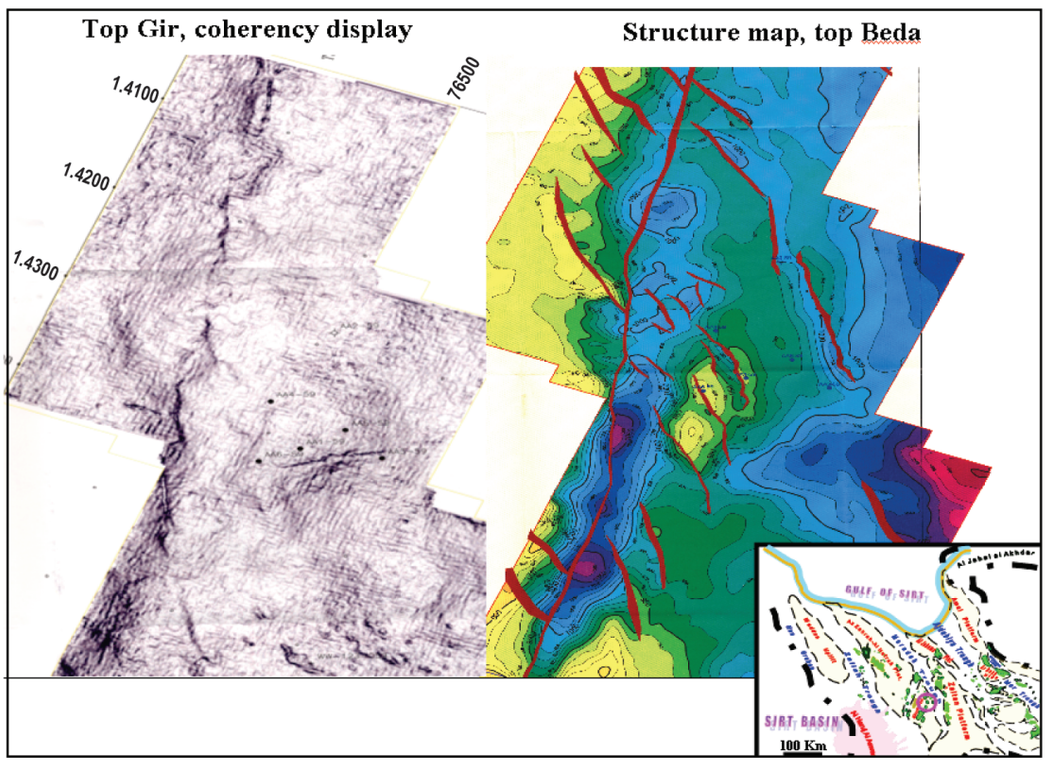


Fig. 17a. Al Bayda Platform, North Balat area, "AA" structure.

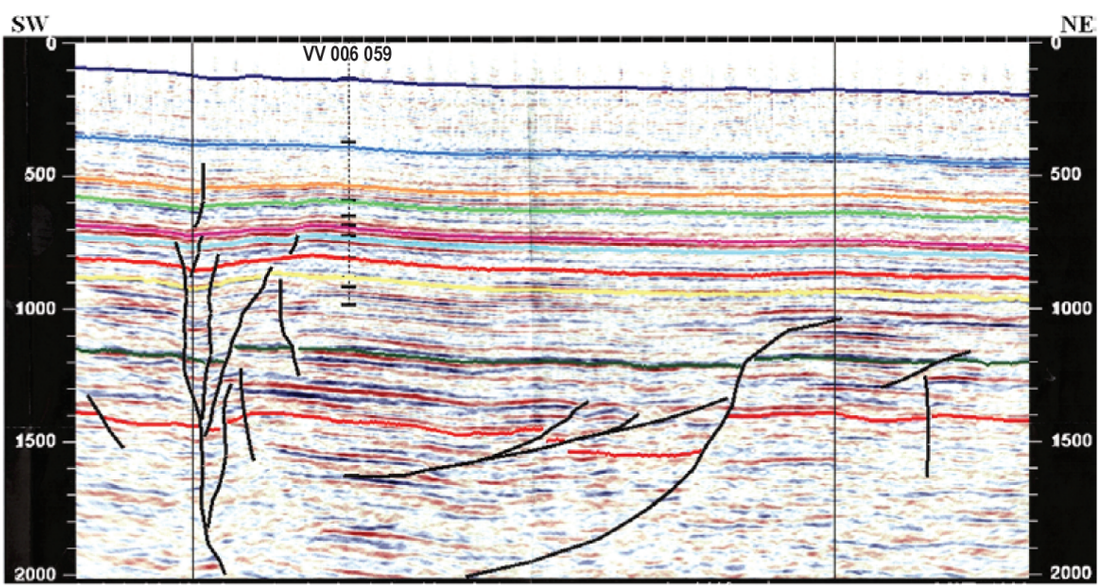


Fig. 17b. NE-SW trending line, North Balat area.

reactivation of NE-SW trending pre-Upper Cretaceous faults.

The seismic lines presented in Figures 21a and 21b are from the eastern edge of the Zaltan Platform (Harash Field). Although they cover only a very small portion of the platform area; they clearly show the northeastward late Tertiary tilting, towards the Ajdabiya Trough.

A complicated picture along the eastern edge of the Zaltan Platform, in the Harash Field is shown in Figure 21a. It is clear that at the time of deposition of the Upper Cretaceous formations the area along the edge was structurally higher, overlain by thinner formations. Only after the late Tertiary tilting (Fig. 21b), was this superior structural situation lost (similar to the Az Zahrah-

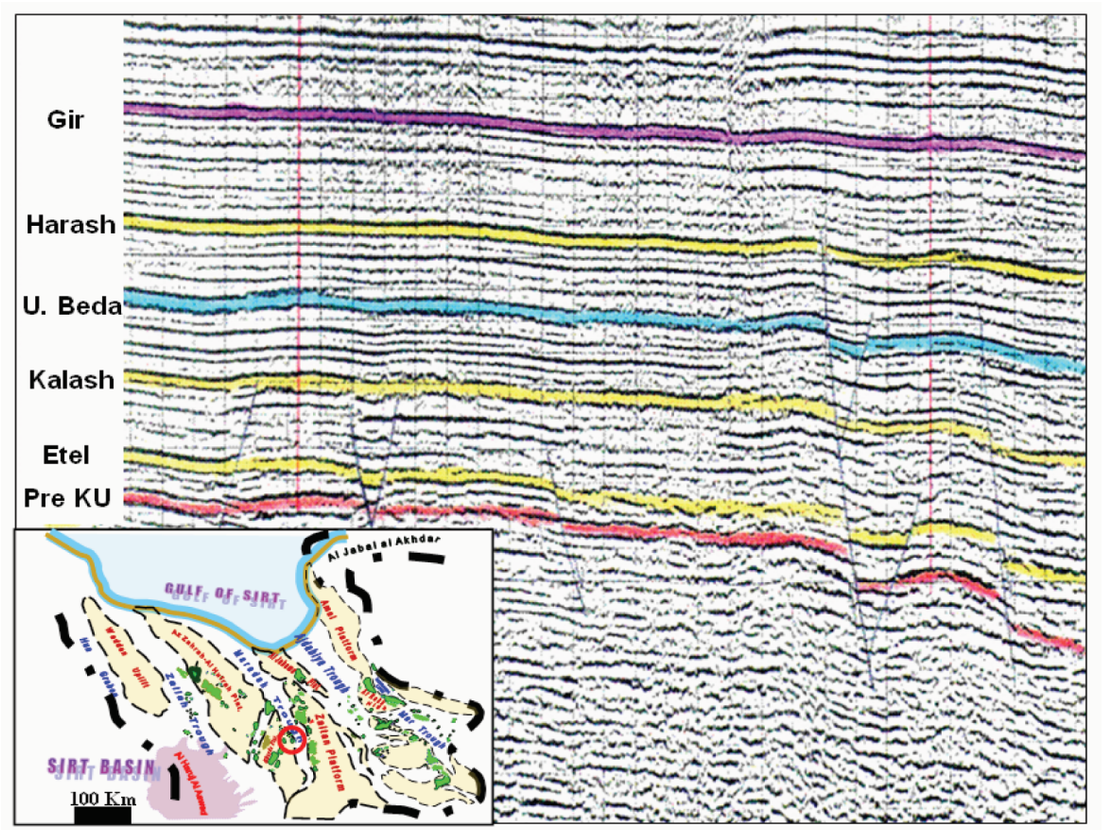


Fig. 18. NW-SE trending line, across Zaggut Field.

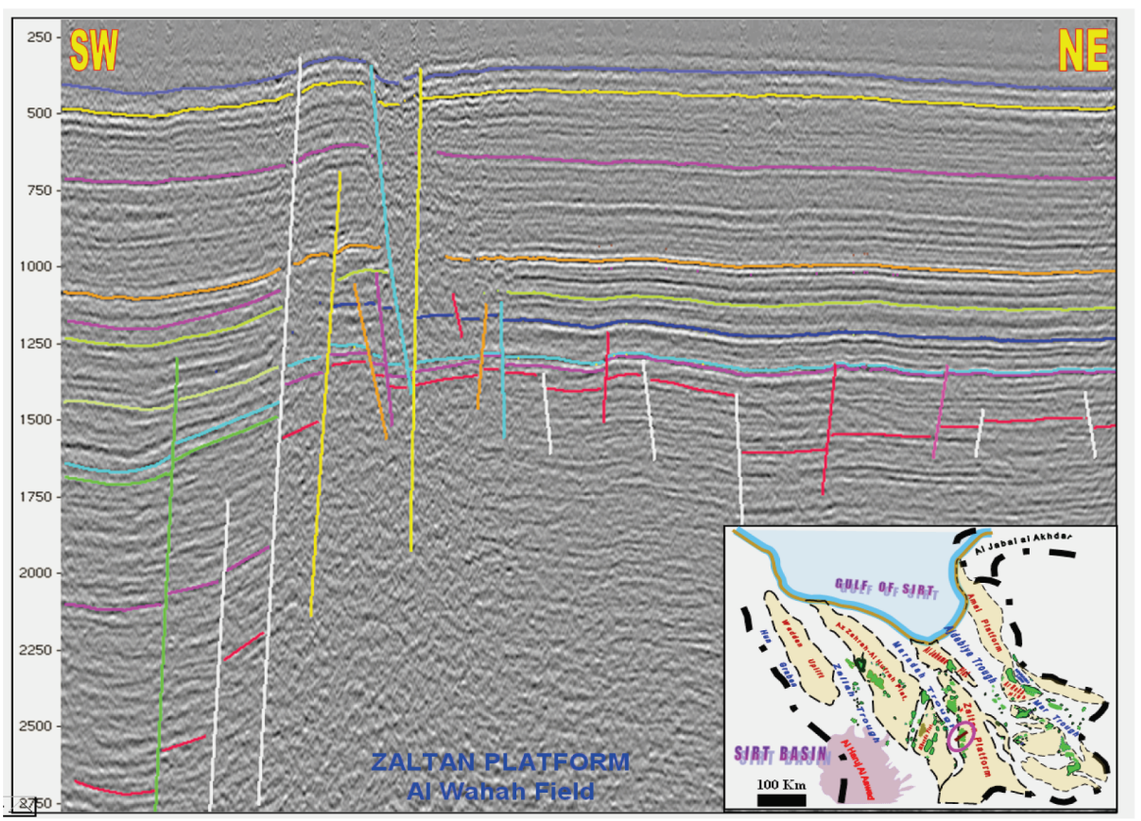


Fig. 19. NE-SW line across the Al Wahah Field, western edge of the Zaltan Platform.

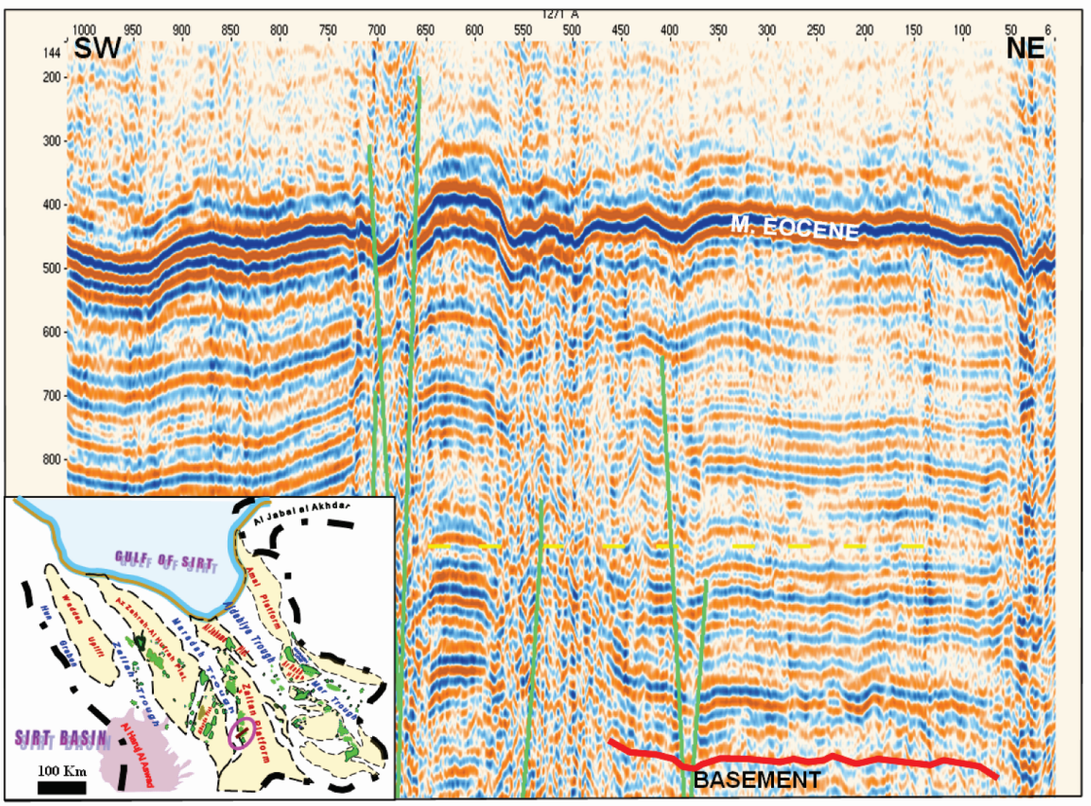


Fig. 20. NE-SW trending line across the Al Daffah Field, western edge of the Zaltan Platform.

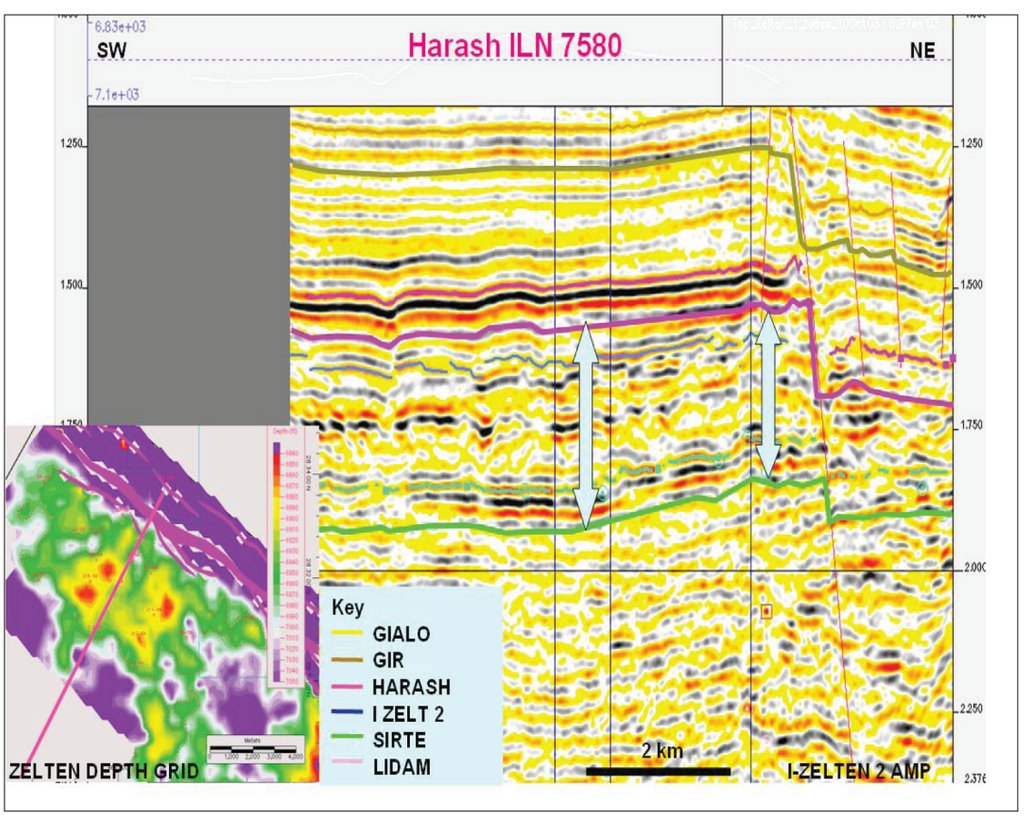


Fig. 21a. NE-SW trending line, Harash area, eastern edge of Zaltan Platform.

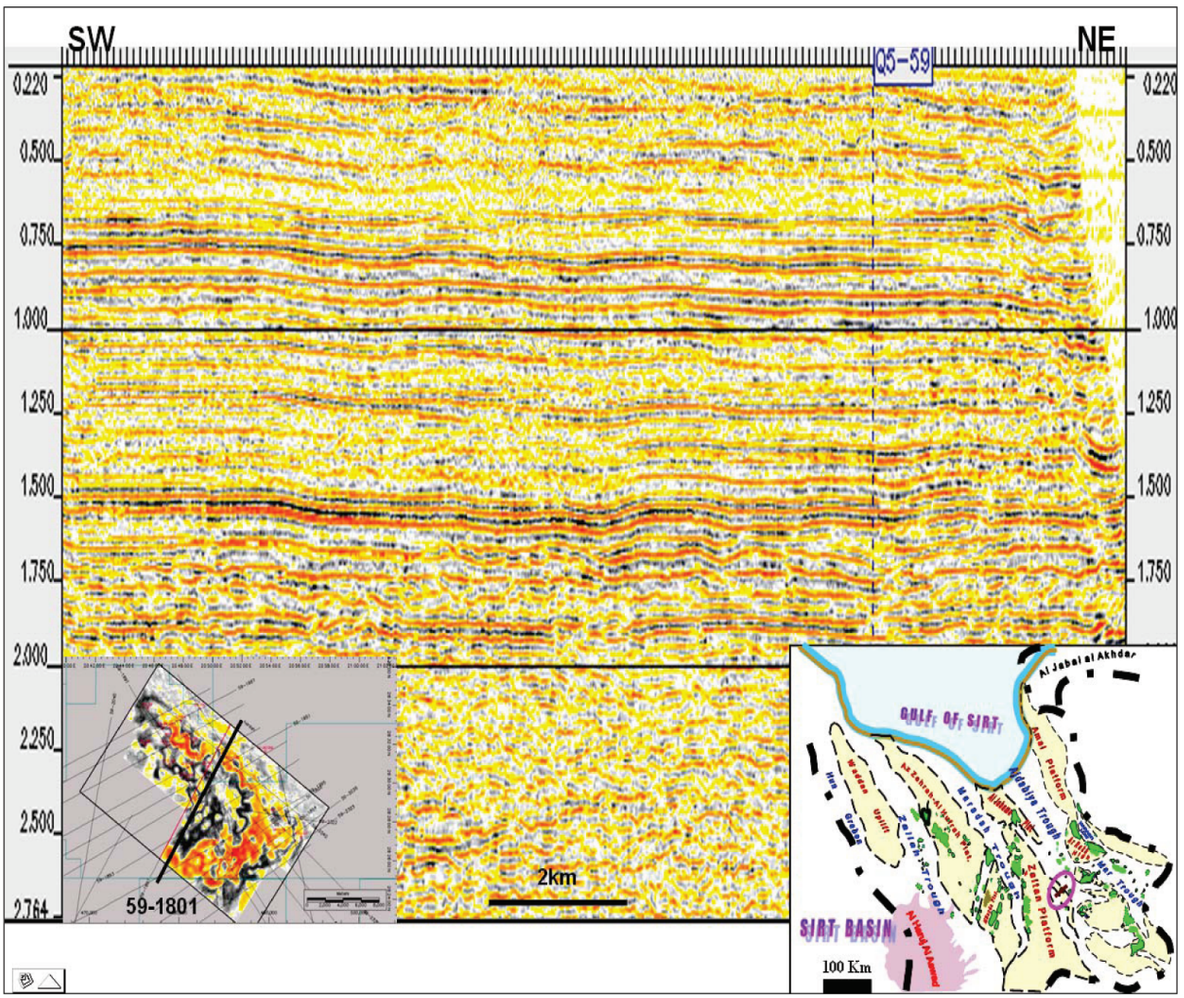


Fig. 21b. NE-SW trending line, Harash Field, eastern edge of Zaltan Platform.

Al Hufrah Platform, Fig. 12) and the present complicated picture evolved.

Another important point to note in this seismic line is the fault displacement which are more at the shallow horizons compared to the deep ones. This type of fault displacement is considered here as reversal blocks movement; which means a faulted tectonic block was higher at earlier stage and reversed its structural position later. These types of fault displacements (larger displacement at the shallower horizons) may be interpreted as strike-slip faults; but the only late Tertiary major tectonic events (subsidence and tiltings discussed in this paper) in the Sirt Basin are the most reasonable explanations for these complicated structural pictures.

Reversal block movements are observed not only along the edges of the platforms; but also are frequently seen in different magnitudes and directions in the trough areas, which make them difficult to be interpreted as strike slip faults due to a single compressional force.

Some relatively young structural lineaments, affecting all the formations of deep and shallow horizons, are observed in different parts of the Sirt Basin. These lineaments are believed to be of tectonic nature and the result of late Tertiary subsidence and tilting of different blocks.

The following seismic line (Fig. 22) shows one of these late Tertiary tectonic lineaments in the northern part of Waha's Block NC-98, along the eastern plunging nose of Rakb High, Eastern Sirt Basin.

Regional structural study of the Zaltan Platform indicates that the northern extension of the platform, called Al Jahamah Platform (see Fig. 1) is extremely complicated by the late Tertiary tectonic events, and differential and reversal block movements are expected to be very common (Fig. 23).

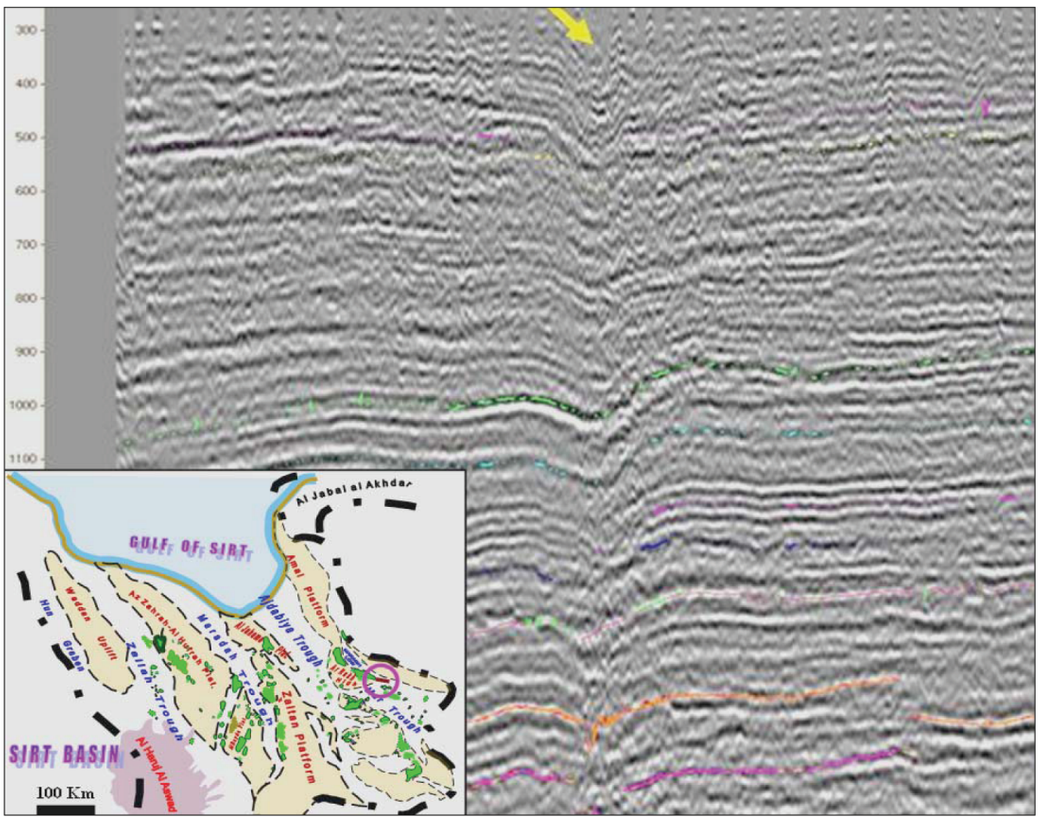


Fig. 22. Late Tertiary structural lineament, eastern nose of Rakb High.

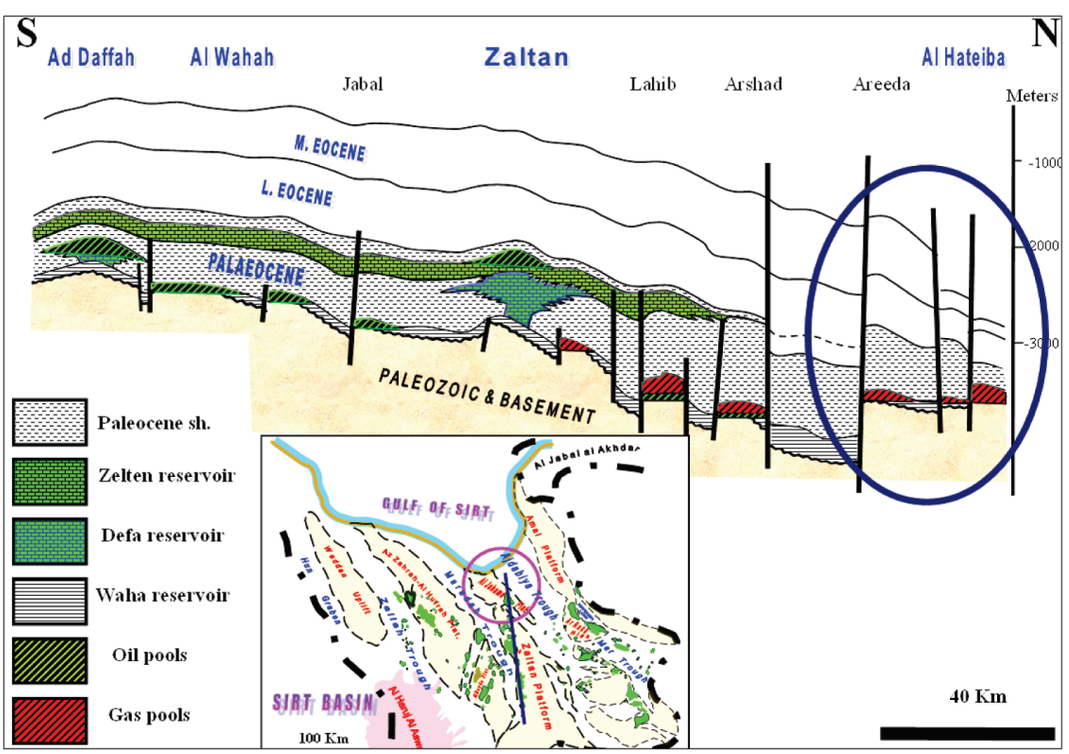


Fig. 23. N-S Regional Cross Section across the Zaltan Platform.

REFERENCES CONSULTED

Abuhajar, M.I. and Roohi, M., 2003. Giant Fields in the Sirt Basin, Libya. North Africa/Mediterranean Petroleum & Geosciences Conference and Exhibition. Tunis, 6-9 October 2003.

Ahlbrandt, T.S., 2002. The Sirte Basin Province of Libya, Sirte-Zelten Total Petroleum System. *U.S. Geological Survey.* only available online at: http:/geology. cr.usgs.gov/pub/ bulletins/b2202-f .

Barr, F.T. and Weegar, A.A., 1972. *Stratigraphic Nomenclature of the Sirte Basin, Libya.* Petrol. Explor. Soc. Libya, 179 p.

Burwood, R., 1997. Petroleum systems of the east Sirte Basin. *Am. Assoc. Petrol. Geol.* **81**, 1365.

Clifford, A.C. 1986. African oil- past, present and future. In: M. T. Halbouty (ed): *Future Petroleum Provinces of the World. Amer. Assoc. Pet. Geol. Mem.*, **40**, 339-372.

Clifford, H.J., Grund, R. and Musrati, H., 1980. Geology of a stratigraphic giant: Messla oil field, Libya. In: M. T. Halbouty, *Giant Oil and Gas Fields of the Decade 1968-1978. Mem. Amer. Assoc. Petrol. Geol.,* **30**, 507-524.

El-Alami, M., Rahouma, S. and Butt, A.A., 1989. Hydrocarbon habitat in the Sirte Basin, Northern Libya. *Petrol. Res. J.,* Tripoli, **1**, 17-28.

El-Alami, M. A., 1996. Habitat of oil in Abu Attiffel area, Sirt Basin, Libya. In: M.J. Salem, A. S. El-Hawat and A. M. Sbeta (eds.). *The Geology of Sirt Basin*, **II**, 337-348, Elsevier. Amsterdam.

Futyan, A. and Jawzi, A. H., 1996. The hydrocarbon habitat of the oil and gas fields of North Africa with emphasis on the Sirt Basin. In: M.J. Salem, A.S. El-Hawat and A.M. Sbeta (eds.). *The Geology of the Sirt Basin*, **II**, 287-308. Elsevier, Amsterdam.

Hallett D., 2002. *Petroleum Geology of Libya.* Elsevier, Amsterdam, 503 p.

Roohi, M., 1996a. A geological view of source-reservoir relationships in the western Sirt Basin. In: M. J. Salem, A. S. El-Hawat and A. M. Sbeta, (eds.)*, The Geology of Sirt Basin,* **II,** 323-336 Elsevier, Amsterdam.

Roohi, M., 1996b. Geological history and hydrocarbon migration pattern of the central Az Zahrah-Al Hufra Platform. In: M. J. Salem, A.S. El Hawat and A. M. Sbeta (eds.), *The Geology of the Sirt Basin,* **II**, 435-454, Elsevier, Amsterdam.

Sanford, R.M., 1970. Sarir oil field, Libya – desert surprise. In: M. T. Halbouty (ed) *Geology of Giant Petroleum Fields. Mem. Amer. Assoc. Petrol. Geol.* **14**, 449-476.

Westaway, R., 1996. Active tectonic deformation in the Sirt Basin and its surroundings. In: M.J. Salem, M.T. Busrewil, A.A. Misallati and M.J. Sola, (eds). *The Geology of Sirt Basin,* **III,** 89-100, Elsevier, Amsterdam.

Petroleum Res. J. Vol. 20 (2007); P. 77–94, 17 Figs.

Seismic Reprocessing: Case Study Barrut Arch, Concession 72, Sirt Basin, Libya

Ali Abuagela, and Naji Miladi*

دراسة حالة إعادة المعالجة السيزمية لقوس باروت بعقد الامتياز رقم 72 بحوض سرت، ليبيا

علي أبو عجيلة وناجي الميلادي

تم إختيار البيانات التي تم مسحها عام 1999ف لاختبار فاعلية إعادة معالجة البيانات السيزمية بمنطقة قوس باروت شمال غربي عقد الامتياز 72 لغرض إعادة المعالجة حيث أوضحت المعالجة الأصلية للمقاطع السيزمية ضعفا في نوعية البيانات وذلك من خلال صعوبة متابعة استمرارية الانعكاس السيزمي، خاصة مع وجود تصدعات بالمنطقة وهو ما زاد في صعوبة التفسيرات السيزمية. إن المشاركيْن في هذا المشروع قد عملا جنبا إلى جنب مع المعالج بصورة دائمة لاختيار أفضل الطرق في كل مرحلة من مراحل المعالجة الانسيابي.

إن المقطع السيزمي النهائي الذي أعيدت معالجته قد أوضح تحسنا ملحوظا وخاصة في استمرارية الانعكاس السيزمي ووضوح التصدعات مقارنة بالمقطع الأصلي وبذلك تم تحاشي خيار تنفيذ برنامج مسح سيزمي جديد باهظ التكلفة.

Abstract: To test the benefits of reprocessing, 2D vibroseis data acquired in 1999 over the Barrut Arch in NW Concession 72 was selected for reprocessing. The original processed sections showed the data to be of poor quality where reflection continuity was difficult to follow. Also, the area is heavily faulted, which increased interpretation difficulties. The project participants worked with the processors on continuous bases in order to select the best parameters from each stage of the processing flow.

The final reprocessed seismic profiles illustrate significant improvement in horizon continuity and fault definition over the original processed data. The very expensive option of acquiring new seismic program was avoided.

INTRODUCTION

Often older vintages of seismic data no longer meet the current requirements and geological objectives of exploration interpreters. When this stage is reached in an exploration project, the only options are to acquire new seismic program or reprocess the existing seismic database with the latest advanced techniques. Reprocessing is significantly more cost effective than the field acquisition of new seismic data. Processing methods in the areas of statics (signal-to-noise enhancement, frequency balancing, and migration) have advanced. Seismic data reprocessing, using state of the art techniques, should result in overall improvement in reflection detail, resolution, and frequency enhancement. Therefore, the reprocessed seismic data will be available for a more meaningful interpretation. Added attention to the statics solution, frequency balancing, and velocity corrections should help reduce or eliminate intersection misties. The objective was to improve horizon correlation and fault definition.

* Veba Oil Operations - Tripoli , Libya.

Geographical Setting

Concession 72 is located over the Ayn An Nagah Sub-Basin. This Sub-basin is the most southern in a series of sub-basins that together form the northwest trending Zallah Trough (Fig.1). The Zallah Trough is the major western component of the regional horst and graben structural fabric of the Sirt Basin (Johnson, 1992). The concession is subdivided into three blocks and is named from north to south; Barrut, Ayn An Nagah, and Al Abrag (Fig.1) (Johnson, 1992).

Geological Setting

The Barrut Arch was structurally active during Oligocene to Post- Eocene. The arch had continued to rise through the Eocene and maintain its north-easterly trend on Concession 72. A fault reactivation occurred after the Eocene when the subsidence of the basin was at its maximum. These faults dissected the arch and cut across adjacent areas. The continued rise of the arch after this period of faulting caused additional displacement along faults which reached

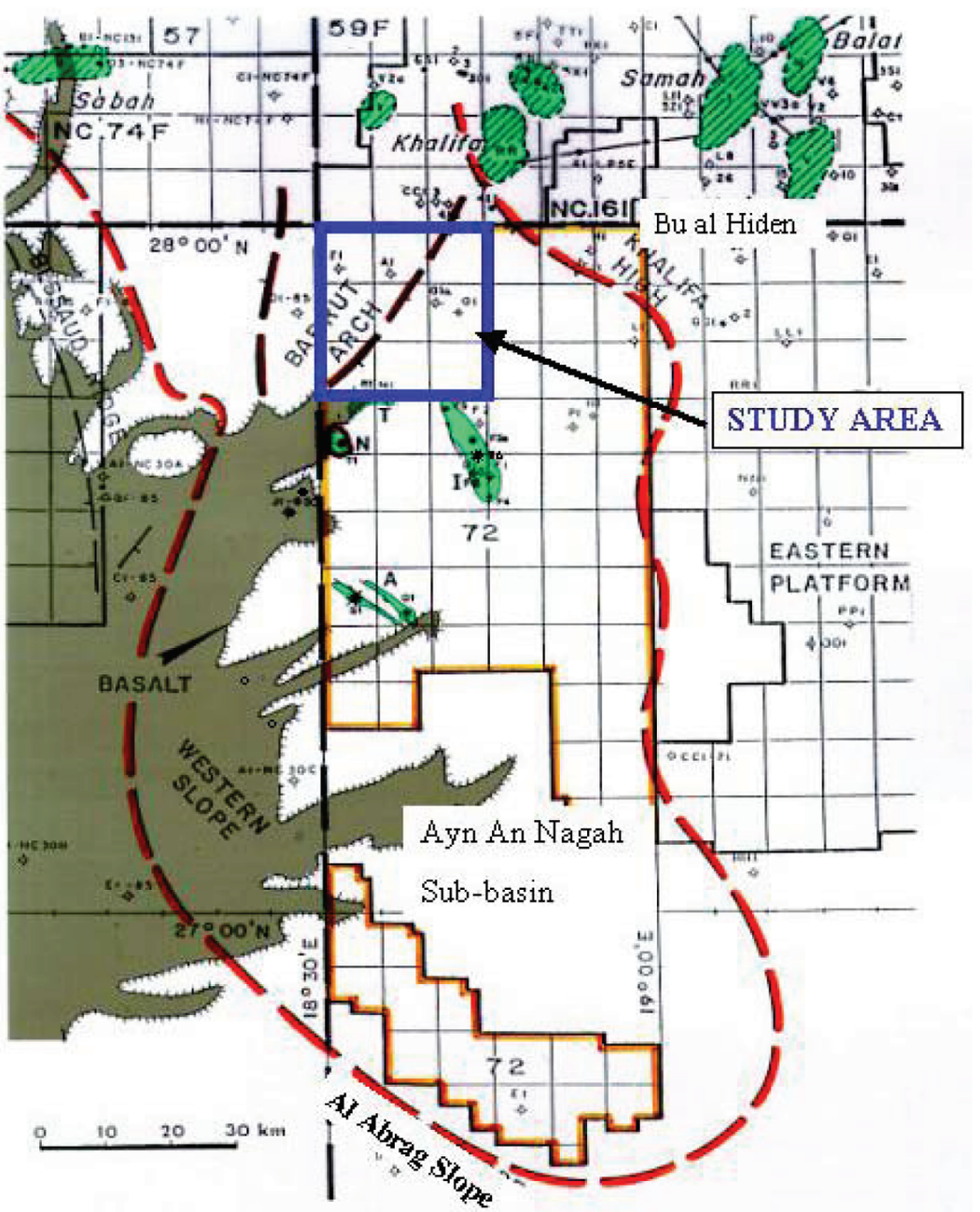


Fig. 1. Concession 72 location map showing Cretaceous boundaries of the Ayn An Nagah Sub-basin and the Barrut Arch.

or had influence further into the Ayn An Nagah Sub-basin. Some of these faults have a rotational or wrench-like character (Johnson, 1992). Additional faulting or fault adjustments may have accompanied the later igneous activity.

Surface Geology

The rocks and sediments exposed on Concession 72 range in age from Eocene to Recent. The oldest exposures are three outcrops of Eocene Gialo Formation located at the crest of the Barrut Arch in northwest Concession 72. The Barrut Arch is the only large scale structural feature exposed at the surface in Concession 72. Its southerly trending axis is two km west of well A1-72 where it then curves to the southwest off the concession. Oligocene and Miocene strata form escarpments which dip to the southeast and define portions of the arch's south-eastern flank. Minor structural features, exposed at the surface on or near the arch, include northwest trending fault traces, a fracture zone and collapse structures. A shallow syncline runs parallel to the arch's south-eastern flank between wells A1-72 and G1a-72.

Basalts are exposed at the surface in the Barrut Arch. The most prominent is a volcanic neck named Gleb el Barrut. It is located 5.2 km south-southwest of well A1-72 and is a radiating dike. Other intrusives, mostly dikes, occur at the surface in this area and have been described in some detail by Roadifer (1958), Geophoto Libya Inc. (1959), Johnson and Gates (1959), and Banar (1967).

SEISMIC SURVEYS

The seismic dataset in the Barrut Arch consists of 276.5 kms of regional 2D conventional seismic data of the surveyed lines acquired by VOO company in 1999 (Table 1). The data coverage is sparse over most of the Barrut Arch (Fig. 2). The quality of the data ranges from poor to good. Structural complexity and surface condition affects the data quality.

Table 1. List of lines re-processed, Concession 72 NW, Barrut Arch area.

Line	First VP	Last VP	First CDP	Last CDP	Length Kms	Direction
72-99-18	101	572	206	1142	18.840	SW-NE
72-99-19	101	781	206	1560	27.200	SW-NE
72-99-20	101	713	206	1424	24.480	NE-SW
72-99-21	101	454	206	905	14.120	SW-NE
72-99-22	101	701	206	1400	24.000	NW-SE
72-99-23	101	494	206	986	15.720	NW-SE
72-99-24	101	636	206	1270	21.400	NW-SE
72-99-25	101	856	206	1710	30.200	NW-SE
72-99-26	101	596	206	1190	19.800	NW-SE
72-99-27	101	531	206	1059	17.200	NW-SE
72-99-28	101	558	206	1114	18.280	NW-SE
72-99-29	101	464	206	926	14.520	NW-SE
72-99-30	101	387	206	772	11.440	NW-SE
72-99-31	101	583	206	1164	19.280	SW-NE
Total					276.48	

The acquisition parameters for this survey are summarized in Table 2 below.

Table 2. Acquisition parameters, Concession 72 NW Barrut Arch.

INSTRUMENTS		RECEIVERS		SOURCE	
Items	Specification	Items	Specification	Items	Specification
Type:	Sercel SN 388	Receiver type:	Sensor SM4-UB 10hz	Type of Vibrators:	Geco-Prakla V4 VVFB 50,000lbs
No. live receiver lines:	1	No. geophones/stn:	48(4stringsof12)	No. Vibrators:	5
No. live channels/line:	120	Pattern:	Rhomboidal	Sweep:	12-72 Hz log . (9db) Hi emphasis
Low cut filter:	Out	String separation:	5m	Sweep Length:	10sec
High cut filter	125 Hz	Geophone separation:	3.33 m	Taper:	300 ms cosine start and end
Sample rate:	2 ms	Overall pattern length:	51.6 m	Polarity:	SEG
Record length:	5000 ms	Overall pattern width:	15m	No. of sweeps/VP:	8 – phase rotated
Coverage	60	Overall pattern width:	40m	vibrators pattern:	Rhomboidal
Polarity:	SEG			Inline move up:	4 m
				Cross line spacing:	6 m
				Total pattern length	48 m
				Total pattern length	24 m
				Source station spacing:	40 m
				Spread parameters:	2500-140-0-140-2500 m

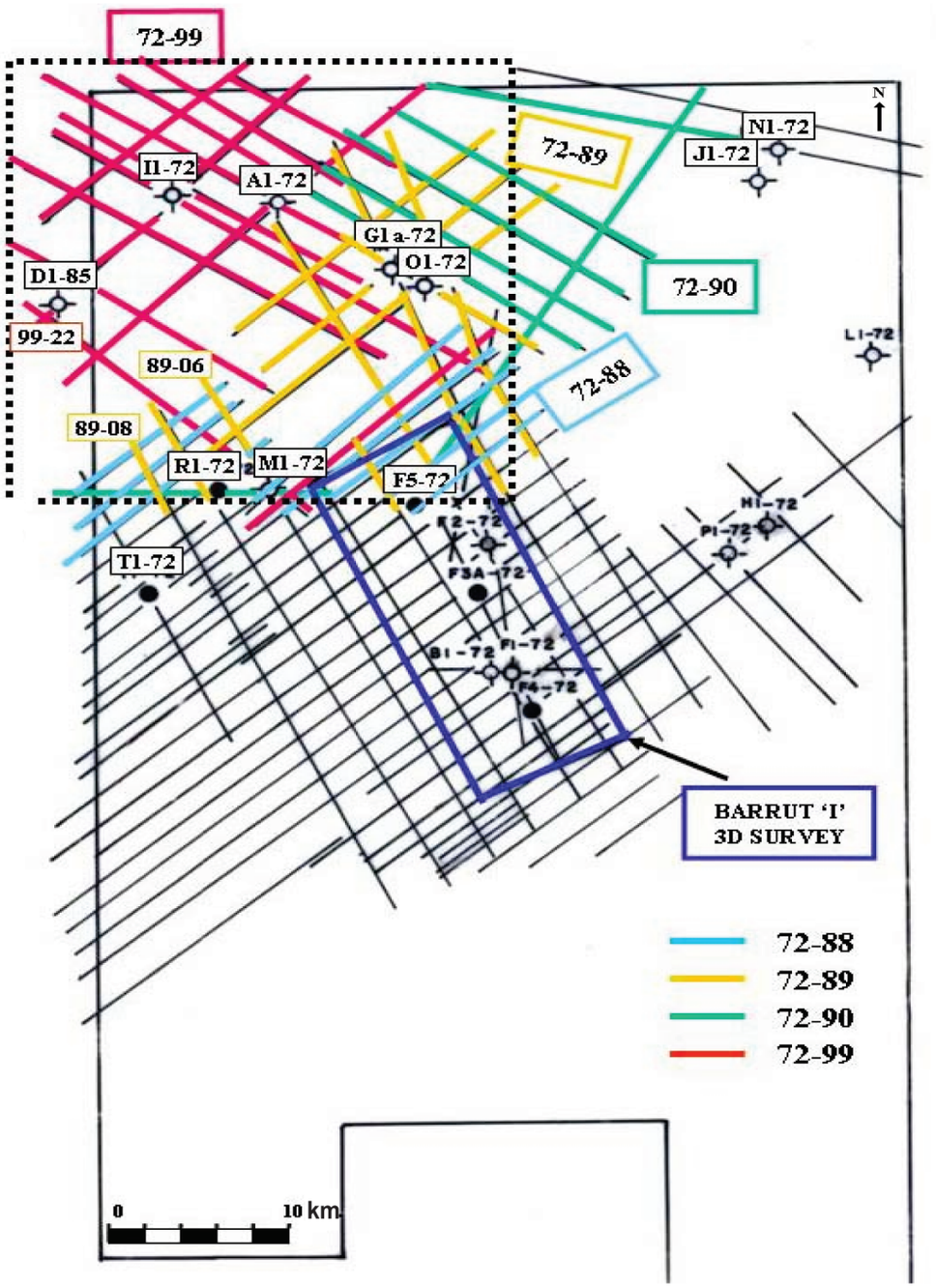


Fig. 2. Base map of Barrut Arch area, Concession 72.

CURRENT PROCESSING

Veba Oil Operations specified that the testing parameters should be performed on line 72-99-25.The summary of reprocessing test sequences are as follows:

Parameter Testing
Preprocessing
Reformat

The field data was received as 3480 cartridge taps. The data was in SEG D (Society of Exploration Geophysicists) demultiplexed format of 5 second record length, and sampling rate of 2ms.

The seismic support data (navigation and geometry) was supplied as SPS (Shell Processing Support) format files on floppy diskettes.

Geometry

The navigation and spread details, provided in

survey (Shell) positioning system (SPS) files, were converted and loaded into internal format. This geometry information was then checked. These included surface and subsurface fold, source, receiver, and midpoint location points.

After applying the geometry to trace headers a number of checks were made to ensure that there is no geometry anomalies between the data and the SPS files.

Data Editing

Interactive trace editing was performed to edit out the isolated noisy and dead traces.

Statics Calculation and Application

Most of the QC (Quality Control) of refraction static has been performed using first-break stacks of the dominant refractor after LMO (linear move out) correction (Fig. 3). The refractor velocity is averaged over each shot point-receiver vector, which entails a natural smoothing filter.

The first-break stack quality should be fair to good and its picking should closely approximate the average of the time-picks. First-break stacking is an efficient technique in many cases. This first-break stack inversion uses direct and reverse shooting with respect to the general direction of acquisition.

Two methods are used for computing refraction static. The first method uses model tomography and is known as GLI (Generalised Linear Inversion and Tomographic Inversion).

The second method is referred to as traveltime decomposition and uses simplified tomography, beyond a simple averaging procedure. Each individual time-pick is decomposed into a source delay, a receiver delay and LMO terms. The Geophone cluster module follows the second method.

Once the geometry has been properly set up, launch the first-break stacking phase in two modes. Stacks are computed and displayed in their ring and pick the stacks. Traces were picked in the direct and reverse shooting.

Static corrections are computed from picks of the first arrivals of refraction stacks. Two stacks are

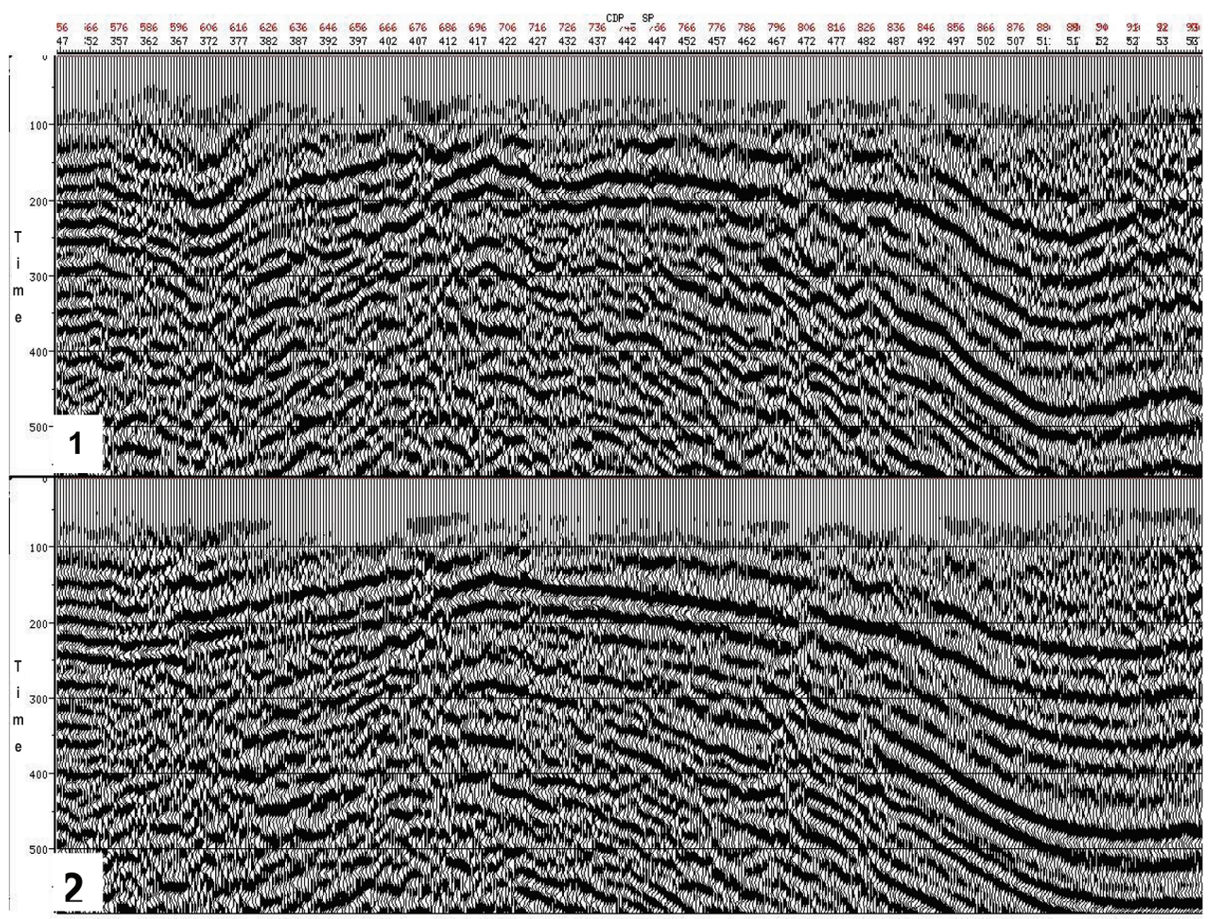


Fig. 3. Stack section showing: 1) stack with field statics, and 2) stack with refraction statics.

computed per source and receiver mode: direct and reverse stacks. Delays are computed for each point .Then, static corrections are computed from delays using weathering and refractor velocity parameters. Picking of elementary traces is used only with the computation of static and the result is saved in TDPIK or WXSTA format.

WXSTA is a program which computes static corrections from the times of the first break picks. The picking results from interactive applications, sorting and gathering of the picks allow construction of relative intercept curves which are handled according to the Gardner method.

Finally the statics were calibrated with the upholes, calculated and checked. The replacement velocity is used to correct from this pseudo datum to the final processing datum, in effect, a bulk shift in time. A replacement velocity of 2000 m/sec and a final datum of 200 m were used.

The result achieved, and the specific requirements to achieve the optimal result are shown below.

Although the first break pick quality was good, this area was characterized by some steeply dipping and discontinuous refractors, the statics application gave similar improvements (Fig. 3).

PRESTACK PROCESSING

Minimum phase conversion.

An auxiliary trace containing the filtered correlated pilot sweep was extracted. A minimum phase equivalent, a filter was calculated and applied to the seismic data.

True Amplitude recovery

Spherical divergence gain functions were tested. The optimal result was decided as the application of $T=V^2T$ (Fig. 4)

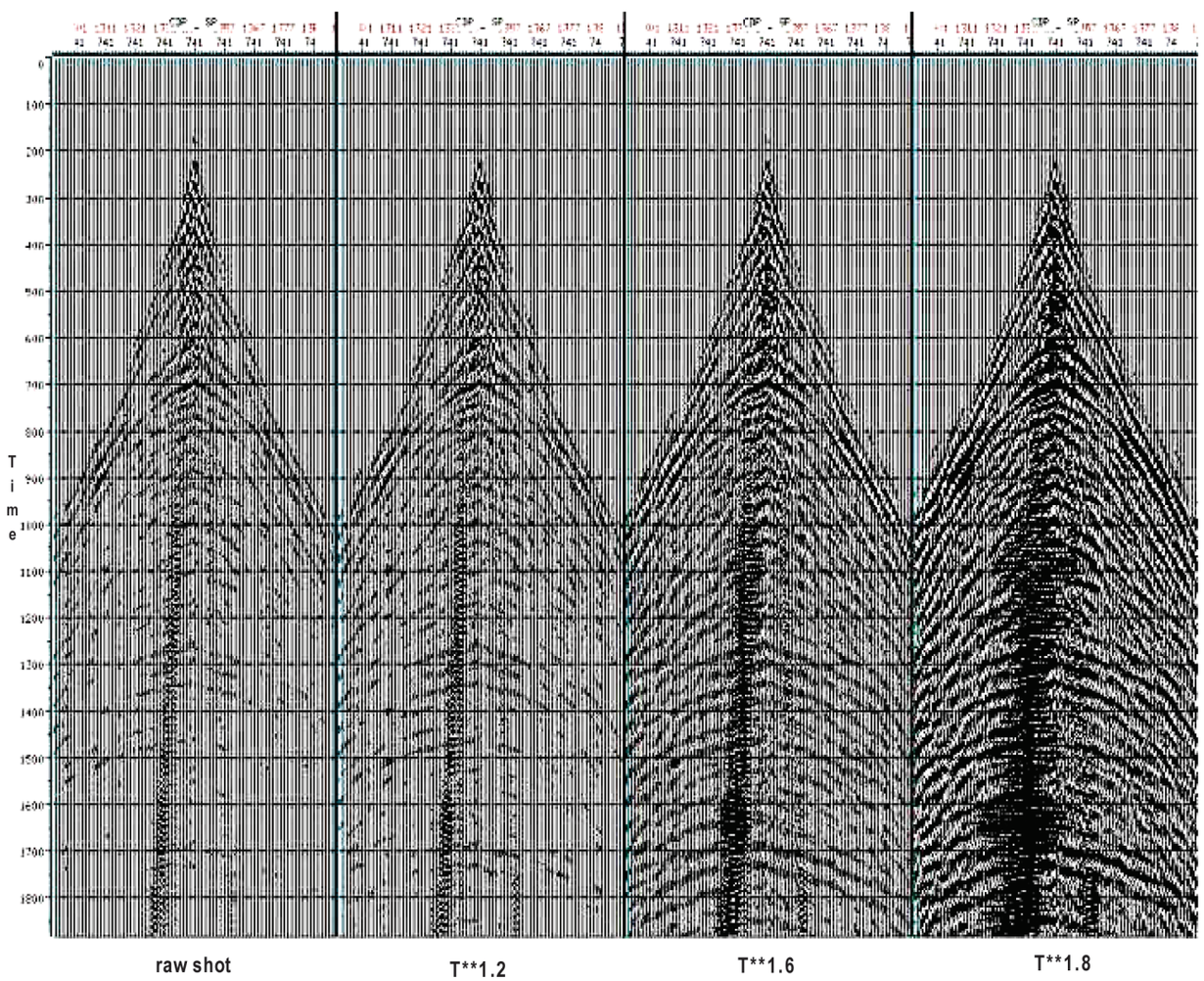


Fig. 4. Amplitude recovery.

Noise Attenuation

FK (frequency-wave number) filter test was performed with number of dips were tested to reduce a low frequency and spatially aliased groundroll. Plots were made of selected records, and the test lines stacked with the FK filter applied (Figs. 5a and 5b).

Deconvolution Before Stack (DBS)

Data was pre-processed with spherical divergence correction and (shot domain FK filtering applied. From the study of the above, the optimum operator length and predictive lag times were found. The test lines were then stacked using different DBS methods, ensemble DBS, one and two window trace DBS, and surface consistent DBS. The surface consistent DBS proved to give the best overall result (Fig. 6).

The final DBS parameters are: Surface consistent predictive deconvolution

Operator=160ms, lag=24ms, window: 0-1200ms

Operator=160ms, lag=12ms, window:

900-2400ms.

Initial Velocity Analysis

The initial or first pass velocity analysis was picked at 1km intervals using groups of 24 Common-midpoints (CMPs). The data was set to the near surface floating datum. The velocity were picked interactively, using constant velocity stacks, semblance, and gather displays is shown in Figure 7.

Residual Statics

The residual static program used is fully surface consistent medium and high frequencies. The analysis window was set to cover the maximum extent of good signalto noise (S/N) ratio data seen on the lines. The parameters for the residual statics applied are:

Window =200-2800 ms, maximum shift =15 ms, internal filter =12-55 Hz.

The residual statics typically provided very good short wavelength static control, and also solved for the longer wavelength static anomalies (Fig. 8).

Prestack Partial Time Migration (DMO)

The DMO used is a Kirchhoff-style based

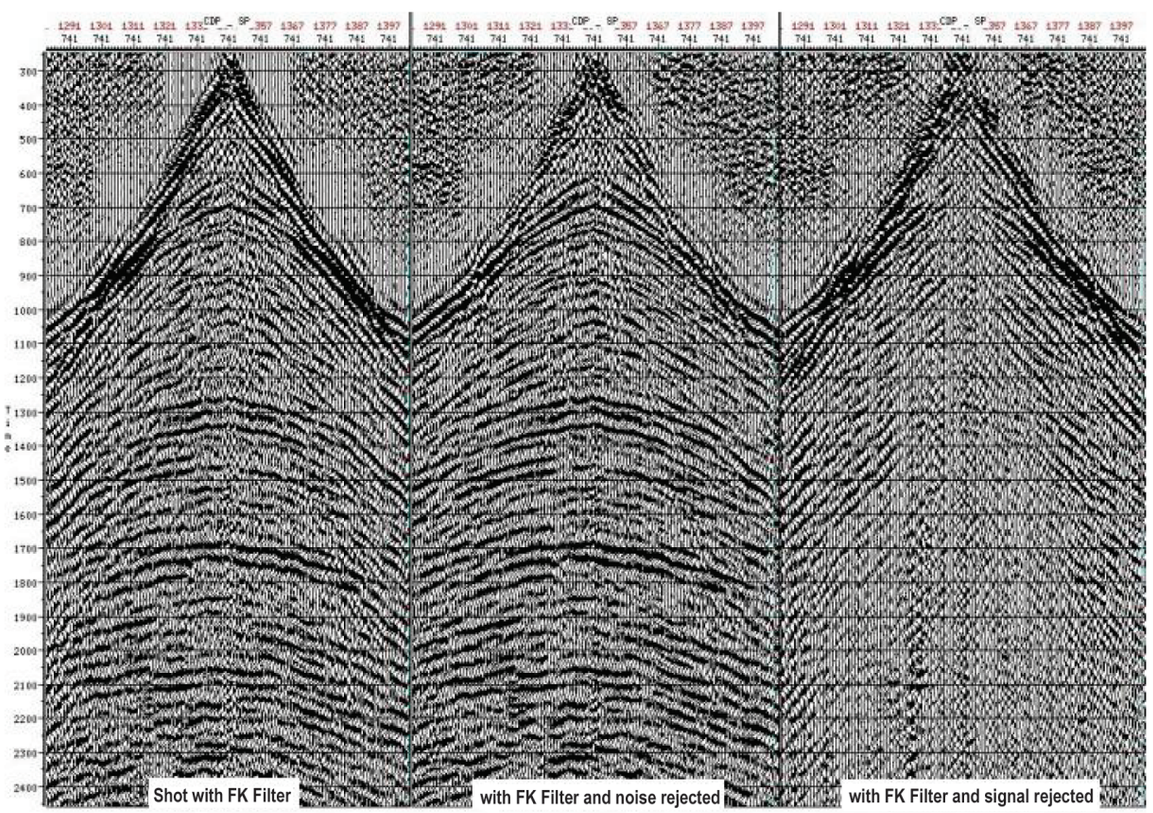


Fig. 5a. FK-filter full fan passing -/+ 4000 ms.

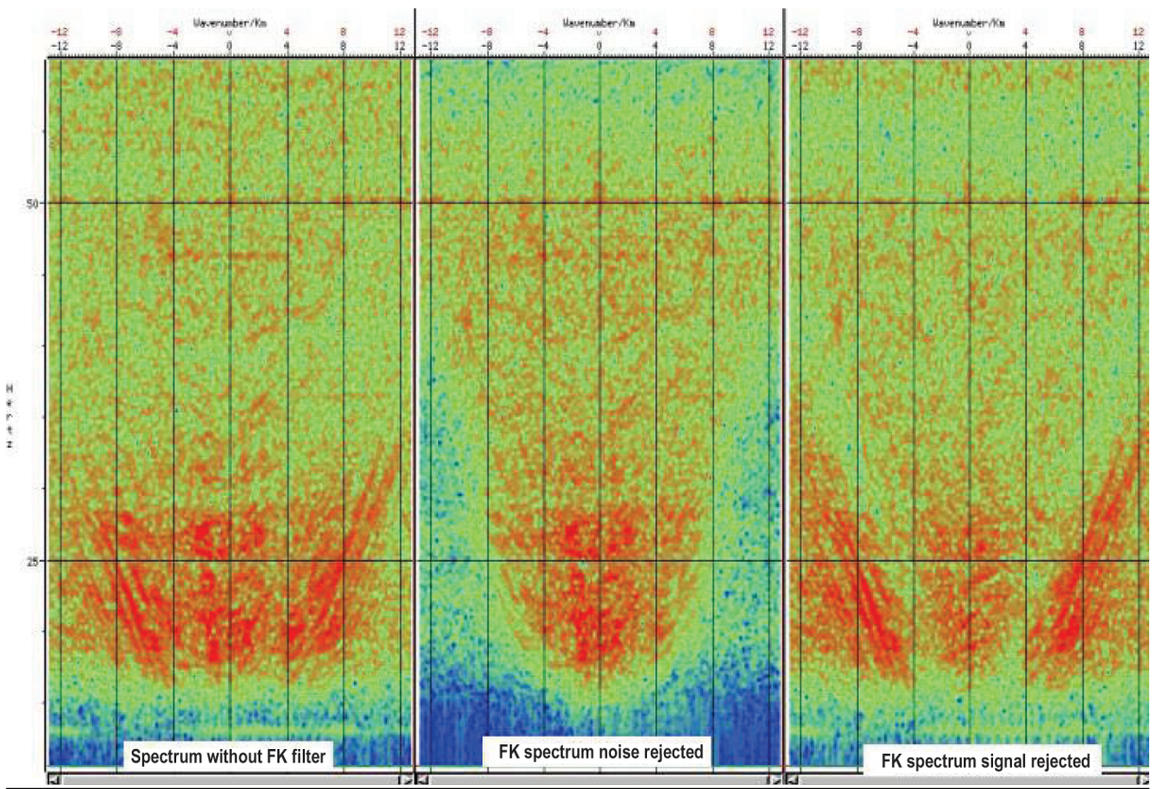


Fig. 5b. FK spectrum.

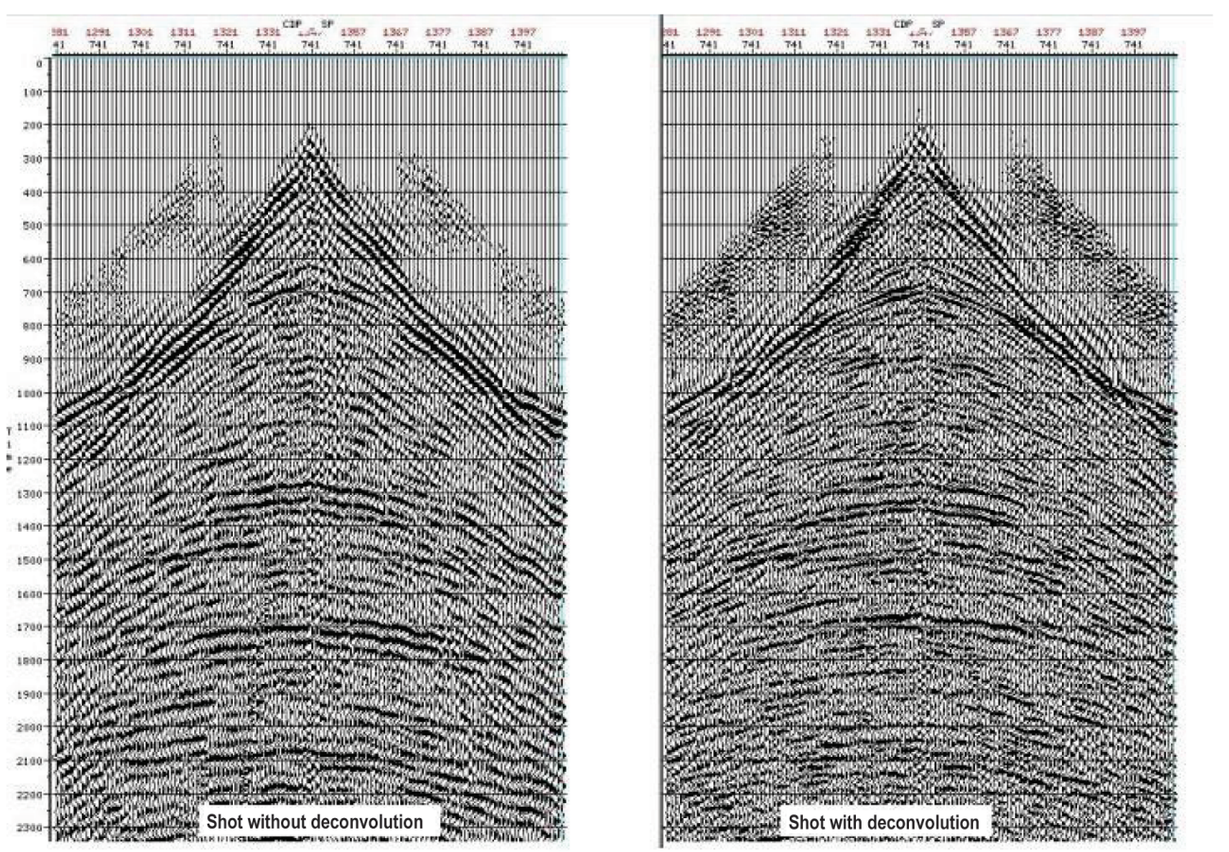


Fig. 6. Surface consistent deconvolution (predictive algorithm).

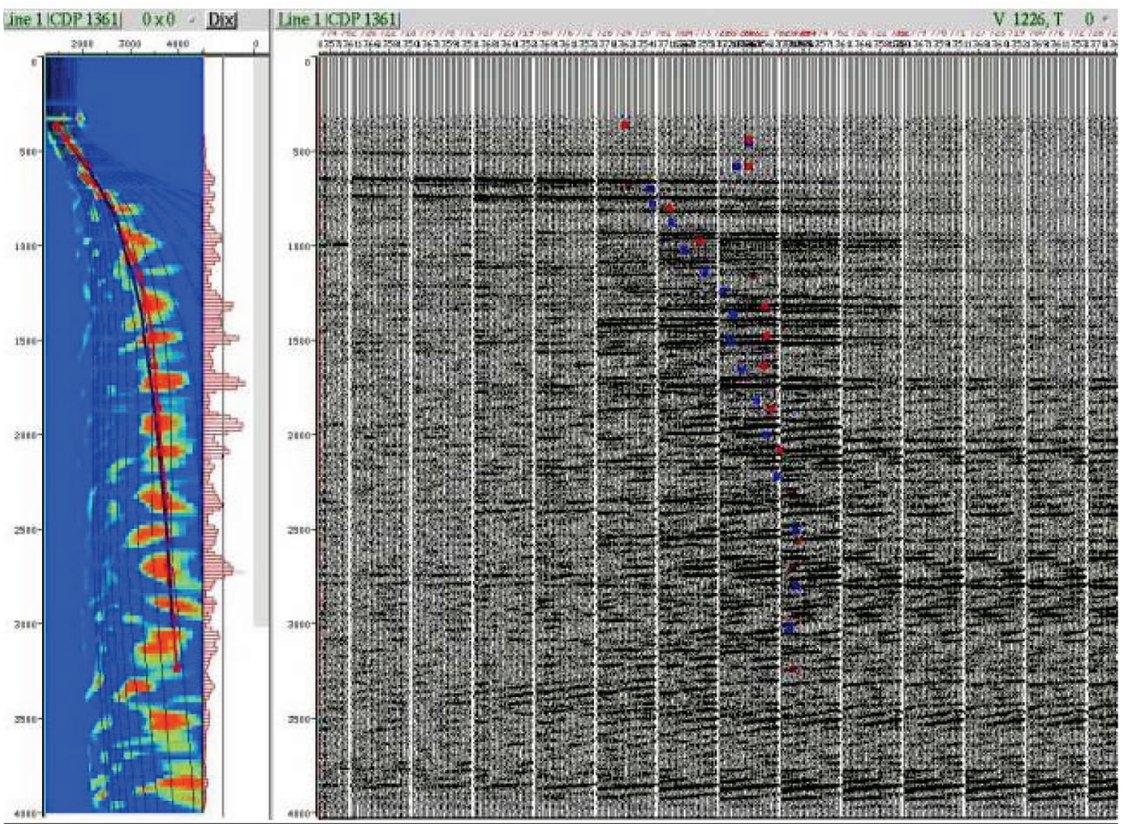


Fig. 7. Velocity spectrum.

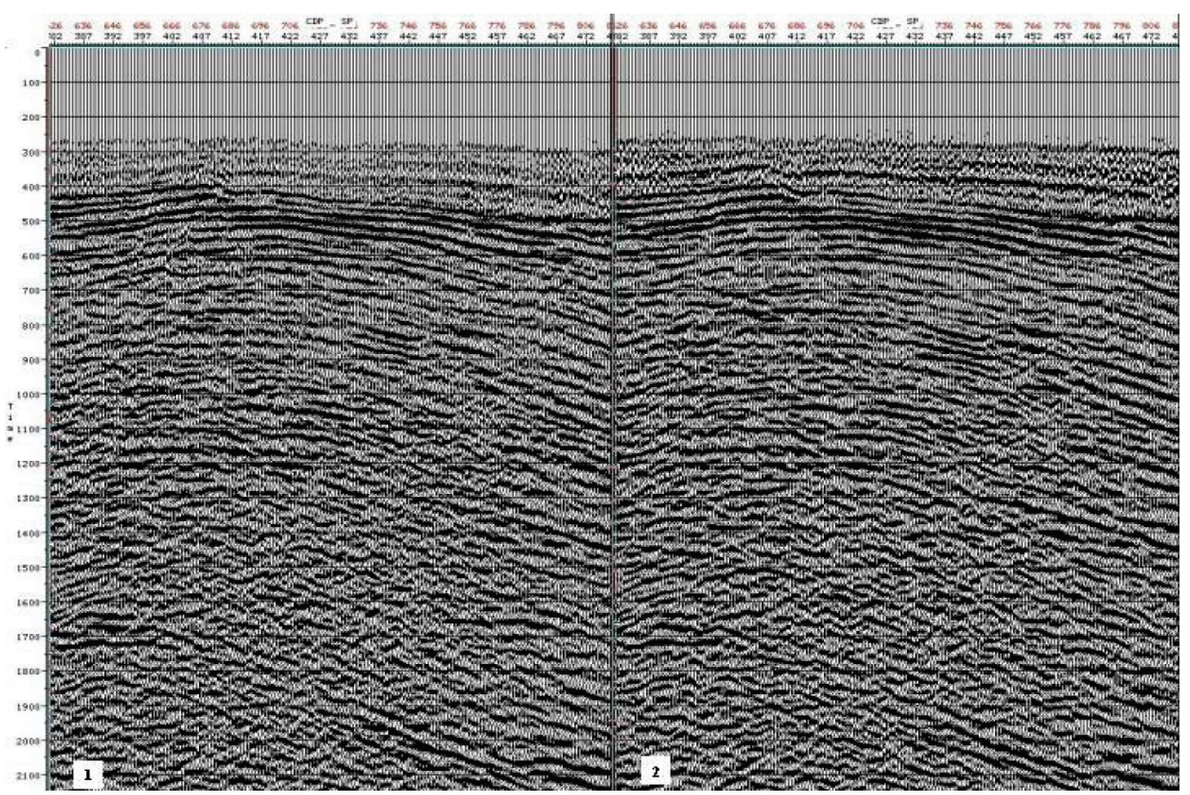


Fig. 8. Part of the stacked section showing: 1) without residual statics, and 2) with residual statics.

algorithm (Schneider, 1978). Data input to the DMO is in common offset order, has full static applied, and is NMO corrected with the 1km velocity field. The offsets were regularized to ensure each offset plane had a trace for each CMP.

The offset interval and DMO dip applied is: offset interval=80m, DMO dip=15 degrees. The DMO produced more significant effects on the steeper dipping data, but generally helped to improve the S/N ratio. (Fig. 9).

Final Velocity Analysis

The final or second pass velocity analysis was picked at 1km intervals using groups 24 CMPS. The data was set to the near surface floating datum, and pre-processed with the DMO and band pass filter applied. The velocities were picked interactively, using variable velocity stacks, semblance, and gather displays.

Second Pass Residual Statics

The same parameters were used as for the first pass of residual statics. The range of statics values from the second pass has never exceeded +/-5 ms.

Variable Muting

Variable muting were picked and refined interactively. The data was re-stacked with the revised mute (Fig.10).

POST STACK PROCESSING

Time Variant (TV) Band-Pass Filter

A time variant band-pass filter was derived from filter scan test .The filter parameters are: Time=0 –1000 / 1000 –2800 ms and Filter=12-55 /12-45 Hz.

Stack

Stack normalization/compensation scaling of the form 1/VN, where N is the stacking fold, was applied in the stacking process.

Final Scaling

Scaling function to balance and enhance the look of data was run. Automatic gain control (AGC)

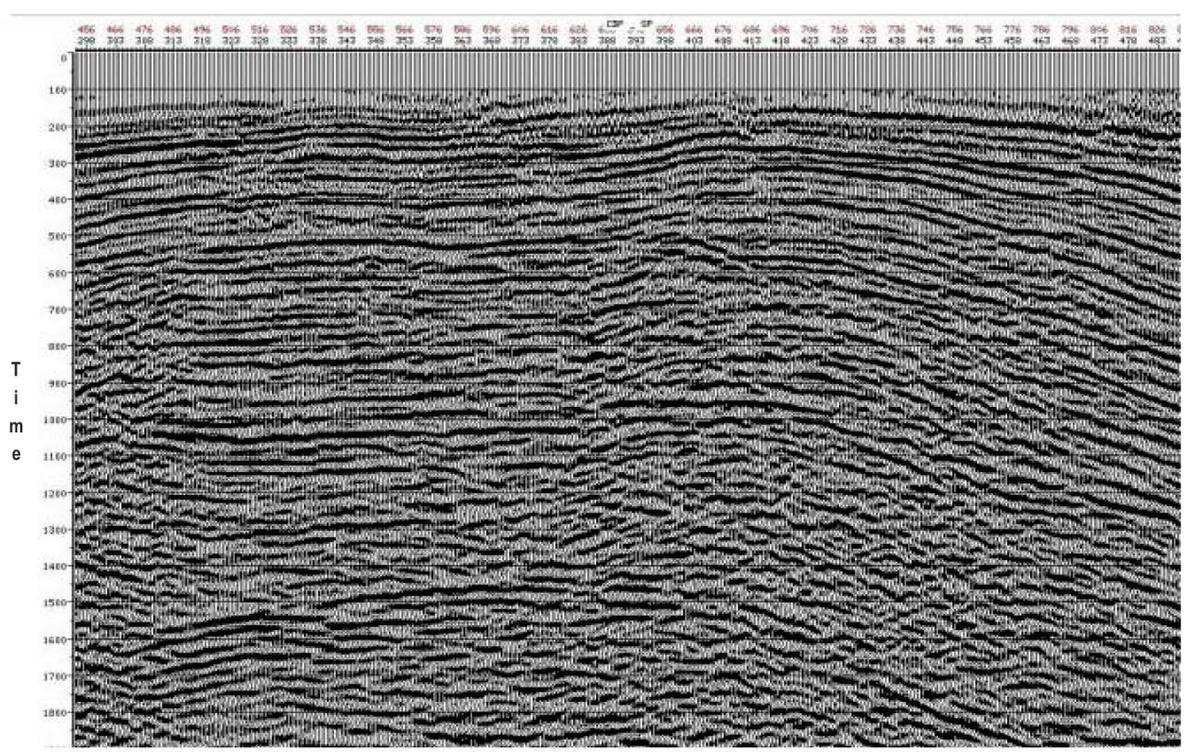


Fig. 9. Stack section of final DMO.

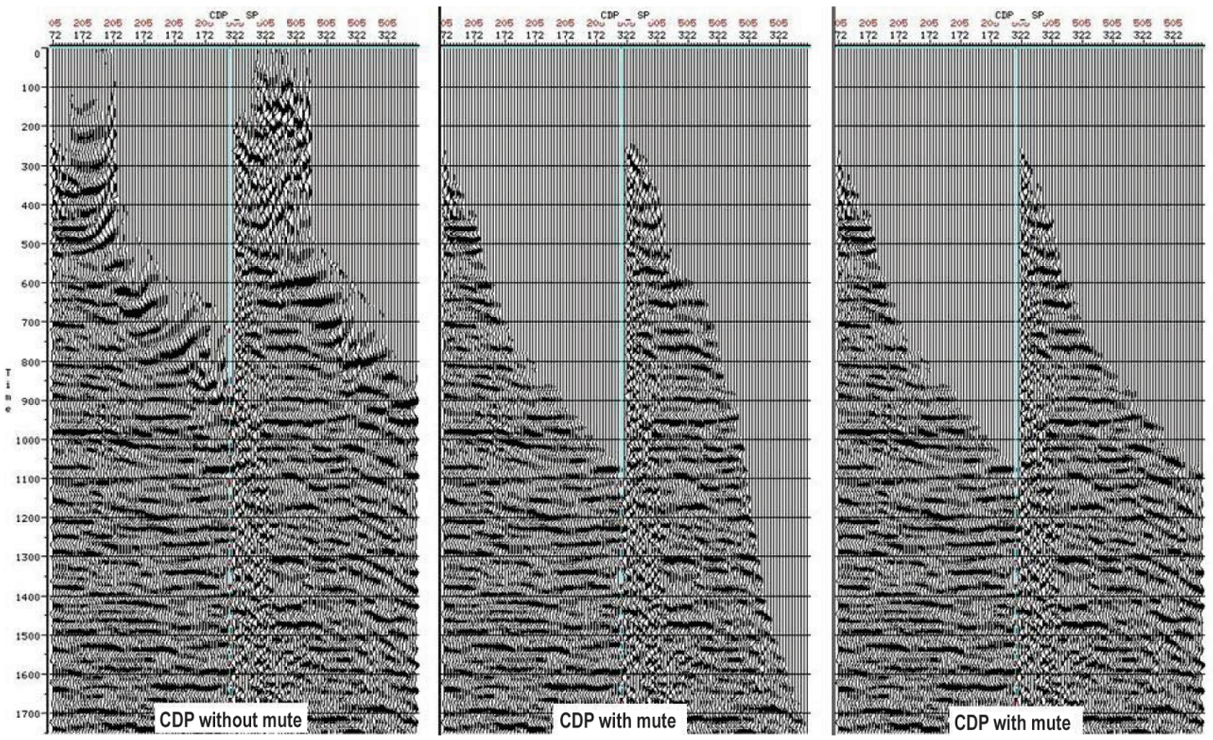


Fig. 10. Showing variable mute (middle) and constant mute (left).

scaling, trace balance (one and multi windows), AGC multi windows proved the most suitable.

The different scaling gates chosen are:

Time = 0 –1000ms AGC = 200ms.
= 1000-2800ms = 600ms.

Random Noise Attenuation in The F-X Domain.

To attenuate the random noise in a spatial-temporal gate, without affecting the spatially coherent events, Frequency-Distance (FX) filtering is performed. The parameters selected as optimal is:

Window in traces= 30, Filter in traces= 9, Filter= 8-45Hz.

Time Migration

An initial set of tests was carried out to test migration algorithms. Finite-difference, FX and Kirchhoff-Time migrations were run. The Kirchhoff-Time migration carried a clear advantage for concession 72NW (Barrut Arch area).

The velocities (Fig.11) input to the migration were tested at various percentages of the final stacking velocities. Results showed that 95% for Concession 72 NW (Barrut Arch Area) is the best (Fig.12).

SPECIAL TEST OF PRESTACK TIME MIGRATION (PSTM)

Prestack Time Migration is a method of imaging seismic data and makes it appear similar to the real geologic cross-section. The Prestack time migration is the data migrated with correct stacking velocities and is a rigorous solution to the problem at conflicting dips. Kirchhoff Prestack migration is a commonly used algorithm for Prestack time migration. It provides high resolution, accurate imaginary and improved velocity estimation (Fig. 13a,b,c, and d). It involves splitting the process into four steps (Fig. 14).

The reprocessing final production parameters are listed below:

REPROCESSING FINAL PRODUCTION PARAMETERS

1. Input: Seg D input data
   Sample rate =2ms length=5000ms 120 traces
2. Demultiplexing and gain removal
3. Editing
4. Geometry assignment
5. Amplitude recovery t**1.6
6. FK-filter full fan
   Passing 4000 m/s

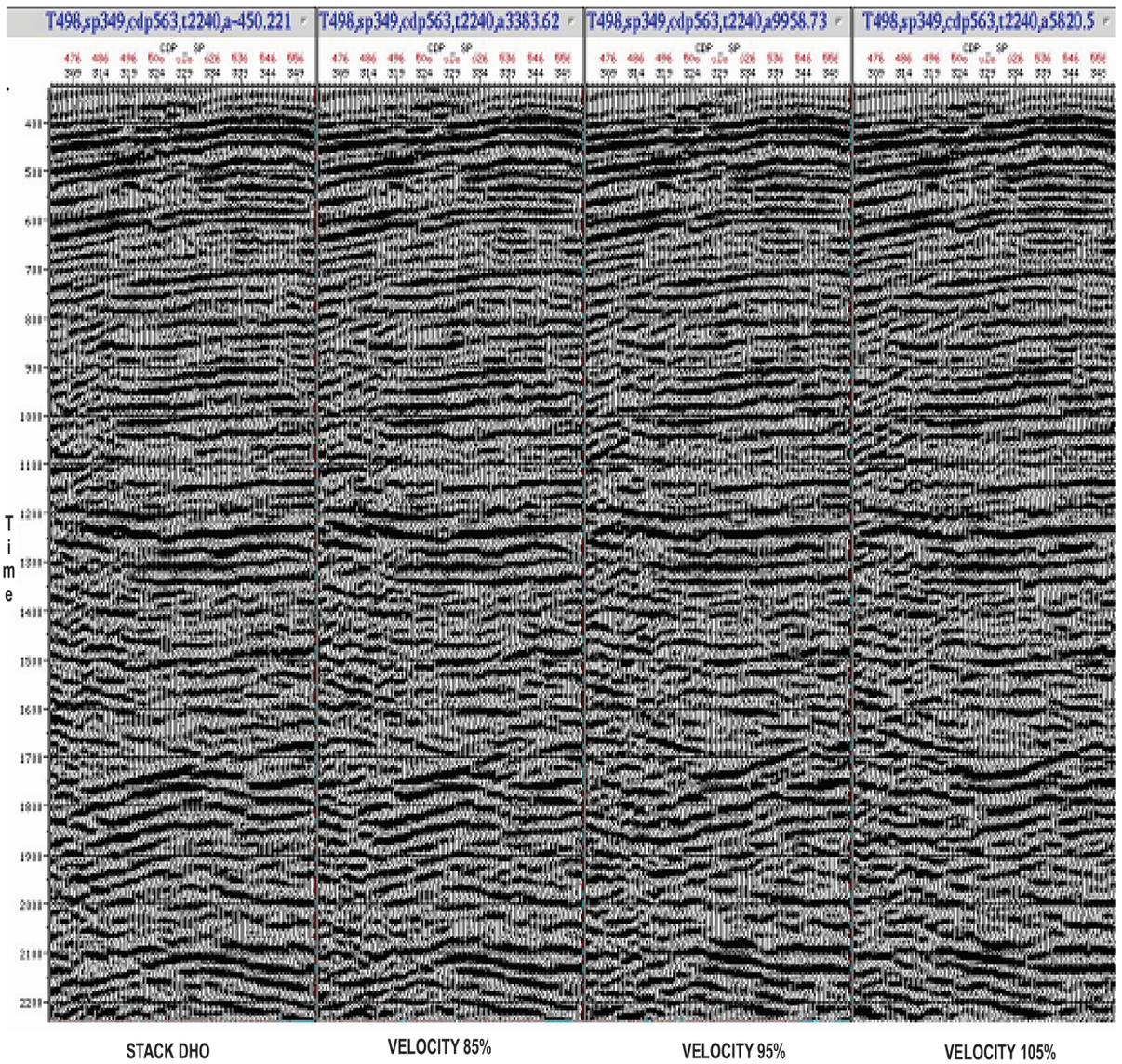


Fig. 11. Migration test at various percentages of the final stacking velocities.

7. Surface Consistent Deconvolution
   Predictive algorithm
   Operator Length=160MS GAP=24MS
   Window 0-1200MS
   Operator Length=160MS GAP=12MS
   Window 900-2400MS
8. Refraction Static Correction
   Datum level : floating datum
   Calculation : first break picking
   Correction velocity: 2000 m/s
9. Automatic Surface Consistent
   Residual statics
   Correction limit: 15 ms
   Gate: 200-2800 ms
10. Normal Moveout Correction
    Velocity analysis every 1200 m
11. Muting: variable muting
12. Dip moveout
    Integral kirchhoff method
13. Stack nominal 60 fold
14. Datum static: datum level 200 m
15. Migration: Kirchhoff method
    Dz= 20 MS
    Using 95% stacking velocities
16. Random Noise Attenuation
    FX-Deconvolution
    Widow 60 traces Operator=19 traces
17. Filter: Type Band-pass

Travel time	low cut-High cut
Sec	Hz
0 - 1.0	12 - 55
1.0 - 2.8	12 – 45

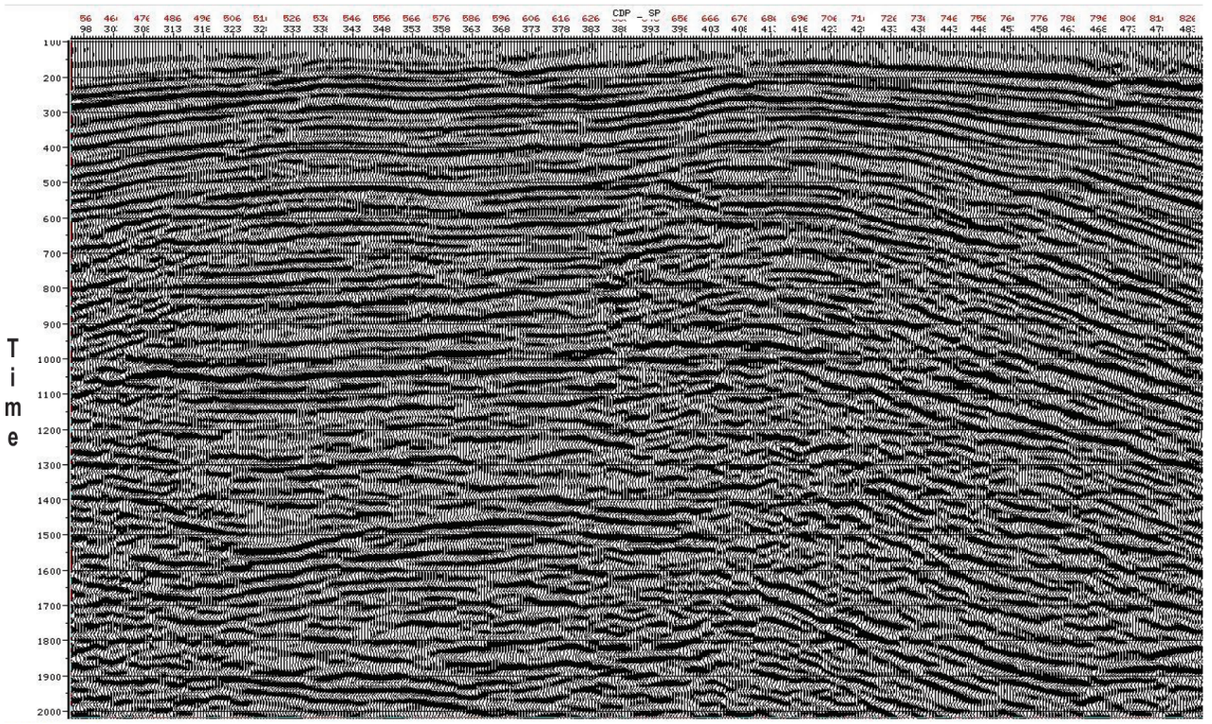


Fig. 12. CDP stack of final migration.

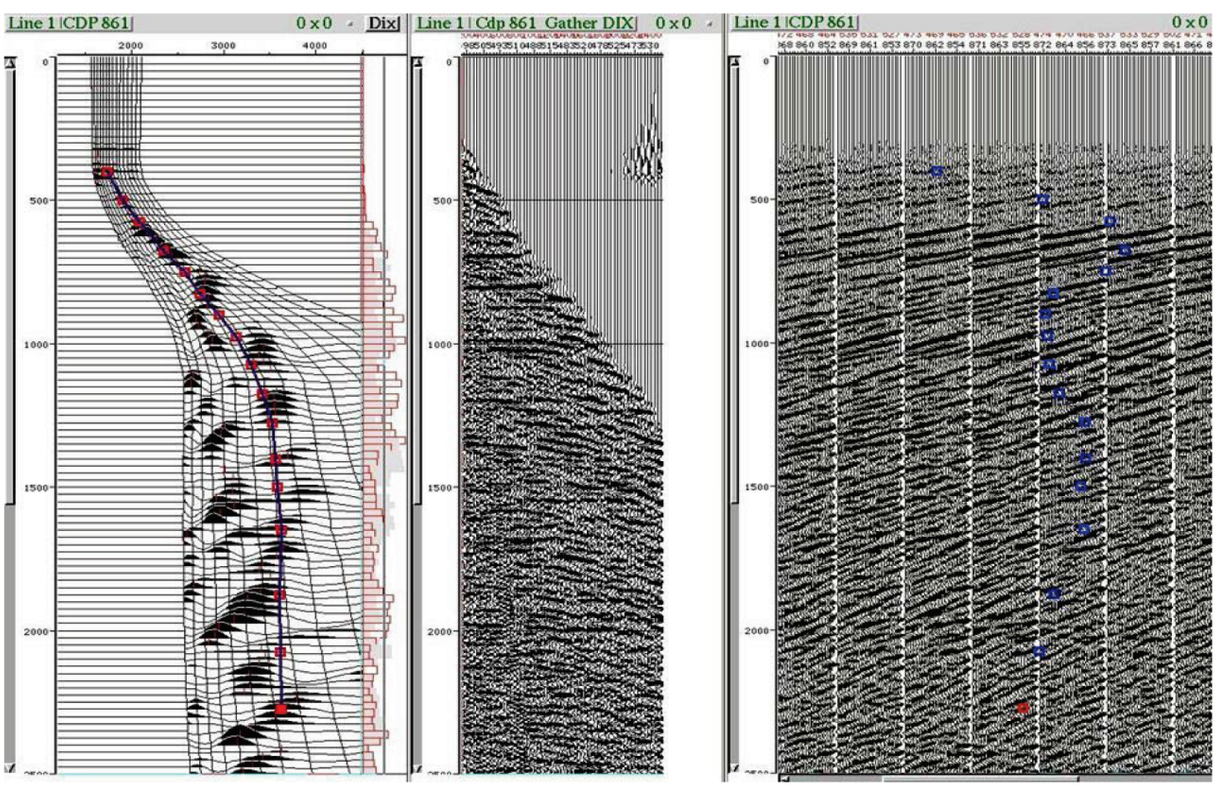


Fig. 13a. Velocity analysis before Prestack time migration at CDP 861.

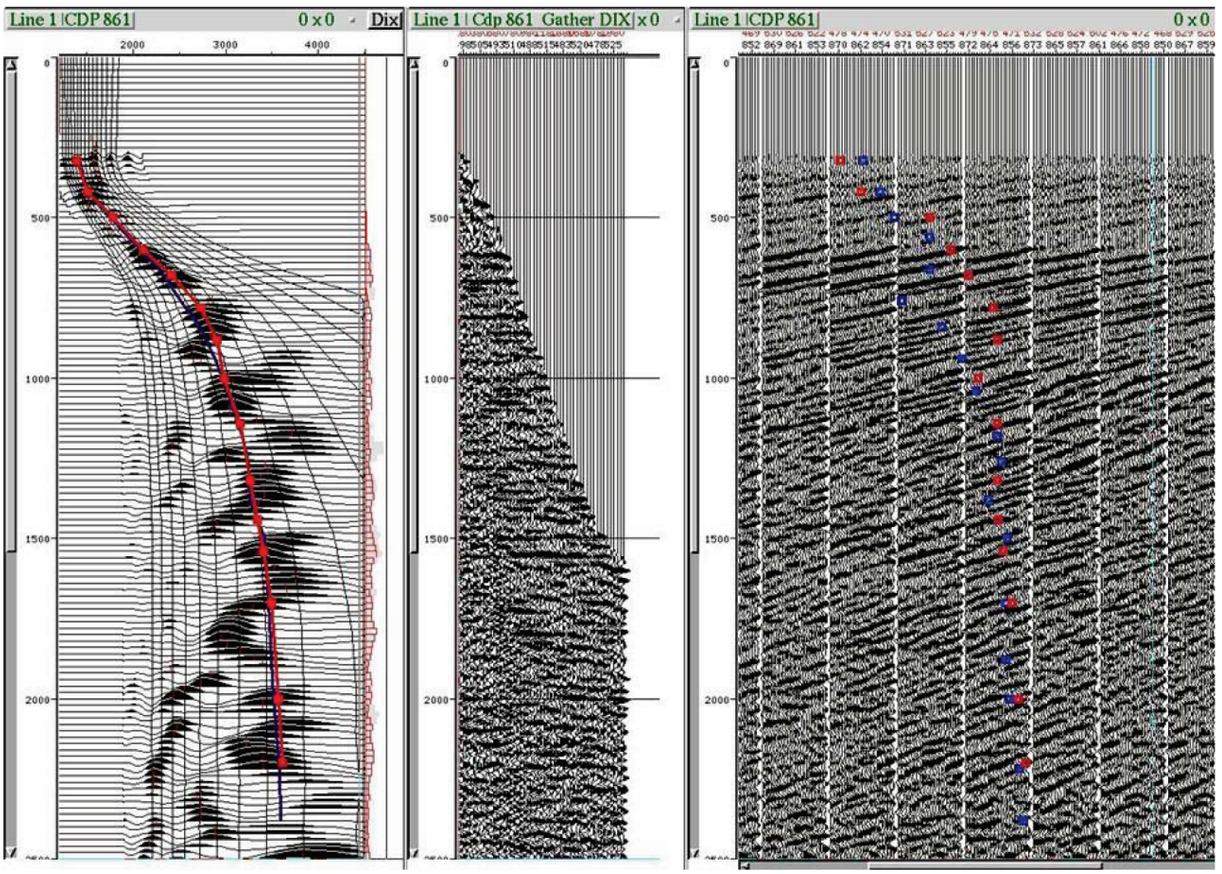


Fig. 13b. Velocity analysis after Prestack time migration at CDP 861.

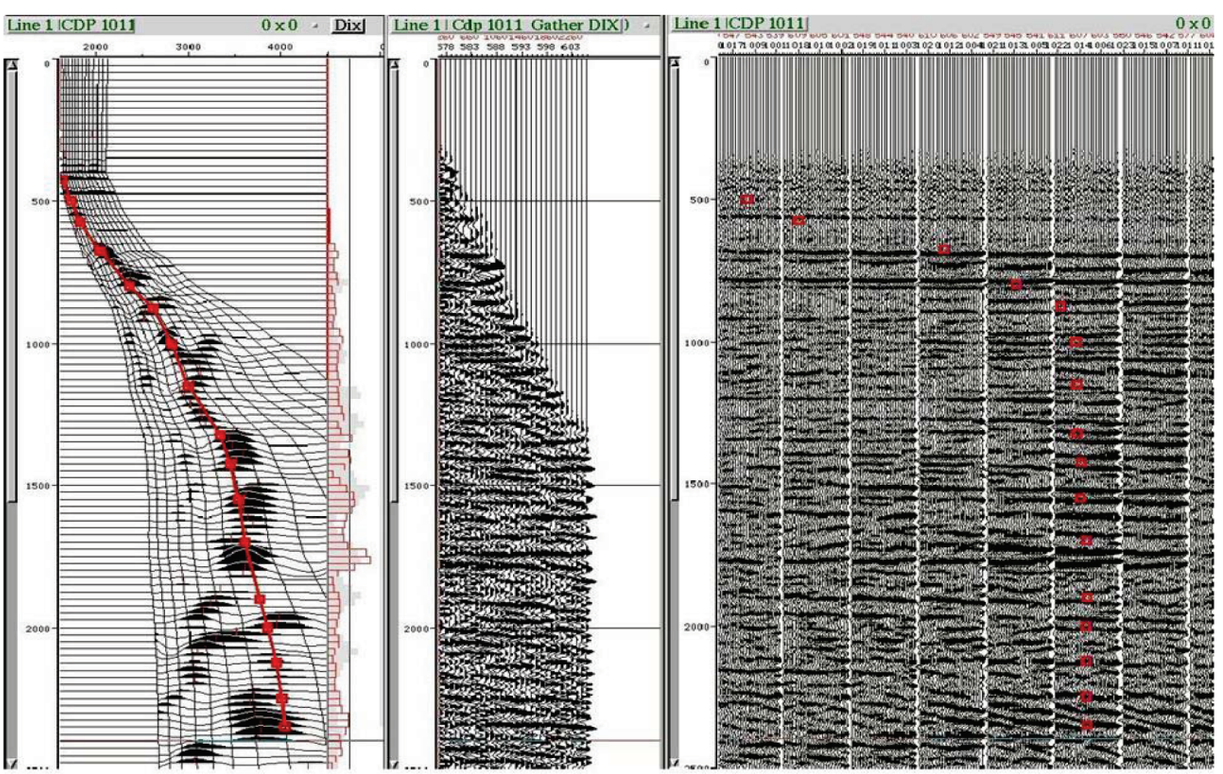


Fig. 13c. Velocity analysis before Prestack time migration at CDP1011.

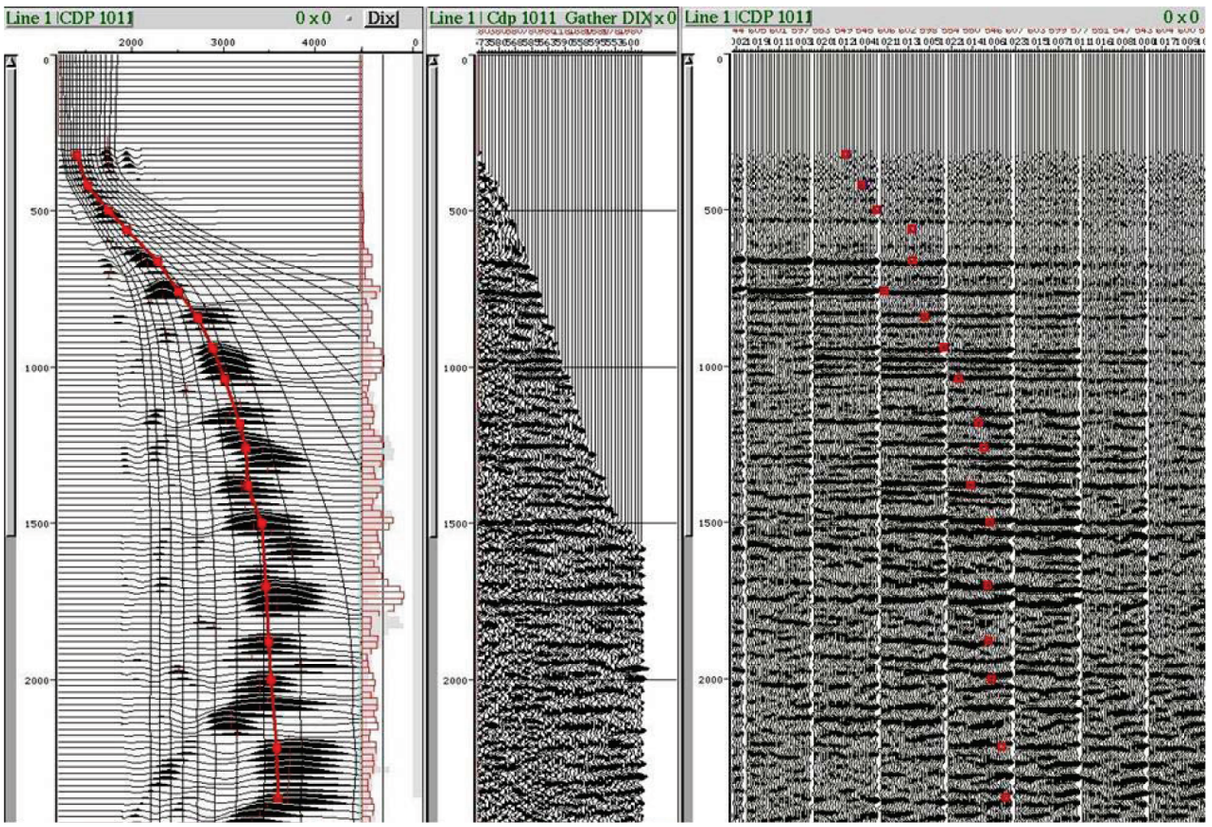


Fig. 13d. Velocity analysis after prestack time migration at CDP1011.

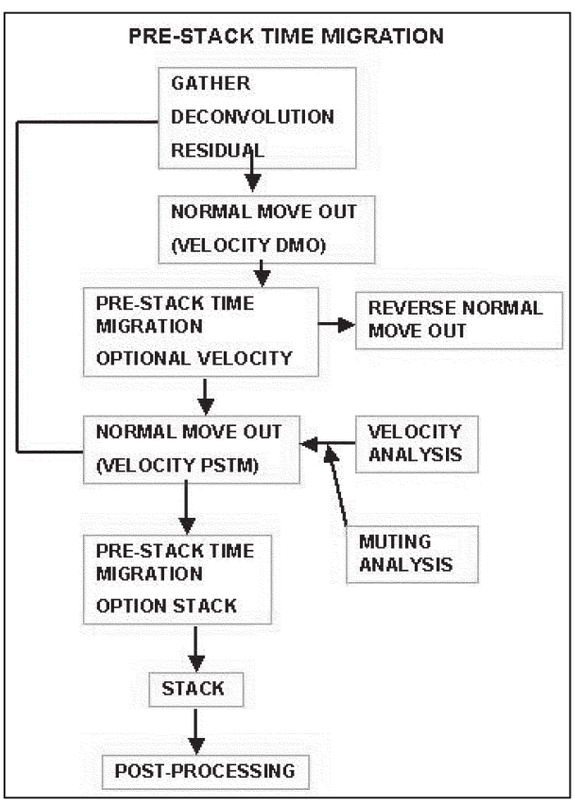


Fig. 14. Prestack time migration flow chart.

18. Equalisation:

Window	0 - 1.0	Gate 200 ms.
Window	1.0 - 2.8	Gate 600 ms.

DISCUSSION OF RESULTS

The fundamental reason behind the reprocessing was to attempt to improve the imaging by using the latest algorithms and best possible seismic processing available. Incremental improvements in the image quality were expected and achieved. The reprocessing produced seismic sections with increased temporal and spatial resolution, facilitating more accurate interpretation of the data. The major difference in the production sequence between the original processing (Fig. 15a and b) and current processing (Fig.16) is attributed to the refraction tomography, Kirchhoff DMO, migration and F-X deconvolution. The processing methodology described in this paper resulted in seismic sections with increased interpretation confidence, which will aid in the understanding of the Barrut Arch deformation and improve the mapping of the structural subdivision shown in Figure 17. Figure 17 shows the stacked

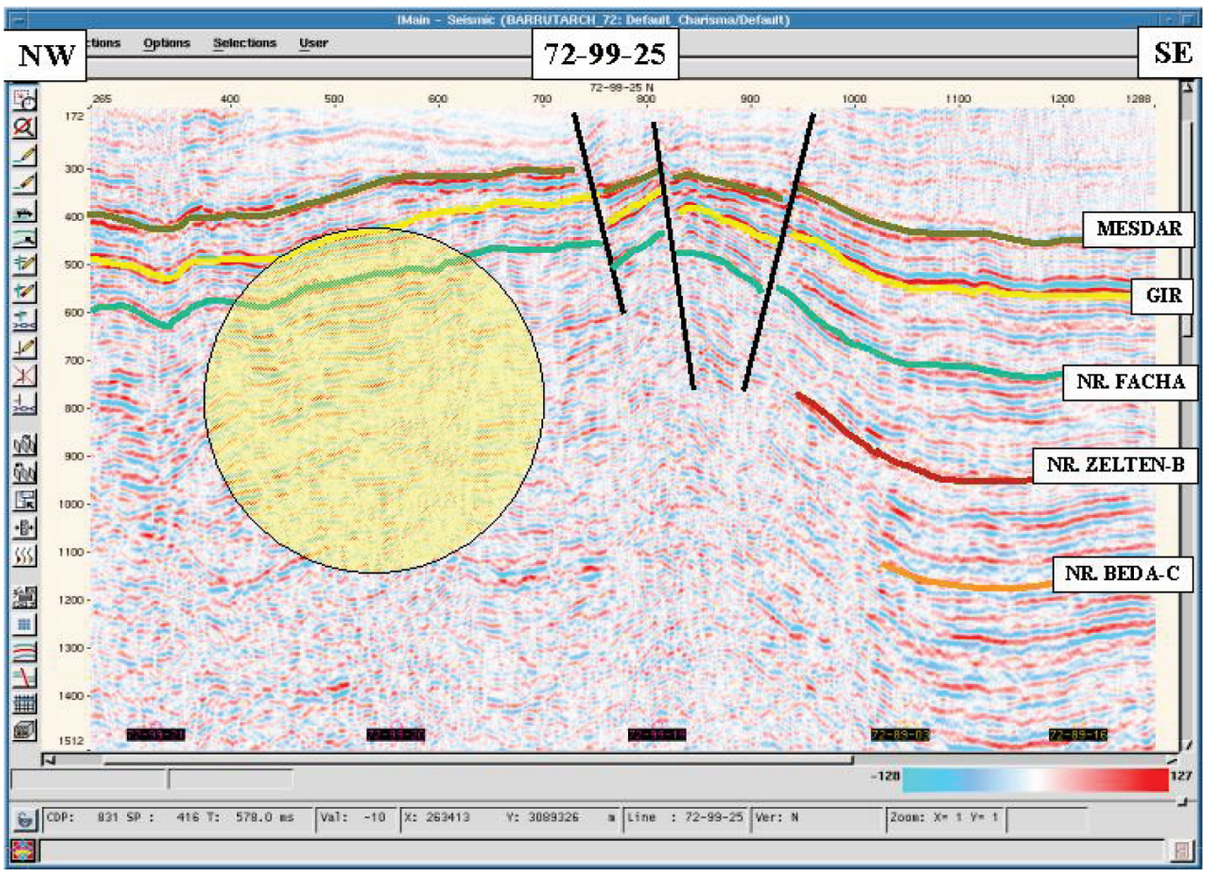


Fig. 15a. Poststack time migration of original processed line 72-99-25.

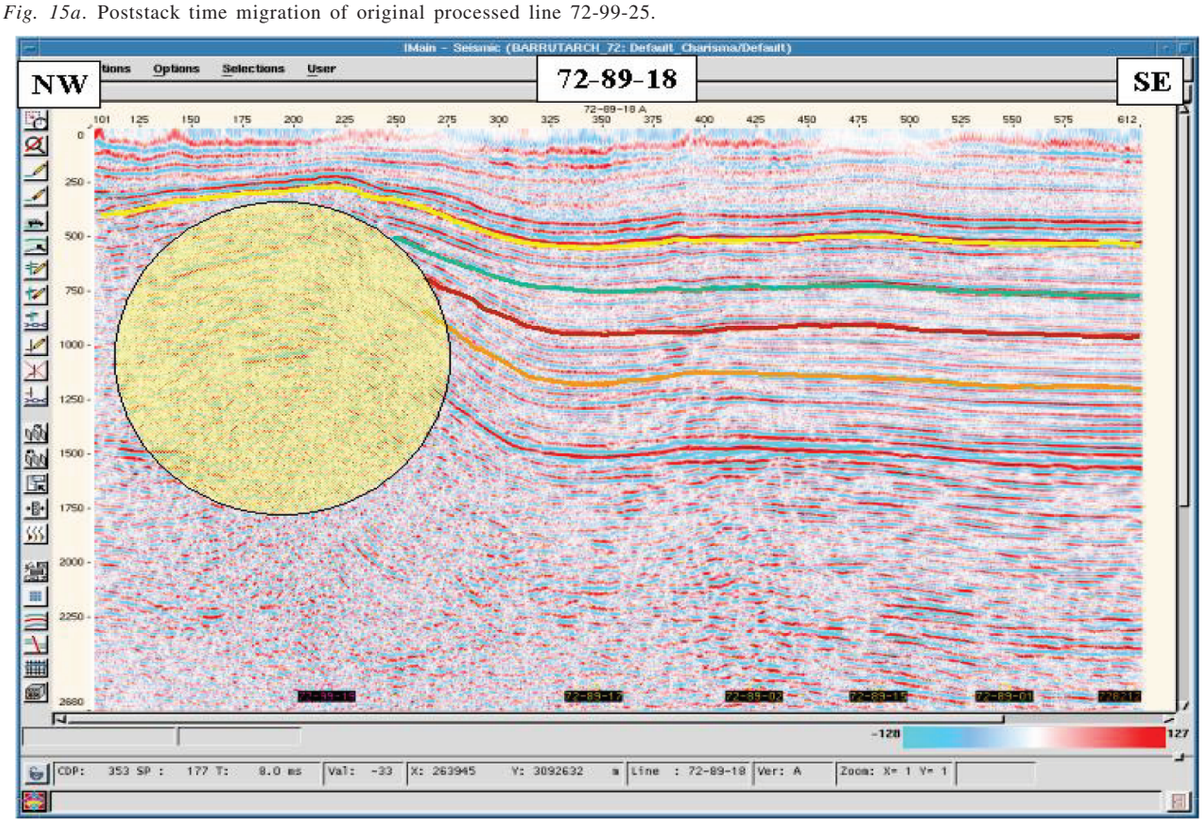


Fig. 15b. Poststack time migration of original processed line 72-89-18.

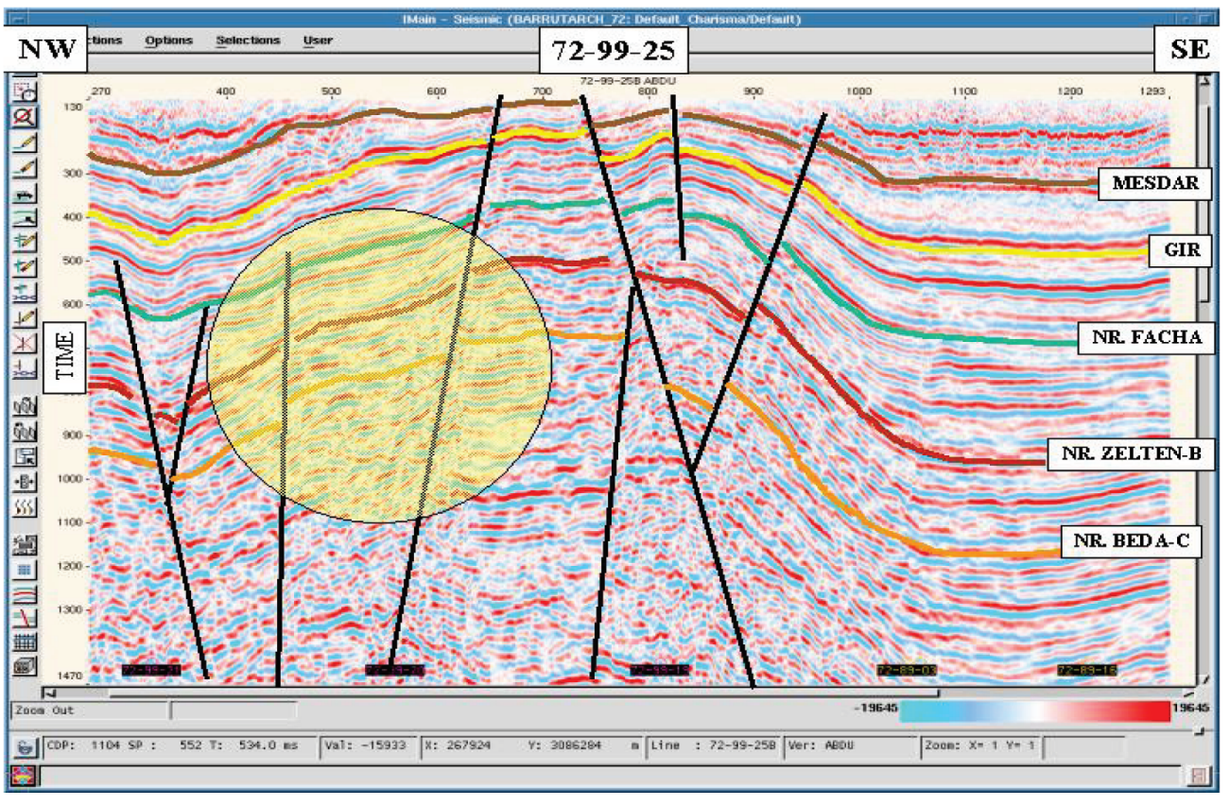


Fig. 16. Poststack time migration of reprocessed line 72-99-25.

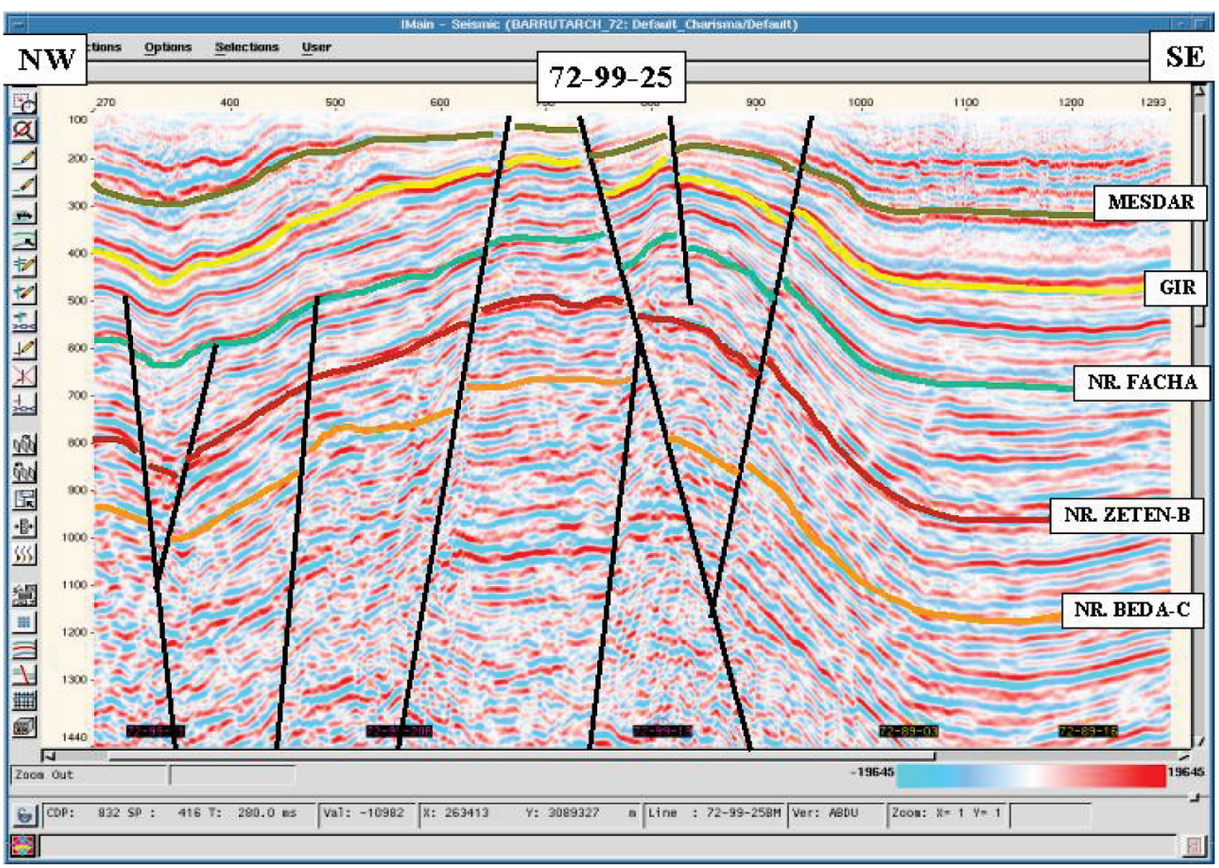


Fig. 17. Prestack time migration of reprocessed line 72-99-25.

section after Prestack time migration. Prestack time migration provided only minor improvement in seismic resolution in comparison with the post stack time migration with F-X deconvolution. Post stack time migration was chosen therefore because this is much more cost effective. Further interpretation of the reprocessed data will also add considerable value to the evaluation of the hydrocarbon potential of the Barrut Arch and may provide some prospective trends for future petroleum exploration.

CONCLUSIONS

1 – Reprocessing of the seismic sections yielded significant improvement over the earlier processed data.

2 – Reprocessing of old data can help in enhancing detail and so should be considered more often.

3 – Seismic reprocessing becomes a very important and relatively cheap alternative to the acquisition of new seismic data as proved in this work.

4 – Seismic reprocessing enhances data quality and ensure confident seismic interpretation, integration with other geosciences data may provide a new impetus for oil and gas exploration along the Barrut Arch area.

5 – The reprocessing produced seismic sections with increased temporal and spatial seismic resolution. This technique provides cost effective results, facilitating more accurate interpretation of the data. Enhanced imaging of the fault pattern and definition as well as the formation sequences has been achieved; this should aid the understanding of rock deformation and improve the mapping of structural subdivisions within the Barrut Arch.

6 – This area needs to be surveyed with 3D seismic data with high enough fold, frequency and quality to allow the desired analysis.

ACKNOWLEDGEMENT

The authors would like to thank the management and the Exploration Department of Veba Oil Operations for making all the data available to us, we also acknowledge their help and encouragement with gratitude.

REFERENCES

Banar, F.J., *1967. Surface and Uphole Geology, Northwest Barrut: LGM 92,* Mobil Oil Libya Ltd., Internal report.

Geophoto Libya Inc., 1959. *Photogeologic Evaluation, Concession 72 Libya*: LIB 60, Mobil Oil of Canada Ltd., (Libyan Branch), internal report.

Johnson, J.T., and Gates, J.K., 1959. *Geology of El Barrut Anticline (Southern Part) Concession No. 72, and Zone iv, Libya*: LIB 73, Mobil Oil of Canada Ltd., (Libyan Branch), Internal report.

Johnson, B.A.1992. *Geological Evaluation of Concession 72: LGM 179*, Veba Oil Operations, Internal Report.

Raodifar, R.E.1958. The *Reconnaissance Geological Survey of Mobil Oil Concession no. 72. Libya;* LIB 27, Mobil Oil of Canada Ltd., (Libyan Branch), Internal report.

Schneider, W.A., 1978. Integral formulation for migration in two and three dimensions. *Geophysics*, **43**, 49-76.

Yilmaz, O., 1987. *Seismic Data Processing*. Society of Exploration Geophysics, Ed. Stephen M. Doherty.

Petroleum Res. J. Vol. 20 (2007); P. 95–102, 10 Figs.

Improved Static Corrections over Sand Dunes for Seismic Line NC151-V532, Western Libya

Abdurrazag M.A. Ushah* and N.R. Goulty**

تحسين التصحيحات الإستاتيكية الناجمة عن الكثبان الرملية للخط السيزمي NC151-V532، غرب ليبيا

عبد الرزاق م. أوشاح و ن. قولتي

هذه الورقة تهتم بدراسة المشاكل الاستيايكية الناجمة عن الكثبان الرملية في الكشف السيزمي بطريقة الانعكاس وذلك بمنطقة عقد الامتياز NC-151 الواقع غرب ليبيا، ففي هذا الامتياز توجد كثبان رملية تمتد إلى عدة كيلومترات ويصل ارتفاعها إلى 100 متر في بعض الأحيان مسببة بذلك صعوبات لوجستية وفنية في عمليات الاستكشاف السيزمي بطريقة الانعكاس، ويرجع ذلك إلى التباين في ارتفاعها وانحدارها الشديد وكذلك إلى انخفاض سرعة الموجات السيزمية فيها والتي تسبب تأخيرا في انتقال الموجات السيزمية (سواء كانت الهابطة منها أو الصاعدة)، حيث يكون من الصعب حساب هذا التأخير الزمني لانتقال هذه الموجات في مثل هذه الكثبان الرملية.

ففي هذه الدراسة تمت مقارنة النتائج المتحصل عليها من استخدام طريقتين لحساب القيم الزمنية المستخدمة في التصحيحات الإستاتيكية، حيث اختير خط من الخطوط السيزمية المارة عبر هذه الكثبان الرملية، وتمت معالجة هذا الخط بمنظومة المعالجة السيزمية ذات البعدين (ProxMAX) . ومن خلال النتائج المتحصل عليها وجد أن طريقة الانكسار المسماة زائد- ناقص والمستخدمة في حساب القيم الزمنية للتصحيحات الإستاتيكية على أساس تصنيف زمن الوقت الزائد لكل مصدر أو لاقط وربطها بالقيم المتحصل عليها تعطي نتائج أفضل من الطريقة الروتينية المستخدمة سابقا والتي تعتمد على إيجاد نموذج تقريبي لسمك الطبقات السطحية وسرعة الموجات السيزمية النافذة خلالها. والسبب أن طريقة الانكسار المستخدمة هذه لا تتطلب إيجاد نموذج تقريبي كما هو سائد في معظم الطرق.

ولحساب القيم الاستاتيكية المتبقية، اختيرت طريقة الـ Maximum power autostatics من عدة طرق موجودة بمنظومة المعالجة السيزمية وذلك لأفضلية النتائج المتحصل عليها وخاصة إذا ما استخدمت هذه الطريقة مع تحليل السرعات مرتين على التوالي بالإضافة إلى ذلك تم استخدام التصحيح المتبقي والمسمى بـ Trim statics وذلك لتحسين نتائج المقاطع السيزمية النهائية.

Abstract*: Concession NC151 is located in the northwestern part of the Murzuq Basin (Libya), which is covered by linear sand dunes that reach heights of ~100 m above the gravel plain. The sand dunes cause large increases in the travel times of reflected events in seismic data. In recent years, the conventional method used to calculate field static corrections has been to interpolate the near-surface velocity structure between upholes. Results are often unsatisfactory on lines that cross the dunes because the reflection events contain false structures that correlate with sand dune topography. These structural artifacts are caused by residual static errors which are too large for automatic statics programs to correct during processing.*

An alternative method of calculating field statics is to pick the first breaks on the Vibroseis field records, calculate the delay times at each station, and use the delay times directly as the field statics after applying a linear adjustment to match them to the upholes. This simple version of the refraction method does not require near-

*Libyan Petroleum Institute, P.O. Box 6431, Tripoli, Libya.
**Department of Earth Sciences, University of Durham, South Road, Durham DH1 3LE, UK.

surface velocity-depth models to be produced, and gives much better results than the conventional field static method. Since this method does not require any near-surface velocity-depth model because it works in time, it can be used in areas with variable LVL or HVL (e.g., sand dunes or permafrost).

The maximum power autostatics method was chosen from several residual statics methods that are available in the ProMAX package. Two iterations of maximum power autostatics and velocity analysis followed by non-surface-consistent trim statics improved the final stacked section.

INTRODUCTION

Robinson and Al-Husseini (1982) addressed the static problem due to sand dunes and described one approach to its solution. Their data were from Rub' Al-Khali, Saudi Arabia, where the dunes are about 1 km wide with a vertical relief of 60-90 m. They have generated a crossplot of traveltime against the elevation of the dune surface, above the sabkha or dune base, using data obtained from many dunes in the area. The crossplot cannot fully resolve either the long or short-wavelength statics in the dunes, but it can be used as an approximation in the computation of datum static corrections.

An important technique for estimating field static corrections is to analyse the first breaks on the seismic field records. In Vibroseis surveys, the first breaks are head-wave arrivals that have been refracted along a higher velocity layer beneath the surface layers. Several refraction methods have been used to estimate the thickness and velocities of the near surface layers. All of these methods are based on the same basic principles for analysis of refracted head waves. Marsden (1993) reviewed the refraction statics methods, starting with the slope/intercept method and ending with time-term technique. He concluded that most methods produce almost identical statics solutions; the differences between them lie in their speed of application.

The presence of extensive sand dunes in NC151 (Fig. 1) causes logistic and technical difficulties for seismic reflection prospecting, due to the steep angle of repose of the sand dune faces and the low seismic

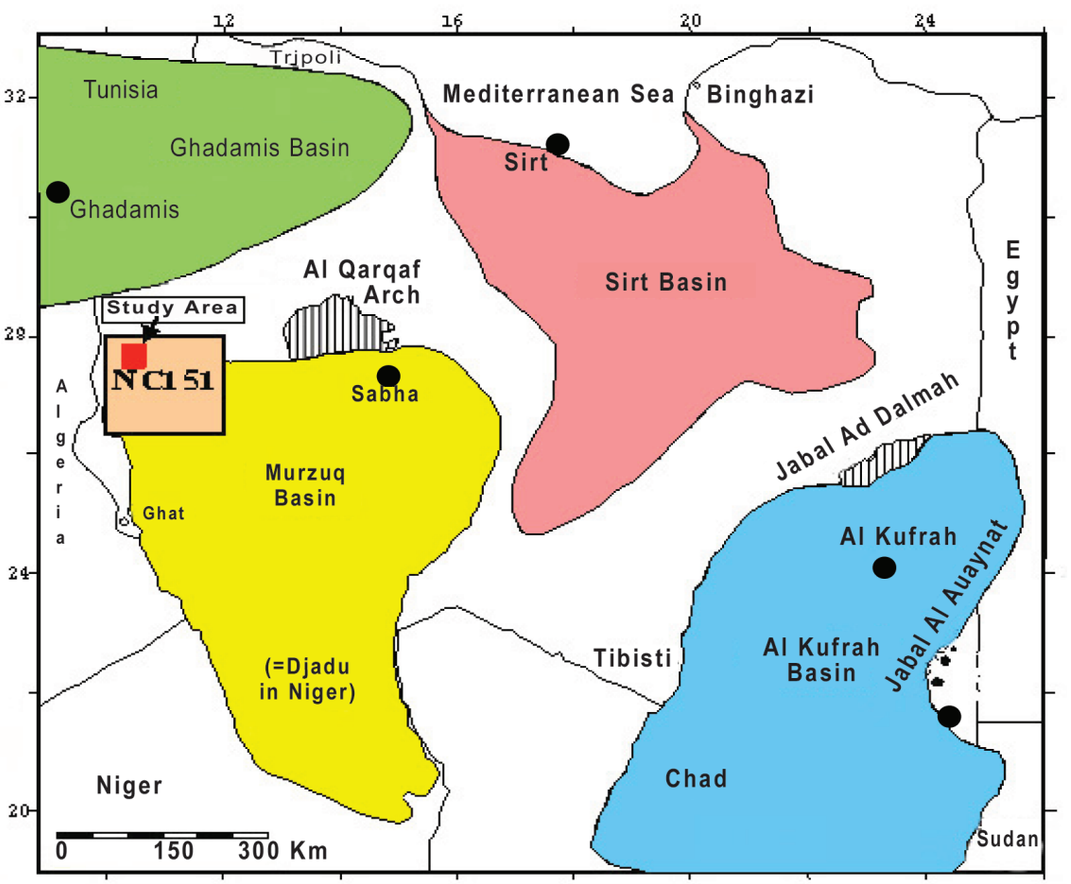


Fig. 1. Generalized location map of sedimentary basins showing study area in Concession NC151.

velocity within them, which causes significant time delays to the reflected waves. These static time shifts in areas of sand dunes are difficult to determine and the conventional method for calculating static corrections does not provide satisfactory results

In this paper, one form of the reciprocal method that may be used for static corrections in seismic reflection surveys is described. It is then applied to seismic line NC151-V532. The estimated receiver and source statics are adjusted to match the uphole data.

FIELD STATICS ESTIMATION

Uphole Surveys

Four upholes were drilled at selected locations along seismic line NC 151-V532 to provide direct measurements of the velocities and thicknesses of the weathering and sub-weathering layers (Fig. 2). Each uphole has been interpreted as a four-layer case with the thicknesses of the top three layers determined and the interval velocities of all four layers determined. Datum static corrections (weathering and elevation corrections) calculated for the four upholes which are located on seismic line NC151-V532 are shown in Table 1.

Conventional Method

For seismic line NC 151-V532, the first two upholes are located on the first two sand dunes (Fig. 3), the other two upholes are located out of the sand dunes (beyond the third sand dune and at the end of the line).The uphole information alone cannot solve the static problems. Additional information is provided by the intersection points with the seismic lines located between the sand dunes. Control points are chosen at pegs to each side of the line intersections close to the flank of each sand dune. At the control points, the thicknesses of layers 1 and 2 and the velocities of the weathering layers are assumed to be the same as at the adjacent line intersection (Table 2). The thickness of layer 3 at each control point is

Table 1. Computation of datum static corrections (weathering and elevation corrections) at the upholes along seismic line NC151-V532.

Variables	Uphole 1161	Uphole 1356	Uphole 1531	Uphole 1641
E_A (Surface elevation)	517.9 m	536.7 m	501.6 m	509.2 m
E_d (Datum elevation)	500.0 m	500.0 m	500.0 m	500.0 m
Z_1 (Thickness of layer1)	16.0 m	10.0 m	16.0 m	4.0 m
Z_2 (Thickness of layer2)	20.0 m	38.0 m	16.0 m	12.0 m
Z_3 (Thickness of layer3)	8.0 m	21.0 m	16.0 m	24.0 m
$E_A - (Z_1 + Z_2 + Z_3) - E_d$	-26.1 m	-32.2 m	-46.4 m	-30.8 m
V_{w1} (Weathering velocity of layer1)	546.0 m/s	459.0m/s	588.0 m/s	435.0 m/s
V_{w2} (Weathering velocity of layer2)	745.0 m/s	786.0m/s	914.0 m/s	749.0 m/s
V_{w3} (Weathering velocity of layer3)	1818.0 m/s	1093.0m/s	1839.0m/s	963.0 m/s
V_r (Replacement velocity)	2609.0 m/s	2500.0m/s	2381.0 m/s	2218.0 m/s
Weathering correction Z_1/V_{w1} Z_2/V_{w2} Z_3/V_{w3}	 29.3 ms 26.8 ms 4.4 ms	 21.7 ms 48.2 ms 19.2 ms	 27.2 ms 17.5 ms 8.7 ms	 9.1 ms 16.0 ms 24.9 ms
Elevation correction = $[E_A - (Z_1 + Z_2 + Z_3) - E_d]/ V_r$	-10.0 ms	-12.9 ms	-19.5 ms	-13.9 ms
Datum correction = - (Weathering correction + Elevation correction)	-50.5 ms	-76.2 ms	-33.9 ms	-36.1 ms

Table 2. Information obtained at upholes (Uh), control points (CP), and intersection points (I\V593, I\V595, I\V597) with other seismic lines.

Type of Points	Station No	Elevation (m)	Thick (m) Layer1	Thick (m) Layer2	Thick (m) Layer3	V_{W1} (m/s)	V_{W2} (m/s)	V_{W3} (m/s)	V_{W4} (m/s)
CP\SOL	1051	504.20	4.00	20.30	6.00	571	832	1591	2932
CP	1056	487.90	4.00	4.00	6.00	571	832	1591	2932
I\V593	1105	496.70	4.00	4.00	6.00	571	832	1591	2932
CP	1146	484.80	4.00	4.00	7.50	571	832	1591	2932
Uh	1161	517.90	16.00	20.00	8.00	546	745	1818	2609
CP	1238	481.70	6.00	2.30	2.90	625	1002	2162	2717
I\V595	1281	471.20	6.00	2.30	0.10	625	1002	2162	2717
CP	1304	468.40	6.00	2.30	6.50	625	1002	2162	2717
Uh	1356	536.70	10.00	38.00	21.00	459	786	1093	2500
CP	1397	481.20	4.00	4.00	15.50	354	952	1818	2703
I\V597	1408	475.40	4.00	4.00	14.00	354	952	1818	2703
Uh	1531	501.60	16.00	16.00	16.00	588	914	1839	2381
Uh\EOL	1641	509.2	4.00	12.00	24.00	435	749	963	2218

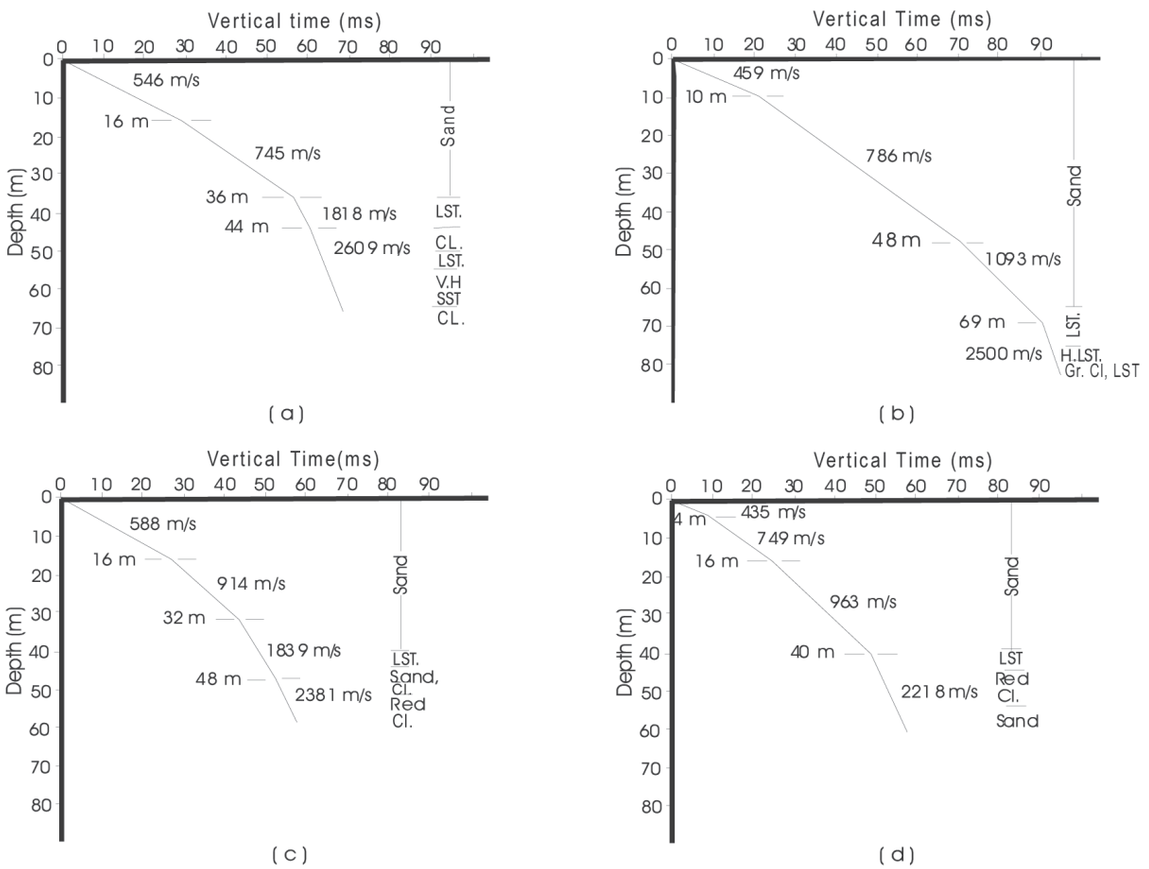


Fig. 2. Interpretation of four upholes survey data depicting four geologic layers. (a) Uphole (VP/SP 1161). (b) Uphole (VP/SP 1356). (c) Uphole (VP/SP 1531). (d) Uphole (VP/SP 1641).

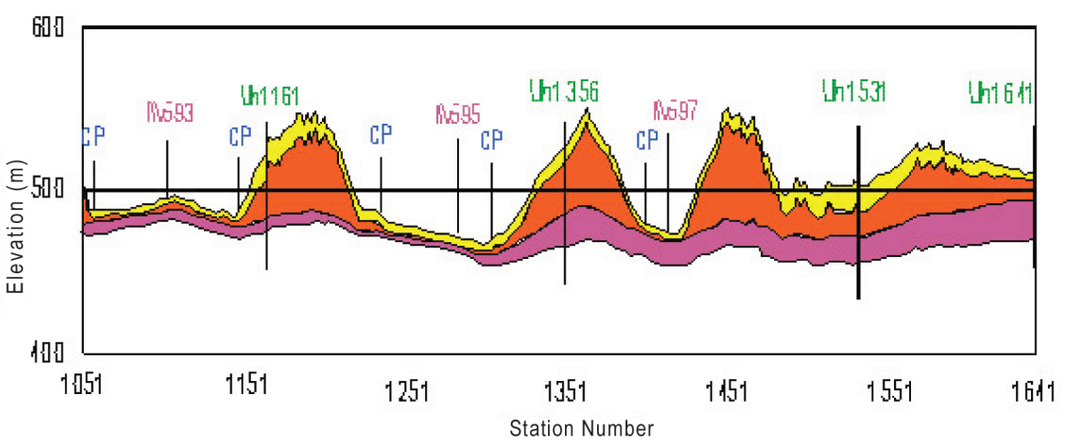


Fig. 3. Layer thickness model (layer 2 forced by factor 0.8).

obtained by linear interpolation between the line intersection and the uphole. Between the upholes and the adjacent control points or line intersections, the thicknesses of all three layers are interpolated using a more complicated scheme described by Ushah (2004). The results are shown in Figure 3.

Several variations on this method were generated by changing the thickness factor that was used in the conventional method (Fig. 3). The results of the field statics for sources and receivers obtained by these variations on the conventional method are shown in Figure 4.

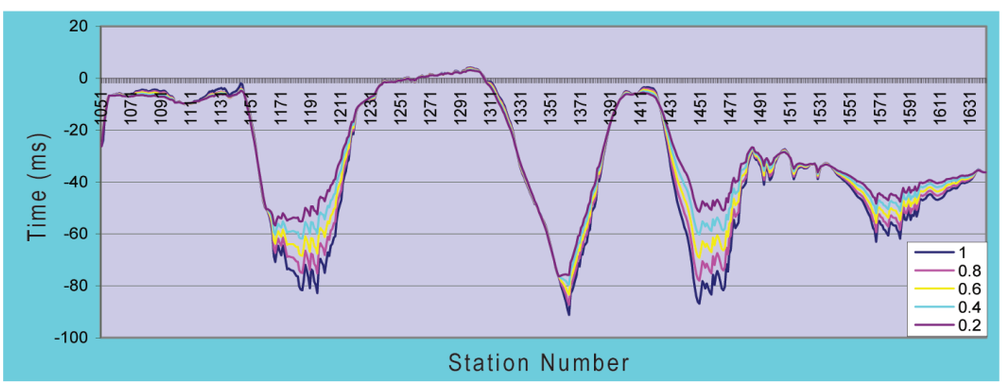
Refraction Method

The plus-minus method developed by Hagedoorn

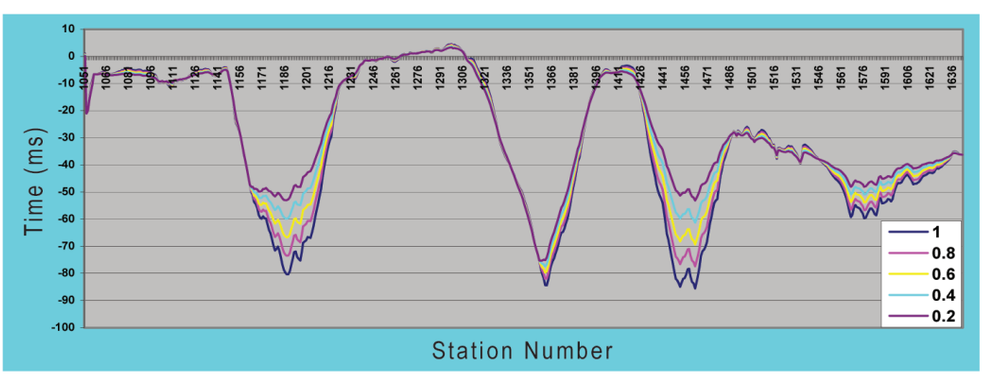
(1959) has been one of the most popular methods of refraction interpretation (Fig. 5). He developed the plus-minus method to estimate bedrock velocity and depth below each geophone station on a reversed seismic refraction profile. Since the reflection data used in this study were acquired using Vibroseis (the first breaks can not be seen directly), the troughs have to be picked manually, and in some cases interpolation is needed to estimate their positions (Fig. 6). Over the sand dunes, the group interval varies between 12 and 20 m instead of 25 m between the sand dunes, and the shortest source-receiver offset varies between 200 m and 257 m instead of 87.5 m. Therefore, the velocities in the near-surface layers are not measured, so the plus times were integrated with the uphole data, and the results are shown in Figure 7. A comparison between conventional and refraction field statics with elevation for a portion of seismic line NC151-V532 was made and is shown in Figure 8.

Examples of Stacked Sections

Seismic line NC151-V532 consisted of 589 split-spread shot gathers, with 25 m source and receiver



(a)



(b)

Fig. 4. Field statics models for line NC151-V532 generated by changing the thicknesses of layer 1 and layer 3 linearly while layer 2 is forced by factors 1.0, 0.8, 0.6, 0.4, and 0.2; (a) Receiver field statics models, (b) Source field statics models.

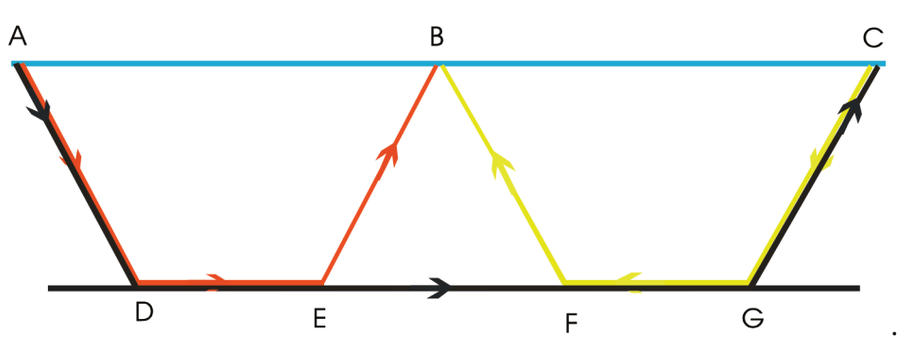


Fig. 5. Raypaths for a reversed refraction profile to illustrate the plus-minus method.

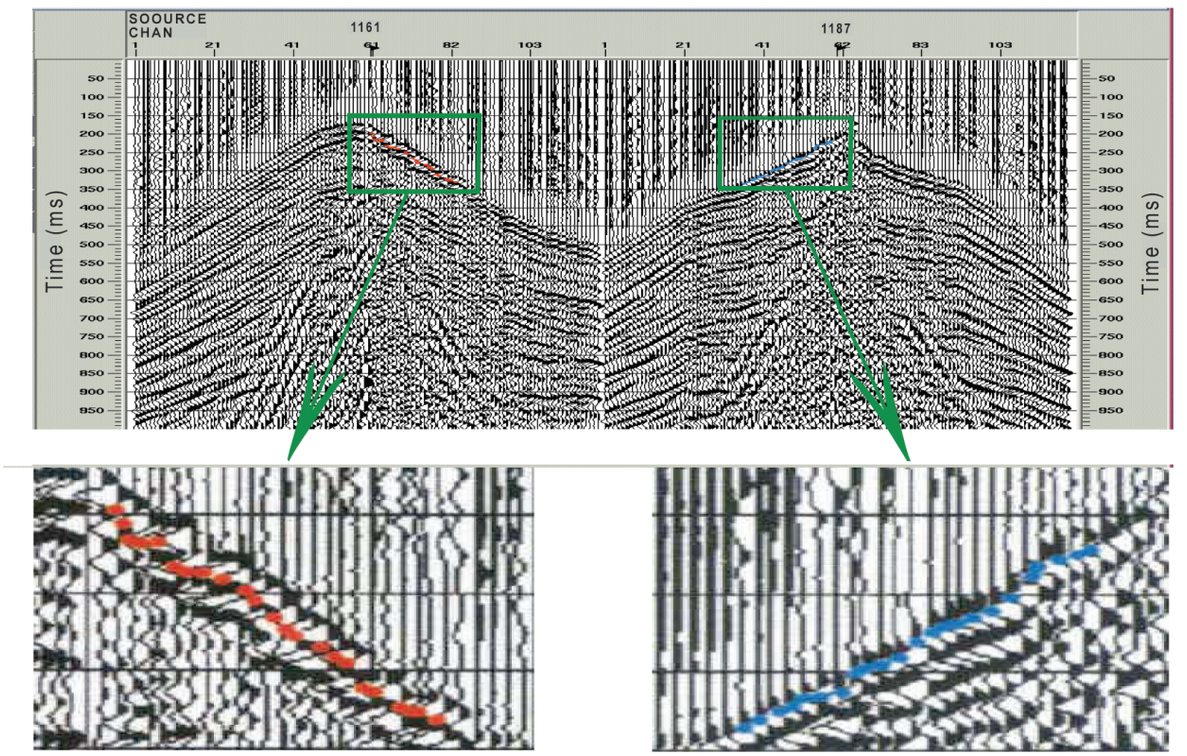


Fig. 6. Common-shot gathers (SP1161 and SP1187) of Vibroseis data from seismic line NC151-V532 after applying a gain ramp ($T^{1.5}$) and automatic gain control (AGC). The red and blue circles represent the picked troughs, corresponding to the centre of the Klauder wavelet, for the first arrivals on the forward and reverse shots, respectively.

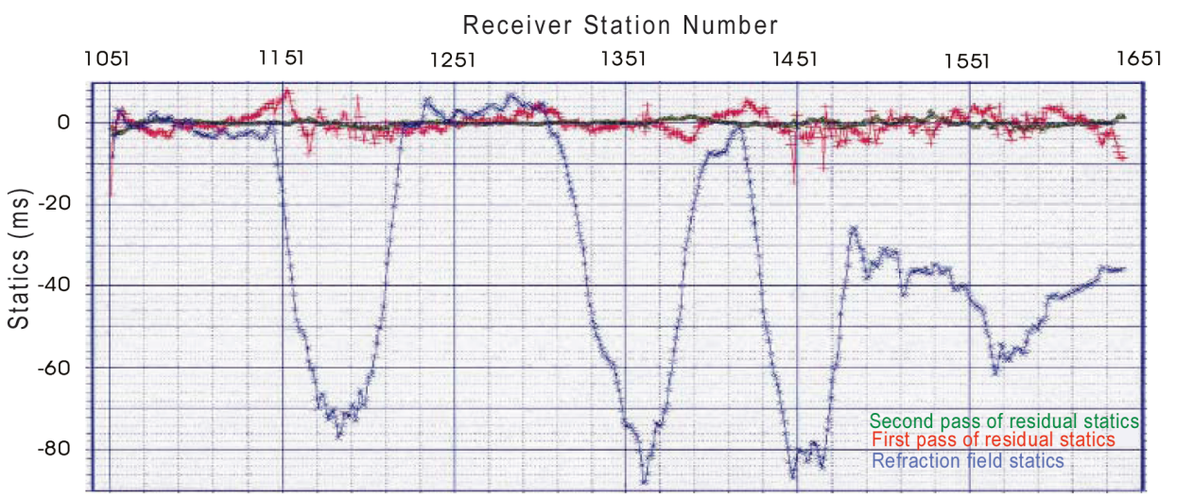


Fig. 7. Receiver field statics (blue) computed as half the plus times ($T^{+}/2$) after adjustment to the upholes, first and second passes of residual statics (red and green) for the same receivers.

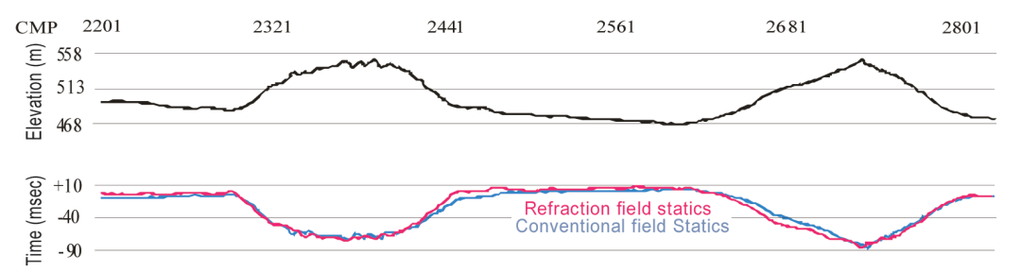


Fig. 8. Common mid point (CMP) elevations on seismic line NC151-V532 (top); refraction and conventional field statics for the same CMPs (bottom).

spacing (along most of the line). Each shot gather consisted of 120 traces with 25 m receiver spacing (but where the line crossed the sand dunes the spacing was less). It has been processed in Durham using the 2-D ProMAX package (Landmark, 1997). The conventional processing steps that were used in processing include geometry set up, filtering and data editing, deconvolution, field statics, CMP sorting, normal movout correction, residual statics and velocity analysis.

Figure 9 shows a portion of the brute stack section for seismic line NC151-V532. In Figure 9, conventional field statics were applied, while in Figure 10a refraction field statics (plus minus method) were applied. The brute stack section with refraction field statics shows better results for removing the long wavelength statics. Figure 10b shows the final stacked section with refraction field statics, automatic mute (stretch mute is 30%), velocity analysis, residual (maximum power) statics (applied twice) and trim statics (with maximum time shift ± 8 ms).

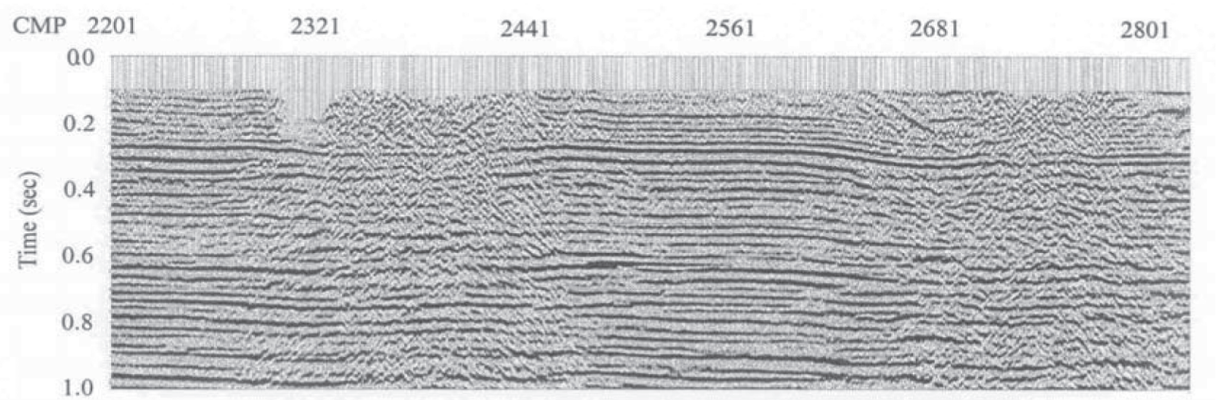


Fig. 9. A portion of the brute stack section of seismic line NC151-V532 after the application of conventional field statics.

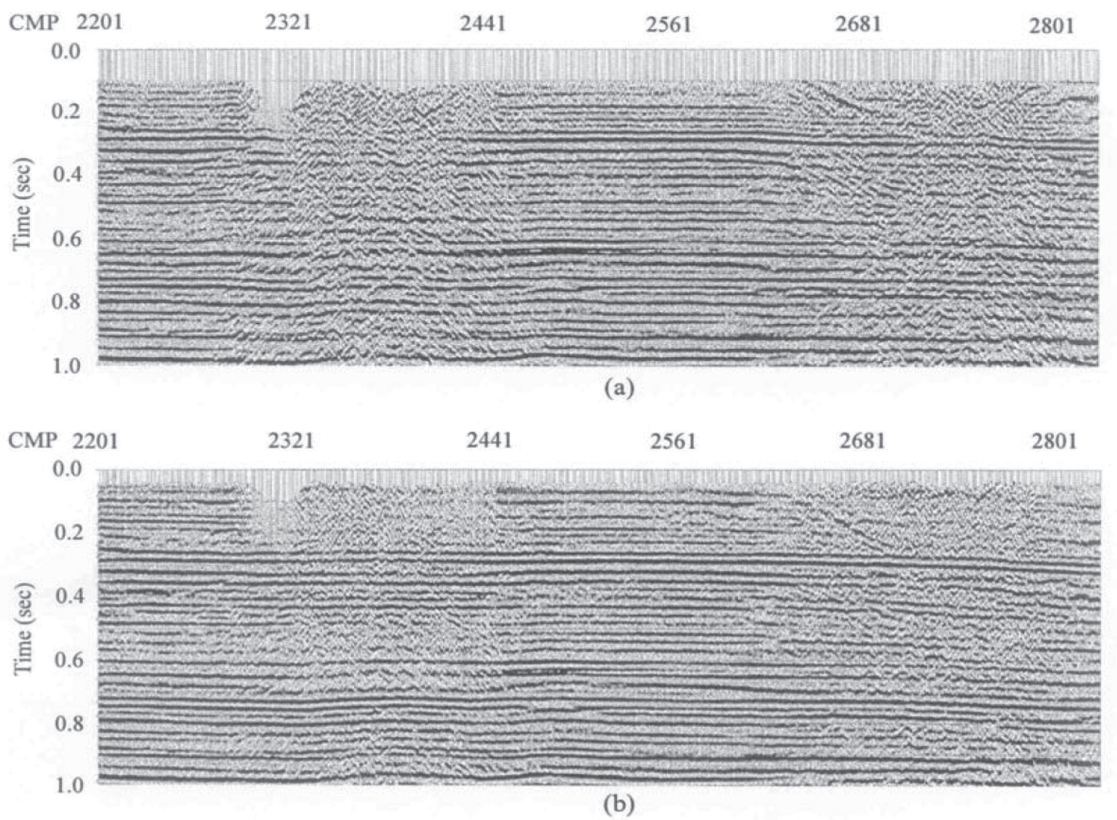


Fig. 10. (a) A portion of the brute stack section of seismic line NC151-V532 after the Application of refraction field statics (plus-minus method) using the upholes as control points, (b) The same stacked section but with refraction field statics, automatic stretch mute 30%, velocity analysis and maximum powerautostatics applied twice, and trim statics.

CONCLUSIONS

The work presented in this paper has dealt with static corrections in sand dune areas in Concession NC151, Murzuq Basin. In this area, one seismic line crossing sand dunes, NC151-V532, was processed using the ProMAX software and two methods of long wavelength statics (refraction and conventional) were applied. It was found that the approximation of each source or receiver field static by $T^+/2$ (where T^+ is the plus time found by the refraction field statics method), with linear interpolation between upholes gives better results than the conventional method of calculating field statics.

For residual statics, the method of maximum power autostatics was found to work well in these data. Improved results were obtained by applying residual statics and velocity analyses twice, followed by trim statics

ACKNOWLEDGEMENTS

We thank the management of Libyan Petroleum Institute for continuous encouragement to produce this work. Also, our appreciation is extended to the chairman and the Exploration Department of Sirte Oil Company for permission to use the data.

REFERENCES

Hagedoorn, J.G., 1959. The plus-minus method of interpreting seismic refraction sections. *Geophysical Prospecting*, **7,** 158-182.

Landmark 1997. *ProMAX Reference Manual*, Volumes 1 and 2.

Marsden, D., 1993. Static corrections-a review: Part II. *The Leading Edge,* **12**, 115-120.

Robinson, D.K. and Al-Husseini, M.I., 1982. Technique for reflection prospecting in the Rub'Al-Khali. *Geophysics*, **47**, 1135-1152.

Ushah, A.M.A., 2004. *Static Problems due to Sand Dunes in NC151, Western Libya*. Ph.D thesis, University of Durham.

Petroleum Res. J. Vol. 20 (2007); P. 103–106, 2 Figs.

Reservoir Characterization in Concession C97-I, Eastern Sirt Basin, Libya

Luca de Vincenzi and Ziad Ayub*

وصف صخور المكمن بعقد الامتياز (C97-I) شرق حوض سرت – ليبيا

لوكا دي فينسينزى وزياد أيوب

يمثل عدم تجانس جيولوجية المكمن بعقد الامتياز (C97-I) مفتاح التحدي فالحجر الرملي ذو النشأة النهرية التابع للجزء العلوي من تكوين السرير الرملي (الكريتاسي المبكر) والحاوي للنفط قد حلت محله وبشكل جزئي تتابعات بركانية مصمتة على هيئة تداخلات من رواهص الفتات البركاني أثناء وبعد فترة ترسيب هذه الصخور الرملية وهي الآن موجودة على عمق 12000قدم. تميزت المرحلة الأولى من الثوران البركاني الغني بالغازات بتوضع الفتات البركاني وتبعه في مرحلة ثانية نشاط ناري على هيئة طفوح بازلتية وقواطع ومتوافقات بركانية. وتأثرت رواسب الفتات البركاني بالطين البركاني والتي تمثل تدفقا حطاميا لرواسب أرضية وانهيارات وتدفقات طينية تكونت أثناء تلامس الحطام البركاني الساخن بمياه خارجية (بحيرة فوهة البركان، أمطار غزيرة) ثم انهالت إلى الأسفل تحت تأثير وزنها ولمسافة العشرات من الكيلومترات في بعض الأحيان.

وبالنظر إلى الأحداث البركانية سالفة الذكر بالمنطقة فقد وجد لدينا ثلاثة مناطق بركانية وهي: براكين مركبة وفتات بركاني وبازلت، وتفرعات من القواطع والمتوافقات البازلتية، ورواهص من الطين البركاني.

ولهذا الحد فقد مكن الحصول على المعلومات التقليدية وتحليلها (الموجة الأولية ومسح ثلاثي الأبعاد وتحويلات آثار تغيير الكتلة والسحنات السيزمية وتحليل المعلومات بالشبكة) من اكتشاف تواجد البازلت ولكنها لم تفلح في التمييز بين الفتات البركاني والحجر الرملي أي المكمن. تم اختيار سرعة الموجة القصيرة والمقاومة كخواص طبيعية تسمح بالتمييز بين الفتات البركاني وصخور الحجر الرملي. وتعتبر خاصية التمغنط ومساعدة الجاذبية والمغناطيسية التقنية المناسبة لدمج أفضل أثناء المعالجة والتفسير والسيزمية ثلاثية الأبعاد. أكدت الدراسات التمهيدية المحتملة إمكانية نجاح المشروع وعرّفت أفضل المعايير للحصول على المعلومات الجيوفيزيائية.

Abstract: *The key challenge in Concession C97-I is the heterogeneous geology of the reservoir: the oil-bearing fluvial sandstones of the Upper Sarir Sandstone Formation (Lower Cretaceous) being partly substituted by a tight volcanic sequence. Volcanism took place during and immediately after the deposition of these sandstones with intercalation of volcaniclastic conglomerates and basalt (volcanoes, sills, and dykes) currently at a depth of 12,000 ft. A first volcanic phase of gas-rich eruptions characterized by deposition of pyroclastics was followed by a second phase consisting of basaltic flows, sills, and dykes. The pyroclastic sediments were affected by lahars, which are matrix-rich debris flows, landslides and mud flows formed when hot pyroclastic debris comes into contact with external water (crater lake, very heavy rainfall) and then slides downward under its own weight at times for tens of kilometers.*

Due to the afore-mentioned volcanic events in the area we have the presence of three volcanic occurrences: volcanic complexes with volcanic-lastics and basalts, sills and dykes swarms of basalt and volcaniclastic laharic conglomerates.

So far, conventional seismic acquisition and processing (P-wave 3D survey, offset volumes trace inversions, seismic facies and neuronal network

* Wintershall-Libya.

analyses) have managed to detect the presence of basalt, but have failed to discriminate volcanoclastic conglomerates from sandstones, i.e. the reservoir. S-wave velocity and resistivity wereselected as physical properties, which allow to differentiate between volcanoclastic and sandstone lithologies. Suitable techniques are magnetotelluric, in association with gravimetric and magnetic for a better integration during processing and interpretation, and 3-component seismic. Propaedeutic feasibility studies confirmed the potential success of the project and defined the most suitable parameters for the geophysical acquisitions.

INTRODUCTION

Concession C97-I is located in the Eastern Sirt Basin at 250 km to the southeast of the town of Al Burayqah. There are two main areas of interest: the Nakhla oil field in the central part and the NPT-high oil fields and prospects in the southeastern part.

Methods

On behalf of Wintershall-Libya, in the third quarter of 2004 the contractor Bureau of Geophysical Prospecting (BGP) acquired a 1kmX1km grid of magnetotelluric stations and a 500mX500m grid of magnetic and gravimetric stations over 400 sq. km on the Nakhla oil field and the NPT high. In the fourth quarter of 2004 the contractors Arab Geophysical Exploration Services Company (AGESCO) and Compagnie Générale de Géophysique (CGG) acquired the first 2D 3-component survey ever recorded in Libya, consisting of 140 full-fold km in the NPT high, where several wells are planned to be drilled in the near future. Figure 1 shows the outlines

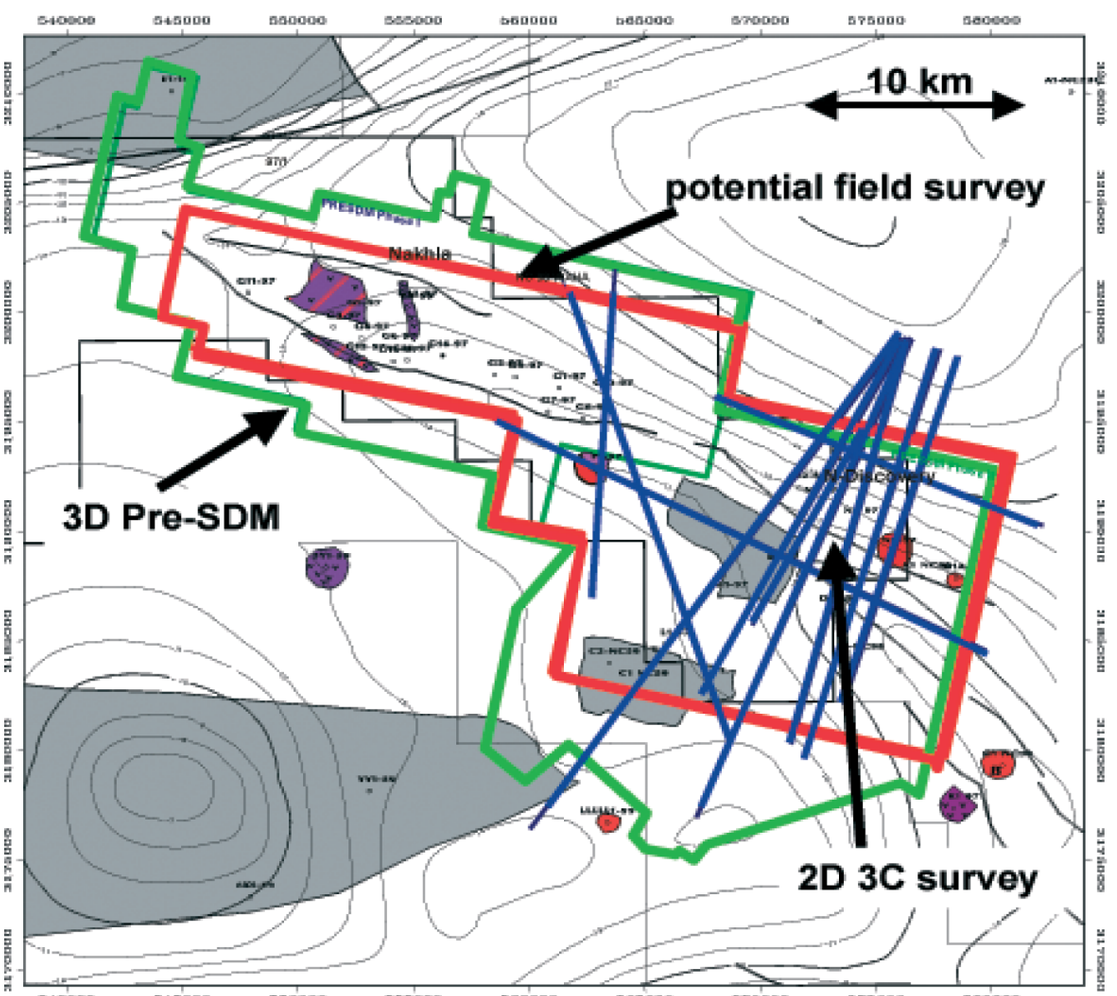


Fig. 1. Geophysical programs and existing data. Curves are Bouguer anomaly (in milligal), red indicates sills and dykes, purple indicates volcanoclastic conglomerates, red and purple indicate volcanic complex, grey indicates basement; the distribution of the lithologies in this picture is based on wells and 3D seismic.

and the location of the geophysical programs and previous existing data, *i.e.* 3D Pre-Stack Depth Migration set.

The processing and intepretation work has included the integration with the existing 3D Pre-SDM and trace-inverted volumes already covering the area of study as well as well logs and cores.

The absence of 3-component and magnetotelluric equipment in Libya was a further challenge for the projects.

RESULTS

After a three-month processing carried out by BGP in Tripoli with the support of Wintershall-Libya's geophysicists and geologists, the results of the potential field work have allowed us to draw a map with the most likely distribution of volcanic lithologies and associate a risk in the future drilling locations (see Figure 2), which was the main objective of the project, as well as to better define the tectonic and the depth of the basement.

According to the theory and the result of the feasibility study, during the 2D 3-component acquisition the P-waves generated by the vibrators have been both reflectedas P-waves by the top of the reservoir and converted and reflected as S-wave. The 3-component processing started at the beginning of January 2005 in CGG's offices in Massy (France) and was completed in October 2005. This included PP-sections and PS-sections and an acoustic and elastic inversion in order to generate Vp/Vs ratio sections, which were integrated with the afore-mentioned results for confirmation of the lithology prediction.

ACKNOWLEDGEMENTS

The authors thank the Libyan National Oil Corporation and Wintershall for the permission to publish and acknowledge BGP, AGESCO and CGG for their important contribution to the success of the project.

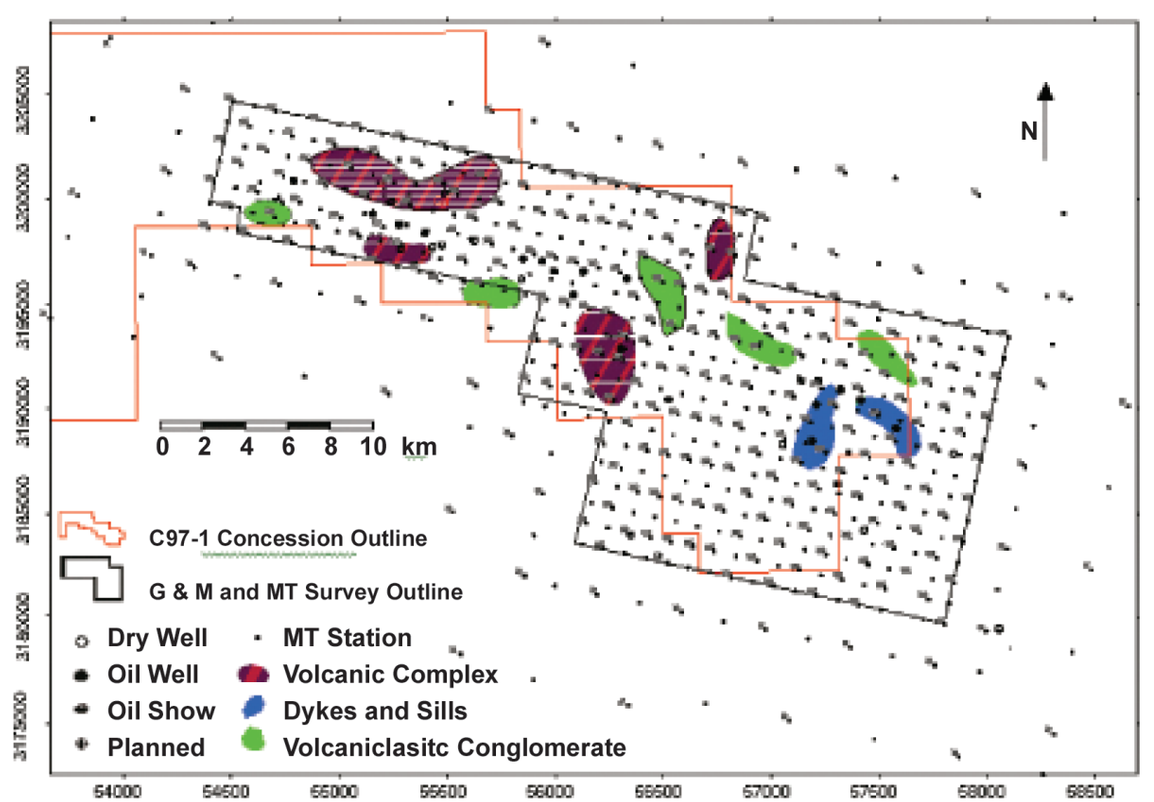


Fig. 2. Map of the most likely distribution of the igneous lithologies in the Sarir Formation.

Petroleum Res. J. Vol. 20 (2007); P. 107–112, 8 Figs.

A Unique High Resolution Imaging Process - a Key to the Understanding of the Reservoir

Stuart Hirsch*, Gary Perry**, and Michael Fleming**

معالجة فريدة عالية الجودة – مفتاح لفهم المكمن

ستورت هيرش وقاري بيري ومايكل فليمج

أدى التصوير عالي الجودة لمقطع زلزالي ثلاثي الأبعاد تم تكامله مع عمليات (AVO) والمعلومات المستمدة من سرود الآبار المتواجدة إلى التعرف على فرصة استثمارية غفل عنها في منطقة حقل كامل الأداء.

Abstract: *Interpretation of high-resolution 3-D seismic imaging integrated with AVO processing and existing well log control results in the identification of byp-assed exploitation opportunities in a mature field area.*

INTRODUCTION

Traditionally, integration of conventional, Pre-stack time-migrated seismic data with detailed interpretations of existing well log control have resulted in the information used to design development plans for newly discovered hydrocarbon accumulations. Through time, wells are drilled to optimally recover these accumulations and several generations of interpretations are produced and refined as a result of the introduction of new data, development of new or enhanced interpretation techniques, or simply by re-evaluating the available well log data under a new or different paradigm.

In many mature field areas, the remaining potential becomes difficult to define and, at this point, the field becomes a candidate for divestiture or abandonment. The use of high-frequency seismic imaging as a stratigraphic discrimination tool and the employment of Amplitude *vs*. Offset (AVO) products as risk reduction tools for the presence (or absence) of hydrocarbon accumulations permits the identification of potential by-passed production opportunities. This paper details the use of this high-frequency technique in the case study of Lake Pelto field.

BACKGROUND

Lake Pelto field (Fig. 1) is located about 120km southwest of New Orleans, Louisiana, in the state waters area of Terrebonne Parish. Discovered in 1929, the field has yielded in excess of 450 Bcf gas and 122 million bbl oil from multiple pay zones in the Pleistocene through the upper Miocene Textularia *"W" (Tex.W)*.[1] More than 300 wells have been drilled for sulphur and hydrocarbon resources. The deepest well drilled to date on the Lake

Pelto feature is 6,556m MD. Principal development of the salt dome feature was carried out by between 1929 and the late 1950s. A later period of development (1955 to 1997) was subsequently carried out in off-structure areas to the east and northeast of the earlier field development .

The latest development has been undertaken by

* Cabot Oil and Gas Corporation.
** Geotrace Technologies Inc.

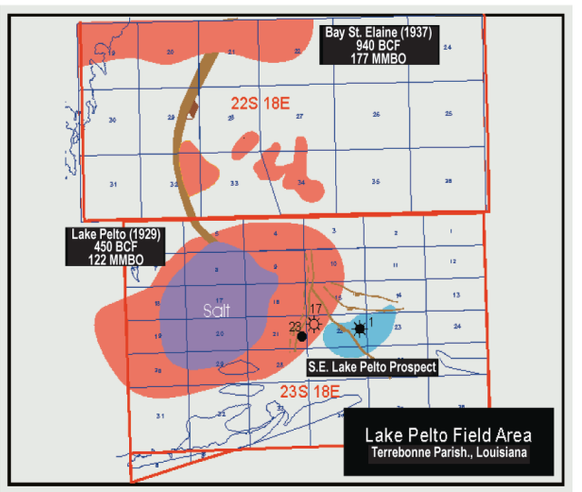


Fig.1. Lake Pelto field area. Location of salt dome and production from Lake Pelto and Bay St. Elaine fields.

Cabot Oil and Gas Corp., which purchased the leases and production in 1998. Cabot has drilled four wells since acquiring an interest in the field area.

GEOLOGICAL SUMMARY

From a regional perspective, the Lake Pelto field area is located within the Upper Miocene Distal-Deltaic Sandstone Subplay[2]. It falls within an area of thick Miocene sedimentation known as the Terrebonne Trough, which is characterized by major salt withdrawal basins, adjoining salt piercement features and regional to sub-regional growth fault systems.

Lake Pelto field proper is itself a salt piercement feature, with salt rising to within 450m of the surface. The deepest salt penetrated is at 3,560m. Faulting is complex and difficult to map in the immediate crestal area and as one nears the steep flanks of the domal feature. At increasing distances to the east of the dome, faulting above the Cibicides carstensi *(Cib. carst.)* is minor, while faulting below the *Cib. carst* is more common. Deep-seated, shale-cored ridges extend both eastward and northward from the dome into the major withdrawal basin that adjoins the domal area.

Major faults are associated with both ridges. These faults extend high up in the stratigraphic section. Faulting to the east dies rapidly away from the dome and does not extend above the *Cib. carst.* at increasing distance from the dome. The shale section marks the onset of hard geopressure and ranges, from a depth of 3,500m near the dome to more than 5,800m off the structure's east flank.

Depositional environments range from inner to middle shelf in the upper Miocene Bigenerina A *(Big. A)* to outer shelf and upper slope in the upper Miocene Textularia "L" *(Tex. L).*

The *Big. A* and younger section is dominantly a sandy interval with few shale breaks, while below the *Big. A* and extending down to the *Tex. L,* the section is dominated by cyclical, coarsening-upward sequences characterized by thick, basal shale units. A major unconformity is evident in the *Cib. carst.* section off the east flank of the Lake Pelto dome.

Production depths range from less than 450m in the Pleistocene to deeper than 5,200m in the Upper Miocene. Gas production dominates below 4,500m and at increasing distances from the dome. Most oil and gas accumulations are associated with structural traps, although an increasing stratigraphic component is evident in areas drilled both north and east of the dome.

DEVELOPMENT CHALLENGE

Using a 1993-1994 vintage 3-D seismic survey, Cabot geoscientists identified several areas that appeared under-exploited. One area, located north of existing production, was characterized by apparent, multiple high amplitude events on a low-relief structural closure that was separated from existing production by a subtle syncline. A second area which is the focus of this paper was located off the east flank of the producing feature in an area with no apparent trapping structure and no distinct stratigraphic separation from depleted producing zones. In both cases, conventional processing exhibited several high amplitude events. However, the data were not suitable to define stratigraphic separation from existing production, nor to discriminate potential reservoir(s) or map their potential lateral extent.

Due to reservoir depths and long producing history of the field complex, better tools were required to discriminate bypassed pay from residual gas in depleted reservoirs. Thus, to reduce the drilling risk of these prospects, Cabot embarked on a seismic reprocessing program that included pre-STM coupled with AVO processing of the 3-D data.

SOUTHEAST LAKE PELTO PROSPECT

Cabot's Southeast Lake Pelto Prospect was first

identified via reconnaissance of the reprocessed, pre-STM 3-D dataset. A Class III AVO amplitude anomaly was seen basinward of previous production (Fig. 2) and was initially linked to the M-4 sand updip Wells 16 and 23. An immediate drainage area problem arose due to an unexplainable excess of 27 Bcfg and 630 million bbl oil produced from the thin M-4 sand intervals in the two wells (4m gross pay at 4,800m MD in Well 17, and 9m gross pay at 4,780m MD in Well 23). This produced area of the M-4 appeared to penetrate the amplitude anomaly.

Additionally, seismic stratigraphy between the producing wells and the prospect area showed neither structural nor stratigraphic separation of the anomaly from the two producing wells. Images using DMO and Pre-STM datasets also failed to show M-4 as a separate unit from the overlying Mc and M-l sands. Even more troubling from drilling risk perspective was the fact that, if a separate prospect existed downdip of the formerly productive wells, it had no apparent trapping mechanism. The production volume vs. drainage-area problem thus became an important consideration affecting any decision to exploit the anomaly.

Prestack Kirchhoff Time Migration

It was decided early in the project to reprocess the 3-D seismic data to obtain a better image subsurface and look for Direct Hydrocarbon Indicators (DHIs). To focus deep reflectors, 3-D Prestack Kirchhoff time migration was utilized. This process simultaneously solves for normal moveout, DMO and migration, placing reflectors in proper spatial positions while retaining as broad bandwidth as possible.

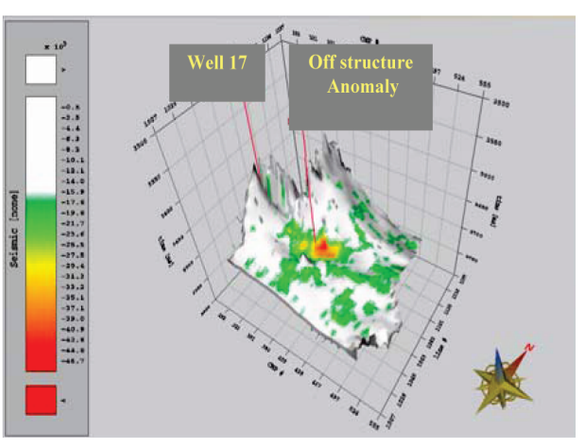


Fig.2. Amplitude of the Mc sand brightens downdip of the depleted reservoir on the high-frequency data.

High-frequency Imaging

Since significant production in south Louisiana is often found in relatively thin sands and in stacked sand sequences, seismic resolution is a key to finding new pay. At 4,880m, about 3.7-sec. Two-Way Travel time (TWT), most seismic data in the area is limited to about 40 to 50 Hz usable frequency. Using quarter wavelength estimation, this means that the thinnest sandstone layer that can be fully resolved is about 65-80 ft thick. To maximize usable frequencies in the reprocessed seismic data, High Frequency Imaging (HFl) was applied. This unique approach to whitening seismic data makes it possible to extract much higher frequencies than traditional methods.

It is a widely known but seldom-used characteristic of seismic that the apparently narrow band trace contains higher frequency information than an extracted wavelet would suggest. By recognizing that convolution is equivalent to polynomial multiplication, and polynomial division is its exact inverse, one can easily demonstrate this characteristic[3]. A synthetic seismogram is constructed by convolving a spike series with a band-limited wavelet, the result being a band-limited trace containing, apparently, only those frequencies that were in the wavelet used. However, by employing polynomial division, the spike series can be obtained from the synthetic seismic trace. In other words, all of the original high-frequency information is contained in the low-frequency trace. Unfortunately, polynomial division cannot be used in the real world, because even the smallest amount of noise introduced into the trace makes the process unstable.

HFI uses vector calculus, rather than polynomial mathematics, to solve the problem by viewing convolution as a vector rotation. The vector that represents the apparent low-frequency seismic is precisely determined, then rotated toward a white spectral position in the chosen vector space. The process is not sabotaged by ambient noise, and the resulting seismic is broad-band with a higher signal-to-noise ratio. In this particular case, using the pre-STM data with 48 Hz maximum usable frequency at 3.7 sec. as input, the HFI yielded 110 Hz data on the high end, an increase of 129%. Now, beds as thin as 4m could be resolved in the zone of interest. This would prove to be extremely beneficial.

Figures 3 and 4 show a comparison of the normal-frequency Pre-STM data and the HFI data on an arbitrary line from the 3-D survey. This line connects

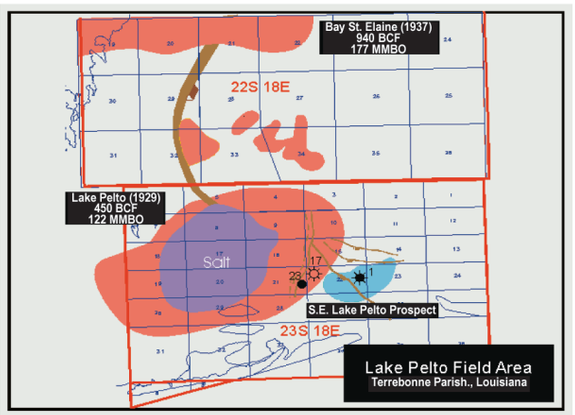


Fig.3. The M-4 sand, producing gas in Wells 17 and 23, is not resolved on the normal frequency pre-STM data

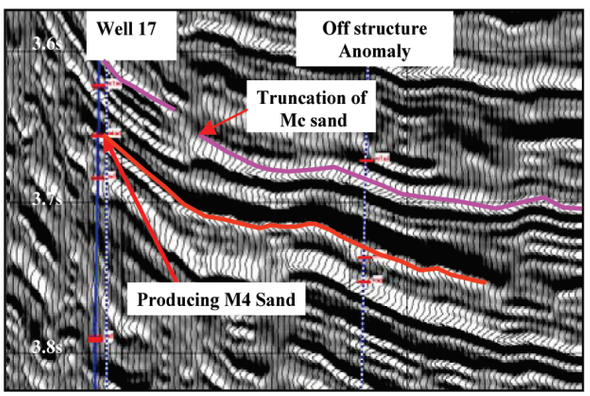


Fig.4. M-4 sand is continuous between Well 17 and the downdip location, although a small fault was verified on the HFI data. The Mc sand, however, shows an abrupt truncation between the wells on the HFI data.

Well 17 to the prospect area anomaly. The HFI section more clearly images the continuity of the M-4 down dip of Well 17, which had been P and A'd after reservoir pressure depletion. Additionally, the Mc sand, which is wet and poorly developed in the updip Well 17, appears to be discontinuous between the two locations on the high-frequency data. It is also evident that a small fault separates the Mc sand seen in the updip wells from the downdip anomaly.

AVO

Since HFI was run on migrated CMP gathers, it was possible to calculate high-frequency AVO attributes on the seismic volume. Wells in the area were analyzed, and it was determined that producing sands fit into Class II or Class III AVO categories. That is, sands that contain gas or oil either had about the same impedance as surrounding shale or had lower impedance. In either case, the AVO effect on a resolved interface at the top of a producing sand is a high-amplitude trough at large angles of incidence.

Both *Intercept* X *Gradient* and *Intercept* X *Poisson's Reflectivity* attributes were useful, as they are good Class III and Class II tools, respectively. The *Intercept* X *Gradient* attribute exhibited a particularly good anomaly, the first DHI located downdip from Well 17. A horizon slice through this 3-D volume is shown in Fig. 5. As can be seen, there is no AVO anomaly at the same level in Well 17.

Frequency Absorption

The broadband data was also scrutinized for absorption effects. As seismic energy passes through an absorptive layer, all frequencies are attenuated, but high frequencies are absorbed more quickly than low frequencies. Sands containing gas are good absorbers and, unlike many AVO effects, higher saturations produce better absorption anomalies. High-frequency seismic is preferable to narrow-band data, since absorption effects are much more apparent in the high end of the spectrum. A 3-D volume indicating degree of absorption was generated for the 3-D area.

An anomaly down dip from Well 17, the second DHI detected at that location, reinforced the AVO work done previously. A horizon slice through this 3-D volume is shown in Figure 6. Notice that the anomaly does not extend updip to Wel1 17 wel1, which had been P&A'd before the 3-D survey was acquired. A vertical profile through this volume is shown in Figure 7.

Based upon interpretation of the HFI reprocessed data and the various AVO and Frequency Absorption Response (FAR) attributes, Cabot geoscientists came to the following conclusions:

- The DHIs were indicative of potential pay in the Mc/M-1 sands rather than in the lower M-4 sand.
- The hydrocarbon present was probably gas.
- The M-4 sand extended downdip into the prospect area but was probably depleted as evidenced by the volumes previously produced updip from this zone in Wells 17 and 23.
- The downdip accumulations had a very strong stratigraphic trapping component.
- A small fault separated the updip limit of the amplitude anomaly in the prospect area from the equivalent interval in Wells 17 and 23. Thus, the decision was made to drill the prospect.

Drilling Results

Well 1 was drilled to a 5,180m TD and completed

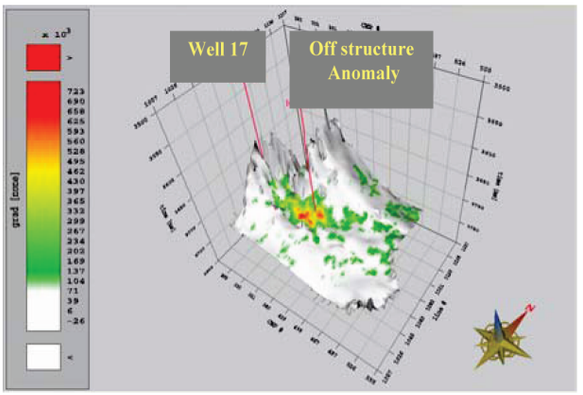


Fig.5. Horizon slice at the Mc sand through the Intercept x Gradient AVO attribute volume. The anomaly in the syncline does not extend updip to Well 17.

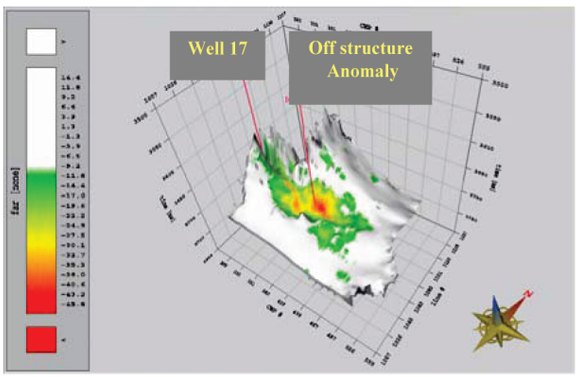


Fig.6. Horizon slice at the Mc sand through the FAR attribute volume. The strong downdip anomaly indicates a substantial gas accumulation.

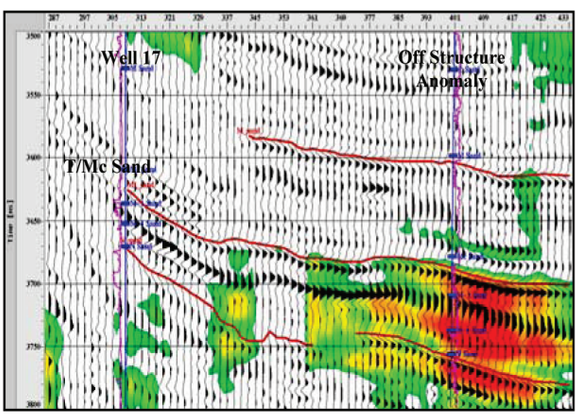


Fig.7. Vertical profile from the FAR attribute volume through Well 17 and the downdip absorption anomaly.

as a producing gas well in the third quarter of 2001. Well log correlation and interpretation confirmed that the Mc sand had developed downdip of Wells 17 and 23, and the upper 15m of sand was clearly gas bearing. Also present was the M-l sand, but not as well developed as in Well 17. Depleted M-4 sand was present and very similar in character to the M-4 sand in Well 17, Figure 8.

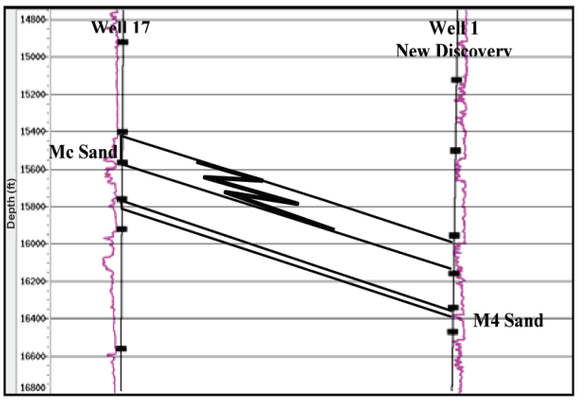


Fig.8. Generalized correlation section showing the Mc and M-4 sands in depleted Well 17 and recently completed Well 1.

CONCLUSIONS

Interpretation of high-resolution seismic imaging, coupled with AVO-attribute analysis, provided the necessary means to interpret subtle changes in stratigraphy and structure that turned Cabot's Southeast Lake Pelto prospect into a viable drilling opportunity. Using the high-frequency processing technique led to the conclusion that, although the Mc and M-1 sand intervals were correlative between the updip Wells 17 and 23 and the downdip prospect area, sand bodies within these intervals were nonetheless stratigraphically distinct units.

Using HFI also permitted discriminating the M-4 sand from potential pay in the overlying Mc and M-l sands. Strong stratigraphic trapping components of the reservoir were verified, as was existence of a very small fault-cutting up through the Mc/M-I sand interval-that previously had not been recognized. AVO characteristics successfully predicted a gas accumulation, and FAR helped determine that the accumulation was, in fact, a virgin reservoir. Seismic interpretation using conventional frequencies would not have resulted in a drilling recommendation for this location, and substantial pay would have been bypassed.

ACKNOWLEDGEMENT

The authors wish to thank Cabot Oil and Gas Corporation and Geotrace Technologies, Inc. for permission to publish this paper.

REFERENCES

[1] Waguespack, S.J., ed., 1983. Lake Pelto field in *Salt domes of south Louisiana*, New Orleans Geological Society, New Orleans, Louisiana, **3**, 42-43.

[2] Chacko, J.J. *et al*.,1992. MC-8. Upper Miocene sandstone– Louisiana Gulf Coast, *Atlas of major central and eastern Gulf Coast gas reservoirs*, Debout, D.G. *et al*. eds., *Bureau of Economic Geology*, Austin, Texas, 11-13.

[3] Stanford Exploration Project, http://sep.stanford.edu/public/docs/gern/ajt/p aper_html/node14.html

Petroleum Res. J. Vol. 20 (2007); P. 113–120, 4 Figs.

Pitfalls in 3D preSDM Imaging

Ian F. Jones*

تصوير هجرة عمق مسبق التراص ثلاثي الأبعاد لا يسهل إدراكه

إيان ف. جونز

ضمن أولى الخطوات التي اعتبرت في مشروع تصوير معين هي كيف يمكن تمثيل نموذج السرعة لتحت السطح. يمكن استعمال كل من التمثيل الطبقي أو المتشابك ولكن في حالة استعمالنا لنماذج طبقية يجب استعمال بعض الافتراضات، ككيف تتغير السرعة عموديا في كل طبقة عن طريق معامل ممال مدمج.

سنحاول في الجزء الأول من الورقة تقييم تأثير تمثيل النموذج على انسياب الصورة، كما سنعتبر تأثير افتراضات محدودة على نتائج هجرة عمق متراص مسبقا بما في ذلك تأثير التباين. وفي الجزء الثاني من هذه العملية سيتم تقييم تأثير العوامل المختلفة على طول الموجة والمحتوى الترددي للبيانات المتدفقة ونفحص الملاحظات المشتركة والتي تفيد بأن التكدس المسبق لصور هجرة عمق كيركوف ذات محتوى ترددي أقل من الوقت المقابل المتعارف عليه.

لقد قمنا باستقصاء العوامل المختلفة التي تؤثر في طول الموجة والمحتوى الترددي أثناء الاندفاع بهدف تقييم أسباب نقص متوقع في نطاق عرض الموجة في البيانات المندفعة ونبرهن على عدم وجود سبب متأصل لعرض موجة بيانات كيركوف (أو العمق) المندفعة لأن تكون أكثر سوءا من البيانات المندفعة الأخرى، ونقدم توصيات تؤكد أفضل محتوى للتردد في مخرجات الصورة المعالجة.

Abstract: *One of the first steps considered in an imaging project is how to represent the velocity model of the subsurface. Both layered and gridded representations can be used, but if we use layered models, then we must also make some assumptions as to how the velocity changes vertically in each layer, via a compaction gradient function.*

In the first part of this paper, we will assess the effect of model representation on an imaging flow and consider the influence of restrictive assumptions on the PreSDM results, including the effects of anisotropy.

In the second part of the paper, we assess the impact of various factors on the amplitude and frequency content of migrated data, and examine the common observation that Pre-stack Kirchhoff depth migrated images sometimes have a lower frequency content than their time-domain counterparts.

We investigate the various factors that influence amplitude and frequency content during migration, with the object of assessing the reasons for potential loss of bandwidth in migrated data, and demonstrate that there is no inherent reason for the bandwidth of Kirchhoff (or depth) migrated data to be worse than other migrated data, and offer recommendations for ensuring optimal frequency content in the processed output image.

INTRODUCTION

The Velocity Depth Model

Current practice in velocity model building usually resorts to one of two representations: the layer-based

* GX Technology EAME Ltd., 180 High Street, Egham, Surrey, TW20 9DN, UK. Corresponding author: ijones@gxt.com

and the gridded (Jones, 2003). The layer-based approach is typical of say a North Sea type environment, where sedimentary interfaces delimit changes in the velocity field. The gridded approach is adopted in environments such as found in the Gulf of Mexico, where the velocity regime is decoupled from the sedimentation, and is governed primarily by vertical compaction gradients (velocity increasing with depth), controlled by de-watering, with iso-velocity contours sub-paralleling the sea bed.

In the example considered here, which is typical of many southern North Sea fields, we have a thick chalk sequence, with a vertical compaction gradient within the chalk. The nature of these compaction gradients can be quite complex, with many subdivisions that are not obviously manifest in terms of a clear seismic response. Due to compaction within the chalk, we can move from a near constant velocity regime in the uppermost part of the chalk, to a steep compaction gradient regime, and then back to a constant (high) velocity region at the base of the chalk, where the chalk has been compressed as much as it can be by the overburden pressure.

Two classes of error can occur in building a model for such bodies:

1. The internal layering in the chalk may not be sufficiently well represented in the layered model, due to the difficulty in picking a clear event when we have a change in compaction gradient rather than a sharp change in reflectivity.

2. Errors in the estimate of the values for the compaction gradient can manifest themselves as apparent anisotropy (Alkhalifa, 1997; Jones*, et al*, 2003).

Both of these errors will result in sub-optimal imaging, including the lateral mispositioning of faults (Alkhalifa and Tsvankin, 1995; Hawkins, *et al*, 2001).

In the example discussed here, we had a thick chalk sequence, wherein the vertical compaction gradient changed subtlety, in a way not readily discernable from the seismic reflection data (Sugrue, et al, 2004). As a consequence, imposing the explicit top and bottom chalk horizons, with an intervening vertical compaction gradient (of the form $v(x,y,z) = vo(x,y) + k(x,y).z$), led to a misrepresentation of the subsurface.

To address this issue, a gridded model building approach was also tried. This relied on dense continuous automatic picking of residual moveout in CRP gathers at each iteration, followed by gridded tomography, resulting in a smoothly varying velocity field which was able to reveal the underlying local changes within the chalk (Hardy, 2003). In Figure 1, we see the differences between a layered representation and a gridded representation of a thick chalk layer.

The Migration Output Bandwidth.

'The depth migration has lower bandwidth': this complaint has often been heard, and examples can be found where it appears to be true. Is this observation an indication of some inherent limitation of Kirchhoff 3D PreSDM or simply of 'bad practice' or economic 'expediency'?

In the following sections, we outline the nature and cause of various factors that have an impact on the frequency content of a migration, and try to assess if these factors affect depth migration more than time migration, or Kirchhoff migration more than alternative schemes (Jones and Fruehn, 2003; Jones and Lambaré,. 2003).

The analysis covers the following topics:

- Spurious Differences
- Aliasing: (Temporal and Spatial)
- Wavelet Changes during Migration: (Frequency, Velocity and Offset Dependent)
- Kirchhoff Migration as a Stacking Process: (Travel-Time Sampling Errors; Sensitivity to Velocity Error; Acquisition Footprints).

SPURIOUS DIFFERENCES

Some aspects of this work deal with 'statements of the obvious': but it could be instructive to re-state them anyway. For example, a common element of confusion in time versus depth comparisons is the degree of post processing. A final time product (with its associated deconvolution and spectral balancing) will naturally look better in terms of signal content, than a raw PreSDM result. Consequently, it is important to perform the appropriate post-processing on the output from the PreSDM before drawing conclusions. In the case of designing spectral balancing operators, we must ensure that the PreSDM output spectrum extends well beyond the signal spectrum.

In addition, whereas a frequency domain finite-difference algorithm explicitly limits the frequency range (FMIN and FMAX parameters), a Kirchhoff scheme (which is usually time domain) does not inherently limit the frequency range. However, in preparation for anti-alias filtering, or variable depth

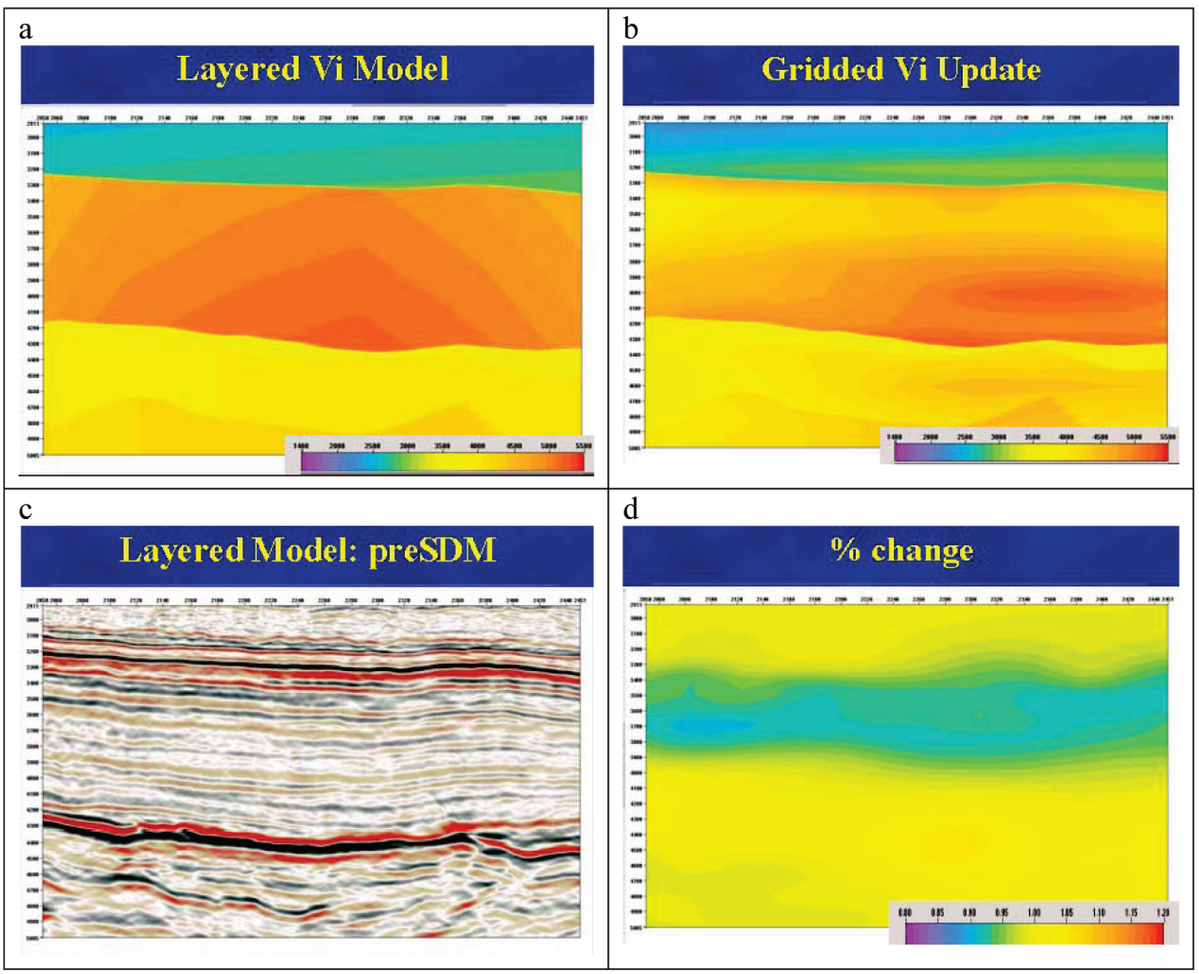


Fig. 1. a: layered model with vertical compaction gradients in the chalk, b: the gridded update, c: the PreSDM from the layered model, d: the percentage change in velocity resulting from the gridded update

step, some Kirchhoff schemes may also select a frequency bandwidth. Thus, in comparisons, we must first ensure that we have migrated that same frequency content.

Temporal Aliasing

For time-sampled data, we have a Nyquist frequency, and if we resample the data say from 2 to 4 ms, then we must first pre-filter the time data in order to avoid aliasing the signal with energy beyond the new Nyquist.

Likewise, during depth migration, we resample data to depth, and must take care that we do not alias temporal frequencies that are not adequately sampled by the output depth step.

This is not usually a problem for finite difference depth migration, as we band-limit the data explicitly during migration. However, for Kirchhoff migration, we have no explicit time-frequency cut-off so must ensure that upon output we do not permit aliased energy to survive.

To accomplish this, we must pre-filter the input time data: to calculate the frequencies permissible in the output depth data, we need to know: *dz* (the output depth sample rate) for the migration, and Vi(t) the interval velocity function. The maximum temporal frequency that can be imaged for a given *dz* is:

$$F_{nyq} = v/(4*dz)$$

For example, for typical marine data, imaged with a 10m depth step, we would need to pre-filter the input data to about 35Hz in the shallow. Figure 2 shows some deep water data where the imaging was performed with a 10m depth step, with and without the appropriate depth-temporal pre-filtering.

This problem of not having pre-filtered the data to guard against temporal aliasing is only important when we image at a 10m depth step (or greater) or

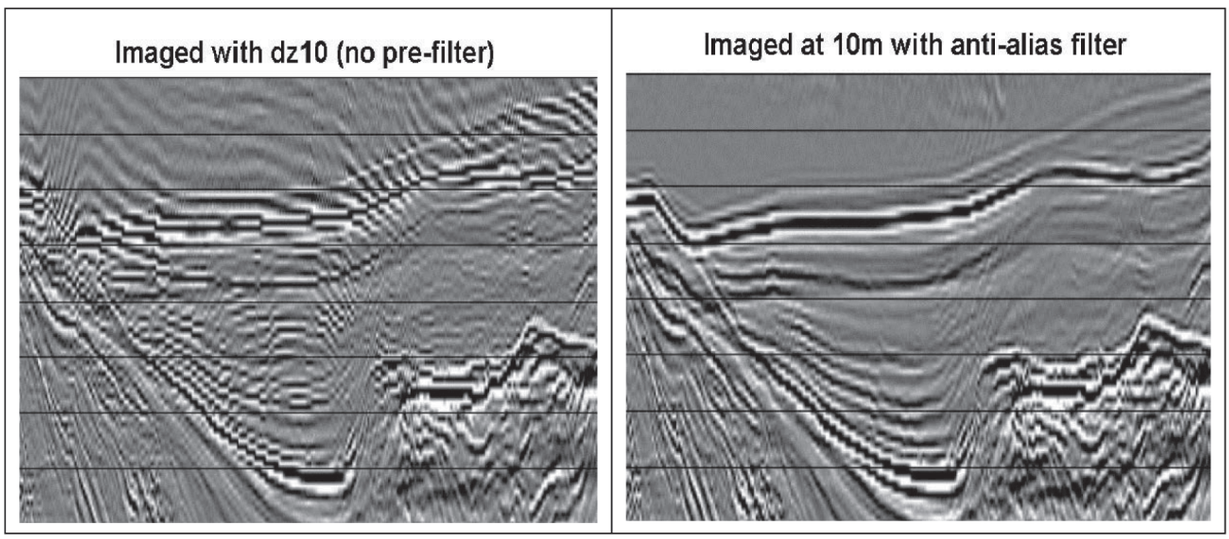


Fig. 2. Effects of not compensating for depth-temporal aliassing in the migration

in the very shallow parts of a marine section, where we have low velocities. Deeper in the data, or with a 5m (or variable) depth step, the problem is not as severe. For some land data, the problem does not usually occur, as we have high near-surface velocities. However, in dune areas, we can have very low surface velocities, so the problem can be even worse.

Recommendations

Estimate the global minimum 1D velocity function that is representative of the 3D velocity field. Compute the corresponding Fmax for the depth step to be used in the migration. Pre-filter the data with the appropriate low-pass filter.

Parameter testing (design of aperture, spatial anti-alias filter, etc) must be performed only on data that have been appropriately pre-filtered.

Spatial Aliasing

During migration, data is moved out along the impulse response to increasingly higher dips, prior to summation to form the output image. For a given inter-trace distance, a given frequency will become aliased for a given dip. In order to prevent the aliased frequencies from being summed into the output image, we apply an anti-alias filter during migration. This will limit the frequency content of dipping reflectors. This observation is true for all migrations, but is more pronounced in Kirchhoff migration, where we explicitly apply an anti-alias filter.

For finite difference schemes (as usually applied in time migration) we do not usually have explicit control of the operator, but aliased frequencies will be rejected as evanescent energy.

Sometimes the design of the anti-alias operator is sub-optimal, as the effect of tapers is not properly taken into account, and the filter kills too much high frequency energy. Thus, omitting the anti-alias filter can sometimes give a better result, especially deeper in the section where high frequency aliased energy is less of a problem.

Recommendations

Produce a test line with the anti-aliasing turned-off, so as to be able to assess any potential damage done to steep dips by the choice of anti-alias parameters. Adjust the anti-alias parameters accordingly.

WAVELET CHANGES DURING MIGRATION

Frequency Dependent Changes

In general, migrating an event of a given dip will lower the frequency content of that event. This lowering of frequency on dipping events is common to both time and depth migrations, but care must be taken to choose the low-cut of display filters so as to preserve the post-migration frequency content of the data.

This also has a corresponding effect on the design of deconvolution operators. It can be observed that

using a deconvolution whose parameters have been chosen by testing on a time migrated image, will give a sub-optimal result when used on a depth migrated image.

Recommendations

Deconvolution tests and parameter selection should preferably be done on the depth migrated data (converted back to time) rather than applying deconvolution operators with parameters selected from previously existing time migrated data.

Velocity Dependent Changes

On a time migrated section, the wavelet is seen in its domain of measurement: namely time. So, ignoring the effects of dispersion and attenuation, the wavelet will appear stationary down the trace. That is to say, its phase and frequency content should not change.

On a depth migrated image however, the wavelet is seen in depth, and its wavelength changes in accordance with the velocity contrasts it sees. The wavelet is stretched as it passes through an interface with a high velocity contrast.

Consequently, the wavelets appear to be of lower frequency in the deeper parts of the section in the depth image. This stretch effect can be removed by a vertical stretch back to time, and if we do this, the frequency content of the wavelet should be similar to that of a time image.

Although we have stated that converting back to time will 'back out' the vertical wavelet stretch, on real data, life is not so simple. Due to the persistence of RMO, the depth domain wavelets are not perfectly aligned in the CRP gathers. Thus upon stacking, we degrade the wavelet character. This distorted wavelet is then converted back to time with a model whose velocity interface sits 'somewhere' within the distorted wavelet. Thus a residual low frequency element remains in the wavelet after conversion back to time. If the input data are in minimum phase, then this effect can be lessened somewhat, as the energy of the wavelet is front-loaded. There is also the interplay with where the horizon boundary sits within the wavelet.

Recommendations

Strive towards a good wavelet compression sequence prior to migration.

Offset Dependent Changes

A more problematic, and fundamental problem related to depth imaging, is the offset dependent stretch of the wavelet in depth (Tygel, *et al*, 1994, 1995). This is analogous to the NMO stretch in time processing (Barnes, 1995).

In the depth domain, the severity of the stretch is proportional to the incidence angle, reflector dip, and to the velocity. Hence the effect is very noticeable for the farther offsets. In addition, the effect stands out at high velocity contrast layers, especially after a velocity inversion, as in this case, the down going rays refract back to the vertical, thus reducing the angle of incidence of subsequent reflections. Consequently the stretch at the base of the high velocity layer appears more pronounced in comparison to deeper events. Hence the effect is most noticeable at unconformities, carbonate, and salt interfaces.

Because the stretch can both increase and decrease with depth, such events are difficult to mute out with a standard processing mute, as the mute functions often must be simply monotonic. To deal with depth stretched wavelets, we need to design an automatic stretch dependent mute.

Recommendations

Stacking mutes should be selected after PreSDM. Consequently the pre-migration mute should be left quite wide. Ideally, an automatic stretch mute, with a parameter to select the stretch threshold could be implemented.

This recommendation is only valid for offset Kirchhoff migration. In a shot migration (as used in a full wave equation scheme) energy is mixed between offsets during the migration, Thus, the mutes must be applied prior to migration.

KIRCHHOFF MIGRATION AS A STACKING PROCESS

If we think of the migration as a sum over hyperbolic trajectories (in time migration) or over more complex asymmetric trajectories (in depth migration), then we can see that summing over an incorrect trajectory will lead to mis-stacking, which translates into a lack of frequency content.

Assuming we have the correct model, there will be 3 main influencing factors on image quality:

- correct sampling of the velocity field (ergo – travel times).
- correct sampling of the input data on the acquisition surface.
- adequate sampling within the Fresnel zone at the image point.

Travel-Time Sampling Errors

There are various theoretical approximations made in ray-tracing or other travel time computation schemes (such as how we treat the curvature of a ray in a velocity gradient). However, a more mundane and damaging effect relates to how we sub-sample the travel times for storage.

In practice the travel time calculation is performed by considering a five-dimensional problem:

- The 2D surface acquisition grid sampled at say 125m* 125m, representing both the source and receiver positions, and
- The 3D subsurface volume sampled at say 100m* 100m* 50m.

For each surface location on the 2D grid, we compute the one-way travel time to each of the nodes in the 3D subsurface volume. In general, the cost of computation increases as the cube of the depth (solving to a depth of 2km costs 8 times more than solving for a depth of 1km). Given that in general an input trace will not lie on the surface nodes used for calculation, we must read the travel time tables associated with the four nearest neighbours and then interpolate. Also, given that the desired output points will not lie on the 3D volume nodes, we must also interpolate those values between nearest neighbours.

These interpolations introduce some error. To avoid them, ideally we should compute travel times for the true surface locations of all shots and receivers, and do so for all desired output depth samples (*i.e*. at the seismic sampling, typically 25m* 25m* 5m). However, the volume of space required to store all travel times is very large (*e.g*. For a 10km* 10km* 10km volume, this would typically be 400 terabytes).

In the near surface, the travel time isochrons tend to have greater curvature, as the wavefield has not spread-out too much. If we sample the travel times on a surface grid of say 200*200m, and then interpolate these values down to 25*25m during the migration, we will have some interpolation error. If we use a simple linear interpolator to resample the travel times to the migration output grid spacing, then we will usually see a grid pattern artifact in depth slices through the resulting images. (N.B. In practice it is the slowness that are interpolated).

Recommendations

QC the degree of artifact by inspecting 3D depth slices through the final image. The artifact is usually strongest at shallower depths. If necessary, use a non-linear interpolation and/or use the smallest 'affordable' grid;

Sensitivity to Velocity Error

As we have noted, an error in the travel times, due to whatever cause, results in mis-stacking in the Kirchhoff summation. This not only leads to a loss of stack power, but also to a loss of frequency content (Jones*, et al*, 1998). Both time migration and depth migration will suffer from loss of amplitude and frequency due to this mis-stacking.

However, depth migration is more sensitive to lateral velocity change (in fact, time migration ignores it to the extent that time migration operators are symmetric) Due to this greater sensitivity to velocity, a depth migration will suffer more than a time migration for a given velocity error.

Recommendations

Output all CRP gathers from the 3D PreSDM final run. Then obtain a dense RMO velocity correction field - eg use an automatic velocity analysis tool to continuously analyse velocity along lines spaced at 200m: gathers can be converted back to time for this. Velocities can be output every 100 or 200m along the lines, to yield a 200m* 200m RMO correction grid, after appropriate editing and smoothing.

Acquisition Footprints

A Kirchhoff migration assumes that the input data are regularly sampled in x, y, and offset, so that the resulting wavefield can be adequately reconstructed during imaging. If we have a gap in the input, there will be an amplitude anomaly in the output, as the corresponding Huygen's 'secondary wavelets' will not sum appropriately (Fig. 3).

In the case of acquisition footprints, time processing is helped by bin-centred DMO and subsequent interpolation prior to migration. Finite Difference PreSDM requires regular bin-centred input, so we avoid the problem as with time imaging.

If the surface distribution is too irregular, and we do not want to accept the expense of pre-stack regularization, then a simple fold compensation-weighting scheme can be applied. This simply scales the input traces in proportion to their distance from their neighbours. This will fail if the gaps are too big, but can yield some improvements. Figure 4 shows the image of an unconformity at target level beneath a production platform, resulting in some coverage gaps, especially for short offsets. Fold compensation can reduce impulse response noise 'generated' by the holes.

Recommendations

Perform regularization/interpolation prior to Kirchhoff PreSDM.

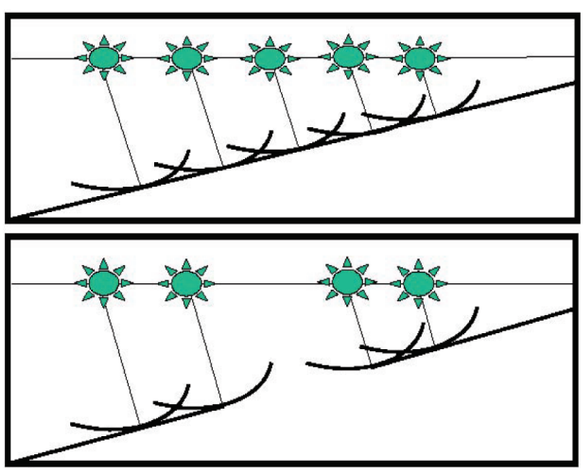


Fig. 3. Irregular input sampling gives non uniform amplitude behaviour in the resultant image.

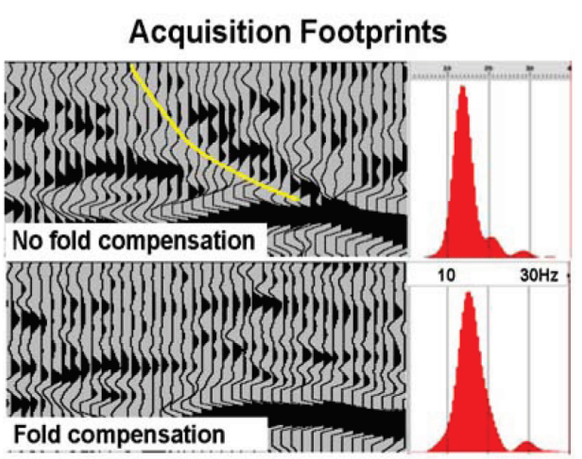


Fig. 4. Impulse response noise for data not pre-conditioned to compensate for surface sampling irregularity. The spectrum of the compensated data is broader in this case (but not always).

CONCLUSIONS

3D PreSDM is still considered an 'expensive' process, consequently pressure is always on to 'save money'. However, if money is 'saved' by either compromising the model representation or not outputting full bandwidth gathers, then more money will be lost by having to work with sub-optimal images.

A representation of the earth's subsurface that is suitable for the data under investigation should be used.

All gathers should be output from a PreSDM: these gathers should be subjected to the full conventional processing expected for any high-fidelity time-processing sequence (*e.g.* careful mute selection, wavelet deconvolution, signal spectral balancing, residual anti-multiple, *etc*).

A series of recommendations have been given in the body of the text. Following the majority of these recommendations should safeguard against most of the factors that act to degrade depth image quality.

ACKNOWLEDGEMENTS

Thanks to Amerada Hess, bp, Repsol, Shell Expro, & Total, for kind permission to use their data, and to Juergen Fruehn, Mick Sugrue, Mike Bridson and Mike Goodwin for producing some of the data examples.

REFERENCES

Alkhalifah, T., and Tsvankin, I., 1995. Velocity analysis for transversely isotropic media. *Geophysics*, **60,** no.5, 1550-1566.

Alkhalifah, T., 1997. Velocity analysis using nonhyperbolic moveout in transversely isotropic media. *Geophysics*, **62**, no.6, 1839-1854.

Barnes, A. E., 1995. Discussion on 'Pulse distortion in depth migration', by M. Tygel, J. Schleicher, and P. Hubral (GEO-59-10-1561-1569). *Geophysics*, **60,** no. 06, 1942-1947.

Hardy, P.B., 2003. High resolution tomographic MVA with automation, SEG/EAGE summer research workshop, Trieste.

Hawkins, K., Leggot, R., Williams, G.,and Kat, H., 2001. Addressing anisotropy in 3D pre-stack depth migration: a case study from the Southern North Sea. *The Leading Edge*, **20**, No.5, 528-543.

Jones, I.F., Bridson, M.L., and Bernitsas, N.X., 2003. Anisotropic ambiguities in TI media. *First Break*, **21**, No.4, 31-37.

Jones, I.F., 2003. A review of 3D preSDM velocity model building techniques. *First Break*, **21**, No.3, 45-58.

Jones, I.F., Fruehn, J., 2003. Factors affecting frequency content in 3D preSDM imaging. *The Leading Edge*, **22**, No.2, 128-134.

Jones, I.F. and Lambaré, G., 2003. Wave equation versus ray based imaging. *First Break*, **21**, No.2, 11-13.

Jones, I.F., Ibbotson, K., Henry, B., Strachan, A., Baud, H., 1998. Enhancements to 3D preSDM salt-flank imaging. *Journal of Seismic Exploration*, **7**, No.3/4, 329-346.

Sugrue, M., Jones, I.F., Evans, E., Fairhead, S., Marsden, G., 2004. Enhanced velocity estimation using gridded tomography in complex chalk. Geop*hysical Prospecting*, **52**, No.6, p683-691.

Tygel, M., Schleicher, J., Hubral, P., 1994. Pulse distortion in depth migration. *64th Ann Internat. Mtg. Soc. Expl. Geophys.*., Expanded Abstracts, 1359-1362.

Tygel, M., Schleicher, J. and Hubral, P., 1994. Pulse distortion in depth migration. *Geophysics*, **59,** no. 10, 1561-1569. (*Discussion in GEO-60-6-1942-1949).